



**NTNU – Trondheim**  
Norwegian University of  
Science and Technology

# A Comparative Life Cycle Assessment of PV Solar Systems

**Kristine Bekkelund**

Master of Energy and Environmental Engineering

Submission date: August 2013

Supervisor: Anders Hammer Strømman, EPT

Norwegian University of Science and Technology  
Department of Energy and Process Engineering



EPT-M-2013-18

**MASTER THESIS**

for

Kristine Bekkelund

Spring 2013

Life Cycle Assessment of Thin Film Solar Panels

*Livssyklusanalyse av solcellepaneler***Background**

A significant amount of research is currently devoted to the exploration of material and technology alternatives for photovoltaic systems. The number of these technology options and their permutations is significant. Given the present situation with formidable focus on the reduction of greenhouse gas emissions, it is important to assess technologies with a holistic perspective. Life Cycle Assessment (LCA) is the prominent tool for such analyses. LCA is a methodological framework for analyzing the environmental aspects of products and product systems throughout their whole life cycle. Understanding how the variety of existing and emerging PV technologies compare to each other, with respect to environmental aspects, is essential to provide direction for research, investments, and policies.

**Objective**

The primary objective of this project is to assess the life cycle impacts of thin film PV solar panels. The aim is to improve on and reconcile existing studies. The secondary objective is to identify environmental bottlenecks and possible options to improve these. Selection of cases to be investigated will be undertaken in dialogue with supervisors.

**The analysis should include following elements**

- 1) Assessment of state of the art in LCA of thin film PV systems.
- 2) Description of the thin film PV production value chain and processing technologies.
- 3) Compilation of empirical data on thin film PV production and benchmarking with existing inventories.
- 4) Life cycle assessment on the selected thin film technologies.
- 5) Analysis and discussion.

-- " --

Within 14 days of receiving the written text on the master thesis, the candidate shall submit a research plan for his project to the department.

When the thesis is evaluated, emphasis is put on processing of the results, and that they are presented in tabular and/or graphic form in a clear manner, and that they are analyzed carefully.

The thesis should be formulated as a research report with summary both in English and Norwegian, conclusion, literature references, table of contents etc. During the preparation of the text, the candidate should make an effort to produce a well-structured and easily readable report. In order to ease the evaluation of the thesis, it is important that the cross-references are correct. In the making of the report, strong emphasis should be placed on both a thorough discussion of the results and an orderly presentation.

The candidate is requested to initiate and keep close contact with his/her academic supervisor(s) throughout the working period. The candidate must follow the rules and regulations of NTNU as well as passive directions given by the Department of Energy and Process Engineering.


Risk assessment of the candidate's work shall be carried out according to the department's procedures. The risk assessment must be documented and included as part of the final report. Events related to the candidate's work adversely affecting the health, safety or security, must be documented and included as part of the final report. If the documentation on risk assessment represents a large number of pages, the full version is to be submitted electronically to the supervisor and an excerpt is included in the report.

Pursuant to "Regulations concerning the supplementary provisions to the technology study program/Master of Science" at NTNU §20, the Department reserves the permission to utilize all the results and data for teaching and research purposes as well as in future publications.

The final report is to be submitted digitally in DAIM. An executive summary of the thesis including title, student's name, supervisor's name, year, department name, and NTNU's logo and name, shall be submitted to the department as a separate pdf file. Based on an agreement with the supervisor, the final report and other material and documents may be given to the supervisor in digital format.

- Work to be done in lab (Water power lab, Fluids engineering lab, Thermal engineering lab)  
 Field work

Department of Energy and Process Engineering, 1. February 2013

  
\_\_\_\_\_  
Olav Bolland  
Department Head

  
\_\_\_\_\_  
Anders H. Strømman  
Academic Supervisor

## **Comment to master thesis description**

In agreement with supervisor and co-supervisor, a slight change in the object of the master thesis has been done. It has been decided to perform a comparative life cycle analysis on different PV technologies rather than conducting a detailed analysis on thin film alone. The scope has been broadened to include multicrystalline silicon PV technology in order to assess the relative competitiveness with thin film PV technology in terms of environmental impact. Life cycle inventories should be collected and harmonized. In addition, it has been decided to perform a sensitivity analysis on selected parameters and compare the results with existing renewable energy technology, in this case wind power. The main focus of the sensitivity analysis will be on climate change (GWP). Future implications and possible improvements of the PV value chain should be discussed.



## Preface

This is the preface of the report "A Comparative Life Cycle Assessment of PV Solar Systems" written during the spring of 2013, as part of my master degree in "Science and Technology - Energy and Environment" at the Norwegian University of Science and Technology (NTNU) in Trondheim, Norway. I have learnt a lot from working with this master thesis and have gained interesting insight in the infinite field of photovoltaics.

I would like to thank all the people who have shared their valuable knowledge with me: First, I would like to thank my supervisor Anders Hammer Strømman for academic support and guidance during weekly meetings. Thank you for facilitating the working schedule to better suit my needs during this semester. A big thank you goes to my co-supervisor, Thomas Gibon, for having an open door at anytime, useful discussions and help with all of my questions. I would also like to thank Joe Bergesen for quick feedback on all my questions! Thank you to Jon Helge Lande and Marit Torp at Elkem in Kristiansand for clarifying information on the Elkem Solar Silicon production process, Anders Arvesen for help on GWP values from wind power, Turid Worren Reenaas and Marika Edoff for thin film information, Linda Ager-Wick Ellingsen for excel-help!

This past year has posed unexpected challenges. I would not have been able to get through it without some very special people around me:

I would like to thank my classmates at the program of Energy and Environment; you know who you are! Thank you for all the laughter and jokes during lunches and dinners, keeping the spirit up! Thank you for all the fun times and hard work we have shared together through five amazing years in Trondheim! I would also like to thank all of the wonderful people in NTNUI Swing and folkedans; for giving me something else than school to think about and sharing my love for dance.

A special thank you goes to my good friends Eline Rangøy and Astrid Eikill for all the support, love and encouragement during some rough periods, giving me the motivation to keep up my work. Thank you for being so understanding!

Finally, I would like to thank my loving family, especially my mother, Anne-Grete Ruud Bekkelund, for continuously supporting me through good and bad times, and for always believing in me.

Kristine Bekkelund  
Trondheim, August 2013





## Abstract

In this report, a comparative life cycle assessment (LCA) of a rooftop, grid-connected photovoltaic (PV) system has been conducted. The primary objective has been to assess the environmental impacts resulting from the PV system over its entire lifetime, while the secondary goal has been to perform a sensitivity analysis on selected parameters and compare the results with the impacts from wind power. Four different cases have been assessed: Mc-Si Sim, mc-Si ESS, CdTe and CIGS. The difference between the multicrystalline silicon (mc-Si) cases were the production method for solar grade silicon: One case used the most common, chemical method; the modified Siemens process (mc-Si Sim), while the other case used the metallurgical route developed by Elkem Solar (mc-Si ESS).

With a few minor exceptions, mc-Si Sim gave the highest environmental impacts, including the global warming impacts (GWP). The thin film technologies, CdTe and CIGS, had significantly lower impact potentials than the mc-Si cases, while the difference between the two were small. The relative contribution from processes to the impacts scores were different within each case investigated: The energy intensive steps for silicon purification were large contributors in the mc-Si cases, in addition to the PV module manufacturing, which was the dominating contributor in the thin film cases. In all cases, the metal depletion potential was dominated by the inverter and cabling components, due to their use of metals like copper and tin. Metallization pastes used in the mc-Si solar cell production contributed to toxicity potentials. Contributions from other processes in the PV value chains were less significant. The GWP-scores in kg CO<sub>2</sub>-eq./m<sup>2</sup> of PV system were found to be 260 for mc-Si Sim, 155 for mc-Si ESS, 75 for CdTe and 86 for CIGS. Main contributors were the energy feed stock used in the solar grade silicon production (mc-Si cases), and the primary aluminium and glass used in manufacturing of the PV module (all cases). A base case was used for comparison with existing LCA studies, giving corresponding GWP-scores of 42,5, 30,8, 16,8 and 20,6 g CO<sub>2</sub>-eq./kWh, which are within the range of published values.

The current thin film technologies are already competitive with wind power in terms of GWP. By performing different combinations of improvement measures, all cases, except mc-Si Sim, could achieve GWPs as low as 5,1-5,8 g CO<sub>2</sub>-eq./kWh (below the minimum value of wind power). Switching the electricity supply towards a higher share of renewable energy and improving in the conversion efficiencies will have a significant effect in reducing the GWP. To improve the material efficiency, manufacturing waste should be reduced and recycled, and the solar cells should be made thinner. The silicon purification methods need to be made more energy efficient by e.g. implementing energy recovery, using biogenic carbon sources as reduction agents or switch from using the modified Siemens method to using more energy efficient methods like the Elkem Solar Silicon production process or the Fluidized Bed Reactor process. Recycled aluminium or steel should be used for the frame of the PV module and the mounting structure. End-of-life PV modules should be recycled to reduce the demand for primary material, e.g. aluminium, glass and rare metals.



## Sammendrag

I denne rapporten har det blitt gjennomført en sammenlignende livssyklusanalyse (LCA) av et solcellepanel, som er montert på tak og koblet til strømmettet. Hovedmålet har vært å vurdere miljøpåvirkningene fra solcellepanelet over hele livsløpet, mens det sekundære målet har vært å gjennomføre en sensitivitetsanalyse på utvalgte parametere og sammenligne resultatene med miljøpåvirkningene fra vindkraft. Fire ulike alternativer ble undersøkt: Mc-Si Sim, mc-Si ESS, CdTe og CIGS. Forskjellen mellom de multikrystallinske silisium (mc-Si) alternativene var metoden som ble bruk til å produsere superrent silisium: Et alternativ brukte den mest vanlige, kjemiske metoden; den modifiserte Siemens-prosessen (mc-Si Sim), mens det andre alternativet brukte en metallurgisk metode utviklet av Elkem Solar (mc-Si ESS).

Potensialet for miljøpåvirkninger var med få unntak høyest for mc-Si Sim, inkludert global oppvarming (GWP). Tynnfilmteknologiene, CdTe og CIGS, hadde signifikant lavere potensialer for miljøpåvirkning enn mc-Si tilfellene, mens forskjellen mellom de to var små. Det relative bidraget fra ulike prosesser til potensialene for miljøpåvirkning var ulikt innenfor hvert enkelt alternativ: Den energikrevende stegene for rensing av silisium var de største bidragsyterne i mc-Si-tilfellene, i tillegg til modulproduksjonen, som var den dominerende bidragsyteren i tynnfilm-tilfellene. I alle tilfellene dominerte komponenter til inverter og kabler potensialet for mineraluttømming pga. bruken av metaller som kopper og tinn. Bruk av metalliseringspasta i produksjonen av mc-Si solceller bidro til toksisitetspotensialene. Bidraget fra andre prosesser i verdikjeden var av mindre betydning. GWP verdiene i kg CO<sub>2</sub>-ekv./m<sup>2</sup> solcellepanel ble beregnet til å være 260 for mc-Si Sim, 155 for mc-Si ESS, 75 for CdTe og 86 for CIGS. De største bidragsyterne var knyttet til energikildene som brukes i produksjonen av superrent silisium, og aluminium og glass som brukes i solcellemodulen. Det ble brukt et referansescenario for sammenlikning med eksisterende LCA studier, noe som ga tilhørende GWP-verdier lik 42,5, 30,8, 16,8 og 20,6 g CO<sub>2</sub>-ekv./kWh. Dette er innenfor verdiområdet som er publisert i andre studier.

De eksisterende tynnfilmteknologiene er allerede konkurransedyktige med vindkraft når det gjelder GWP. Ved å utføre ulike kombinasjoner av forbedringstiltak kunne alle alternativer, untatt mc-Si Sim, oppnå så lav GWP som 5,1-5,8 g CO<sub>2</sub>-ekv./kWh (under minimum verdien for vindkraft). Å vri energiforsyningen mot en høyere andel av fornybar energi og å forbedre virkningsgraden til solcellemodulen vil ha en betydelig effekt for å redusere GWP. For å forbedre materialeeffektiviteten, bør produksjonsavfall reduseres og resirkuleres, og solcellene bør gjøres tynnere. Rensemetodene for silisium bør bli mer energieffektive ved å f.eks. implementere energigjenvinning, bruke biogene karbonkilder som reduksjonsmiddel eller bytte fra å bruke den modifiserte Siemens prosessen til å bruke mer energieffektive metoder som den metallurgiske prosessen utviklet av Elkem Solar eller "Fluidized Bed Reactor" prosessen. Resirkulert aluminium eller stål bør brukes i rammen til solcellemodulen og i monteringskonstruksjonen for solcellepanelet. Kasserte solcellemoduler bør gjenvinnnes

for å redusere etterspørselen etter primære materiale, f.eks aluminium, glass og sjeldne metaller.

## Table of contents

1	Introduction .....	1
1.1	Background .....	1
1.2	LCA and existing studies .....	2
1.3	Objective and outline of the report.....	3
2	Current status and future prospective of the PV technology.....	5
2.1	Production of solar cells/PV modules .....	5
2.2	Technology mix.....	6
2.3	Installed capacity .....	8
2.4	Future prospects - scenarios and roadmaps .....	10
3	PV theory.....	13
3.1	How a solar cell works .....	13
3.2	Important characteristics for the PV system performance.....	15
3.2.1	Conversion efficiency .....	15
3.2.2	Performance ratio .....	16
3.2.3	Lifetime.....	18
3.2.4	Direct normal irradiation.....	18
3.2.5	Lifetime electricity generation .....	18
4	Life cycle assessment methodology.....	19
4.1	Concept.....	19
4.2	Goal and scope definition.....	20
4.3	Life cycle inventory analysis .....	21
4.4	Life cycle impact assessment.....	22
4.4.1	Selection of impact categories, category indicators and characterization models .....	22
4.4.2	Classification.....	22
4.4.3	Characterization .....	22
4.4.4	Normalization .....	23
4.4.5	Grouping.....	23
4.4.6	Weighting .....	23
4.5	Interpretation .....	23

4.6	Mathematical background .....	24
4.6.1	Direct and indirect emissions .....	24
4.6.2	The open Leontief model .....	24
4.6.3	Basic contribution analysis .....	25
4.6.4	The foreground and background system .....	27
4.6.5	Advanced contribution analysis .....	28
4.6.6	Multiple outputs and allocation methods .....	29
5	System description.....	31
5.1	Goal and scope of the study .....	31
5.2	Functional unit.....	32
5.3	System boundaries .....	32
5.3.1	Foreground system.....	32
5.3.2	Background system .....	35
5.4	Characterization method and categories for impact assessment.....	36
5.4.1	Characterization and impact categories .....	36
5.4.2	Cultural perspective .....	37
5.4.3	Software .....	37
6	Multicrystalline silicon PV production value chain .....	39
6.1	Metallurgical grade silicon.....	39
6.2	Solar grade silicon.....	41
6.2.1	Elkem Solar Silicon production process .....	41
6.2.2	Modified Siemens process .....	43
6.2.3	Union Carbide process .....	44
6.2.4	Fluidized Bed Reactor process .....	45
6.3	Ingot.....	47
6.4	Wafer .....	49
6.5	Multicrystalline silicon solar cell.....	50
6.6	Multicrystalline silicon PV module .....	55
7	Thin film PV .....	56
7.1	Configuration and structure of thin film solar cells.....	56
7.2	Advantages .....	58
7.3	Disadvantages.....	59

8	CdTe PV production value chain .....	62
8.1	Background .....	62
8.2	Substrate.....	63
8.3	Front electrical contact.....	63
8.4	Buffer layer .....	64
8.4.1	Chemical bath deposition.....	64
8.5	Absorber layer .....	65
8.5.1	Close-spaced sublimation.....	66
8.5.2	Electrodeposition .....	66
8.5.3	Sparry pyrolysis.....	67
8.5.4	Screen printing .....	68
8.5.5	Vapour transport deposition.....	68
8.5.6	Metal organic chemical vapour deposition.....	69
8.6	Cadmium chloride vapour treatment.....	70
8.7	Back electrical contact .....	70
8.8	CdTe solar cell and PV module .....	71
9	CIGS PV production value chain.....	74
9.1	Background .....	74
9.2	Substrate.....	75
9.3	Back electrical contact .....	76
9.4	Absorber layer .....	76
9.4.1	Co-evaporation processes .....	77
9.4.2	Selenization/sulfurization of precursor materials.....	79
9.5	Buffer layer .....	80
9.5.1	Alternative buffer materials .....	81
9.6	Sodium incorporation .....	81
9.7	Front electrical contact.....	82
9.8	CIGS solar cell and PV module .....	82
10	The rest of the PV production value chain.....	86
10.1	Balance of system .....	86
10.2	Rooftop PV system .....	86
11	Life cycle inventory.....	88

11.1	Collection of inventories.....	88
11.1.1	Case 1: Mc-Si Sim .....	88
11.1.2	Case 2: Mc-Si ESS.....	89
11.1.3	Case 3: CdTe .....	90
11.1.4	Case 4: CIGS.....	90
11.1.5	Overview.....	91
11.2	Yield ratios .....	92
12	Results and analysis.....	94
12.1	Relative performance .....	94
12.2	Advanced contribution analysis .....	96
12.2.1	Case 1: Mc-Si Sim .....	96
12.2.2	Mc-Si ESS .....	99
12.2.3	Case 3: CdTe .....	103
12.2.4	Case 4: CIGS.....	104
12.3	Sensitivity analysis .....	107
12.3.1	Conversion efficiency .....	109
12.3.2	Performance ratio .....	110
12.3.3	Lifetime.....	111
12.3.4	Direct normal irradiation.....	112
12.3.5	Lifetime electricity generation .....	113
12.3.6	Electricity mix .....	115
12.3.7	Energy efficiency (electricity) .....	117
12.3.8	Material efficiency.....	118
12.3.9	Overall performance envelopes.....	120
13	Discussion and conclusion.....	124
13.1	Objective completeness .....	124
13.2	Result robustness .....	126
13.2.1	Quality of analysis .....	126
13.2.2	Benchmarking.....	131
13.3	Insights and implications .....	139
13.4	Conclusion .....	143
	References.....	145



Appendices .....	167
A Inventory MG-Si .....	167
A.1 Mc-Si Sim.....	167
B Inventory SoG-Si.....	168
B.1 Mc-Si Sim.....	168
B.2 Mc-Si ESS.....	169
C Inventory ingot.....	173
C.1 Mc-Si Sim.....	173
D Inventory mc-Si wafer .....	174
D.1 Mc-Si Sim.....	174
D.2 Mc-Si ESS.....	174
E Inventory solar cell .....	178
E.1 Mc-Si Sim.....	178
E.2 Mc-Si ESS.....	179
E.3 CIGS .....	182
F Inventory PV module.....	188
F.1 Mc-Si Sim.....	188
F.2 Mc-Si ESS.....	189
F.3 CdTe .....	192
F.4 CIGS .....	197
G Inventory mounting structure .....	202
G.1 Mc-Si Sim.....	202
G.2 Mc-Si ESS.....	202
G.3 CdTe and CIGS .....	203
H Inventory inverter and cabling .....	204
H.1 Mc-Si Sim.....	204
H.2 Mc-Si ESS.....	204
H.3 CdTe and CIGS .....	205
I Inventory rooftop PV-system .....	207
I.1 Mc-Si Sim.....	207
I.2 Mc-Si ESS.....	207
I.3 CdTe .....	208

I.4	CIGS .....	209
J	Overview of existing LCA studies .....	210
J.1	Mc-Si PV systems .....	210
J.2	CdTe PV systems .....	211
J.3	CIGS PV systems.....	212

## List of figures

Figure 2.1: Global annual PV cell/module production, 2000-2011 (Jäger-Waldau, 2012, edited for readability).....	5
Figure 2.2: Overview of PV cell technologies (Raugei et al., 2007b, edited for readability). ....	6
Figure 2.3: Market share of PV cell technologies, 1999-2011 (de Wild-Scholten, 2011; *modified to include numbers for the year 2011 from Fraunhofer ISE (2012))......	7
Figure 2.4: Global annual installed PV capacity, 2000-2012 (based on numbers from EPIA (2013)). Note that ROW-numbers for 2012 are directly integrated into relevant regions. ROW: Rest of the world. MEA: Middle East and Africa. APAC: Asia Pacific.....	8
Figure 2.5: Cumulative installed PV capacity, 2000-2012 (based on numbers from EPIA (2013)). ROW: Rest of the world. MEA: Middle East and Africa. APAC: Asia Pacific. ....	9
Figure 2.6: Conversion efficiency targets for commercial PV modules, from IEA roadmap on PV technology (IEA, 2010). ....	12
Figure 3.1: Basic operation of a solar cell (Malm, 2008). The solar cell is illuminated with solar irradiation ( $h\nu$ ), which excites electrons (negative) across the bandgap of the semiconductor, leaving holes (positive) behind in the valence band. ( $E_v$ = energy of valence band [eV], $E_g$ = bandgap energy [eV], $E_c$ = energy of the conduction band [eV]. $I$ = current [A], $V$ = voltage [V]). ....	15
Figure 3.2: The I-V characteristics of a solar cell with the maximum power point (constructed based on information from Markvart (2000)). $P_{max}$ = maximum power output produced by the solar cell [W], $I_m$ = current at maximum power output [A], $V_m$ = voltage at maximum power output [V], $I_{sc}$ = short circuit current [A], $V_{oc}$ = open circuit voltage [V].....	17
Figure 4.1: : The main steps of conducting an LCA (ISO, 2006a, edited for readability). ....	20
Figure 5.1: Mc-Si PV system - Flowchart for the foreground system in the mc-Si Sim-case and mc-Si ESS-case. ....	33
Figure 5.2: Thin film PV system - Flowchart for the foreground system in the CdTe-case and the CIGS-case.....	35
Figure 6.1: Principle sketch of metallurgical silicon production (Rosenkilde, 2012, edited for readability). ....	40
Figure 6.2: Schematic view of Elkem Solar Silicon production process, where production of MG-Si and SoG-Si happens in an integrated process (ABB, 2012). MG-Si is produced and then purified to yield SoG-Si. ....	42
Figure 6.3: Schematic representation of the Siemens bell-jar reactor for SoG-Si production ..	44
Figure 6.4: Schematic representation of a fluidized bed reactor for SoG-Si production.....	46
Figure 6.5: SoG-Si in form of Siemens chunks (left) and FBR granules (right) (REC, 2011b). ..	47
Figure 6.6: Multicrystalline ingot production using the Bridgeman technology (Luque & Hegedus, 2011, edited for readability). ....	48
Figure 6.7: Multicrystalline ingot production using the block-casting process technology (Luque & Hegedus, 2011, edited for readability).....	48

Figure 6.8: Principle sketch of multi wire sawing (Luque & Hegedus, 2011, edited for readability). .....	49
Figure 6.9: Multicrystalline silicon wafer (Rosenkilde, 2012). .....	50
Figure 6.10: Open tube quartz diffusion furnace for phosphorus diffusion (during p-n junction formation in the mc-Si solar cell production) (Luque & Hegedus, 2011, edited for readability). .....	51
Figure 6.11: Conveyor belt furnace for phosphorus diffusion (during p-n junction formation in the mc-Si solar cell production) (Luque & Hegedus, 2011, edited for readability). .....	52
Figure 6.12: Screen printing for electrical contacts during mc-Si solar cell production (Luque and Hegedus, 2011, edited for readability). .....	53
Figure 6.13: Atmospheric pressure chemical vapour deposition system for the deposition of antireflective coating onto the front surfaces of the mc-Si solar cells (Markvart, 2000, edited for readability). .....	54
Figure 6.14: Multicrystalline silicon solar cell (front) (Khan, 2009). .....	55
Figure 7.1: Schematic cross-section of superstrate configuration (left) and substrate configuration (right) for thin film solar cells (Romeo et al., 2004). .....	57
Figure 8.1: Chemical structure of CdTe (Biccari, 2012a, edited for readability). .....	62
Figure 8.2: Schematic illustration of close-spaced sublimation of the CdTe absorber layer (Luque & Hegedus, 2011). The substrate is the cross-lined rectangle. Film thickness $d$ and growth rate are shown at the bottom of the figure. ....	66
Figure 8.3: Schematic illustration of electrodeposition of the CdTe absorber layer (Luque & Hegedus, 2011). The substrate is the cross-lined rectangle. Film thickness $d$ and growth rate are shown at the bottom of the figure. ....	67
Figure 8.4: Schematic illustration of spray pyrolysis of the CdTe absorber layer (Luque & Hegedus, 2011). The substrate is the cross-lined rectangle. Film thickness $d$ and growth rate are shown at the bottom of the figure. ....	67
Figure 8.5: Schematic illustration of screen printing of the CdTe absorber layer (Luque & Hegedus, 2011). The substrate is the cross-lined rectangle. Film thickness $d$ is shown at the bottom of the figure. ....	68
Figure 8.6: Schematic illustration of vapour transport deposition of the CdTe absorber layer (Luque & Hegedus, 2011). The substrate is the cross-lined rectangle. Film thickness $d$ and growth rate are shown at the bottom of the figure. ....	69
Figure 8.7: Schematic illustration of metal organic chemical vapour deposition of the CdTe absorber layer (Luque & Hegedus, 2011). The substrate is the cross-lined rectangle. Film thickness $d$ and growth rate are shown at the bottom of the figure. ....	69
Figure 8.8: Patterning scheme for monolithic cell interconnections in an integrated CdTe PV module (Bosio et al, 2011, edited for readability). P1 is performed by laser scribing, while P2 and P3 are usually performed by mechanically scribing. ....	72
Figure 8.9: Cross-section of a finished CdTe PV module in superstrate configuration (standard structure). Note that a layer of antireflective coating may be applied to the front surface of the substrate facing the incident light. ....	73

Figure 9.1: Tetragonal crystal structure of CIS (Biccari, 2012b, edited for readability).....	74
Figure 9.2: Illustration of an in-line deposition system for co-evaporation of CIGS absorber layer from line-sources (McEvoy et al, 2012). .....	78
Figure 9.3: Diagrams representing the recipes in the co-evaporation methods used for deposition of the CIGS absorber layer (Razykov et al., 2011, edited for readability). The methods are defined according to the variation in the copper (Cu) content.....	79
Figure 9.4: Illustration of the selenization of precursors materials for deposition of the CIGS absorber layer (McEvoy et al, 2012). The process happens in two steps: A stack of metal (Cu, In, Ga) layers are deposited by e.g. sputtering, thermal evaporation or electrodeposition, before the stack is selenized in H <sub>2</sub> Se atmosphere and converted into CIGS.....	80
Figure 9.5: Deposition and patterning sequence to obtain a monolithically integrated CIGS PV module (McEvoy et al., 2012, edited for readability). The window layer refers to the front contact.....	83
Figure 9.6: Patterning scheme for monolithic cell interconnections in an integrated CIGS module (Kushiya et al., 2009, edited for readability). P1 is performed by laser scribing, while P2 and P3 usually are performed by mechanically scribing.....	84
Figure 9.7: Cross-section of a finished CIGS PV module in substrate configuration (standard structure). Note that a layer of antireflective coating (e.g. EVA) may be applied to the front surface of the low iron cover glass facing the incident light. ....	85
Figure 10.1: Illustration showing the difference between a solar cell, a PV module and a PV array (U.S. Department of Energy, 2012c). .....	87
Figure 12.1: Relative performance of PV technologies (UCTE el mix). Impact scores normalized to highest impact score across the different PV technologies. The aggregated impact value for the case with the highest score is given per m <sup>2</sup> of PV system. (For abbreviations see Table 5.1).7 .....	95
Figure 12.2: Mc-Si Sim, UCTE el mix. Relative contribution from foreground processes to impact categories normalized to highest impact score across the different PV technologies. Aggregated impact results per m <sup>2</sup> PV system. (For abbreviations see Table 5.1). .....	97
Figure 12.3: Mc-Si ESS, UCTE el mix. Relative contribution from foreground processes to impact categories normalized to highest impact score across the different PV technologies. Aggregated impact results per m <sup>2</sup> of PV system. (For abbreviations see Table 5.1).....	100
Figure 12.4: CdTe, UCTE el mix. Relative contribution from foreground processes to impact categories normalized to highest impact score across the different PV technologies. Aggregated impact results per m <sup>2</sup> of PV system. (For abbreviations see Table 5.1).....	103
Figure 12.5: CIGS, UCTE el mix. Relative contribution from foreground processes to impact categories normalized to highest impact score across the different PV technologies. Aggregated impact results per m <sup>2</sup> of PV system. (For abbreviations see Table 5.1). The graph has been cut off at 60% normalized contribution, and the MDP has in reality a normalized contribution of 84%.....	105
Figure 12.6: GWP [g CO <sub>2</sub> -eq./kWh] related to change in PV module conversion efficiency. GWP values for wind power included for comparison (windband).....	109

Figure 12.7: GWP [g CO <sub>2</sub> -eq./kWh] related to change in performance ratio of the PV system. GWP values for wind power included for comparison (windband).....	110
Figure 12.8: GWP [g CO <sub>2</sub> -eq./kWh] related to change in lifetime of the PV system. GWP values for wind power included for comparison (windband).....	111
Figure 12.9: GWP [g CO <sub>2</sub> -eq./kWh] related to change in the direct normal irradiation. GWP values for wind power included for comparison (windband).....	112
Figure 12.10: GWP [g CO <sub>2</sub> -eq./kWh] related to change in the ratio of electricity generation relative to base case. GWP values for wind power included for comparison (windband)....	114
Figure 12.11: GWP [g CO <sub>2</sub> -eq./kWh] related to change in electricity supply mix (marked off on figure). GWP values for wind power included for comparison (windband). ....	116
Figure 12.12: GWP [g CO <sub>2</sub> -eq./kWh] related to improvements in energy efficiency (electricity). GWP values for wind power included for comparison (windband). ....	117
Figure 12.13: GWP, HTP, MDP, PMFP and POFP related to improvements in material efficiency, measured per kWh electricity produced by the PV system. Impact values for natural gas without CSS and for wind power included for comparison (windband).....	119
Figure 12.14: Overall performance envelopes for GWP values. Worst case scenario: Coal power, no improvements. Best case scenario: Hydropower, 20% improved energy efficiency, 10% improved material efficiency. Dark line: Base case scenario, UCTE electricity mix, no improvements. ....	121

## List of tables

Table 5.1: Midpoint categories in the ReCiPe characterization model (Goedkoop et al., 2012). .....	36
Table 8.1: Methods for CdTe film deposition (Razykov et al., 2011). .....	65
Table 9.1: Methods for CIGS film deposition (Razykov et al., 2011).....	77
Table 6.1: Data sources for the life cycle inventories used in this study.....	92
Table 6.2: Overview of data sources used in this study and in which appendices the LCIs can be found. ....	92
Table 6.3: Yield ratios for foreground processes in the two mc-Si cases. ....	93
Table 12.1: Overview of parameters for the base case scenario.....	108
Table 12.2: Choice for x-value limits - ratio of lifetime electricity generation relative to base case.....	113
Table A: Inventory for MG-Si production, mc-Si Sim-case. ....	167
Table B: Inventory for SoG-Si production by using the modified Siemens method, mc-Si Sim- case.....	168
Table C: Inventory for SoG-Si production by using the metallurgical production method by Elkem Solar, mc-Si ESS-case. ....	169
Table D: Inventory for mc-Si ingot growing, mc-Si Sim-case. ....	173
Table E: Inventory for mc-Si wafer production, mc-Si Sim-case.....	174
Table F: Inventory for mc-Si wafer production (including wafer growing), mc-Si ESS-case..	174
Table G: Inventory for mc-Si solar cell production, mc-Si Sim-case. ....	178
Table H: Inventory for mc-Si solar cell production, mc-Si ESS-case.....	179
Table I: Inventory for deposition of back contact in solar cell, CIGS-case. "UNEP" refers to number from Gibon et al. (forthcoming), while "ESU" refers to numbers from Jungbluth et al. (2012), p. 86. ....	182
Table J: Inventory for deposition of absorber layer in solar cell, CIGS-case. "UNEP" refers to number from Gibon et al. (forthcoming), while "ESU" refers to numbers from Jungbluth et al. (2012), p.86. ....	183
Table K: Inventory for deposition of buffer layer in solar cell, CIGS-case. "UNEP" refers to number from Gibon et al. (forthcoming), while "ESU" refers to numbers from Jungbluth et al. (2012), p.86. ....	184
Table L: Inventory for deposition of front contact in solar cell, CIGS-case. "UNEP" refers to number from Gibon et al. (forthcoming), while "ESU" refers to numbers from Jungbluth et al. (2012), p.86. ....	185
Table M: Inventory for bus bar attach to solar cell, CIGS-case. "UNEP" refers to number from Gibon et al. (forthcoming), while "ESU" refers to numbers from Jungbluth et al. (2012), p.86. .....	185

Table N: Inventory for scribing of solar cells for cell interconnection, CIGS-case. "UNEP" refers to number from Gibon et al. (forthcoming), while "ESU" refers to numbers from Jungbluth et al. (2012), p.86. ....	186
Table O: Inventory for test of solar cell performance, CIGS-case. "UNEP" refers to number from Gibon et al. (forthcoming), while "ESU" refers to numbers from Jungbluth et al. (2012), p.86.....	187
Table P: Inventory for mc-Si PV module manufacturing, mc-Si Sim-case.....	188
Table Q: Inventory for mc-Si PV module manufacturing, mc-Si ESS-case. ....	189
Table R: Inventory for CdTe PV module manufacturing, CdTe-case. "UNEP" refers to number from Gibon et al. (forthcoming), while "ESU" refers to numbers from Jungbluth et al. (2012), p. 79-80.....	192
Table S: Inventory for CIGS PV module manufacturing, CIGS-case. "UNEP" refers to number from Gibon et al. (forthcoming), while "ESU" refers to numbers from Jungbluth et al. (2012), p.86.....	197
Table T: Inventory for on-roof mounting structure, mc-Si Sim-case. ....	202
Table U: Inventory for on-roof mounting structure, mc-Si ESS-case. ....	202
Table V: Inventory for on-roof mounting structure, CdTe-case and CIGS-case. "UNEP" refers to number from Gibon et al. (forthcoming), while "ESU" refers to numbers from Alsema et al. (2006) and de Wild-Scholten et al. (2006). ....	203
Table W: Inventory for inverter and cabling, mc-Si Sim-case. ....	204
Table X: Inventory for inverter, mc-Si ESS-case. ....	204
Table Y: Inventory for cabling, mc-Si ESS-case.....	205
Table Z: Inventory for inverter, CdTe-case and CIGS-case. "UNEP" refers to number from Gibon et al. (forthcoming), while "ESU" refers to numbers from Alsema et al. (2006) and de Wild-Scholten et al. (2006).....	205
Table AA: Inventory for cabling, CdTe-case and CIGS-case. "UNEP" refers to number from Gibon et al. (forthcoming), while "ESU" refers to numbers from Alsema et al. (2006) and de Wild-Scholten et al. (2006).....	206
Table BB: Inventory for complete rooftop mc-Si PV system, mc-Si Sim-case.....	207
Table CC: Inventory for complete rooftop mc-Si PV system, mc-Si ESS-case.....	207
Table DD: Inventory for complete rooftop CdTe PV system, CdTe-case. "UNEP" refers to number from Gibon et al. (forthcoming), while "ESU" refers to numbers from Alsema et al. (2006) and de Wild-Scholten et al. (2006). ....	208
Table EE: Inventory for complete rooftop CIGS PV system, CIGS-case. "UNEP" refers to number from Gibon et al. (forthcoming), while "ESU" refers to numbers from Alsema et al. (2006) and de Wild-Scholten et al. (2006). ....	209
Table FF: Overview of recent LCAs assessing the GWP of rooftop and ground mounted mc-Si PV systems.....	210
Table GG: Overview of recent LCAs assessing the GWP of rooftop and ground mounted CdTe PV systems.....	211



Table HH: Overview of recent LCAs assessing the GWP of rooftop and ground mounted CIGS PV systems..... 212



## List of abbreviations

2DS	2°C scenario
AC	Alternate current
AM	Air mass
APAC	Asia Pacific
APCVD	Atmospheric pressure chemical vapour deposition
ARC	Anti-reflective coating
a-Si	Amorphous silicon
AZO	Aluminium-doped zinc oxide
BIPV	Building Integrated Photovoltaic
BOS	Balance of system
BZO	Boron-doped zinc oxide
CAT	Centre for Alternative Energy (Britain)
CBD	Chemical bath deposition
CCS	Carbon capture and storage
CdTe	Cadmium telluride
CGS	Copper gallium diselenide
CIGS	Copper indium gallium diselenide
CIS	Copper indium diselenide
c-Si	Crystalline silicon
CSS	Closed-spaced sublimation
CTO	Cadmium stannate
CVD	Chemical vapour deposition
DC	Direct current
DNI	Direct normal irradiation

DSSC	Dye-sensitised solar cells
ECN	Energy Research Centre of the Netherlands
ED	Electrodeposition
EPBT	Energy payback time
EPIA	European Photovoltaic Industry Association
eq.	Equivalents
ESS	Elkem Solar Silicon production process
EVA	Ethylene vinyl acetate
FBR	Fluidized Bed Reactor process
FTO	Fluorine-doped tin oxide ( $\text{SnO}_2:\text{F}$ )
FU	Functional unit
GHG	Greenhouse gases
GWP	Global warming potential
HVE	High-vacuum evaporation
IEA	International Energy Agency
IPCC	Intergovernmental Panel on Climate Change
ISO	International Organization for Standardization
ITO	Tin-doped indium oxide ( $\text{In}_2\text{O}_3:\text{Sn}$ )
Klif	Climate and Pollution Agency of Norway
LCA	Life cycle assessment
LCI	Life cycle inventory
LCIA	Life cycle impact assessment
mc-Si	Multicrystalline silicon
MEA	Middle East and Africa
MG-Si	Metallurgical grade silicon
MOCVD	Metal-organic chemical vapour deposition

NMVOC	Non-methane volatile organic compounds
NREL	National Renewable Energy Laboratory
OECD	Organisation of Economic Co-operation and Development
OPV	Organic photovoltaics
PEG	Polyethylene glycol
PEN	Polyethylene naphthalate
PET	Polyethylene terephthalate
PI	Polyimide
PV	Photovoltaic
QDSC	Quantum dot solar cells
REC	Renewable Energy Corporation
REN21	Renewable Energy Policy Network for the 21st century
ROW	Rest of the world
SAS	Sulfidization after selenization scheme
sc-Si	Single crystalline silicon
SENSE	Sustainability Evaluation of Solar Energy Systems
SLG	Soda-lime glass
SoG-Si	Solar grade silicon
SOLTECTURE	Solar Construction Sustainability Technology
SP	Screen printing
SS	Stainless steel
SSB	Statistics Norway
STC	Tetrachlorosilane
TCO	Transparent conducting oxide
TCS	Trichlorosilane

UCTE	Average European electricity mix (Union for the Coordination of Transmission of Electricity)
UNEP	United Nations Environment Programme
VTD	Vapour transport deposition
ZTO	Zinc stannate

# 1 Introduction

## 1.1 Background

Environmental concerns are gaining increased importance as the world's population continues to grow, putting heavy pressure on the Earth's resources. Climate change due to increased global warming is an especially important environmental issue. An increase in the global average temperature will have significant, adverse impacts both on humans, ecosystems and nature, e.g. leading to more extreme weather, ocean acidification, extinction of species, drought, desertification, melting of glaciers and rising global average sea level.

The demand for energy is increasing, particularly as developing countries pursue industrialization. The energy mix used to cover this increasing demand has a large influence on climate change. Today, most of the energy supplied globally comes from fossil fuels, leading to emissions of greenhouse gasses (GHG) like carbon dioxide (CO<sub>2</sub>), further enhancing the global warming. According to the fourth assessment report from the United Nations Intergovernmental Panel on Climate Change (IPCC), "*Most of the observed increase in global average temperatures since the mid-20th century is **very likely** due to the observed increase in anthropogenic GHG concentrations*" (IPCC, 2007). To limit the long-term increase in global average temperature to 2,0-2,4°C, it is necessary to reduce the global CO<sub>2</sub>-emissions with 50-80% within 2050 (compared to the levels in 2000) (IPCC, 2007).

Looking at the total change from 1970 to 2004, global GHG emissions due to human activities grew with 70%, while the annual carbon dioxide emissions grew by about 80% (IPCC, 2007). Due to slow processes and feedback mechanisms in nature, the impacts caused by GHG emissions may become even larger than what is projected. This calls for serious action, using both climate mitigation and adoption strategies. An increased use of renewable energy technologies, substituting the fossil energy sources, is considered to be a necessary and important part of the solution if the global warming challenge is to be tackled. In addition, the fossil energy sources are being depleted and other energy sources need to replace them when this time comes.

The utilization of solar energy is expected to increase in the next years. The sun offers an infinitely large amount of energy, and sunlight can be directly converted into electricity by using photovoltaic (PV) systems. The use of PV technology for energy production is considered to be one of the more promising renewable energy technologies, having the potential to contribute significantly to a sustainable energy supply and help mitigate GHG emissions (Sumper et al., 2011). Originally, PV technology was developed for space applications in the 1950s. In the wake of the oil crisis in the early 1970s, PV technology gained increasing interest and has since experienced an exponential growth (Markvart, 2000). Today, PV systems are the third most important renewable energy source after

hydropower and wind power in terms of installed capacity (European Photovoltaic Industry Association (EPIA), 2013).

Multiple interconnected PV cells of semiconducting materials make up a PV module, which converts solar light photons into electricity. When incident sunlight hit the modules, electrons are triggered by photons with a certain wavelength to flow through the materials and direct current (DC) electricity is produced (Sumper et al., 2011). PV modules can be mounted on roofs of buildings, integrated in building facades or assembled into large power plants (ground mounted). A typical PV system consist of one or several PV modules connected together in an array and the balance of system (BOS). The BOS includes the mounting structure of the PV module and the power-conditioning equipment for converting the generated DC current to alternate current (AC) with the proper form and magnitude required by the power grid (Sumper et al., 2011). The majority of PV modules are today used for grid-connected power generation. However, in remote areas and developing countries, PV modules may be used for off-grid power generation (European Commission, 2012b). Current commercial PV technologies are crystalline silicon technology (dominating) and thin film technologies. Multicrystalline silicon (mc-Si) PV technology currently accounts for about 45% of the global PV production. However, thin film technologies is considered to be an important option for present and future low cost PV modules (Filippidou et al., 2010).

## 1.2 LCA and existing studies

Traditional environmental impact analysis have generally focused on a restricted number of life cycle steps (Sumper et al., 2011). This is a narrow approach because it gives a limited picture of the environmental impacts from a product. In the case of renewable energy systems, the largest environmental impacts occur during the production and installation steps (Sumper et al., 2011).

Life cycle assessment (LCA) is a tool for assessing the environmental impacts of a product or product system over its entire life cycle. This involves quantifying the inputs of material and energy, and the output of pollutants and waste during the life cycle stages of the system studied, all the way from raw material/resource extraction to end-of-life management. Both direct and indirect impacts generated by the product system are accounted for. The LCA approach gives the possibility to compare the environmental performance of different product systems performing the same function.

A number of detailed studies on LCA of PV systems have been published (see appendices J.1-J.3). The majority of these studies focus on global warming impacts (GWP) and energy-payback time (EPBT). Other environmental impacts are often not considered. Recent LCA studies on mc-Si PV technology give GWP values in the range of **18,0-72,4 g CO<sub>2</sub>-equivalents (eq.)/kWh** (Fthenakis & Alsema, 2006; Alsema et al., 2006; Pacca et al., 2007; Fthenakis & Kim, 2007; Stoppato, 2008; Fthenakis et al, 2008; Ito et al. 2008, Ito et al., 2009;



Ito et al., 2010; Filippidou et al., 2010; Dominguez-Ramos et al., 2010; de Wild-Scholten 2011; Westgaard et al., 2012; de Wild-Scholten & Gløckner, 2012). The available LCA literature on thin film PV technologies are of a smaller extent, especially for the CIGS technology. These technologies are not as mature as the mc-Si PV technology and have only been commercially produced for a few years. Recent LCA studies gives GWP values in the range of **15,5-66,0 g CO<sub>2</sub>-eq./kWh** for CdTe PV technology (Kato et al., 2001; Raugei et al., 2005; Fthenakis & Alsema, 2006; Fthenakis & Kim, 2007; Raugei et al., 2007a; SENSE, 2008; Fthenakis et al., 2008; Ito et al., 2008; Ito et al., 2009; de Wild-Scholten & Schottler, 2009; Ito et al., 2010; Filippidou et al., 2010; Dominguez-Ramos et al., 2010; Held & Ilg, 2011; de Wild-Scholten, 2011) and **20,5-95,0 g CO<sub>2</sub>-eq./kWh** for CIGS PV technology (Raugei et al., 2005; Raugei et al., 2007a; SENSE, 2008; Ito et al., 2008; de Wild-Scholten & Schottler, 2009; Ito et al., 2009; Ito et al., 2010; Dominguez-Ramos et al., 2010; Clarius, 2011; de Wild-Scholten 2011, Ito et al, 2011).

The high variability in the results makes it difficult to compare the published studies. There are several reasons for the large range in the GWP values. The different studies use different methods, with different system boundary conditions, rely on different data sources and inventory methods, model the PV technology at different locations, use different production processes to manufacture the PV system, use different electricity mix, and consider different lifetimes, conversion efficiencies and analytical periods (Pacca et al., 2007; Sumper et al., 2011). Since PV technology can be utilized in a range of applications, it is important to be aware of what type of PV system is analysed and if it is grid-connected or standalone.

### **1.3 Objective and outline of the report**

The primary objective of this report is to assess the environmental life cycle impacts of a rooftop, grid-connected PV solar system, without solar tracking, by performing a comparative LCA on four cases. Special weight will be put on the GWP. The cases investigated are mc-Si Sim, mc-Si ESS, CdTe and CIGS. The difference between the mc-Si cases are the solar grade silicon (SoG-Si) production methods. A metallurgical process route will be represented by the metallurgical upgrading process developed by Elkem Solar (mc-Si ESS), while a chemical process route will be represented by the modified Siemens process (mc-Si Sim), the most common SoG-Si production method today. The secondary objective will be to perform a sensitivity analysis on selected parameters. The results will be compared with the impacts (mainly GWP) of a wind power system. In addition, environmental issues and possible options on how to improve these will be identified.

First, an brief overview on PV technologies will be presented together with some key-numbers on the global production and installation of PV technology, to provide background information on the status of PV technology today. Future prospects for the PV technology will be presented in the same chapter. Theory on how a solar cell works and important parameters for the PV system performance will then be explained. The methodology of LCA

will be presented to give a reference to how the work has been conducted. The system description will present assumptions and choices made for the LCA study, before the PV value chains for the different technologies are presented in separate chapters. An overview on data collection will be given, defining the cases investigated in this report. The results from the LCA and sensitivity analysis will be investigated and explained in the result part. Finally, the results will be toughly discussed and compared with similar studies, giving a conclusion in compliance with the objective, wrapping up the report.

## 2 Current status and future prospective of the PV technology

This chapter will provide background information on the present status and future prospective of PV technology.

### 2.1 Production of solar cells/PV modules

The production of solar cells and PV systems has doubled every two year since 2002 (European Commission, 2012d). This equals an average annual growth rate of 40% since 2000 (The International Energy Agency (IEA), 2010). The current globalization trend is that the production of PV modules and its components is shifting to Asia (de Wild-Scholten, 2011). China and Taiwan are large producers, accounting for more than 65% of the global production of PV cells and modules (Jäger-Waldau, 2012). Figure 2.1 shows the development in global annual PV production between 2000 and 2011.

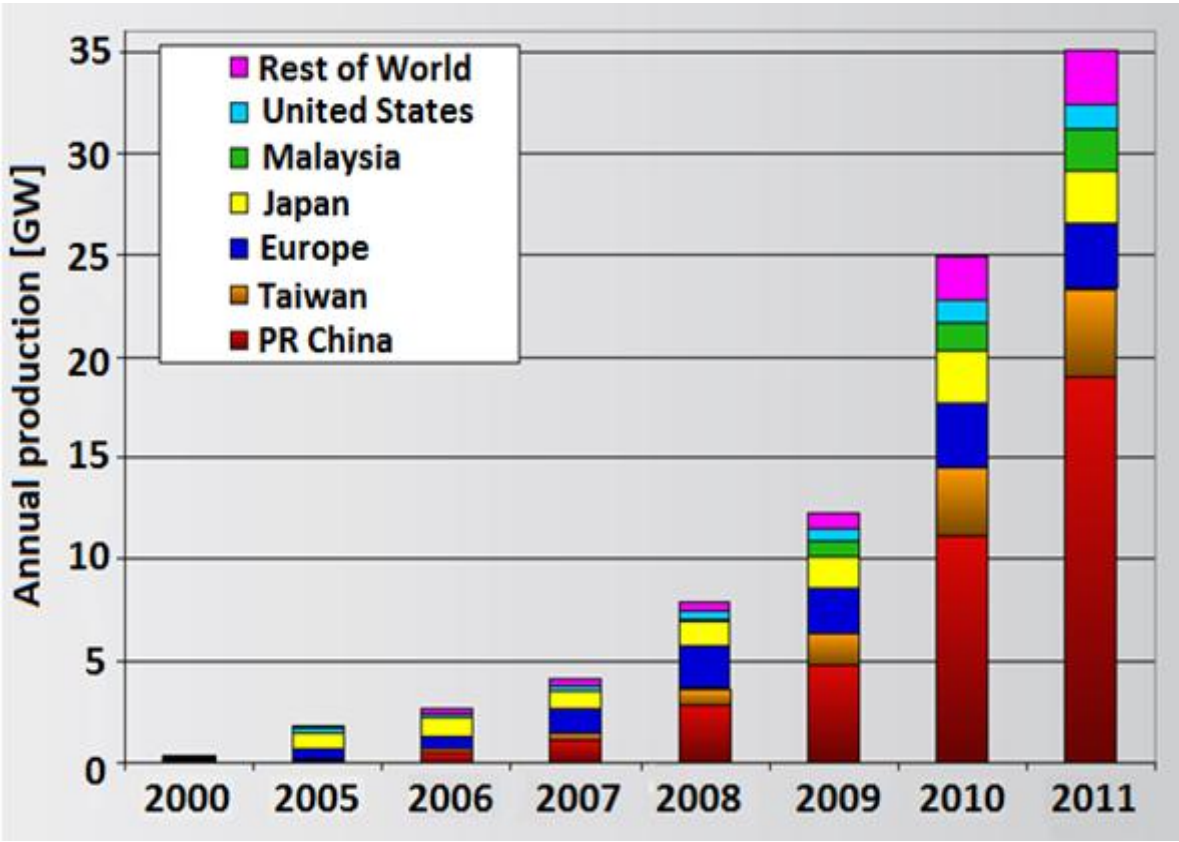


Figure 2.1: Global annual PV cell/module production, 2000-2011 (Jäger-Waldau, 2012, edited for readability).

## 2.2 Technology mix

Commercial PV technologies are built on crystalline silicon (c-Si) or thin film solar cells (see Figure 2.2). The crystalline silicon PV technology is often referred to as first generation technology and is subdivided into single crystalline (sc-Si), multicrystalline (mc-Si) and ribbon cast multicrystalline solar cells. These technologies are considered to be reasonable mature, and most of the research is directed toward production (Malm, 2008).

The thin film PV technologies are referred to as second generation technology. The most common thin film technologies are amorphous silicon (a-Si), cadmium telluride (CdTe) and copper indium gallium diselenide ( $\text{Cu(In,Ga)Se}_2$ , CIGS). These technologies aim at using less material, while maintaining the efficiencies of the first generation technology (McIntyre, 2010).

The categorization of the third generation technologies is more complex, but in general it refer to PV technologies which are not yet produced commercially on a larger scale (Malm, 2008) e.g. organic (OPV), dye-sensitised (DSSC), quantum dot (QDSC) and quantum well solar cells. These technologies can be made from chemicals which are processed into inks, coatings and paints and applied over large areas (McIntyre, 2010).

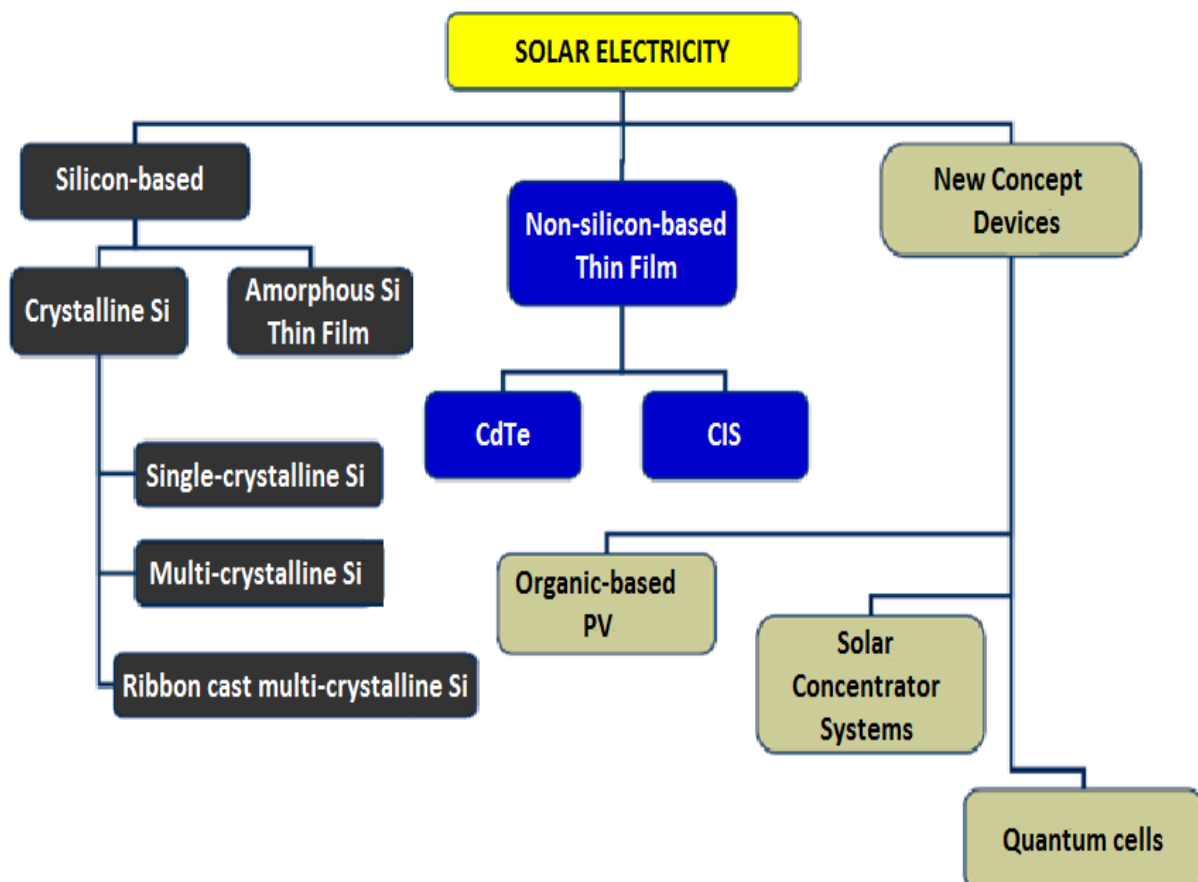


Figure 2.2: Overview of PV cell technologies (Raugei et al., 2007b, edited for readability).

The development in market share of PV technologies from 1999-2011 is shown in Figure 2.3. (Note that mono c-Si is the same as sc-Si). Presently, the best established and most used PV technology is the crystalline silicon PV. Crystalline silicon PV has accounted for about 80-85% of the global PV production capacity the last decade (Platzer, 2012). Sc-Si PV modules have a slightly higher efficiency than mc-Si PV modules, but the cost of production is lower for the mc-Si PV technology. As the names suggest, the difference between sc-Si and mc-Si is that sc-Si is made of wafers cut from an ingot of a single silicon, while mc-Si is made of wafers containing many different crystals of silicon (Hsu et al., 2012).

The thin film PV technologies had a market share of 19% in 2009 (Razykov et al., 2011), but due to the fact that the ramp up of new PV production has not followed that of the crystalline silicon, this market share has decreased since then (Jäger-Waldau, 2012). However, the market share of thin film PV technologies are expected to increase in the near future (Razykov et al., 2011). Overall, the mc-Si PV technology is currently the dominating PV technology on the market.

For 2011, the market shares for the different PV technologies were the following: 40% sc-Si, 45% mc-Si, 1% ribbon cast multicrystalline silicon, 3% a-Si, 8% CdTe and 3% CIS (Fraunhofer Institut für Solare Energiesysteme (ISE), 2012).

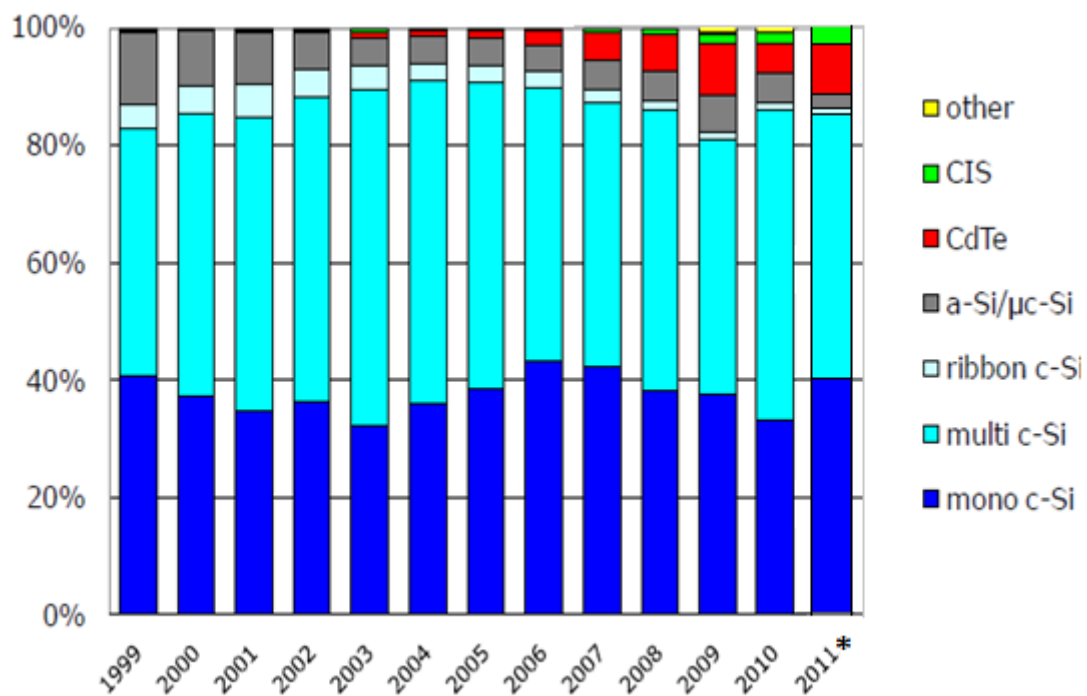


Figure 2.3: Market share of PV cell technologies, 1999-2011 (de Wild-Scholten, 2011; \*modified to include numbers for the year 2011 from Fraunhofer ISE (2012)).

### 2.3 Installed capacity

The global PV market, in terms of annual installed PV capacity, stabilized in 2012, representing a turning point. 31,1 GW of new PV capacity was installed globally, roughly the same as in 2011 (EPIA, 2013).

Figure 2.4 shows the development in annual installed PV capacity between 2000 and 2012. The top five markets, accounting for over two thirds of the newly installed PV systems, were Germany (7,6 GW), followed by China (5,0 GW), Italy (3,4 GW), the USA (3,3 GW) and Japan (2,0 GW) (EPIA ,2013).

Even though the market for PV systems in Europe declined for the first time compared to previous years, Europe accounted for 55% of the new PV capacity in 2012. The market decline in Europe were mainly due to reduced incentives, general policy uncertainty and a drop in the Italian market (Renewable Energy Policy Network for the 21st century (REN21), 2013a).

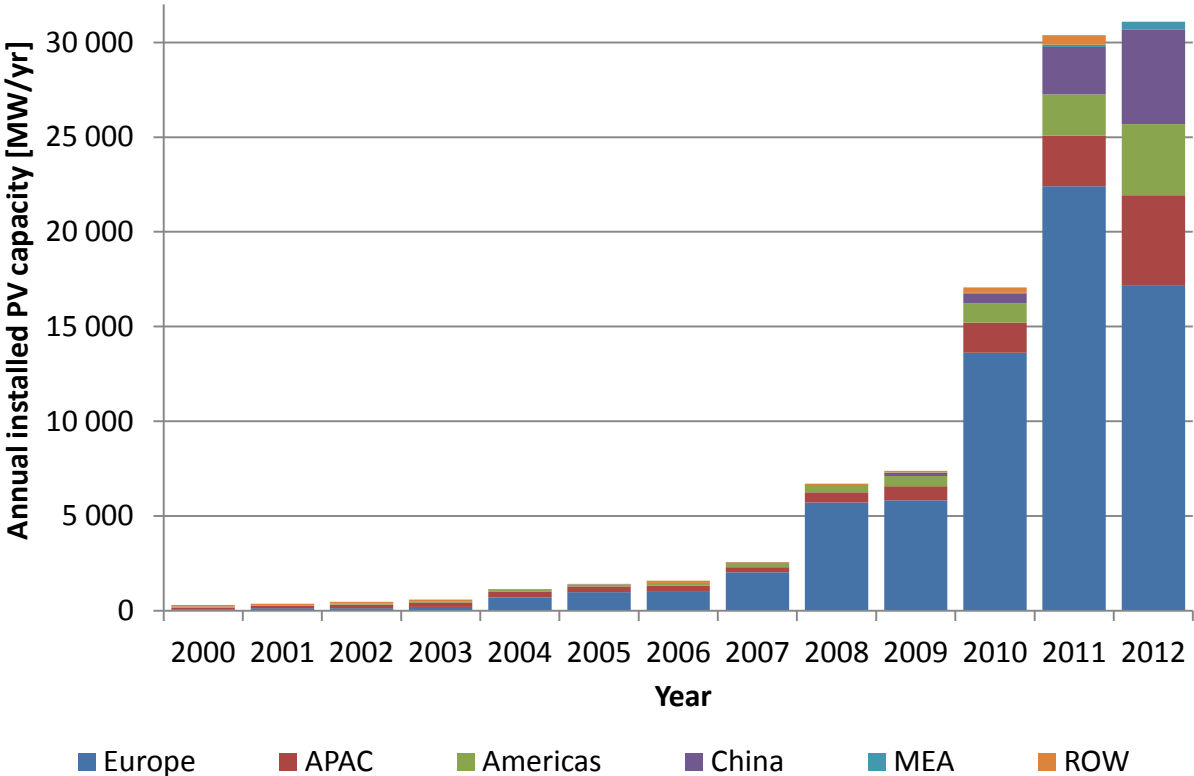


Figure 2.4: Global annual installed PV capacity, 2000-2012 (based on numbers from EPIA (2013)). Note that ROW-numbers for 2012 are directly integrated into relevant regions. ROW: Rest of the world. MEA: Middle East and Africa. APAC: Asia Pacific.

The global cumulative installed PV capacity reached 102,2 GW in 2012 (EPIA, 2013). These numbers represent both grid-connected and off-grid PV systems. However, the majority of installed PV capacity is grid-connected, the off-grid PV systems only accounting for approximately 1% of the global PV capacity (REN21, 2013a).

Figure 2.5 shows the development in cumulative installed PV capacity between 2000 and 2012. The top five countries in terms of cumulative installed PV capacity are Germany (32 GW), followed by Italy (16 GW), China (8,3 GW), the USA (7,8 GW) and Japan (6,9 GW) (EPIA, 2013). China, the USA, Japan, Australia and India are among those countries who have not yet fully utilized their PV potential. Other countries are on the brink of starting to deploy PV systems, especially countries from sunbelt regions like Africa, the Middle East, South East Asia and Latin America (EPIA, 2013).

Europe is the leading region in PV installations, with about 70% of the global cumulative PV capacity. The acceleration in deployment of PV systems has been due to economical incentives and support schemes. PV systems currently covers 2,6% of the European electricity demand (EPIA, 2013). By 2020, PV energy may provide 12% of the European electricity demand according to an energy demand forecast developed by the European Commission (2012c).

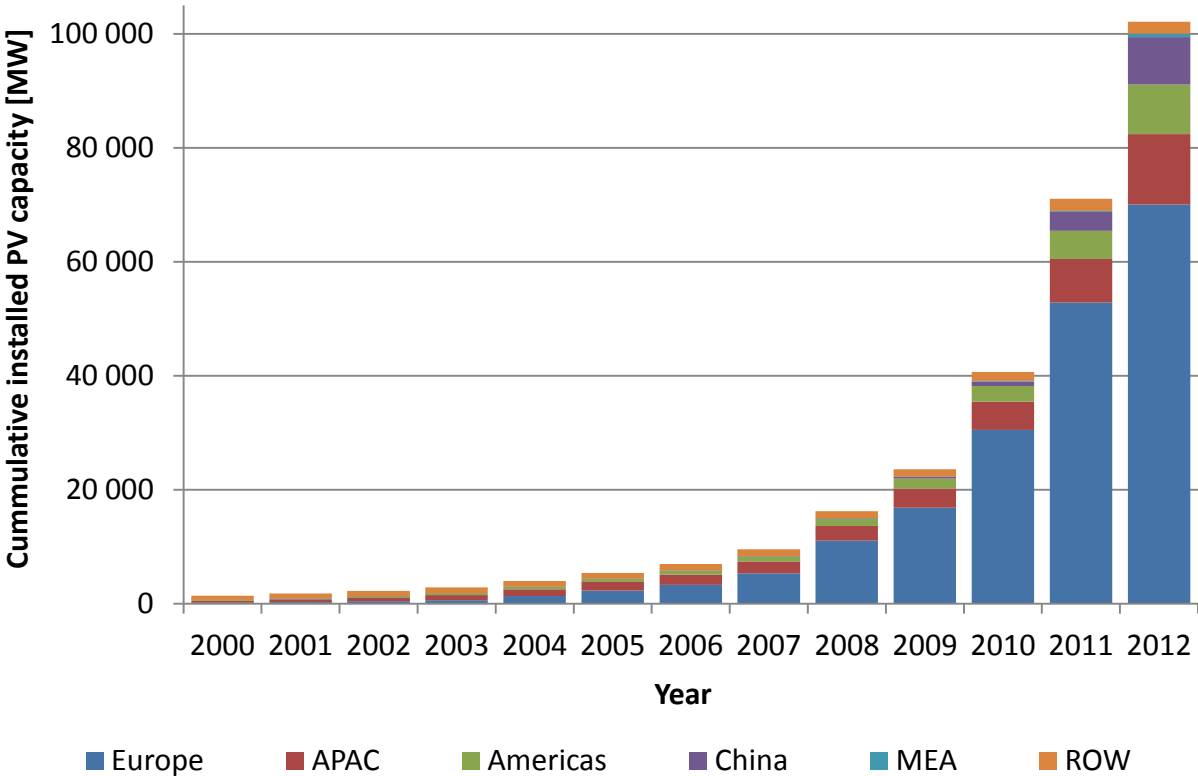


Figure 2.5: Cumulative installed PV capacity, 2000-2012 (based on numbers from EPIA (2013)). ROW: Rest of the world. MEA: Middle East and Africa. APAC: Asia Pacific.

PV systems can be applied in a diverse range of applications. The market for PV is often divided into four end-use-sectors (adapted from IEA, 2010):

- **Residential systems:** Mounted on individual buildings. Size up to 20kW.
- **Commercial systems:** Mounted on commercial office buildings, schools, hospitals and retail. Size up to 1 MW.
- **Utility systems:** Mounted on roofs or ground. Size from 1 MW and higher.
- **Off grid applications:** Not connected to the utility grid. Varying in size.

So far, the residential systems accounts for the largest share (more than 40%) of the global cumulative installed PV capacity (IEA, 2010; Razykov et al., 2011).

## 2.4 Future prospects - scenarios and roadmaps

At the end of 2012, PV systems covered 0,6%, or 110 TWh, of the total global electricity demand (EPIA, 2013). During the last years, several scenarios and roadmaps about the potential growth and implementation of PV systems have been published. To give an insight on how the PV market may evolve, this section will present predictions for future installed PV capacity and PV electricity generation.

In "*Global market outlook for photovoltaics 2013-2017*", published by the European Photovoltaic Industry Association (EPIA, 2013), two scenarios have been derived to forecast the global PV market in 2017:

- **The business-as-usual scenario:** Represents the lowest estimate and a pessimistic development, where support mechanisms and feed-in-tariffs are phased out.
- **The policy-driven scenario:** Represents the highest estimate and an optimistic development, where new support mechanisms are introduced and there is a strong political will to promote PV technology as a major power source.

According to these two scenarios, the global annual PV market (i.e. annual PV installations) could reach between 48 and 84 GW in 2017, while the cumulative installed PV capacity could reach 288-423 GW (EPIA, 2013).

The International Energy Agency (IEA) has published several reports on the future development of energy demand and energy technology mix. In the report "*Medium-Term Renewable Energy Market Report 2013 - Market Trends and Projections to 2018*" (IEA, 2013d), the cumulative installed PV capacity is projected to reach 268 GW in 2017 and then 308 GW in 2018. 1,3% of the total global electricity generation is projected to be supplied by PV systems in 2018, generating 368 TWh of electricity.

"*World Energy Outlook*" has been published annually by IEA since 1993. The report provides projections on energy demand and supply by using a large-scale simulation model designed



to replicate how energy markets function (IEA, 2012b). In "*World Energy Outlook 2012 - Renewable energy outlook*" (IEA, 2012c) three different scenarios have been used to examine future energy trends towards 2035:

- **The current policies scenario:** Illustrates the current course. Only policies and measures which have been adopted or are already initiated by the middle of 2012 are accounted for.
- **The new policies scenario:** Includes existing policies already implemented and recently announced commitments and plans not yet adopted.
- **The 450 scenario:** Includes policies adopted to put the world on an energy pathway consistent with having approximately 50% chance of limiting the increase in global average temperature to 2°C in the long term, compared with preindustrial levels. In order to not surpass the 2°C-limit, the concentration of greenhouse gases in the atmosphere should stabilize at 450 parts per million of CO<sub>2</sub>-eq.

These scenarios projects that PV systems will contribute to an electricity generation of between 524 and 1 371 TWh in 2035. This equals 1,3-4,3% of the total global electricity generation. However, according to IEA (2012c), the new policy scenario is the most central scenario of the report. In this scenario, the PV electricity generation increases 26-fold in the time period 2010-2035, up to 846 TWh, making up 2,3% of the total global electricity generation. The global cumulative installed PV capacity reaches approximately 600 GW within the same time period.

"*Energy Technology Perspectives*" has been published every two years since 2006 by IEA. This report represents the IEA's most long-term outlook, presenting the main results for 2050 (IEA, 2013a). The scenarios are created by using both back casting and forecasting (IEA, 2013c). By using back casting, the end state is already decided, and possible pathways on how to reach this end state have to be found. By using forecasting, the pathways are chosen first, and the end states are then the outcome of the analysis. In "*Energy Technology Perspectives 2012 - Pathways to a clean energy system*" (IEA, 2012a), the main scenario is the **2°C scenario** (2DS). This scenario describes how the overall energy system will evolve towards 2050, if the energy-related CO<sub>2</sub>-emissions are reduced with more than 50% compared to year 2009 and further reduced thereafter (IEA, 2013b). This pathways gives an 80% chance to limit the increase in the global average temperature to 2°C (IEA, 2013b). The 2DS scenario projects that PV systems account for approximately 6,5% of the total global electricity generation in 2050 with a possible annual production of 2 667 TWh.

A technology roadmap on solar photovoltaic energy were published by IEA in 2010. The IEA PV technology roadmap builds on the **blue map scenario** from "*Energy Technology Perspectives 2008 - Scenarios and strategies to 2050*" (IEA, 2008), which describes how energy technologies may be transformed by 2050 to achieve the global goal of reducing the annual CO<sub>2</sub>-emissions by 50% compared to year 2005 (IEA, 2010). This is consistent with a

long-term rise in global average temperature of 2-3°C, assuming that the cut in energy related CO<sub>2</sub>-emissions is combined with deep cuts in other greenhouse gas emissions too (IEA, 2008). However, the IEA PV technology roadmap forecasts a more rapid PV deployment than that of IEA (2008): While IEA (2008) projects that PV systems will provide 6% of the global electricity generation in 2050, the roadmap projects that PV systems will provide 5% of the global electricity production already in 2030 and 11% of the global electricity production in 2050. This is based on a global cumulative installed PV capacity of approximately 3 155 GW in 2050, with the possibility to provide 4 572 TWh of electricity.

According to the IEA PV technology roadmap, there will be a shift from residential to larger-scale PV systems over time. For PV technology to be competitive with other energy technologies, PV systems need to achieve grid parity, i.e. solar PV generation costs equal to retail electricity grid prices (REN 21, 2013b). The IEA PV technology roadmap predicts that PV residential and commercial systems will reach grid parity in many regions by 2020.

The IEA PV technology roadmap sets conversion efficiency targets for commercial PV modules. Current commercial PV modules have conversion efficiencies of around 8-20%, depending on the PV technology used (see chapter 3.2.1). Figure 2.6 shows the potential efficiency improvements over the next 20 years forecasted by the IEA PV technology roadmap. The PV industry should strive towards producing PV modules in 2030 with the following conversion efficiencies: 25% for sc-Si, 21% for mc-Si, 15% for a-Si, 15% for CdTe and 18% for CIGS.

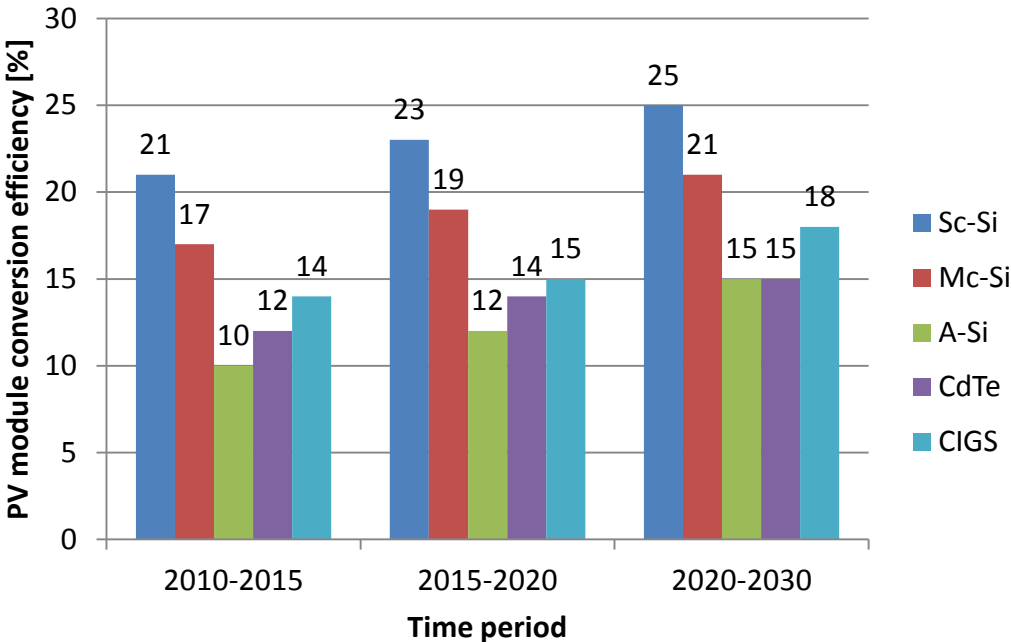


Figure 2.6: Conversion efficiency targets for commercial PV modules, from IEA roadmap on PV technology (IEA, 2010).

### 3 PV theory

Solar cells operate by utilizing the *photovoltaic effect*, which was discovered by Alexandre-Edmond Becquerel in 1839 (Malm, 2008). The phenomenon can be explained by the origin of its name: *Photo* from the Greek word *phos*, which means light, and *voltaic* which means electrical. In other words, the photovoltaic effects is about electricity generation from light illumination.

A semiconductor can convert sunlight directly into electricity by exploiting the photovoltaic effect (Markvart, 2000). By adding impurities to a semiconductor (doping), the electrical properties of the semiconductor can be controlled, and this property is utilized in PV applications. The photovoltaic effect will be explained in detail in the first section of this chapter, while the second section will explain important parameters affecting the PV system performance.

#### 3.1 How a solar cell works

In this section, silicon will be used as example for an in-depth explanation of the photovoltaic effect and how a solar cell works (adapted from Markvart, 2000).

A silicon atom lacks four electrons in its outer shell. These missing electrons can be provided by neighbouring silicon atoms, forming bonds between the atoms and ending up in a crystal structure. The energy of an electron in a crystal structure is distributed in different *energy bands*. When the outer shell of a silicon atom is filled up, like it is in a crystal structure, the energy of the electrons is in the *valance band*. The *conduction band* is a higher energy band, separated from the valance band by a *bandgap*, a very important feature of a semiconductor. However, in order for the silicon to able to lead current, the electrons need to be able to move. When they are bound in a crystal structure, the electrons have no free spaces to move to and a semiconductor of pure silicon will therefore act as an insulator. A pure semiconductor is called *intrinsic*.

Silicon and other semiconductors may only lead electricity if electrons are introduced into the conduction band or removed from the valance band. This can be done by introducing an impurity to the silicon; the silicon is doped. If the silicon is doped with a substance where the atoms have five electrons in their outer shell (e.g. phosphorus), four of these electrons will fill the valance band, while the last extra electron will find its place in the conduction band. The extra electrons in the conduction band are free to move and results in a negative current. The silicon has become a *n-type semiconductor*.

The other doping alternative is to dope the silicon with a substance where the atoms have only three atoms in their outer shell instead (e.g. boron). Since the silicon atom is missing four electrons in its other shell, there is a lack of electrons, and there will be a "*hole*" in the

valance band. These holes act as mobile, positively charged particles, thus creating a positive current. The silicon is in this case called a *p-type semiconductor*.

In the making of a silicon solar cell, doping is used to create a p-type region and a n-type region. The interface between these two regions is called a *p-n junction*, having a strong electric field. Since the junction is formed by the same semiconductor material in a crystalline silicon cell, the junction is called a *homojunction*. The opposite is a *heterojunction*, formed by two different semiconductor materials. The electric field is caused by electrons in the n-region near the surface diffusing into the p-region and holes diffusing in the opposite direction into the n-region. This electric field is build up until it is not possible for the charged particles to move between the regions. However, if the solar cell is exposed to sun light, the bound electrons may be thermally excited to a higher energy state and generate a current. The sun light can be seen as a flux of photons which carry a certain amount of energy. If the photon energy exceeds the bandgap energy, the electrons get energy to move from the valance band to the conduction band. Since a hole is left behind in the valance band, *electron-hole pairs* are created and a current is generated. The electrical current can be used in an external load and the charged carriers are circulated through the system. Figure 3.1 shows the basic operation of a solar cell.

In 1956, Joseph J. Loferski showed that the optimum energy bandgap for PV solar energy conversion is 1,5 eV (Miles et al., 2005). In practise, semiconductors with energy bandgaps between 1,0 and 1,7 eV are used in PV applications (Miles et al., 2005). A direct-bandgap material, e.g. CdTe and CIGS, absorbs the incident light more efficiently then an indirect-bandgap material, like e.g. c-Si (Markvart, 2000).

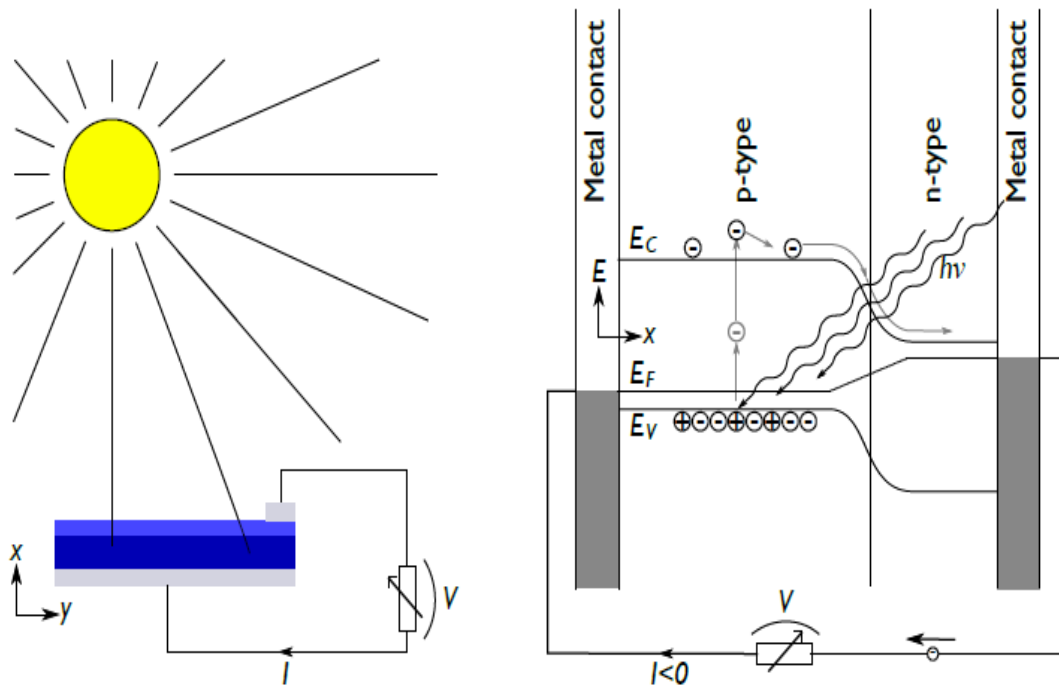


Figure 3.1: Basic operation of a solar cell (Malm, 2008). The solar cell is illuminated with solar irradiation ( $h\nu$ ), which excites electrons (negative) across the bandgap of the semiconductor, leaving holes (positive) behind in the valence band. ( $E_V$  = energy of valence band [eV],  $E_F$  = bandgap energy [eV],  $E_C$  = energy of the conduction band [eV].  $I$  = current [A],  $V$  = voltage [V]).

### 3.2 Important characteristics for the PV system performance

There are several factors affecting how much electricity is produced by a PV system during its lifetime. This section will explain these parameters, as well as the lifetime electricity generation from a PV system.

#### 3.2.1 Conversion efficiency

The conversion efficiency of a PV module describes the how much of the incoming solar irradiation is converted into electricity by the PV module.

The conversion efficiency,  $E$ , of a solar cell/PV module is then defined by the following equation:

$$E = \frac{P_{max}}{P_{irradiation}} = \frac{I_m V_m}{P_{irradiation}} \quad (3.1)$$

where  $P_{max}$  is the maximum possible power produced by the solar cell/PV module [W],  $I_m$  is the current at maximum power output [A],  $V_m$  is the voltage at maximum power output [V]

and  $P_{irradiation}$  is the power of the incident radiation [W]. The maximum values refer to measurements done under standard test conditions, i.e. irradiance equal to  $1 \text{ kW/m}^2$ , standard reference AM 1,5 spectrum (sunlight after crossing 1,5 atmosphere) and temperature equal to  $25^\circ\text{C}$  (Markvart, 2000; Muños-García et al., 2012).

There are different power losses in a PV cell, affecting the maximal power output ( $P_{max}$ ) from the solar cell (adapted from Markvart, 2000):

- **Incomplete absorption of light/transmission losses:** Only the part of the incident solar radiation with photon energy equal or higher than the bandgap energy of the semiconductor material is absorbed in the solar cell.
- **Thermal losses:** As the photon energy increases above the bandgap energy of the semiconductor material, the energy in excess of this bandgap value does not generate electron-hole pairs, but is lost to the lattice as heat (Miles et al., 2005).
- **Recombination losses:** Recombination is the opposite of current generation. The electrons which absorb the incident photon energy have to be transferred to the junction to be able to generate voltage in the cell. If the photon energy hits an electron far away from the junction, the electron may meet a hole on its way to the junction and recombine. The energy absorbed by the electron is offset by the hole and the electron falls back into the valence band.
- **Top-surface reflection losses**
- **Top contact shading of the solar cell**

The conversion efficiency for commercial mc-Si PV modules normally ranges from 12 to 17% (Jäger-Waldau, 2012). Commercial sc-Si PV modules have a conversion efficiency of 14-20% (Jäger-Waldau, 2012). For thin film PV modules, the conversion efficiency for commercial CdTe PV modules range from 9 to 13,1% (Razykov et al., 2011; U.S. Department of Energy, 2012a), while the conversion efficiency for commercial CIGS PV modules range from 10,7 to 14% (Razykov et al., 2011; U.S. Department of Energy, 2012b).

### 3.2.2 Performance ratio

The performance ratio is the ratio of the actual and theoretically possible energy output of the PV system. In other words, it describes the proportion of electricity which is produced in reality after other inefficiencies of the PV-system, such as ohmic losses, thermal losses and conduction losses, are taken into account (Markvart 2000; SMA Solar Technology AG, 2010). The losses from a PV system can be related to e.g. losses in inverter and cabling, shading of the PV system and dust/snow covering the surface of the PV module (Photovoltaic-software, 2013). The performance ratio is also sometimes referred to as the fill factor.

Figure 3.2, showing the I-V characteristics of a solar cell, can be used to illustrate the concept of performance ratio: The red square represents an ideal solar cell with no losses. The yellow

square represent a solar cell where the different losses have been taken into consideration. The performance ratio is then a measure of how far the I-V characteristics of an actual solar cell differ from those of an ideal solar cell (Keithley Instruments Inc., 2010).

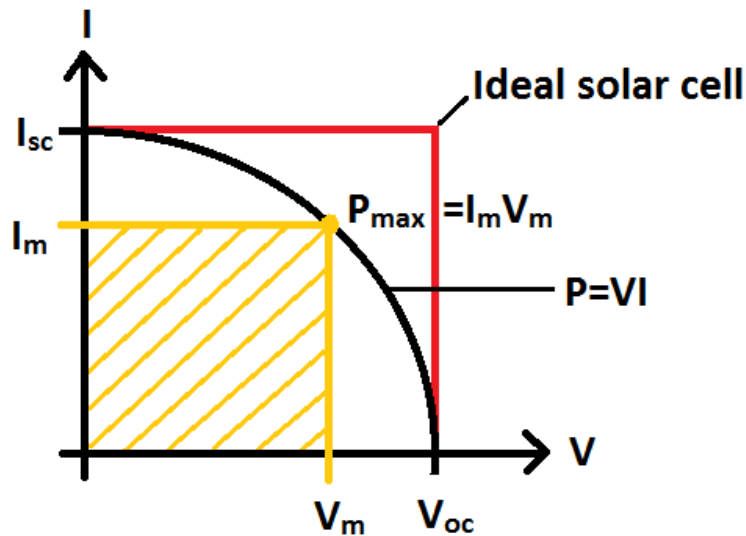


Figure 3.2: The I-V characteristics of a solar cell with the maximum power point (constructed based on information from Markvart (2000)).  $P_{max}$  = maximum power output produced by the solar cell [W],  $I_m$  = current at maximum power output [A],  $V_m$  = voltage at maximum power output [V],  $I_{sc}$  = short circuit current [A],  $V_{oc}$  = open circuit voltage [V].

The performance ratio of a solar cell/PV module,  $PR$ , is defined by the following equation (Markvart, 2000):

$$PR = \frac{P_{max}}{I_{sc}V_{oc}} = \frac{I_m V_m}{I_{sc}V_{oc}} \quad (3.2)$$

where  $P_{max}$ ,  $I_m$  and  $V_m$  are as described earlier in chapter 3.2.1,  $I_{sc}$  is the short circuit current [A] and  $V_{oc}$  is the open circuit voltage [V].

The performance ratio typically range from 70 to 90% (Fraunhofer ISE, 2012). In existing LCA-studies, the most commonly used performance ratios are 75% for rooftop PV systems and 80% for ground mounted PV systems.

### 3.2.3 Lifetime

The lifetime of a PV systems is defined as the time period that the PV system is in operation, including routine maintenance and repairs, before severe degradation in its ability to produce electricity (Hsu et al., 2012). The lifetime of a PV system may vary from manufacturer to manufacturer. Usually, PV systems are expected to have a life time of at least 20 years and up to 30 years (Berger et al., 2010; Zuser & Rechberger, 2011). However, very few PV systems have been installed for long enough; only a small share of all globally installed PV systems is older than 10 years (Centre for Alternative Technology (CAT), 2013).

### 3.2.4 Direct normal irradiation

The solar irradiation reaching the PV system is dependent on both geographical location, time of year/day and the inclination (orientation) of the PV module. The optimal inclination is such that the incoming irradiation is normal to the PV module.

The direct normal irradiation (DNI) is the part of the (global) solar radiation which is not reflected, scattered or absorbed by air molecules, clouds and particulate matter in the atmosphere, and reaches a surface perpendicular (normal) to the incoming solar radiation (Markvart, 2000). It is measured in kWh/m<sup>2</sup>/year.

### 3.2.5 Lifetime electricity generation

All of the parameters explained in chapters 3.2.1-3.2.4 affects the electricity generated by a PV system during its lifetime. The lifetime electricity generation,  $G$  in kWh/m<sup>2</sup>, of a PV-system is described by the following equation (Fthenakis et al., 2008):

$$G = I \times E \times PR \times L \quad (3.3)$$

where  $E$  is the PV module conversion efficiency [%],  $PR$  is the performance ratio [%],  $L$  is the lifetime of the PV system [years] and  $I$  is direct normal irradiation [kWh/m<sup>2</sup>/year].



## 4 Life cycle assessment methodology

This chapter will give an overview of the most important aspects of life cycle assessment (LCA). The general procedure of conducting a LCA, as well as the mathematical background will be presented.

### 4.1 Concept

Life cycle assessment is a tool for assessing the environmental impacts of a product or product system over its entire life cycle. In a LCA, the different phases of a product's life cycle, like extraction of natural resources/raw material, production and manufacturing, distribution, use, maintenance, end-of-life treatment, recycling and final disposal, are included (International Organization for Standardization (ISO), 2006a). All of the emissions and resources connected to the different life cycle phases are accounted for. LCA is therefore often called a cradle-to-grave approach. It is necessary to have a holistic view when assessing environmental impacts, in order to get the most correct picture of the environmental burdens connected to a product or service delivered from a system (Strømman, 2010). LCA try to tackle this challenge. To ensure a holistic perspective, it is not only important which life cycle phases are included, but also which upstream processes in the economy should be included.

By using LCA, issues of problem shifting can be revealed (Strømman, 2010). The term problem shifting can be used in two ways: In the process of solving an environmental problem, the problem might either be shifted to another stage in the value chain or create a new environmental problem. This makes it crucial to have a consistent system description with clearly stated system boundaries (see chapters 4.2 and 4.6.4).

LCA makes it possible to compare technological systems with respect to their environmental impacts (Strømman, 2010). Further, LCA results can be used to inform decision makers, act as guidance for legislation, policy targets and marketing, and for identifying where improvements can be made in the value chain of a product or product system (ISO, 2006a).

The principle and guidelines of conducting a LCA are stated in the ISO 14040 and ISO 14044 from the International Organization for Standardization. According to ISO 14040 (2006a), conducting LCA can be broken down into four main steps (Figure 4.1):

- Goal and scope definition
- Inventory analysis
- Impact assessment
- Interpretation

These steps will be presented and explained in the following sections.

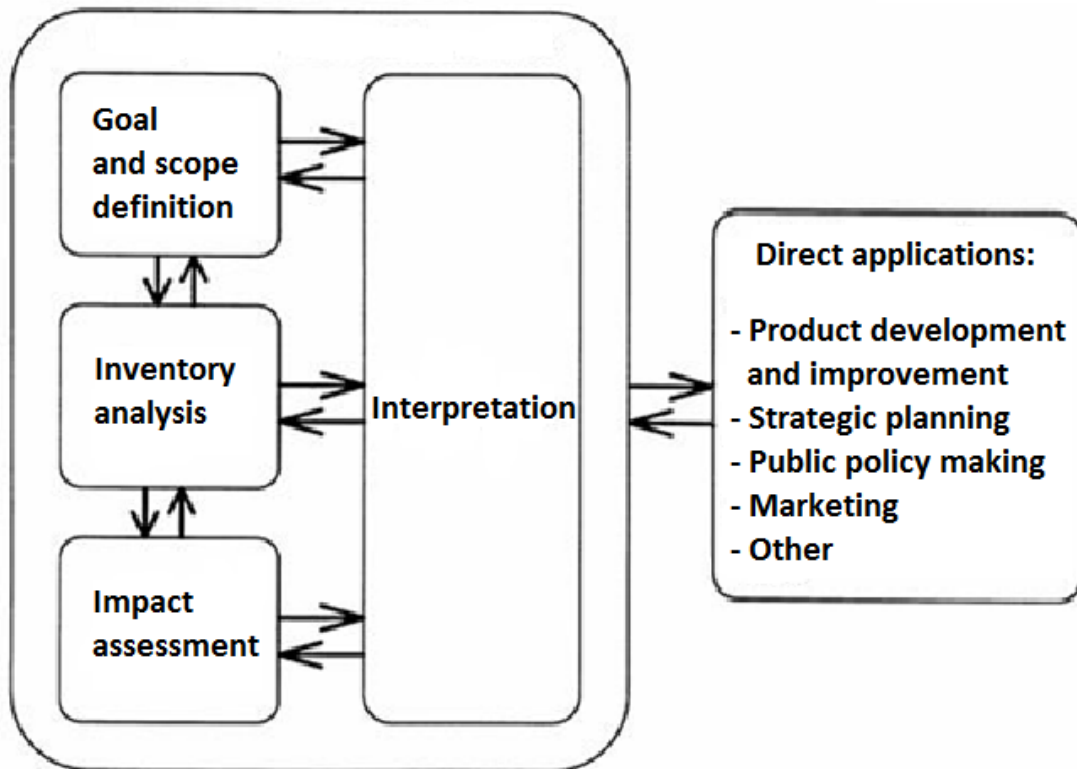


Figure 4.1: : The main steps of conducting an LCA (ISO, 2006a, edited for readability).

## 4.2 Goal and scope definition

The first thing that needs to be defined when conducting a LCA, is the goal and scope of the analysis. According to ISO 14040 (2006a); *"The goal of an LCA states the intended application, the reasons for carrying out the study and the intended audience"*. I.e. the goal of the LCA tells the reader what the purpose with the study is and who might find the results of the study useful.

Then the LCA study has to be narrowed down and clearly defined through the scope. This involves making several decisions. The product system in question has to be described with clearly stated system boundaries. This means deciding which processes (life cycle phases) should be included and accounted for, and to what level of detail the product system is modelled. The level of detail will have implications for the data requirements and - quality. It is important to include which assumptions have been made and which limitations the study might have. Omitting a process from the system description, which in reality has significant influence on the environmental impacts from the product/product system, will affect the conclusions of the study.

An important part of the scope process is to decide the functional unit (FU). The functional unit should describe what kind of function or service the product system delivers. ISO 14044 (2006b) states: *"The primary purpose of a functional unit is to provide a reference to which the inputs and outputs are related"*. All of the environmental impact results from the LCA will be measured relative to the functional unit, so the functional unit itself also has to be measurable. This makes it possible to compare results with other similar LCA studies with the same functional unit. However, it is important to have in mind that the system description may vary from study to study.

Impact categories and method for impact assessment are also chosen in the scope process. Selecting impact categories means selecting which types of environmental impacts are to be studied. To avoid problem shifting, it is recommended to not have a too narrow focus area (Andresen, 2008).

The decisions made in this step has a large influence on the outcome of the study, but as LCA is an iterative technique (ISO, 2006a), modifications may be done along the way to better satisfy the goal of the study.

### **4.3 Life cycle inventory analysis**

In the life cycle inventory analysis, relevant data on inputs, outputs and emissions needed for conducting the LCA are collected and calculated. These data forms the life cycle inventory (LCI) of the product system. The inventory constitute the computational basis of the analysis, and it is therefore of great interest to collect as complete information as possible on mass- and energy balances (Johansen, 2008). Data gathering is an iterative process. During the process, new data requirements, limitations or other issues may be discovered. To ensure that the goal of the LCA is still met, these new discoveries may lead to modifications of the goal and/or scope of the study (ISO, 2006a).

The data which need to be collected, can be separated into two groups: Foreground data and background data (see chapter 4.6.4) The foreground data describes the part of the system where there is a need for high resolution and detailed data, i.e. specific data related to the life cycle processes. The background data are data connected to upstream processes in the value chain, where less detail is required, and generic data available in databases are often used.

The availability of data is varying, and this is why the inventory analysis is often considered to be the most time consuming and demanding step of a LCA. Even though some data may be public available, most data often need to be collected for the particular case of the study (Andresen, 2008). This can be done by contacting companies/industries involved in the different process stages. Confidentiality matters can make the collection process difficult. Numbers on inputs, outputs and emissions are case sensitive and give companies a competitive advantage, especially if the technology is a "one-of-a-kind". Therefore these data are often not given out unless required by law or if promise of confidentiality is given.

Omitting inventory from an LCA report because of confidentiality, limits the possibility to compare similar LCA studies with each other (less transparency). In countries where legislation demands a minimum of certain emissions to be reported, the data gathering may be easier to conduct. If obtaining first hand data from the industry is impossible, data from databases and open literature could be used instead. However, the uncertainty in data may be larger. A sensitivity analysis could therefore be performed to identify to which extent changes in key parameters will affect the results (Johansen, 2008).

#### **4.4 Life cycle impact assessment**

In the life cycle impact assessment (LCIA), the collected inventory is used to evaluate potential environmental impacts of the product system. This stage can be divided into **three mandatory steps** (chapters 4.4.1-3) and then be extended further by conducting **three additional, optional steps** (chapters 4.4.4-6) (ISO, 2006a):

##### **4.4.1 Selection of impact categories, category indicators and characterization models**

In this step, which types of environmental impacts to include, represented by impact categories, and how they should be quantified through corresponding indicators and characterization method are determined (Pålsson & Mattsson, 2011). This is done in compliance with the goal and scope of the LCA. Normally, the choice of characterization model decides which impact categories are chosen, since the characterization model often include predefined selection and set-up of impact categories (Pålsson & Mattsson, 2011).

##### **4.4.2 Classification**

The classification consist of assigning the items of the LCI to the different impact categories, i.e. organizing the inventory items according to what type of environmental impact they have the potential to cause. Each entry of the LCI may contribute in more than one impact category.

##### **4.4.3 Characterization**

The characterization process consists of calculating the category indicator results (ISO, 2006a), i.e. the inventory results are converted into impact potentials within the different impact categories (Pålsson & Mattsson, 2011).

Each type of substance emitted, contribute differently to the impact potential of an impact category. Therefore, to find the contribution from the emissions of a specific substance to an impact category, the emissions of the substance have to be multiplied with a

characterization factor. The characterization factor describes how the substance contributes to the impact potential measured relative to a reference substance (see chapter 4.6.3) This is done for each type of emissions and the resulting impact values are summed for the respective impact category (European Commission, 2012a).

#### **4.4.4 Normalization**

Normalization means that the midpoint results from the characterization step are normalized relative to a reference situation, i.e. the relative contribution from the impact categories is calculated. This gives an indication on how important impacts from the studied system are compared to the reference situation, e.g. relative to total impacts on a regional, national or international scale.

#### **4.4.5 Grouping**

The grouping process involves dividing the results from the characterization step into different categories or groups. This may create a clearer overview of the environmental impact. After the grouping, the emissions are sorted on a nominal basis (input vs. output, global vs. local) or ranked by a given hierarchy according to priority (Pålsson & Mattsson, 2011). It is important to note that this is based on value choices.

#### **4.4.6 Weighting**

Performing the weighting step consist in making value choices, assigning different weight of importance to the different impact categories and their results, and then aggregating them into one total score representing the total environmental impacts of the product system. It is important to note that this score is not scientifically based. Doing this form of aggregation, may make the results easier to understand for the public, but introduces a lot of uncertainties.

### **4.5 Interpretation**

The last step of an LCA is to analyse the results from the impact assessment step. This means looking into how the different processes and emissions (stressors) contribute to the different impact categories (see chapter 4.6.3 and 4.6.5). The interpretation should identify the most important environmental issues and options on how to possibly reduce the impacts investigated. A sensitivity analysis may be conducted to see how sensitive the results are for certain changes in the data and/or assumptions. The quality of the data in the LCI and limitations with the study should be discussed. In accordance with the defined goal and scope of the study, a conclusion is reached.

## 4.6 Mathematical background

In this section, the mathematical basis of conducting an LCA will be given (adapted from Strømman, 2010). The theory presented here has its outset from the open Leontief model, based on linear modelling.

### 4.6.1 Direct and indirect emissions

The product/product system which is studied shall deliver a certain amount of function or service, described as the functional unit. In order to provide this functional unit, direct activity is initiated in the process which the functional unit is required from. However, this initial process requires inputs from other process to be able to produce the functional unit, and these processes again require inputs from other processes and so on. This causes chains of requirements, so-called indirect activity. Both the direct activity and indirect activity causes emissions. The direct emissions are the emissions generated by the process which the functional unit is required from, while the indirect emissions are the emissions generated by all other processes due to the requirement of the functional unit.

### 4.6.2 The open Leontief model

#### *The requirement matrix*

The relations between the processes studied in a LCA are described in a requirement matrix,  $A$ . The coefficients in this matrix,  $a_{ij}$ , represent how much input from process  $i$  is required per unit output from process  $j$ :

$$a_{ij} = \frac{\text{amount of } i \text{ required}}{\text{output of } j} \quad (4.1)$$

In the case where  $i = j$ , the process in question has an internal demand of input from itself. This coefficient is often zero. The columns of  $A$  can be interpreted as the cooking recipe for each product produced. Information on inputs to the different processes has to be collected, both type of inputs and the amount needed. It is important to remember that the inputs are required per unit output. If numbers on inputs for the total output produced by a process are collected, these numbers need to be normalized by dividing by the total output.

### ***The production balance***

The total production output from each process is described by a vector  $x$ . Each coefficient in this vector,  $x_i$ , describes the total output from a process  $i$  to cover a given demand. By setting up a production balance, the total production output is related to the intermediate demand and the external demand:

$$x = Ax + y \quad (4.2)$$

Vector  $Ax$  represents the intermediate demand, i.e. the demand of products between the different processes. Vector  $y$  represents the external demand, i.e. the demand of products which the product system has to deliver. This is typical the functional unit. If process  $i = 1$  is the process which produce the functional unit, the first coefficient of  $y$  is set equal to 1, while the rest coefficients are set equal to 0.

### ***The Leontief Inverse***

The output of the processes, i.e. the  $x$  vector, is unknown and has to be solved. By rearranging equation 4.2, this gives:

$$x = (I - A)^{-1}y = Ly \quad (4.3)$$

where  $L = (I - A)^{-1}$  and is called the Leontief Inverse. The coefficients of the matrix  $L$ ,  $l_{ij}$ , represent the output from process  $i$  required per unit output of external demand from process  $j$ . The columns of  $L$  can be interpreted as the output required per unit external demand of product from each process. The interpretation of  $x$  is then the total output required to cover a specific external/final demand. To be able to solve equation 4.3, the determinant of  $(I - A)$  has to be positive.

## **4.6.3 Basic contribution analysis**

### ***Total stressors/emissions***

Now, the established matrices, vectors and equations can be used to calculate the total emissions from the product system and what type of environmental impacts these emissions may lead to. The emissions from the different processes can be described by a stressor intensity matrix,  $S$ . The coefficients of  $S$ ,  $s_{ij}$ , describe how much of a stressor  $i$  is emitted per unit product output from process  $j$ . The data on stressors have to be collected simultaneously with data on requirements used in the  $A$  matrix. The total amount of stressors generated by the product system can then be found by using equation 4.4:

$$e = Sx = SLy \quad (4.4)$$

The coefficients of vector  $e$ ,  $e_i$ , represent the total amount of each type of stressor  $i$  generated due to the external demand given in vector  $y$ .

It is useful to find out how the different processes contribute to the total stressors. First, the  $x$  vector has to be diagonalized (denoted with a  $\wedge$ ). To distribute the stressors over the different processes, the following equation can be used:

$$E = S\hat{x} = S\widehat{L}y \quad (4.5)$$

The coefficients of matrix  $E$ ,  $e_{ij}$ , describes the amount of stressor  $i$  generated/caused by process  $j$  due to the given external demand  $y$ .

### **Total impacts**

The stressors then need to be transformed into impacts. This is what is done in the LCIA step. The use of impact categories makes it easier to interpret the environmental loads resulting from the product system, then if a complete list of stressors was to be given. To be able to perform this transformation, a matrix of characterization factors,  $C$ , is introduced. The characterization factors are used to convert emissions of different substances with the same type of environmental impacts into equivalents of a reference substance, describing the specific impact. The coefficients of  $C$ ,  $c_{ij}$ , then represents the characterization factor for a stressor  $j$  within an impact category  $i$ . One stressor may contribute in more than one impact category.

An example on a impact category is climate change, where the characterization factor is global warming potential (GWP) and the reference substance is CO<sub>2</sub>-equivalents (eq.). Each substance contributing to climate change, has its own specific GWP value measured in kg CO<sub>2</sub>-eq. per kg emission of the substance. E.g. methane (CH<sub>4</sub>) has a GWP of 21 kg CO<sub>2</sub>-eq. per kg emissions of CH<sub>4</sub> (time horizon 100 years). This means that the emissions of CH<sub>4</sub> contribute 21 times more to climate change than what the same amount of emission of CO<sub>2</sub> would do. Multiplying the GWP value (characterization factor) with the total emission of CH<sub>4</sub>, will give the contribution of this substance to climate change, measured in CO<sub>2</sub>-eq.

For a given external demand, the total impacts,  $d$ , is then found by equation 4.6:

$$d = Ce = CSx = CS\widehat{L}y \quad (4.6)$$

The coefficients of vector  $d$  represent the total amount of impact potential within each impact category  $i$ .

The total impacts may be distributed over the different processes in order to see how each of them contributes to the different impact categories. This is done by using equation 4.7:

$$D_{pro} = CE = CS\hat{x} = CS\widehat{L}y \quad (4.7)$$



The total impacts may also be distributed over the different stressors in order to see how each of them contributes to the different impact categories. First, vector  $e$  has to be diagonalized. Then equation 4.8 can be used:

$$D_{str} = C\hat{e} = C\widehat{Sx} = C\widehat{SLy} \quad (4.8)$$

#### 4.6.4 The foreground and background system

The product system which is studied in detail in the LCA is called the foreground system. The data used to model the processes in the foreground system are compiled specifically for the given study and are denoted with the index  $f$ . The requirement matrix  $A_{ff}$  describes the requirements between the foreground processes. The value chains upstream of the foreground system are modelled using generic data from databases. These processes are called background processes, denoted with the index  $b$ . The requirement matrix  $A_{bb}$  described the requirements between the background processes. Obviously there are interactions between the foreground system and background system. The upstream inputs from the processes in the background to the processes in the foreground are described by the  $A_{bf}$  matrix.

The foreground data on inputs and emissions, as well as the upstream inputs from the background system to the foreground system are collected first hand by the person conducting the LCA. The background data on inputs and emissions are known in databases, and data collection on these background processes is not necessary. Typically, the foreground system is unidirectional, while the background system will contain loops between the processes since they represent a larger part of the economy. The interface between the foreground system and the background system is called the system boundary, and decides to which extent specific data collection is necessary before generic data can be used. How reliant the results are upon generic data versus specific data will indicate the uncertainty in the results. The larger the fraction of impacts from the foreground system compared to the fraction of impacts from the background system, the more precise the results are.

The total system can now be described by a requirement matrix  $A$  with four subsections:

$$A = \begin{bmatrix} A_{ff} & 0 \\ A_{bf} & A_{bb} \end{bmatrix} \quad (4.9)$$

The foreground system is represented in the top left subsection, the background system is represented in the bottom right subsection, while the inputs from the background system to the foreground system is represented in the bottom left subsection. The  $A$  matrix is often rather presented as a  $(I - A)$  matrix because this makes it easier to read. The matrix  $I$  is the identity matrix, a diagonal matrix with only ones on its diagonal. For the  $(I - A)$  matrix, the diagonal is stated by a series of ones, while the off diagonal are generally negative.

The associated stressors generated from the foreground and background system can be expressed in a total stressor matrix  $S$ :

$$S = [S_f \ S_b] \quad (4.10)$$

The stressors generated from the foreground system,  $S_f$ , are represented to the left, while the stressors generated from the background system,  $S_b$ , are represented to the right.

#### 4.6.5 Advanced contribution analysis

An advanced contribution analysis may be conducted to better understand how the foreground processes contribute to the various impacts. This means distributing the total impacts from the foreground processes,  $D_{pro}$ , over direct impacts from the foreground processes themselves, as well as over the upstream impacts, i.e. indirect impacts from the background processes, related to the different foreground process.

The total system is described by the requirement matrix  $A$  and the stressor matrix  $S$  as previously stated in equation 4.9 and equation 4.10. The output from the foreground processes,  $x_f$ , can be found by equation 4.11:

$$x_f = (I - A_{ff})^{-1}y_f \quad (4.11)$$

For each of the foreground processes, a demand,  $M_{bf}$ , is placed upon the different background processes:

$$M_{bf} = A_{bf}\hat{x}_f \quad (4.12)$$

The output from the background processes to each of the foreground processes,  $X_{bf}$ , is then described by equation 4.13:

$$X_{bf} = (I - A_{bb})^{-1}M_{bf} = (I - A_{bb})^{-1}A_{bf}\hat{x}_f \quad (4.13)$$

The direct impacts generated by the foreground processes,  $D_{pro,ff}$ , is found by using equation 3.14.

$$D_{pro,ff} = CS_f\hat{x}_f \quad (4.14)$$

The indirect impacts generated by the background processes, related to each of the foreground processes,  $D_{pro,bf}$ , is found by using equation 4.15:

$$D_{pro,bf} = CS_bX_{bf} = CS_b(I - A_{bb})^{-1}M_{bf} = CS_b(I - A_{bb})^{-1}A_{bf}\hat{x}_f \quad (4.15)$$

The total impacts related to each of the foreground processes are then given by equation 4.16:

$$D_{pro,f} = D_{pro,ff} + D_{pro,bf} \quad (4.16)$$

#### 4.6.6 Multiple outputs and allocation methods

Many processes generate multiple outputs, e.g. combined heat and power and recycling. Usually, these types of processes can be distinguished by what type of by-products they produce:

- **Exclusive by-products:** These are products which are not produced separately elsewhere. Example: New scrap from metal processing.
- **Ordinary by-products:** These are products where the production processes are linked together in a way that makes it impossible to produce one product without producing the other too. Example: Combined heat and power.
- **Joint products:** These products are a result of a "default" process design, where the process is actually designed to have multiple outputs. Example: Combined transport of passengers and goods in an aircraft.

When a process produces more than one product, one has to use allocation methods to assign the environmental burdens from the process to each of the products. Allocation can also be related to multiple inputs, e.g. waste incineration. There are three main types of allocation approaches:

- **The disaggregation approach:** One tries to collect a more detailed inventory for the process which makes it possible to create separate inventory models for the different products.
- **The substitution approach:** Sometimes also referred to as the avoided product method or system expansion method. The product system is expanded to include more than one production technology. One (or more) of the by-products is produced by an alternative technology, substituting the part of the original technology producing this by-product(s). One product from the product system is left "unadjusted", being produced by the original technology. This product is credited with the avoided production of the other by-product(s) from an alternative technology. The choice of alternative technology can have different effects on the allocation results depending on which type of technology is selected and should be chosen with care. One may perform a sensitivity analysis with respect to the various technology alternatives.
- **The partitioning approach:** The products are assigned a share of the environmental impacts by using a chosen property, e.g. mass, energy, energy or price (economic allocation). The chosen partitioning variable should reflect the driving force of the multiple production process and is between zero and one.

Since allocation is not used directly by the author of this report, the allocation methods will not be explained in further detail. For details on equations for the methods, the reader is referred to Strømman (2010).

## 5 System description

This chapter will present the goal and scope of this analysis. The choice of functional unit, the system boundaries for the study, the impact categories and method for impact assessment will be presented and explained.

### 5.1 Goal and scope of the study

The primary goal is to assess the environmental life cycle impacts of a rooftop, grid-connected PV solar system, without solar tracking, by performing a LCA. The GWP will be investigated in detail, as climate change is a highly important environmental issue. Different PV technologies will be investigated by performing a comparative LCA on four cases: Mc-Si Sim, mc-Si ESS, CdTe and CIGS solar cells. The difference between the multicrystalline silicon (mc-Si) cases are the solar grade silicon (SoG-Si) production methods, using one metallurgical and one chemical process route. The metallurgical process route will be represented by the metallurgical upgrading process developed by Elkem Solar (mc-Si ESS), while the chemical process route will be represented by the modified Siemens process, the most common SoG-Si production method today (mc-Si Sim).

The secondary objective will be to perform a sensitivity analysis. By performing a sensitivity analysis, one seeks to identify how "sensitive" a model is to changes in the value of the parameters of the model and to changes in the structure of the model (Breierova & Choudhari, 1996). In this report, the focus will be on parameter sensitivity. A series of simulations will be performed, by varying different parameters in a base case scenario to investigate how the changes affects the environmental performance of the PV system (i.e. the impact potentials). The change in parameters is done one at a time, i.e. changing the value of only one specific parameter in the base case scenario and keeping the rest of the parameters constant. The following selected parameters will be varied:

PV module conversion efficiency, performance ratio, lifetime, direct normal irradiation, lifetime electricity generation, electricity mix, energy efficiency (main focus electricity) and material efficiency.

The impact results from the sensitivity analysis will be compared with impact results from 1 kWh of electricity supplied to the grid by wind power. The range of impact values from the wind power system will be referred to as the *windband*, meaning the impact values between the minimum and the maximum of what is found in chosen literature. The main focus will be on the GWP.

An *overall performance envelope* for the four PV cases will be identified by combining all the selected parameters and using their minimum and maximum values. The overall

performance envelope for each PV technology will then describe the possible GWP-range for each specific PV system.

Both the results from the LCA and the sensitivity analysis will contribute to identifying environmental issues and possible options on how these can be improved.

## **5.2 Functional unit**

As mentioned earlier, the functional unit has to be measurable and should describe what kind of function or service the product/product system delivers. The purpose of a PV system is to generate electricity, measured in kWh. Intuitively, an appropriate functional unit for this analysis would be 1 kWh of electricity supplied to the grid by the PV system. Choosing this as a functional unit would make it possible to compare the results from this analysis with other competing electricity generating technologies. However, as seen in chapter 3.2.5, there are several factors affecting how much electricity is produced by a PV system. Choosing 1 kWh of electricity as a functional unit would mean making additional choices for the conversion efficiency, performance ratio, lifetime and direct normal irradiation. Since the electricity generated by the PV system is influenced by changes in these parameters, it has been decided to use a functional unit of 1 m<sup>2</sup> of PV system instead.

## **5.3 System boundaries**

In this LCA study the lifecycle of a PV system is evaluated. It is important to have clearly stated system boundaries in order to know which processes to include and to gather specific data on (foreground processes), and which processes where generic data are sufficient to use (background processes).

### **5.3.1 Foreground system**

#### ***Mc-Si PV system***

The foreground processes included in the analysis of the mc-Si Sim-case and ESS-case, where process specific data have been collected, are the following:

- Production of metallurgical grade silicon (MG-Si)
- Production of solar grade silicon (SoG-Si)
- Multicrystalline silicon ingot growing
- Multicrystalline silicon wafer sawing
- Solar cell production
- PV module production

- Mounting structure
- Inverter and cabling
- Manufacturing of the final rooftop PV system

A flowchart of the mc-Si foreground system studied is given in Figure 5.1. Note that the production of MG-Si and SoG-Si is happening in an integrated process for the mc-Si ESS-case.

The following processes are not included in the mc-Si Sim-case:

- Product packaging for mc-Si solar cells, only included for wafer and module.
- Slurry recycling in the wafer production.
- Waste-/waste water treatment.
- Waste for landfill or incineration.
- Raw material transportation.
- Infrastructure for production of MG-Si, SoG-Si and ingot growing (factories).

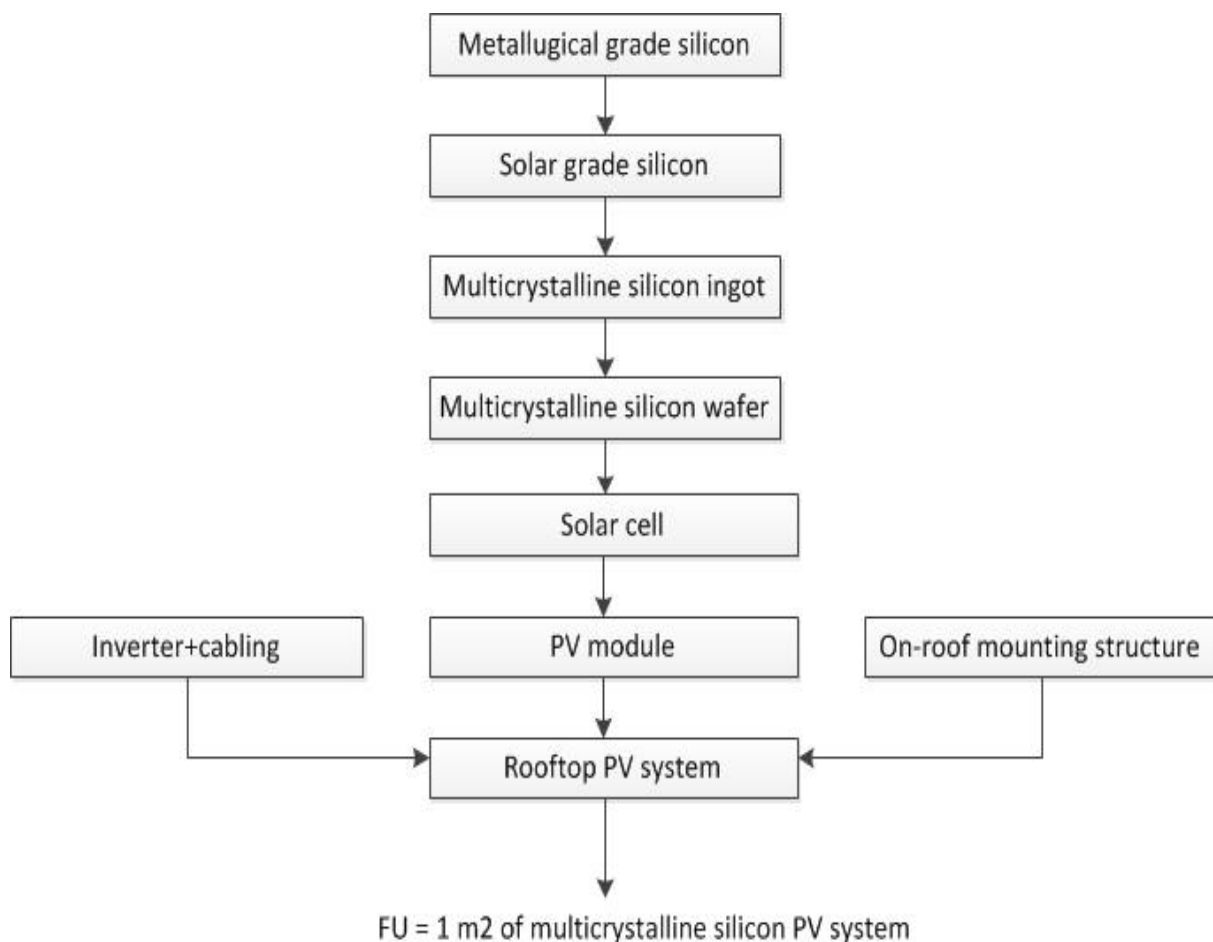


**Figure 5.1: Mc-Si PV system - Flowchart for the foreground system in the mc-Si Sim-case and mc-Si ESS-case.**

Further, the following processes are not included in the foreground system for any of the two mc-Si cases:

- End-of-life treatment of solar cells and PV systems, e.g. recycling and disposal.
- Recycling of intermediate waste in the production line (exception: slurry recycling included in the mc-Si ESS case).
- Installation and maintenance of PV modules.
- Transport of intermediate products in the production line.

### ***Thin film PV system***

The foreground processes included in the analysis of the CdTe-case and the CIGS-case, where process specific data have been collected, are the following:

- Preparation of substrate
- Deposition of the front contact layer (transparent conducting oxide, TCO)
- Deposition of the absorber layer
- Deposition of the buffer layer
- Deposition of the back contact layer
- Solar cell and PV module manufacturing
- Mounting structure
- Inverter and cabling
- Manufacturing of the final rooftop PV system

Note that unlike the mc-Si cases (one or both), the thin film cases includes transport of intermediate products in the production line and waste management for PV module manufacturing.

A flowchart of the thin film foreground system studied is given in Figure 5.2. Note that the production of solar cell and PV module happens in an integrated step.



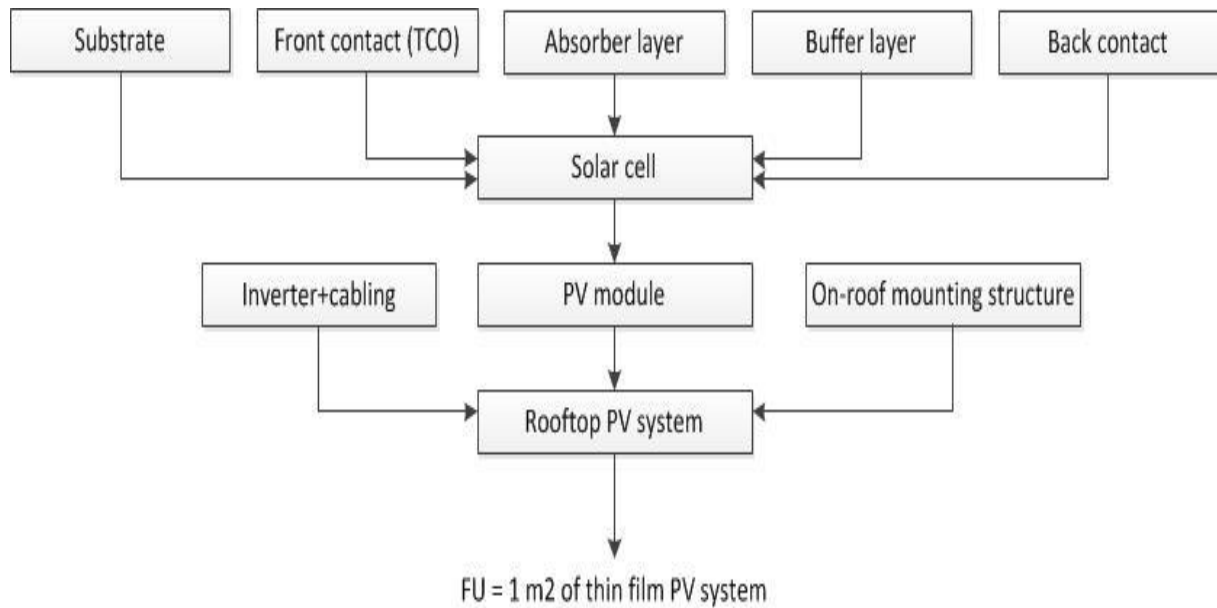


**Figure 5.2: Thin film PV system - Flowchart for the foreground system in the CdTe-case and the CIGS-case.**

The following processes are not included in the CdTe-case:

- Frame for the PV module.
- Recycling of intermediate metal waste in the production line, e.g. absorber and back contact metals.

Product packaging of PV module are not included in the CIGS-case.

Further, the following processes are not included in the foreground system for any of the two thin film-cases:

- End-of-life treatment of solar cells and PV systems, e.g. recycling and disposal.
- Installation and maintenance of PV modules.

### 5.3.2 Background system

The background data will be supplied from a public, Swiss LCI database called Ecoinvent (version 2.2). Ecoinvent is a comprehensive and complete database, containing more than 4000 generic LCI datasets for several process categories. The datasets are based on industrial data and compiled by international research institutes and LCA consultants (Ecoinvent Centre, 2012). Currently, Ecoinvent is considered to be the best existing LCI database (Strømman, 2010).

## 5.4 Characterization method and categories for impact assessment

### 5.4.1 Characterization and impact categories

The life cycle impact assessment stage is conducted by using the ReCiPe characterization model. This model takes the provided life cycle inventory and transforms these data into indicator scores for the different impact categories. The ReCiPe method offers the possibility of determining the environmental impact within 18 midpoint categories and/or within three endpoint categories.

The midpoint categories represent a problem oriented approach where the impact categories represent different types of environmental stress. The endpoint categories translate the stress into environmental consequences, by grouping the midpoint categories into three endpoint categories representing environmental damages. This method is therefore called a damage oriented approach. The endpoint categories may be easier to understand and interpret, but an important drawback is that they introduce a larger uncertainty.

In this study, the midpoint categories will be used, since they are more robust. Having 18 midpoint categories ensures a complete picture of the environmental impacts from the product system. The midpoint categories are listed below in Table 5.1 together with their belonging characterization factor.

**Table 5.A: Midpoint categories in the ReCiPe characterization model (Goedkoop et al., 2012).**

IMPACT CATEGORY	CHARACTERISATION FACTOR	ABBREVIATION	UNIT
Agricultural land occupation	Agricultural land occupation potential	ALOP	m <sup>2</sup> ×yr
Climate change	Global warming potential	GWP	kg CO <sub>2</sub> -eq.
Fossil depletion	Fossil depletion potential	FDP	kg oil-eq.
Freshwater ecotoxicity	Freshwater ecotoxicity potential	FETP	kg 1,4-DCB-eq.
Freshwater eutrophication	Freshwater eutrophication potential	FEP	kg P-eq.
Human toxicity	Human toxicity potential	HTP	kg 1,4-DCB-eq.
Ionising radiation	Ionising radiation potential	IRP	kg U <sup>235</sup> -eq.
Marine ecotoxicity	Marine ecotoxicity potential	METP	kg 1,4-DCB-eq.
Marine eutrophication	Marine eutrophication potential	MEP	kg N-eq.
Metal depletion	Metal depletion	MDP	kg Fe-eq.

	potential		
Natural land transformation	Natural land transformation potential	NLTP	m <sup>2</sup>
Ozone depletion	Ozone depletion potential	ODP	kg CFC-11-eq.
Particulate matter formation	Particulate matter formation potential	PMFP	kg PM <sub>10</sub> -eq.
Photochemical oxidant formation	Photochemical oxidant formation potential	POFP	kg NMVOC-eq.
Terrestrial acidification	Terrestrial acidification potential	TAP	kg SO <sub>2</sub> -eq.
Terrestrial ecotoxicity	Terrestrial ecotoxicity potential	TETP	kg 1,4-DCB-eq.
Urban land occupation	Urban land occupation potential	ULOP	m <sup>2</sup> ·yr
Water depletion	Water depletion potential	WDP	m <sup>3</sup>

#### 5.4.2 Cultural perspective

In addition to the choice of using midpoint or endpoint categories, the choice of cultural perspective has to be made. Each cultural perspective represents a set of choices and assumptions on different issues like time perspective and technology development. There are three cultural perspectives in ReCiPe (adapted from Goedkoop et al., 2012):

- **Individualist:** The individualist perspective represents a technological optimism as regards to human adaptation. The individualist have short time interests; therefore the time horizon is relatively short. In addition, the individualist only believes in undisputed environmental impacts.
- **Hierarchist:** The hierarchist perspective represents the "average human view". The most common policy principles regarding time frame and other issues are the basis for this perspective. The hierarchist is often used in scientific models (ReCiPe, 2012).
- **Egalitarian:** The egalitarian perspective represents a precautionary view; therefore the time horizon is relatively long. This perspective is extreme with regards to environmental issues. Impact types do not have to be fully established, but will be considered if some indications exists.

This study will use the most common used cultural perspective; hierarchist.

#### 5.4.3 Software

The study will be conducted by using a software called Arda, developed at Norwegian University of Science and Technology (NTNU). The collected life cycle inventory is plotted

into a template describing the foreground system with its material- and energy use, resource extraction and emissions, together with the linkage of inputs from the background system to the foreground system. In other words, the requirement matrices  $A_{ff}$  and  $A_{bf}$ , together with the stressor matrix  $S_f$  are put into the template. The template is uploaded to the software, which links the inventory to the Ecoinvent database (describing the background system, see chapter 5.3.2) and the ReCiPi Hierarchy method. According to choices made by the analyst, results are produced.

## 6 Multicrystalline silicon PV production value chain

In this chapter, the value chain of the SoG-Si based PV production and processing technologies will be explained. Since the scope of this report is limited to the assessment of multicrystalline silicon- and thin film solar cells, other crystalline technologies like single crystalline silicon and ribbon silicon cells will not be presented here. The different production steps making up the foreground system described in Figure 5.1 will be explained. Note that only the value chain upstream of the PV module, including the module itself, will be presented in this chapter.

### 6.1 Metallurgical grade silicon

Silicon is the second most abundant element in the Earth's crust, comprising approximately 26% of it (Saga, 2010). Silicon does not exist naturally in its elemental form, but as silicon dioxide ( $\text{SiO}_2$ ) in sand, rock and quartz (Amendola, 2011). The silicon dioxide must be converted to elemental silicon (Si), with very low levels of contaminants in order to be useful in PV applications (Amendola, 2011). The first step in this purification process is to produce metallurgical grade silicon (MG-Si).

Most of the MG-Si is commercial produced by carbothermic reduction of silicon dioxide (Jungbluth et al., 2012). Quartz is feed into a electric arc furnace at a very high temperature (1 400 - 2 000°C), where it reacts with a carbon based reduction agent (Martello, 2012). Examples on reduction agents are coal, coke, charcoal and wood chips (Jungbluth et al., 2012).

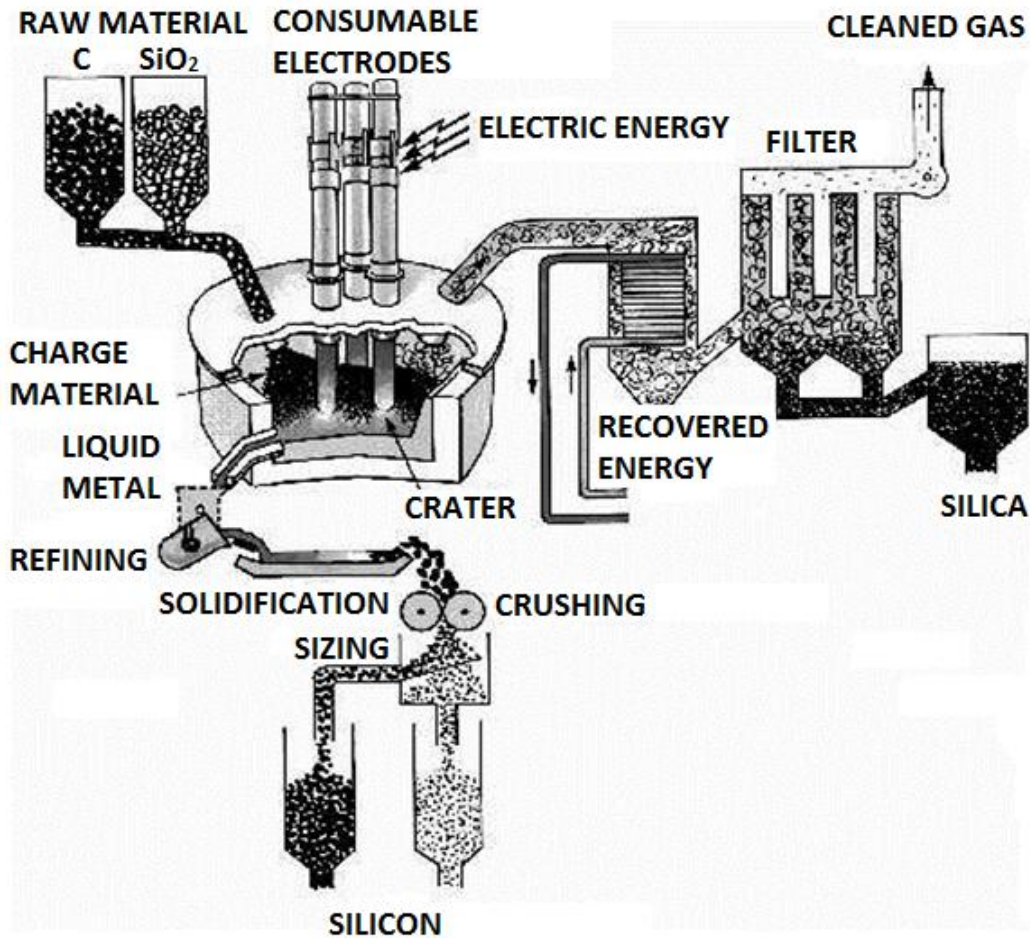


Figure 6.1: Principle sketch of metallurgical silicon production (Rosenkilde, 2012, edited for readability).

Figure 6.1 shows the principle of MG-Si production. The raw materials; the carbon based reduction agent and quartz in form of silicon dioxide, are charged to the top of the furnace. The furnace is supplied with electricity through three graphite electrodes inserted in the raw material mix. The electricity demand is typically 10-15 kWh/kg MG-Si (Rosenkilde, 2012). In the furnace, the silicon dioxide is reduced by the carbon in the reduction agent. The oxygen in the silicon dioxide is removed by rebinding to the carbon and forming carbon monoxide gas (CO). Since the electrodes also consist of carbon, they become a part of the reduction process themselves and new electrode material has to be fed continuously to the process (Andresen, 2008). Through tap holes in the bottom of the furnace, the molten silicon is tapped out. The produced MG-Si typically has a silicon purity of 98-99%. The main impurities are iron, aluminium and calcium (Luque & Hegedus, 2011).

The basic reaction which takes place in the carbothermic reduction process can be described by the following equation:



Gases in the furnace which have not reacted with each other, leaves the furnace in the off-gas, containing e.g. silica dust and carbon dioxide (Martello, 2012). The silica dust is collected from the off-gas in filters close to the gas-outlet and stored for sale. The off-gas also contains energy which can be recovered. This has been done at the MG-Si production plant of Elkem at Thamshavn, Norway. By doing this, they have reduced the external electricity demand by around 20% (Andresen, 2008).

## 6.2 Solar grade silicon

A purity of 98-99% silicon for the MG-Si is not pure enough for solar cell application. The MG-Si has to be further purified in order to reach a high purity of 99,9999% (six nines pure). Silicon with this purity is called solar grade silicon (SoG-Si). There are currently two main purification methods; a metallurgical route and a chemical route. For the description of a metallurgical route, the technology of Elkem Solar will be presented. Considering a chemical route, the three most common methods will be presented. In 2008, about 95% of the SoG-Si produced was produced using one of these three chemical methods (Gløckner et al., 2008). However, for this report, only two of the methods described in this chapter will be used in the LCA conducted; the Elkem Solar Silicon process and the modified Siemens process (see chapter 5.1).

### 6.2.1 Elkem Solar Silicon production process

Elkem Solar in Kristiansand, Norway, has developed a metallurgical process for producing SoG-Si by upgrading/refining of MG-Si. This process is called the Elkem Solar Silicon production process (ESS).

ESS consists of five independent process steps for purifying silicon, where the production of MG-Si and SoG-Si happens in one integrated process (ABB, 2012). This significantly reduces the energy demand for producing SoG-Si compared to the modified Siemens process. According to Elkem Solar, the energy consumption of their ESS process is 1/4 of the energy consumption of the modified Siemens process (Elkem Solar, 2012b). ESS involves pyrometallurgical refinement and treatment with acid solutions (Braga et al., 2008). The process steps will be explained in the following (see Figure 6.2):

**1. MG-Si production:** MG-Si is produced by carbothermic reduction of quartz in an electric arc furnace (see chapter 6.1).

**2. Slag treatment and crushing:** This is the first of three sequential purification steps to reduce the amount of impurities in the MG-Si and remove boron (ABB, 2012). Liquid MG-Si is transferred from the arc furnace and undergoes a pyrometallurgical slag treatment. After the treatment, the MG-Si is solidified and crushed.

**3. Leaching:** To reduce the level of phosphorus and other metallic impurities, the crushed MG-Si undergoes a hydrometallurgical cleaning process. This involves cleaning with acids.

**4. Direct solidification:** By direct solidification (see chapter 6.3), phosphorus and other metallic impurities are further removed. The result is a solidified ingot.

**5. Post treatment:** The solidified ingot produced in step 4 is cut into bricks of 10 kg and then cleaned with acids. Excessive concentrations of impurities contained in parts of the ingot are cut off.

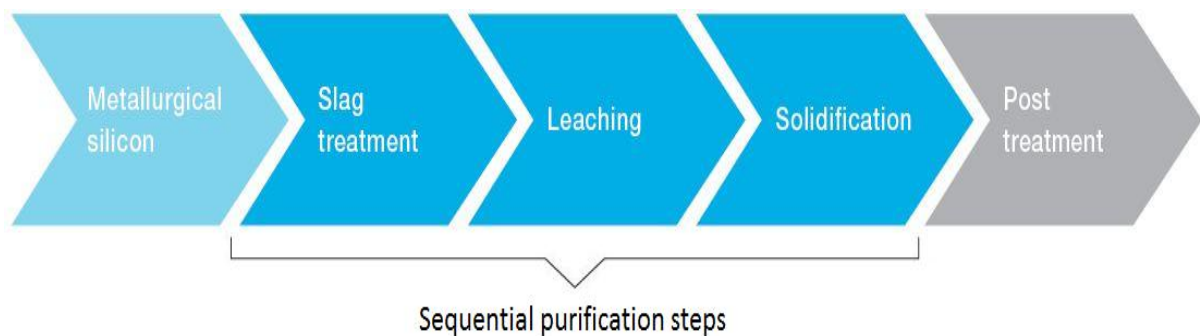


**Figure 6.2: Schematic view of Elkem Solar Silicon production process, where production of MG-Si and SoG-Si happens in an integrated process (ABB, 2012). MG-Si is produced and then purified to yield SoG-Si.**

Using ESS to produce SoG-Si avoids the formation of chlorosilane gas when the MG-Si is purified. The SoG-Si produced by the ESS method is currently used in mix-in ratios of 40-80%. However, the conversion efficiency of solar cells using 100% SoG-Si produced by the ESS method is the same as solar cells using SoG-Si produced by the modified Siemens method (de Wild-Scholten & Gløckner, 2012). An average conversion efficiency of almost 17% has been obtained for multicrystalline silicon solar cells using SoG-Si produced by this method (Elkem Solar, 2012a). It is not possible to give a more in depth discussion about this process due to intellectual property rights.



### 6.2.2 Modified Siemens process

The modified Siemens process is currently the most common method used for commercial SoG-Si production. This process involves chemical purification of MG-Si, by thermal decomposition of trichlorosilane gas ( $\text{SiHCl}_3$ , TCS).

First, hydrogen chloride gas (HCl) is mixed with powdered MG-Si in a fluidized bed reactor. In the fluidized bed reactor, hydrochlorination of MG-Si happens at  $300^\circ\text{C}$  (Rosenkilde, 2012) and gaseous chlorinated silicon compounds, trichlorosilane (85%) and tetrachlorosilane ( $\text{SiCl}_4$ , STC, 15%) are produced. This can be described by the following chemical equations (Rosenkilde, 2012):



The TCS is separated from the STC by distillation, and then further purified. The by-product, STC, can either be converted back to into TCS and be reused as production input, or be used to produce fumed silica (Odden et al., 2008; LDK Solar, 2011b).

Finally, the high purity TCS gas is feed into a Siemens bell-jar reactor together with hydrogen gas (Figure 6.3). In the reactor, there are thin high-purity silicon rods electrically heated to  $1100^\circ\text{C}$ . These have a diameter of about 0,5 cm and a height of about 2 m (Markvart, 2000). The TCS gas is reduced and decomposed by the hydrogen gas, and solar grade silicon deposit onto the rods (LDK Solar, 2011b). The main chemical reaction can be expressed by the following equation:



The residue product, hydrogen chloride, is recovered. Other by-products are also formed in the reactor:  $\text{SiCl}_4$ ,  $\text{H}_2$ ,  $\text{SiHCl}_3$  and  $\text{SiH}_2\text{Cl}_2$  (Ciftja et al., 2008).

When the rods have reached the desired diameter of 12,5 cm (Markvart, 2000) because of the silicon deposition, they are removed from the reactor. This final solidification step is called chemical vapour deposition (CVD). The silicon rods are broken into chunks and packaged. The inner walls of the Siemens reactor have to be cooled to avoid silicon deposition on them (Ciftja et al., 2008).

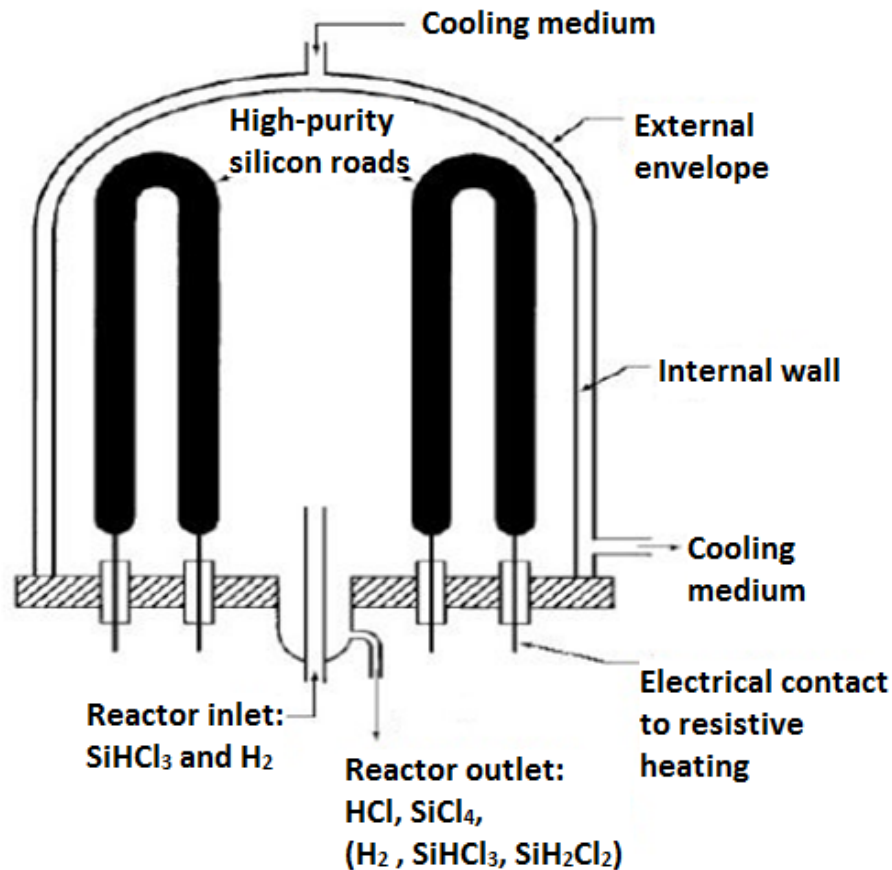


Figure 6.3: Schematic representation of the Siemens bell-jar reactor for SoG-Si production (Ciftja et al., 2008, edited for readability).

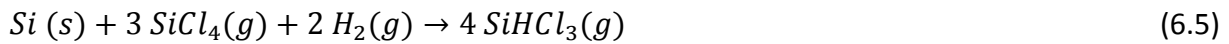
There are some drawbacks of using the modified Siemens process for SoG-Si production. The modified Siemens process is very energy intensive and demands roughly 200 kWh/kg SoG-Si (Amendola, 2011). Not all of the TCS feed into the Siemens reactor deposits on the silicon rods. Only 20-25% of the silicon in the TCS is deposited onto the rods (Odden et al., 2008). The rest leaves the reactor together with the off-gas. The TCS and STC leaving the reactor can be recycled and reused.

The TCS and STC produced during the modified Siemens process require careful handling, because they are explosive in the presence of water and hydrochloric acid. In addition, they are also highly volatile, corrosive and toxic (Braga et al., 2008).

### 6.2.3 Union Carbide process

The Union Carbide process is similar to the modified Siemens process, except that this process uses silane gas ( $\text{SiH}_4$ ) as precursor material for SoG-Si production instead of

trichlorosilane (TCS) gas. First, tetrachlorosilane (STC) is reduced by hydrogen through a mass bed of MG-Si in a fluidized bed reactor, producing TCS. Equation 5.2 and equation 5.3 is then replaced by the following equation:



After several purification steps, where TCS is converted back to silane, SoG-Si is produced by thermal decomposition of silane gas in a Siemens bell-jar reactor (see chapter 6.2.2). This can be described by following equation:



The solar power company Renewable Energy Corporation (REC) uses this technique. Some advantages with this process are that the pyrolysis in the Siemens reactor can be operated at a lower temperature than the modified Siemens process, the conversion efficiency is higher and no corrosive compounds are produced (Ciftja et al., 2008). However, this process requires more purification steps than the modified Siemens process before the silane-compound can enter the Siemens reactor.

#### 6.2.4 Fluidized Bed Reactor process

The Fluidized Bed Reactor (FBR) process also makes use of silane gas, but is different from the Union Carbide Process with regards to how the silane gas is deposited and transformed into SoG-Si in the final step. FBR uses seed granules of purified silicon, instead of high-purity silicon rods for the silicon deposition (REC, 2013a). The Siemens bell-jar reactor in the final step is replaced by a fluidized bed reactor.

Figure 6.4 illustrate the FBR process. The silicon seed granules are fed into the fluidized bed reactor, while heated silane gas and hydrogen gas enters below in the reactor and exits above. The silicon granules are "fluidized" by the stream of gas, making them flow like a liquid, and the silane gas is decomposed and deposits silicon layers onto the granules (REC, 2013a). The reaction is the same as described in equation 6.6. The deposition causes the silicon granules to grow larger and heavier until they exit when they have reached a sufficient size. FBR is a continuously process where new silicon granules, silane gas and hydrogen gas are feed into the fluidized bed reactor at a steady rate.

Alternatively, trichlorosilane gas (TCS) can be used instead of silane gas. The company REC uses silane gas in their FBR process, while the company Wacker uses TCS gas.

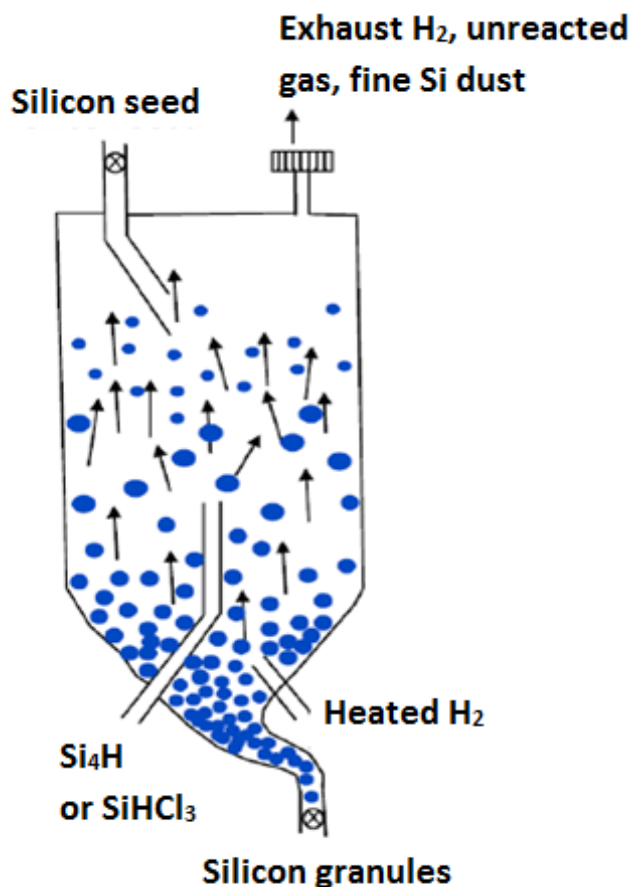


**Figure 6.4: Schematic representation of a fluidized bed reactor for SoG-Si production (Rosenkilde, 2012, edited for readability).**

FBR have several advantages. The energy consumption is less than when using a Siemens reactor, due to the fact that there is no need for cooling of the reactor during the silicon deposition. The silicon deposition also takes place at a lower temperature than for the modified Siemens process. According to REC (2013a), their FBR process uses 80-90% less energy than what the modified Siemens method does.

The silicon seed granules have a larger total surface area than the silicon rods used in the modified Siemens and Union Carbide process, so more SoG-Si is produced per cubic meter of reactor space (REC, 2013a). The Siemens and Union Carbide process are batch processes, while the FBR is a continuous process. FBR has therefore less downtime or setup effort required.

The final SoG-Si product of the FBR process is given in granules, a ready to use form, while the use of a Siemens reactor requires the breaking of rods into chunks of SoG-Si. Figure 6.5 illustrate the difference between these end products.



**Figure 6.5: SoG-Si in form of Siemens chunks (left) and FBR granules (right) (REC, 2011b).**

Disadvantages with FBR are the powder generation due to homogeneous decomposition of silane gas in the free reactor space and hydrogen absorption into the SoG-Si deposition layer (Ciftja et al., 2008).

### **6.3 Ingot**

The production of multicrystalline silicon is usually done by a method called direct solidification (Rosenkilde, 2012). Crystalline silicon improves the conversion efficiency of solar cells and leads to further purification of the SoG-Si. The direct solidification process starts with SoG-Si being put in quartz crucibles and then heated above its melting point in a special furnace. Then the molten SoG-Si is cooled down slowly from the bottom, crystallization takes place and the multicrystalline silicon is casted into ingot blocks (Rosenkilde, 2012). The ingot blocs may weigh up to 250 - 330 kg (de Wild-Scholten & Alsema, 2004; Luque & Hegedus, 2011).

When the ingot casting is done in one step, the fabrication technology is called the Bridgeman technology. This is the most used technology. However, if the melting of the SoG-Si and the subsequent cooling/crystallization happens in two different crucibles, the technology is called a block-casting process (Luque & Hegedus, 2011). Using the Bridgeman technology, the cooling of the molten SoG-Si is done by descending the crucible out of the furnace (Figure 6.6). During the block-casting process, the cooling of the molten SoG-Si is happening in a second crucible by adjusting the heating elements (Figure 6.7).

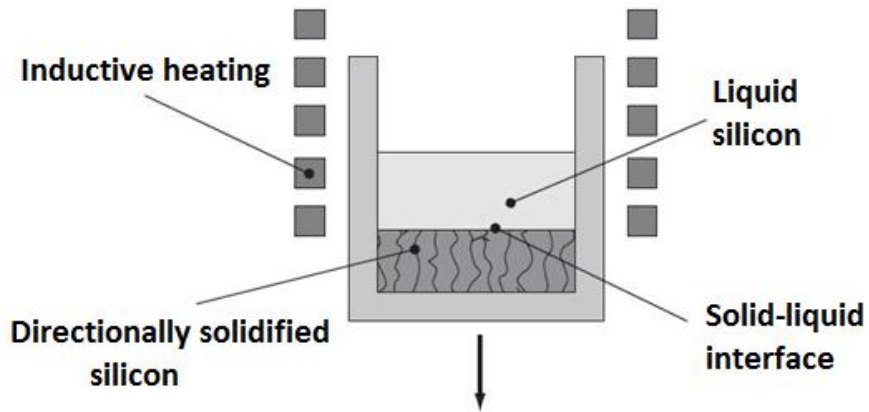


Figure 6.6: Multicrystalline ingot production using the Bridgeman technology (Luque & Hegedus, 2011, edited for readability).

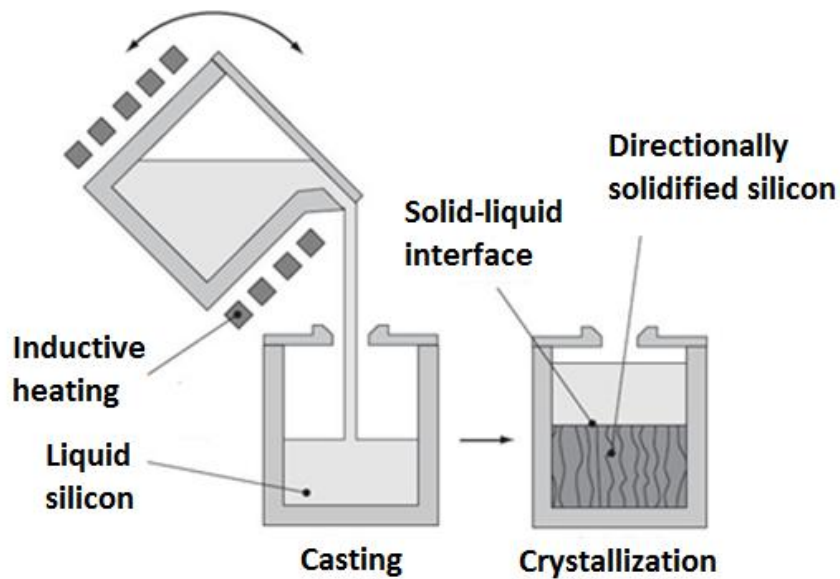


Figure 6.7: Multicrystalline ingot production using the block-casting process technology (Luque & Hegedus, 2011, edited for readability).

The edges of the ingot blocks have insufficient quality, due to contamination from the crucible, and are therefore cut off. Usually, the sides, the bottom and part of the top of the ingot blocks are remelted to produce subsequent ingots (de Wild-Scholten & Alsema, 2004).

## 6.4 Wafer

The mc-Si ingots have to be cut into wafers; very thin discs of mc-Si. The ingot is first cut into square blocks in order to meet dimensional specifications. Typical wafer sizes are 125x125 mm<sup>2</sup> or 156x156 mm<sup>2</sup> (used in this report). The mc-Si blocks are cut into wafers by multi wire sawing. The principle of this technology is showed in Figure 6.8.

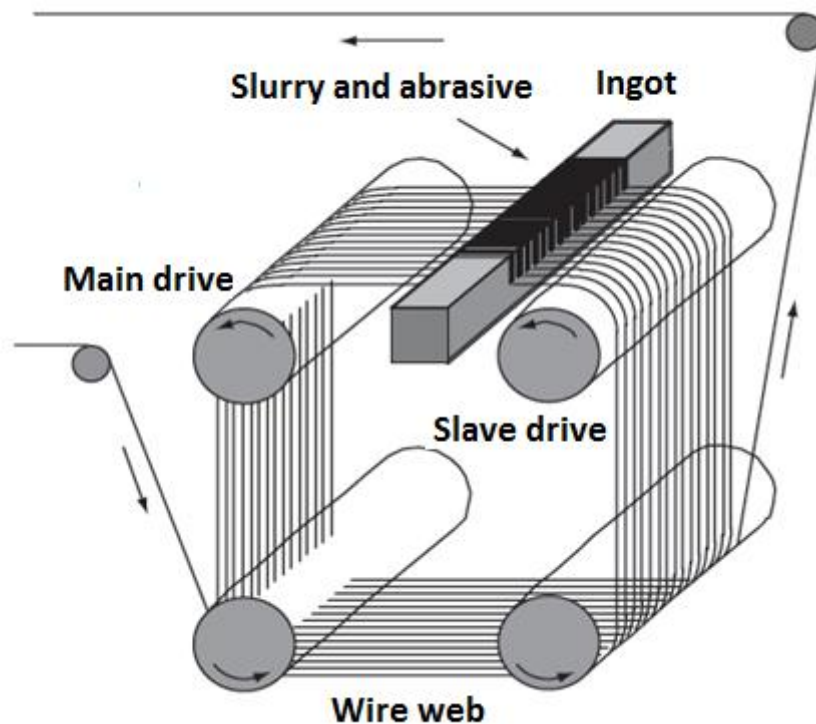


Figure 6.8: Principle sketch of multi wire sawing (Luque & Hegedus, 2011, edited for readability).

Briefly explained, a thin steel wire (140-200  $\mu\text{m}$ ) is supplied from a spool, wound around four moving rollers (wire guides) and tensioned in a way that in the end makes up a moving wire web (Luque & Hegedus, 2011). To be able to cut through the hard mc-Si columns, an abrasive slurry consisting of silicon carbide particles and PEG coolant (poly ethylene glycol), is supplied through nozzles over the wire web. The used slurry may be recycled. The mc-Si columns is pushed against this wire web and sliced into several thousand wafers simultaneously. This is the advantage of the multi wire sawing technology; a high wafer throughput. The wire is usually moving in one direction with a speed of 10 - 15 m/s during the cutting (Rosenkilde, 2012). A second spool collects the used wire.

Some of the mc-Si is lost as saw dust. This loss is called a kerf loss and is about 150-180  $\mu\text{m}$  per wafer produced (Rosenkilde, 2012). The final wafers typically have a thickness of 180-200  $\mu\text{m}$  (Jungbluth et. al., 2012).



**Figure 6.9: Multicrystalline silicon wafer (Rosenkilde, 2012).**

After the multi wire cutting, the wafers are cleaned with chemicals like e.g. tenside, sodium hydroxide, potassium hydroxide, acetic acid and hydrochloric acid (Jungbluth et al., 2012).

## **6.5 Multicrystalline silicon solar cell**

In order to transform the wafer into a solar cell, the wafer has to undergo several chemical, thermal and deposition treatments (Markvart, 2000). Particular important layers of the mc-Si solar cell are the n-type layer to form the p-n junction and two metal layers to form the electrical contacts. The main process steps will be described in the following:

**1. Surface cleaning and etching:** To remove microscopic damage to its surface, the wafer is subject to several wet cleaning steps in chemical baths. The wafer is then etched by alkaline solutions (sodium hydroxide or potassium hydroxide) to remove sawing parts.

**2. Phosphorus diffusion for p-n junction formation:** The front of the wafer has to be doped in order to create a p-n junction. Usually, the starting multicrystalline wafers are of p-type, i.e. boron-doped (Markvart, 2000). Phosphorus is a n-type impurity, and this substance is introduced to the front surface of the wafer. The phosphorus diffusion requires a high



temperature of 830-860°C (Luque & Hegedus, 2011). The doping process can be performed in two ways, either by use of a open tube quartz diffusion furnace or by use of a conveyor belt furnace.

When using an open tube quartz diffusion furnace for the phosphorus diffusion (Figure 6.10), the dopant source is a liquid of phosphorus oxychloride ( $\text{POCl}_3$ ). The wafers are loaded in quartz boats and placed in the quartz furnace. The dopant is carried into the quartz furnace by bubbling nitrogen through it, while oxygen is simultaneously fed into the furnace. The oxygen reacts with the dopant and creates phosphorus oxide ( $\text{P}_2\text{O}_5$ ), which in turn transforms into silicon dioxide ( $\text{SiO}_2$ ) and atomic phosphorus. The phosphorus then diffuses into the wafer. After the diffusion, oxygen left on the wafer is chemically removed.

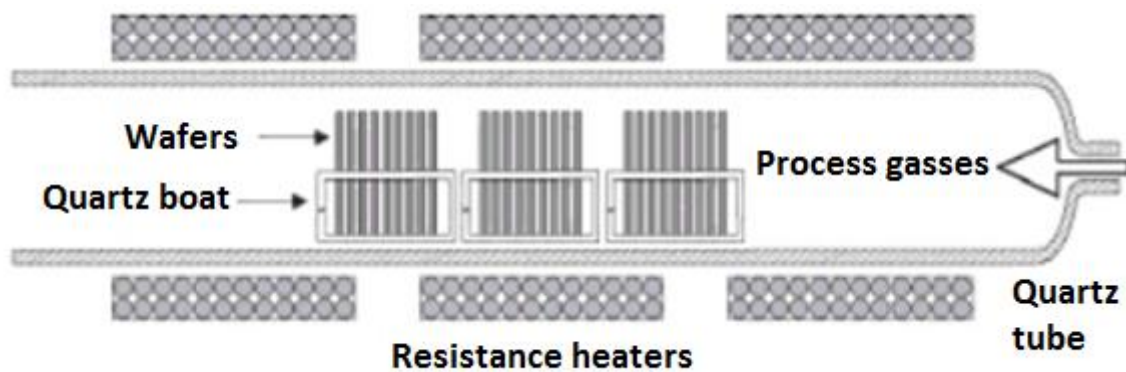


**Figure 6.10: Open tube quartz diffusion furnace for phosphorus diffusion (during p-n junction formation in the mc-Si solar cell production) (Luque & Hegedus, 2011, edited for readability).**

The phosphorus diffusion is performed in a continuous way and with a higher throughput than when using a conveyor belt furnace (Figure 6.11). Before being fed into the conveyor belt furnace, the wafers are sprayed with liquid containing phosphorus (dopant).

Alternatively, the dopant can be screen printed, spun-on, deposited by CVD or applied as a gas into the wafer (Luque & Hegedus, 2011). The temperature in the furnace is controlled by infrared heating. Disadvantages with the conveyor belt furnace are that ambient air can get into the furnace, and that the hot conveyor belt can introduce metallic impurities.

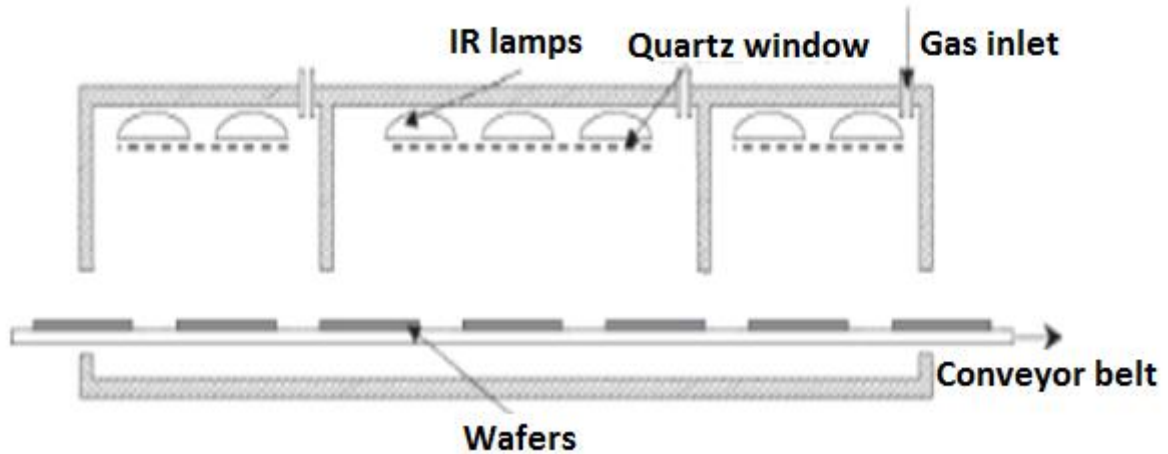


**Figure 6.11: Conveyor belt furnace for phosphorus diffusion (during p-n junction formation in the mc-Si solar cell production) (Luque & Hegedus, 2011, edited for readability).**

The edges and back surface of the wafers have also been exposed for phosphorus diffusion. This has created unwanted n-type regions. To remove these regions, the wafers are placed in a plasma etching machine where these regions are etched off.

**3. Front and back metal contacts:** Screen printing is used for the formation of electrical contacts. A mesh (grid) of steel wires embedded in an emulsion makes up the screen (Markvart, 2000). At the places where metal is to be deposited, the emulsion is removed by photographic techniques. A conductive metal paste is then squeezed through the screen onto the wafer and deposits the metal grid (Figure 6.12). Usually, a paste containing silver is used for contacting the phosphorus diffused front of the wafer, while another paste containing a mixture of silver and aluminium is used for contacting the bulk p-type silicon wafer at the back.

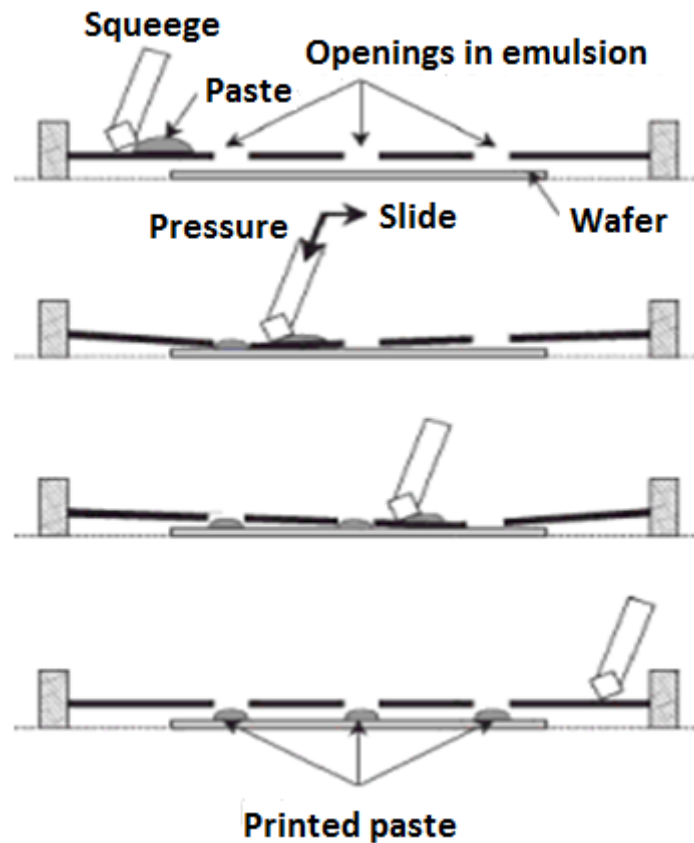


Figure 6.12: Screen printing for electrical contacts during mc-Si solar cell production (Luque and Hegedus, 2011, edited for readability).

After the screen printing, the pastes undergo a firing process in a conveyor belt furnace at high temperature. This causes the metal electrodes to be connected with the silicon electrodes (LDK Solar, 2011a), forming a conductive path for the electrical current. There are also small amounts of glass in the paste which provide a good adhesion to the silicon surface (Markvart, 2000).

**4. Antireflection layer deposition:** An anti-reflective coating (ARC) is deposited onto the front surface of the solar cell in order to enhance its absorption of sunlight (LDK Solar, 2011a). Currently, silicon nitride ( $\text{Si}_3\text{N}_4$ ) is the preferred option for antireflection coating, because it has beneficial effects on the electronic properties of the silicon wafers. Titanium oxide ( $\text{TiO}_2$ ) is another option. The silicon nitride is deposited onto the front surface of the wafer by using atmospheric pressure chemical vapour deposition (APCVD), involving the reaction of silane gas and ammonia (Luque & Hegedus, 2011) (see Figure 6.13). Sometimes step 4 is performed before the deposition of electric contacts (step 3).

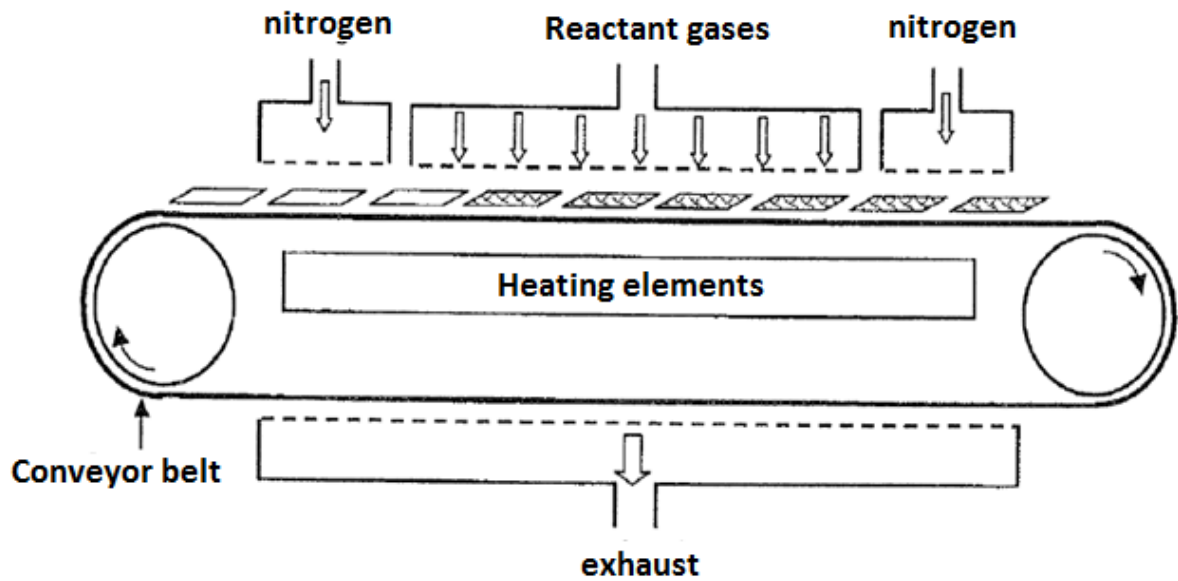


Figure 6.13: Atmospheric pressure chemical vapour deposition system for the deposition of antireflective coating onto the front surfaces of the mc-Si solar cells (Markvart, 2000, edited for readability).

**5. Testing and sorting:** Testing is done under standard conditions, before the solar cells are sorted into classes according to current and voltage performance.

A picture of the front surface of a finished multicrystalline silicon solar cell can be seen in Figure 6.14. The thin horizontal metal strips, called fingers, supply electrical current to a larger bus bar (the two vertical strips). Typical dimensions for the metal grid is 100-200  $\mu\text{m}$  wide fingers (Khan, 2009), spaced with 3 mm, and 2 mm wide bus bars (Markvart, 2000).

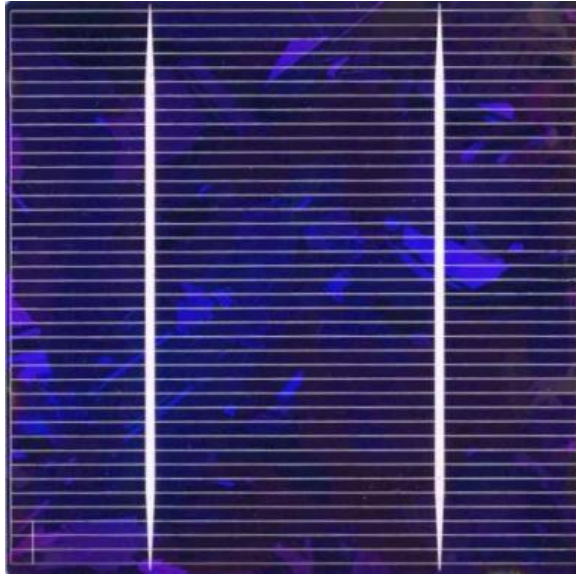


Figure 6.14: Multicrystalline silicon solar cell (front) (Khan, 2009).

## 6.6 Multicrystalline silicon PV module

The solar cells are interconnected in series with copper strings and encapsulated to form a module. Today, most of the modules on the markets consist of 60-72 mc-Si cells (Jungbluth et al., 2012). A typical module has the following composition of layers:

- 1. Front cover of tempered glass or low iron solar glass:** Protects against the elements and maximizes the conversion efficiency of the PV module.
- 2. Encapsulant:** A transparent, electrically insulating, thermoplastic polymer, most commonly ethylene vinyl acetate (EVA). The back of the solar cells may also be covered with a layer of EVA.
- 3. Solar cells and metal interconnectors.**
- 4. Foil of Tedlar (most used), Tefzel or Mylar forming the back cover.** (Tedlar is a mix of polyester and polyvinyl fluoride).

To protect against humidity an additional layer of aluminium foil can be included in the sandwich of the layers above. By applying heat at about 150°C and pressure under vacuum, the layers are laminated (Markvart, 2000). For improving the adhesion between the layers, primers are used. Connections are insulated. Finally, the edges of the module are purified, sealed and protected with an aluminium frame.

A junction box is applied to the module to enable connections among modules when they are series connected to form a PV system (Solar World, 2012).

## 7 Thin film PV

The first section in this chapter will provide an overview on the general structure of thin film solar cells. The second and third sections will give an overview of what is perceived as advantages and disadvantages of thin film PV technology compared to crystalline silicon PV technology.

### 7.1 Configuration and structure of thin film solar cells

Thin film solar cells are built up of several, very thin layers of different materials. The thickness of a thin film layer may vary from a few nanometers to tens of micrometers (Chopra et al., 2004). The term "thin film" refers to the processes used to deposit the film layers, and not to the thinness of the film layer (Solar Thin Films, 2007b). Today, there is mainly three thin film PV technologies which are produced commercially: Amorphous silicon (a-Si), cadmium telluride (CdTe) and copper indium gallium diselenide (Cu(In, Ga)Se<sub>2</sub>, CIGS). These names refers to the semiconductor material being used for solar absorption in the thin film solar cell. A purity of at least 99,999% is required for the semiconductors deployed in the production of thin film PV modules (Marwede et al., 2013). Due to their high optical absorption coefficient, a layer of approximately 2 μm is sufficient to absorb most of the useful parts of the light spectrum. This report will focus on the two thin film PV technologies with the currently highest conversion efficiencies, CdTe and CIGS.

In general, thin film solar cells consist of substrate, front electrical contact, buffer layer (n-type), absorber layer (p-type) and back electrical contact. The substrate can be either glass, metal or polymer foil. The substrate constitute a passive layer in the solar cell and has to be mechanically stable, have a matching thermal expansion coefficient with the other deposited layers and be inert during the solar cell manufacturing (Chopra et al., 2004). The metal foils can be made of e.g. stainless steel (SS), molybdenum (Mo) or titanium (Ti), while the polymer foils can be made of e.g. polyimide (PI), polyethylene terephthalate (PET) and polyethylene naphthalate (PEN) (Aliyu et al., 2012).

Thin film solar cells can be grown in a substrate or a superstrate configuration, depending on the direction through which light enters the solar cell (Aliyu et al., 2012). The two types of configurations are illustrated in Figure 7.1: If the solar cell has a superstrate structure, the light enters the solar cell through the substrate base on which the cell layers were deposited. This means that the substrate has to be reasonable transparent, i.e, glass or polymer foil, to allow enough light to pass into the cell (Aliyu et al., 2012). If the solar cell has a substrate structure, the light enters through the "opposite" side, trough the front contact. Metal foils can therefore only be used in the substrate structure, while polymer foils can be used in both configurations. A substrate configuration requires an encapsulating glass, while this is not required for a superstrate configuration (Biccari, 2012c). Which type of configuration is

used for the different types of thin film solar cells depends on which configuration yields the highest solar cell conversion efficiency and which type of substrate is used.

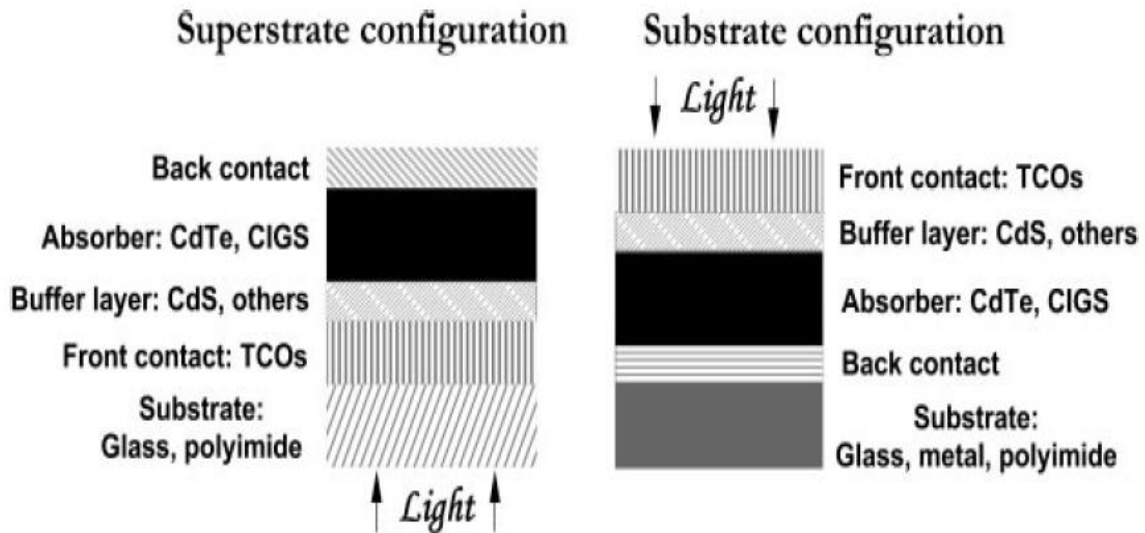


**Figure 7.1: Schematic cross-section of superstrate configuration (left) and substrate configuration (right) for thin film solar cells (Romeo et al., 2004).**

The front contact is a transparent conductive oxide (TCO). A TCO is a n-type semiconductor with good electrical conductivity, ensuring transport of the photo-generated current to the external circuit without too much resistance loss, and high transparency in the visible spectrum, ensuring that enough light is let through to the underlying parts of the solar cell. (Chopra et al., 2004; Singh & Patra, 2010).

The buffer layer and the absorber layer are two different semiconductor materials which forms a heterojunction in the solar cell. An electrical field is created in the interface between these two layers (see chapter 3.1). The main role of a buffer layer is to passivate the surface of the absorber layer (Malm, 2008). A maximum amount of irradiation should be able to pass through the buffer layer, in order to reach the junction region and absorber layer, i.e. no photocurrent generation occurs in the buffer layer (Chopra et al., 2004). The buffer layer should be as thin as possible and have a bandgap as high as possible to ensure minimum resistive loss and low series resistance. The front electrical contact (i.e. the TCO) is applied to the n-type buffer layer, while the back electrical contact is applied to the p-type absorber layer.

## 7.2 Advantages

Compared with crystalline silicon solar cells, thin film solar cells have several advantages which makes them an interesting and competitive alternative, especially for future global growth in PV production and installed capacity. This section will present some of the perceived advantages of thin film PV technology compared to the crystalline silicon PV technology.

Thin film solar cells have up to 99% lower semiconductor material requirements due to the fact that they are made of semiconductors with direct bandgap (see chapter 3.1), absorbing the solar spectrum much more efficiently than crystalline silicon and making very thin layers sufficient for light absorption (MiaSolé, 2011; Solar Construction Sustainability Technology (SOLTECTURE), 2013;). Silicon is an indirect bandgap material, requiring wafers of at least 50  $\mu\text{m}$  to ensure effective light absorption (Chopra et al., 2004).

Fewer process steps ( $\approx 1/3$  less) are required in the production of thin film solar cells, making the thin film PV value chain significantly more energy efficient than the crystalline silicon PV value chain (SOLTECTURE, 2013). Especially avoiding the energy intensive process steps of metallurgical grade- and solar grade silicon production is beneficial. The energy consumption in the thin film PV value chain is at least 50% lower than for the crystalline silicon PV value chain (SOLTECTURE, 2013). It should also be noted that CdTe and CIGS solar cells do not have to undergo the passivation process like crystalline silicon solar cells have to (Razykov et al., 2011).

To create interconnections between crystalline silicon solar cells, metal ribbons are attached to the cells at discrete points (Solar Thin Film Inc., 2007b). Each solar cell must be provided with a front- and back metal grid. Each of these front contacts must be connected to the back contact grid of the next solar cell for series connection (McEvoy et al., 2012). When producing thin film PV modules, the production process results in integrally connected modules, i.e. monolithic interconnections of individual cells, avoiding costly individual cell handling and separate interconnections (Markvart, 2000). This means that with the thin film PV technology, the complete module can be produced with the cell interconnections made during layers deposition (see chapters 8.8 and 9.8 for further details).

Usually, rigid glass is used as the substrate for thin film PV modules. Glass requires careful handling to avoid damages and substantial support for fabrication and installation due to its weight. However, thin film solar cells can also be grown on flexible, low weight substrates like metal- or polymer foils, enabling them to be utilized in a range of applications. They can be utilized for Building Integrated Photovoltaic (BIPV), where they are laminated directly into building facades and other surfaces. Flexible thin film PV can achieve a high specific power of over 2 kW/kg, which make them very attractive for space applications (Aliyu et al., 2012). Flexible substrates enable continuously manufacturing (i.e. roll-to-roll manufacturing), offering advantages such as lower equipment size (up to 30 times smaller, i.e. lower costs),



higher material utilization, increased fabrication scalability and high speed of deposition (Aliyu et al., 2012).

Thin film PV technologies have performance attributes. When their cell temperatures increase, solar cells become less efficient at converting solar energy into electricity (Jungbluth et al., 2012). The conversion efficiency of CdTe and CIGS solar cells are less susceptible to cell temperature increases, enabling CdTe and CIGS PV modules to generate relatively more electricity under high ambient (and therefore high cell) temperatures than silicon crystalline PV modules (Jungbluth et al., 2012; DayStar Technologies Inc, 2013b). CdTe and CIGS PV modules also absorb low and diffuse light under cloudy and overcast weather, shading, dawn and dusk conditions, while crystalline silicon PV modules operate much less efficiently during such conditions (Jungbluth et al., 2012; AVANCIS GmbH, 2013). This makes thin film PV modules suited for regions with less direct sunlight, such as Northern Europe (DayStar Technologies Inc, 2013b).

### **7.3 Disadvantages**

This section will present some of the perceived disadvantages of thin film PV technology compared to the crystalline silicon technology.

So far, thin film solar cells/PV modules, have been less efficient than the crystalline silicon ones (see chapter 3.2.1). However, the conversion efficiencies achieved in research laboratories have proven to be promising. The record for conversion efficiencies for crystalline silicon solar cells are 25,0% for sc-Si and 20,4% for mc-Si, while the conversion efficiencies on module levels are 22,9% for sc-Si and 18,5% for mc-Si. CdTe and CIGS technology are not far from reaching the conversion efficiency levels of mc-Si: On solar cell levels, both CdTe and CIGS solar cells have achieved a conversion efficiency of 19,6%. CdTe PV modules has a conversion efficiency record of 16,1% and CIGS a record of 15,7% (all efficiency numbers from Green et al., 2013). Note that all of these results have been confirmed under standard conditions: Irradiance  $1 \text{ kW/m}^2$ , standard reference AM 1,5 spectrum and temperature  $25^\circ\text{C}$ . Even though higher conversion efficiency records have been published, these have not been verified under standard conditions.

CdTe and CIGS technology employ rare metals like tellurium (Te), indium (In) and gallium (Ga). These metals are by-products of other "parent" metals: Tellurium is mainly a by-product of copper- and nickel-mining and processing (primary source), but is also produced in a certain amount during mining of zinc, gold and lead (Marwede & Reller, 2012; Simon et al., 2013). Indium is a by-product of zinc production. Gallium is extracted from bauxite and zinc ores and is a by-product of aluminium production. The gallium content is usually very low and the extraction difficult to perform (Zuser & Rechberger, 2011). Better refining methods are required to achieve a higher gallium production.

Cost and availability of tellurium, indium and gallium may limit the market growth of CdTe and CIGS PV technologies, in particular for use in large-scale terrestrial applications (Razykov et al., 2011; Marwede et al., 2013). Several studies have been performed to investigate this issue. CdTe PV systems accounted for 20-40% of the total global tellurium production in 2010 (Marwede & Reller, 2012). Some studies have shown that accessible tellurium reserves and annual tellurium production to a certain extent can limit the market growth of CdTe PV systems, while others have found an absolute tellurium shortage to be unlikely, but with the possibility of temporarily bottlenecks in supply, especially if the tellurium production capacities are not scaled up fast enough. (Marwede & Reller, 2012; Marwede et al., 2013). Provided a substantially improvement in material efficiency and an increased built up of efficient collection and recycling systems, Marwede & Reller (2012) showed that a significant share of tellurium consumed in CdTe PV modules could be supplied from PV production scrap, i.e. excess material from deposition processes and material in rejected PV modules and from end-of-life PV modules. Concerning indium, Dhere (2007) stated that an estimated amount of 20 GW CIGS PV modules could be produced per year, without overstraining the indium supply. If the indium from CIGS modules were recycled, the production of CIGS PV modules could be increased to 50 GW per year (Dhere, 2007). In the end, the future technological progress of the thin film solar cells themselves and the production processes will influence the amount of scarce metals used in the PV modules.

There has been some concerns related to the potential negative environmental impacts of cadmium (Cd) contamination from CdTe and CIGS PV modules. Cadmium can be found in the CdTe absorber layer in the CdTe PV modules and in the CdS buffer layer in both the CdTe and CIGS PV modules. CdTe PV systems accounted for 0,6% of the total cadmium amount consumed in 2005 (Raugei & Fthenakis, 2010). CdTe PV technology has no chance to do away with cadmium, while CIGS PV technology can eliminate the CdS buffer layer by using another type of buffer material (Razykov et al., 2011, see chapter 9.5.1). Elemental cadmium is highly toxic. It can cause adverse effects on kidney and bone, and give lung cancer (Biccari, 2012a). Cadmium in a non-metallic form, like CdTe and CdS, is not so toxic as metal cadmium, they have an extremely low water solubility and a low vapour pressure (Biccari, 2012a).

It has been done extensive research to map the risks associated with using cadmium in thin film PV modules. It has been shown that cadmium is a stable compound as long as it is contained within the thin film PV modules, i.e. enclosed and sealed within two glass sheets (Raugei & Fthenakis, 2010). During a building fire, the risk of cadmium emissions to the environment are found to be minimal, as the CdTe is captured in the molten glass (Razykov et al., 2011). CdTe and CIGS PV modules should be properly disposed of during manufacturing rejections and after end-of-life to ensure safe recovery of cadmium and prevent it from leaking into the environment.

Cadmium is an inevitable by-product of zinc- (primary source), lead- and copper-mining, meaning that the annual amounts of raw cadmium generated are entirely determined by the production rates of these metals (Razykov et al., 2011). The use of cadmium in CdTe PV modules may be considered as beneficial to the global environment by sequestering a non-negligible amount of cadmium from otherwise potentially harmful left-over stockpiles (Raugei & Fthenakis, 2010). Previous research has shown that the cadmium emissions from the life cycle of CdTe PV systems are one to three orders of magnitude lower than the cadmium emissions from other types of electricity generation (Marwede & Reller, 2012).

## 8 CdTe PV production value chain

In this chapter, the value chain of the CdTe based PV production and processing technologies will be explained. The background for the CdTe PV technology will be presented first, before the different production steps making up the foreground system described in Figure 5.2 will be explained. Note that only the value chain upstream of the PV module, including the module itself, will be presented in this chapter.

### 8.1 Background

Cadmium telluride (CdTe) belongs to the II-VI semiconductor family. It is a chalcogenide semiconductor, meaning that it consists of one electropositive element (few electrons in the outer shell, easily "lost", here Cd) and one chalcogen element (belongs to group 16 of the periodic table, here Te). Its chemical structure is shown in Figure 8.1.

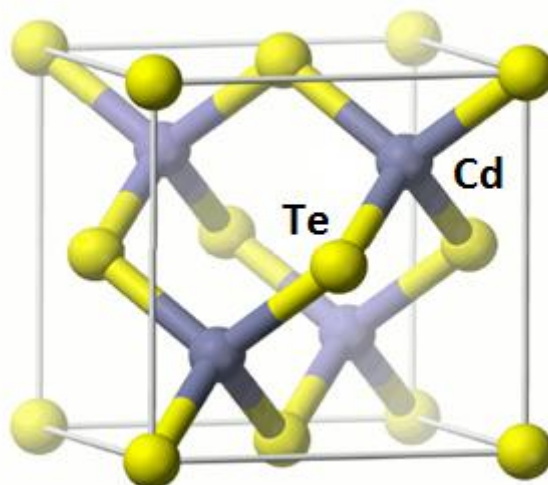


**Figure 8.1: Chemical structure of CdTe (Biccari, 2012a, edited for readability)**

CdTe is a direct-bandgap material with a bandgap energy of 1,45 eV, which is close to the ideal value for PV conversion efficiency (Fang et al., 2011; see chapter 3.1). In addition to this, CdTe has a high chemical and thermal stability, p-type conductivity and a very high optical absorption coefficient of  $10^5 \text{ cm}^{-1}$  (Morales-Acevedo, 2006; Fang et al, 2011). All in all, this makes CdTe an excellent material for PV application. CdTe solar cells usually consist

of a p-type absorber layer of CdTe and a n-type buffer layer of CdS (cadmium sulfide), forming a heterojunction.

CdTe is the thin film PV technology which has achieved the highest production level so far (Chu, 2011). One PV producer has been particularly important for the commercial mass production of CdTe PV modules; the company First Solar. This company became the first PV producer in the world to exceed 1 GW per year production rate in 2009 (Wolden et al., 2011). In 2012 First Solar was the second largest PV producer in the world, independent of technology (Lian, 2013).

## 8.2 Substrate

CdTe solar cells can be grown in a substrate or a superstrate configuration (see chapter 7.1). In the case of CdTe PV, the superstrate configuration yields a higher efficiency and this is therefore the most commonly used configuration for CdTe solar cells. The type of glass used for substrate depends on the temperature of the following deposition processes. A low-cost, soda-lime glass (SLG) can be used for temperatures below 550°C, while an alkali-free glass, e.g. borosilicate, can be used for higher temperatures, typically 550-600°C (Romeo et al., 2004; Chopra et al., 2004). Presently, the borosilicate glass is considered to be too expensive to utilize in commercial production (McEvoy et al., 2012). To reduce the reflection at the air/glass interface, an antireflective coating may be applied on the rear surface of the substrate glass, i.e. the surface of the substrate facing towards the incoming radiation (Razykov et al., 2011; EV Group, 2013).

If the CdTe solar cell is grown in a substrate configuration, this requires a substrate of metal foil or a metal-coated glass substrate (Razykov et al., 2011). Using this type of configuration is not actively pursued due to the limiting back contact. The back contact exhibits poor quality because the interface is degraded during the high-temperature processing of the heterojunction (CdTe/CdS) and cells are shunted (Razykov et al., 2011).

## 8.3 Front electrical contact

The front contact is a highly transparent and n-type conducting layer of TCO. In order to form an ohmic contact and have a good band alignment with the n-CdS buffer layer, the TCO layer needs to have an electron affinity below that of CdS. This upper limit is an electron affinity of 4.5 eV (Romeo et al., 2004). For CdTe solar cells, the most commonly used TCOs are fluorine-doped tin oxide ( $\text{SnO}_2:\text{F}$ , FTO) or tin-doped indium oxide ( $\text{In}_2\text{O}_3:\text{Sn}$ , ITO). There is a drawback of using ITO as front contact: In addition to being an expensive material, ITO is sensitive to annealing treatment, which may alter the electron affinity (Razykov et al., 2011). The TCO is approximately 0.2-1.0  $\mu\text{m}$  thick and is usually deposited onto the substrate by spray pyrolysis, atmospheric pressure chemical vapour deposition or sputtering (Biccarri, 2012a).

High-efficient PV-devices may be produced utilizing a bi-layer of TCOs. The bi-layer consist of a low-resistive TCO and then a much thinner layer of a high-resistive TCO. The thin high-resistive TCO layer minimizes the forward current through pinholes in the buffer layer (Morales-Acevedo, 2006). The most common example on use of bi-layer in the CdTe solar cell structure is a layer of ITO (deposited onto the substrate glass), and then a very thin layer of tin oxide ( $\text{SnO}_2$ ) (Chopra et al., 2004).

Other TCOs like aluminium-doped zinc oxide (AZO) and cadmium stannate ( $\text{Cd}_2\text{SnO}_4$ , CTO), together with a thin high-resistive layer of zinc stannate ( $\text{Zn}_2\text{SnO}_4$ , ZTO), have also been investigated with varying success, but are so far not yet used in commercial production of CdTe PV modules. CTO has shown better performance than both FTO and ITO, by being more transmissive and conductive, but it requires annealing processes at elevated temperatures, which are not suited for the use of soda-lime glass as a substrate (Miles et al., 2005; McEvoy et al, 2012). The use of AZO has resulted in unstable TCO films. Examples of papers investigating these types of front contact layer for CdTe solar cells are: Wu et al. (2001), Gupta & Compaan (2004) and Wu et al. (2005).

## **8.4 Buffer layer**

The buffer layer in the CdTe solar cell is deposited onto the front contact. It is almost always made of n-type CdS, which has a bandgap of 2,42 eV (Biccari, 2012a). Since the CdS is transparent for light with wavelengths down to 515 nm, the buffer layer is also referred to as the window layer in the CdTe solar cell structure (McIntyre, 2010).

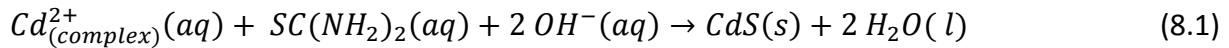
The CdS layer forms a heterojunction with the CdTe layer in the solar cell. In order to minimize the photon absorption losses in the CdS layer, enabling a maximum number of photons to reach the CdTe layer, a thin CdS layer of 50-200 nm is desirable. Finding the right thickness of the buffer layer is a difficult balance, because if the layer is too thin, this may lead to a lower open-circuit voltage and performance ratio through shunting in the device. A thin buffer layer is also desirable due to the high resistance of CdS. The last years progress in the development of CdTe solar cell has been made by reducing the thickness of the CdS layer (Razykov et al., 2011).

Various methods can be used for deposition of the CdS layer: Chemical bath deposition (CBD), evaporation, close-spaced sublimation (CSS), vapour transport deposition (VTD), metal-organic chemical vapour deposition (MOCVD) and sputtering (Razykov et al., 2011; Biccari, 2012a). The most common method, CBD, will be explained in the next subsection.

### **8.4.1 Chemical bath deposition**

The principle of chemical bath deposition is that a substrate is immersed in a dilute solution containing metal ions and a source of hydroxide, sulfide or selenide ions (Nair et al., 1998). A

thin semiconductor film is deposited onto the substrate. In the case of CdS-deposition using CBD, the glass substrates are mounted in an aqueous alkaline bath with a temperature of around 70 -80°C. Cd<sup>2+</sup> - ions, from cadmium sulfate (CdSO<sub>4</sub>) or cadmium iodide (CdI<sub>2</sub>), and S<sup>2-</sup> - ions, from thiourea (SC(NH<sub>2</sub>)<sub>2</sub>), are slowly released and then condensate onto the TCO-coated glass substrate, forming a CdS-layer (Khallaf et al., 2008; Biccari, 2012a). The simplified reaction can be described by the following equation (Cunningham et al., 2002):



CBD gives the possibility to form very thin and continuous layers. This allows for a high transmission of low-wavelength photons through the buffer layer, increasing the absorption in the CdTe layer and thereby increasing the solar cell efficiency (Romeo et al., 2004).

## 8.5 Absorber layer

The CdTe absorber layer is deposited onto the buffer layer. This layer is p-doped due to Cd deficiencies, and no additional doping is required (McEvoy et al., 2012). The CdTe PV technology is very flexible in terms of manufacturing method. Both vacuum and non-vacuum deposition methods, classified into high-temperature and low-temperature processes, can be used in the deposition of the CdTe layer. These methods are given in Table 8.1. All of the deposition methods have achieved solar cell conversion efficiencies above 10%. The thickness of the CdTe layer varies from 2,0-7,0 µm depending on the type of deposition method (McEvoy et al., 2012).

**Table 8.A: Methods for CdTe film deposition (Razykov et al., 2011).**

<b>1.</b>	Thermal evaporation	<b>8.</b>	Sputtering
<b>2.</b>	Electrodeposition	<b>9.</b>	Hot-wall evaporation
<b>3.</b>	Spray pyrolysis	<b>10.</b>	Ion-assisted evaporation
<b>4.</b>	Chemical vapour deposition	<b>11.</b>	Metal-organic chemical vapour deposition
<b>5.</b>	Close-spaced sublimation	<b>12.</b>	Vapour transport deposition
<b>6.</b>	Chemical molecular-beam deposition	<b>13.</b>	Molecular-beam epitaxy
<b>7.</b>	Screen printing	<b>14.</b>	Atomic layer deposition

Typical high-temperature processes (above 500°C) are close-space sublimation and vapour transport deposition, while typical low-temperature processes (below 450°C) are electrodeposition (ED), high-vacuum evaporation (HVE), sputtering and screen printing (SP) (Razykov et al., 2011). Only a few of the processes mentioned in Table 8.1 are suitable for large-scale production, these are briefly explained in the next subsections.

### 8.5.1 Close-spaced sublimation

Close-space sublimation is characterized by a close space between the source and the substrate (see Figure 8.2). This deposition technique utilizes the temperature difference as the driving force for the deposition (Biccari, 2012a). CdTe in the form of powder or granulate is sublimed in vacuum and condenses on the substrate at temperatures between 450 and 600°C (McEvoy et al., 2012). The process have a high material yield and can achieve a deposition rate above 10 μm/min (McEvoy et al., 2012).

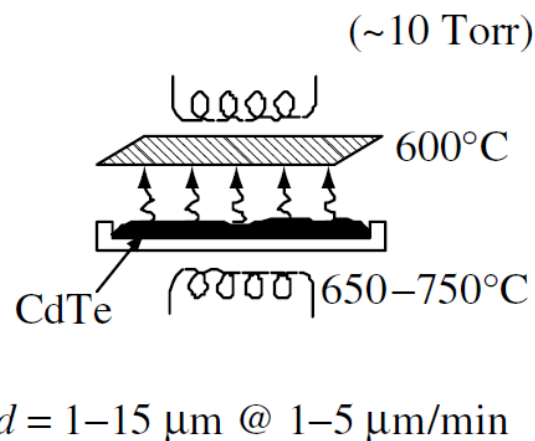
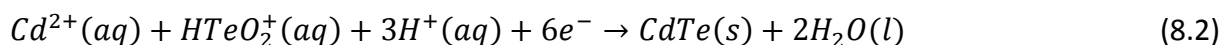


**Figure 8.2:** Schematic illustration of close-spaced sublimation of the CdTe absorber layer (Luque & Hegedus, 2011). The substrate is the cross-lined rectangle. Film thickness  $d$  and growth rate are shown at the bottom of the figure.

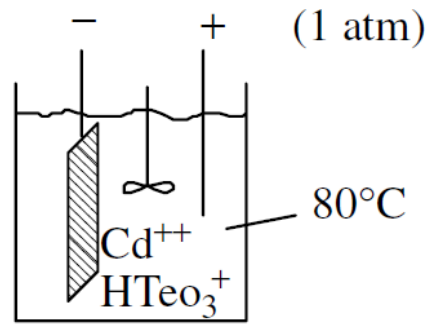
### 8.5.2 Electrodeposition

During electrodeposition (see Figure 8.3), the substrate is immersed into an aqueous solution of e.g.  $\text{CdSO}_4$  and  $\text{Te}_2\text{O}_3$ , holding an temperature of around 80-90°C. An electrical potential is then evenly applied to the front contact layer (TCO) on the substrate. This starts galvanic reduction of Cd and Te from  $\text{Cd}^{2+}$  and  $\text{HTeO}_2^+$  ions in the solution, and a CdTe layer is formed on the substrate. The total reaction can be described by the following equation (McEvoy et al., 2012):



After this reaction, the CdTe has n-type conductivity, but a doping conversion into p-type is achieved by thermal post annealing in a chlorine-containing environment (McEvoy et al., 2012). The process have a low deposition rate, but this can be compensated for by doing the deposition of CdTe layers on a number of substrates in parallel.



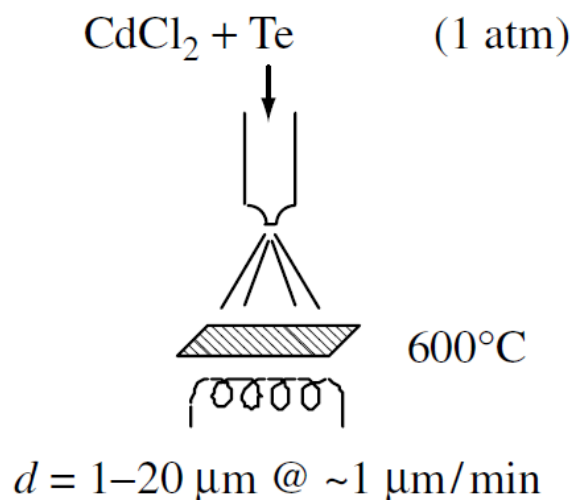


$$d = 1-2 \mu\text{m} @ 0.01-0.1 \mu\text{m}/\text{min}$$

**Figure 8.3:** Schematic illustration of electrodeposition of the CdTe absorber layer (Luque & Hegedus, 2011). The substrate is the cross-lined rectangle. Film thickness  $d$  and growth rate are shown at the bottom of the figure.

### 8.5.3 Spray pyrolysis

Spray pyrolysis (see Figure 8.4) utilizes a slurry containing CdTe, CdCl<sub>2</sub> and a carrier, e.g. propylene glycol (Luque & Hegedus, 2011). The slurry is sprayed onto a heated substrate. When the droplets hit the surface, the compounds are liberated and a CdTe layer is formed on the surface (McEvoy et al., 2012). The process does not require vacuum conditions. It is also sometimes referred to as chemical spraying.



$$d = 1-20 \mu\text{m} @ \sim 1 \mu\text{m}/\text{min}$$

**Figure 8.4:** Schematic illustration of spray pyrolysis of the CdTe absorber layer (Luque & Hegedus, 2011). The substrate is the cross-lined rectangle. Film thickness  $d$  and growth rate are shown at the bottom of the figure.

#### 8.5.4 Screen printing

During screen printing (see Figure 8.5), a Cd- and Te-containing slurry/paste is applied to the substrate through a screen, before undergoing a thermal reaction under the influence of added  $\text{CdCl}_2$ , forming a CdTe layer (McEvoy et al., 2012). Due to some porosity in the CdTe layer, this method requires a thickness in the higher end of the possible range to ensure good operation of the solar cells.

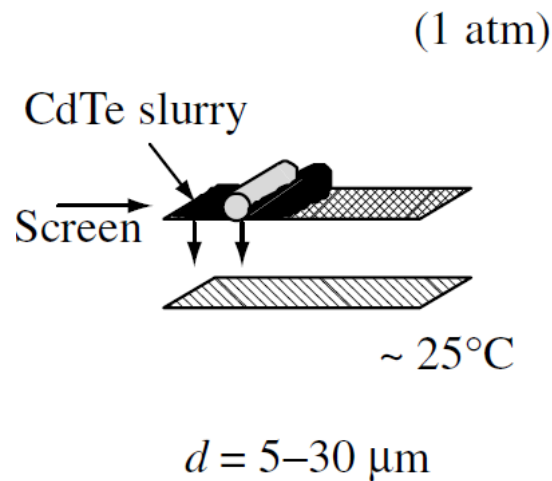


Figure 8.5: Schematic illustration of screen printing of the CdTe absorber layer (Luque & Hegedus, 2011). The substrate is the cross-lined rectangle. Film thickness  $d$  is shown at the bottom of the figure.

#### 8.5.5 Vapour transport deposition

During vapour transport deposition (see Figure 8.6), solid CdTe contained in a heated chamber evaporates and reacts with a carrier gas. When the carrier gas is saturated with Cd and Te, the gas is exhausted through a small opening above or below the moving substrate at a distance of approximately 1 cm (Luque & Hegedus, 2011). The Cd and Te condensate out of the gas and form CdTe onto the substrate.

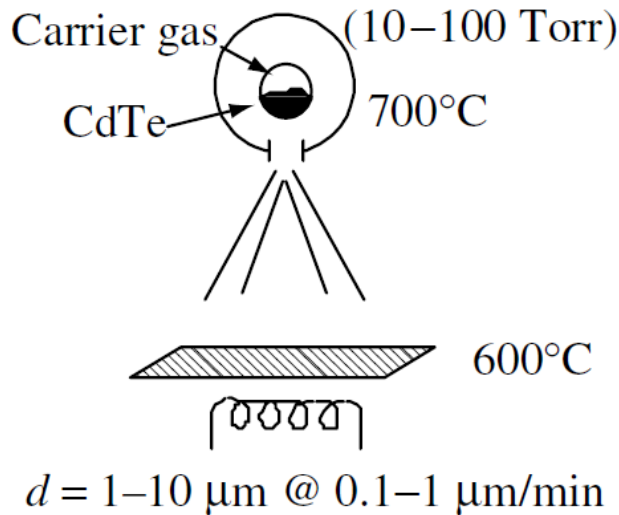


Figure 8.6: Schematic illustration of vapour transport deposition of the CdTe absorber layer (Luque & Hegedus, 2011). The substrate is the cross-lined rectangle. Film thickness  $d$  and growth rate are shown at the bottom of the figure.

### 8.5.6 Metal organic chemical vapour deposition

Metal organic chemical vapour deposition utilizes organic Cd and Te precursors, e.g. dimethyl cadmium and diisopropyl tellurium, in hydrogen carrier gas (see Figure 8.7) (Luque & Hegedus, 2011). The CdTe layer is deposited onto a heated substrate (200-400°C) by pyrolytic decomposition of the carrier gas with the precursors. The deposition rate depends on the substrate temperature.

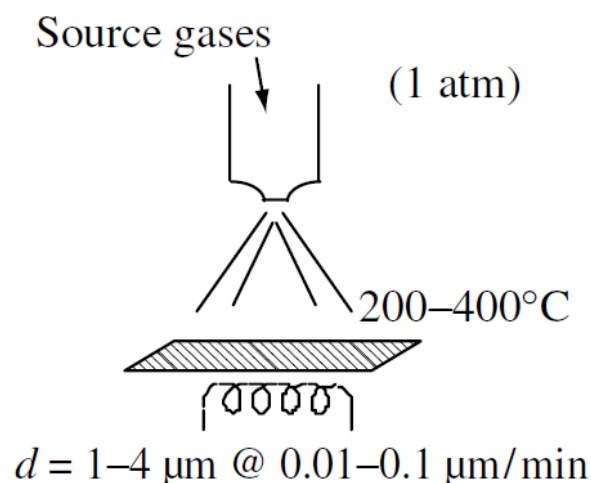


Figure 8.7: Schematic illustration of metal organic chemical vapour deposition of the CdTe absorber layer (Luque & Hegedus, 2011). The substrate is the cross-lined rectangle. Film thickness  $d$  and growth rate are shown at the bottom of the figure.

## 8.6 Cadmium chloride vapour treatment

After the deposition of the CdTe layer, the CdTe solar cell exhibits a poor electrical performance (Romeo et al., 2004). This is independent of which type of deposition process has been used. To improve the cell efficiency (by a factor of 2-3), a chlorine-containing material, CdCl<sub>2</sub> or CHClF<sub>2</sub>, is deposited onto the CdTe layer, before the CdTe/CdS stack are subjected to a heat treatment between 350 and 600°C under a chlorine- and oxygen-containing atmosphere for 10 to 30 minutes, prior to the back contact deposition (Birkmire & Meyers, 2001; Romeo et al., 2004; Gessert et al., 2008). The treatment is called cadmium chloride vapour treatment or junction activation. It has to be performed with care, because over-treatment can result in loss of adhesion, reducing the PV device performance (Wu, 2004). The residual CdCl<sub>2</sub> is removed by a water rinse or mild etch (Birkmire & Meyers, 2001).

## 8.7 Back electrical contact

Forming an efficient and stable ohmic contact on the p-type CdTe layer, is a difficult challenge in the CdTe PV technology. The back contact metal has to have a work function higher than that of the p-type CdTe to form an ohmic contact. CdTe has a work function of 5,7 eV. There is no metal available with such high work functions, so modifications have to be done. By using chemical etching with Br-methanol or a NP solution, the surface of the CdTe layer is heavily p-doped, creating a Te-rich accumulation layer (Morales-Acevedo, 2006; McEvoy et al., 2012). Between the CdTe layer and the back contact, a buffer layer of a p-type, chemically inert semiconductor with a narrow bandgap is applied. (Note that the buffer layer mentioned here, is **not** the same buffer layer as referred to in chapter 8.4). Some buffer material diffuses into the CdTe layer under a post-deposition annealing treatment above 150°C (Birkmire & Meyers, 2001). Finally, a metal layer for low-resistance current collection is deposited. The combined buffer layer and metallization layer will be referred to as the back contact. The most common materials used for the back contact film coating are either copper-based or copper-free:

- **Cu-based materials:** Cu/Au, Cu/graphite, As<sub>2</sub>Te<sub>3</sub>/Cu/Mo, or graphite pastes doped with Hg and Cu like e.g. Cu<sub>x</sub>Te:HgTe/graphite paste and HgTe:Cu/graphite paste/Ag paste (Razykov et al., 2011; Biccari, 2012a)
- **Cu-free materials:** Ni/Al, Ni/P, Sb<sub>2</sub>Te<sub>3</sub>/Mo, Sb/Mo, Sb/Au, HgTe/graphite, Te/Au, ZnTe/Sb<sub>2</sub>Te<sub>3</sub>, Ni, PbTe, SnTe, ZnTe (Biccari, 2012a; Rajendra & Kekuda, 2012).

Earlier, copper-based back contacts were often used, but during the recent years, other alternatives for back contacts have been investigated due to the fact that a back contacts with copper may not be stable over time, leading to efficiency degradation. The copper gradually diffuses into the absorber layer and buffer layer, creating defects and leading to copper accumulation at the heterojunction (U.S. Department of Energy, 2012a). Examples of

research papers on back contact materials for CdTe solar cells are Romeo et al. (2007), Matin et al. (2010) and Irfan et al. (2012).

The back contact is usually deposited by screen printing or sputtering. One of the most common examples are a back contact of nickel (Ni) and aluminium (Al). The thickness of the back contact layer is approximately 0,3-1,5  $\mu\text{m}$ .

## **8.8 CdTe solar cell and PV module**

As previously mentioned (see chapter 7.2), thin film PV technology have the advantage of integrated series connection of solar cells during the different stages of layer deposition. The layers are scribed (separated) into parallel stripes by laser ablation or mechanical machining in three sets, defining the solar cells in area and interconnecting them at the same time (Bonnet, 2000).

The first patterning step, P1, happens through laser scribing of the front contact layer (TCO). The front contact layer is separated for the different cells by scribing lines at a periodic distance of about 1 cm (McEvoy et al., 2012). A second patterning step, P2, is performed through mechanically scribing after the deposition of the buffer- and absorber layers (Aberle, 2009). This patterning step opens the TCO layer underneath for the back contact layer, which is deposited next. The back contact layer forms an ohmic contact to the next cell in the P2 scribing line. Finally, the a third patterning step, P3, is made by mechanically scribing through all the layers, except the front contact layer, separating the back contact of adjacent cells from each other. The patterning steps makes it possible to adjust the solar cell width according to technical needs or commercial requirements. A cell width of 9-10 mm seems to be an optimum value for CdTe solar cells, while the interconnection width is in the order of 200-300  $\mu\text{m}$  (McEvoy et al., 2012). Figure 8.8 shows the monolithic cell interconnections between CdTe solar cells, together with the trenches from the three patterning steps.

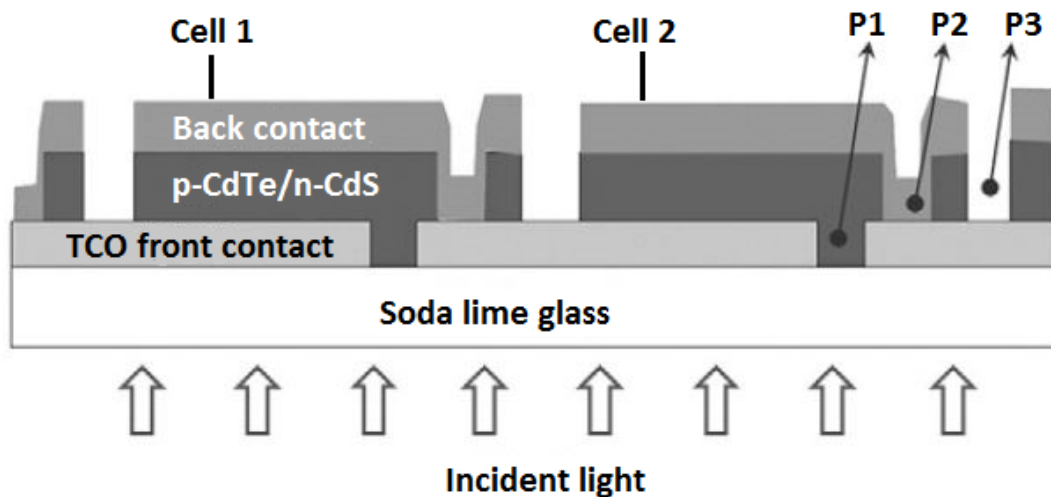


**Figure 8.8: Patterning scheme for monolithic cell interconnections in an integrated CdTe PV module (Bosio et al, 2011, edited for readability). P1 is performed by laser scribing, while P2 and P3 are usually performed by mechanically scribing.**

By using a conducting adhesive, metallic conductors are attached to the first and the last solar cell in the module, and are then further connected by contact bands (Sn-plated Cu ribbons) toward a point of the module where it traverses the back cover (typically glass) (McEvoy et al., 2012). This process is referred to as the bus bar attach.

The back of the module needs to be protected against humidity and other external influences. This is achieved by encapsulating the back of the module with a sheet of EVA, which then undergoes a thermal annealing step under vacuum. EVA works as an adhesive for the attachment of a low iron back cover glass. This process is referred to as lamination. All films at a boundary region of 1-2 cm of the edges of the module have to be removed to provide electric insulation of the module. This is done by sandblasting or laser ablation after the encapsulation with EVA. The contact bands of the module are attached inside a junction box to enable series connection of modules, and if necessary an exterior frame is applied. The module manufacturing is completed by performing testing of the module performance using a solar simulator. The modules are classified according to conversion efficiency and packed for shipment.

The cross-sectional structure of a finished CdTe PV module in the superstrate configuration can be found in Figure 8.9. Note that this is the standard structure, and that there may be other options for the different layers.

Incident light



Substrate: Soda-lime glass	2,0-4,0 mm
Front contact: SnO <sub>2</sub> :F (FTO)	0,2-1,0 μm
Buffer: n-CdS	50-200 nm
Absorber: p-CdTe	2,0-7,0 μm
Back contact: Ni/Al	0,3-1,5 μm
Encapsulant: EVA	0,4-0,7 mm
Low iron cover glass	2,0-4,0 mm

Figure 8.9: Cross-section of a finished CdTe PV module in superstrate configuration (standard structure). Note that a layer of antireflective coating may be applied to the front surface of the substrate facing the incident light.

## 9 CIGS PV production value chain

In this chapter, the value chain of the CIGS based PV production and processing technologies will be explained. The background for the CIGS PV technology will be presented first, before the different production steps making up the foreground system described in Figure 5.2 will be explained. Note that only the value chain upstream of the PV module, including the module itself, will be presented in this chapter.

### 9.1 Background

Copper indium gallium diselenide ( $\text{Cu(In,Ga)Se}_2$ , CIGS) is a mixed alloy of the semiconductors copper indium diselenide ( $\text{CuInSe}_2$ , CIS) and copper gallium diselenide ( $\text{CuGaSe}_2$ , CGS). These semiconductors and their mixed alloys belongs to the I-III-VI<sub>2</sub> semiconductor family and are referred to as chalcopyrites because of their tetragonal crystal structure (Razykov et al., 2011). The chemical structure of CIS is shown in Figure 9.1. In the CIGS structure, each Cu-, In- or Ga atom has four bonds to the Se-atom, while the Se atom has two bounds to the Cu atom and two bonds to the In atom.

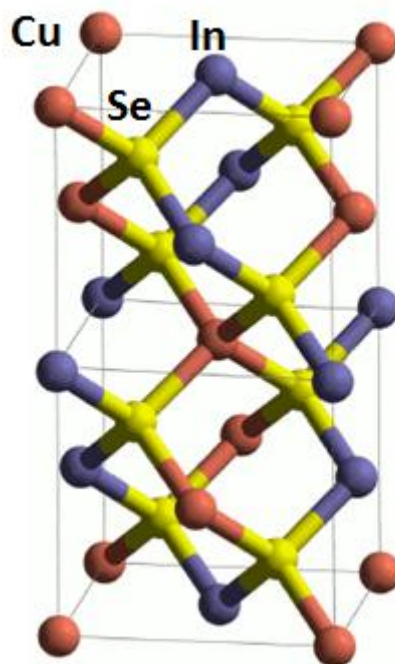


Figure 9.1: Tetragonal crystal structure of CIS (Biccari, 2012b, edited for readability).



The starting point for CIGS PV is CIS, which has several favourable properties for thin film PV application: It has a high optical absorption coefficient of  $3-6 \times 10^5 \text{ cm}^{-1}$  (among the highest for semiconductor materials), possibility to change the resistivity and type of conductivity (can be either p- or n-type) and it gives the possibility for bandgap engineering (Razykov et al., 2011). CIS has a direct-bandgap of 1,0 eV, which is quite low for solar cells. The indium is therefore replaced with an alloy of indium and gallium, giving copper indium gallium diselenide or CIGS. By varying the  $[\text{Ga}]/[\text{In}+\text{Ga}]$  ratio, the bandgap is increased to a value between 1,04 and 1,68 eV. The bandgap increase results in an increase in the open-circuit voltage, thereby increasing the conversion efficiency. Current CIGS solar cells are made with a  $[\text{Ga}]/[\text{In}+\text{Ga}]$  ratio of 20-30%, which gives a bandgap of 1,20-1,25 eV. Increasing the bandgap even further would require a higher Ga content, but these solar cells have proven to be of inferior electronic quality and yield lower-efficiency cells. The Cu/In ratio affects the electronic properties of CIGS and it is essential to have good control of the stoichiometry (Markvart, 2000).

CIGS solar cells usually consist of a p-type absorber layer of CIGS and a n-type buffer layer of CdS, forming a heterojunction. Compared with other semiconductor materials, CIGS has one of the highest current densities, having the potential to produce high current outputs, as well as they preserves their performance properties in a better way (Solar Thin Films Inc, 2007a). They are also suitable for large-area, automated production. A distinctive feature of the CIGS PV technology is that there are no dominant manufacturing process and no standardization on the manufacturing process (Kushiya, 2012).

Today, CIGS is the most efficient thin film PV technology. So far, most of the commercial CIGS PV producers have a production volume far below 100 MW/year (Kushiya, 2012). One exception is the Japanese company Solar Frontier K.K., which exceeded 1 GW PV production capacity in 2011.

## 9.2 Substrate

As for the CdTe solar cells, CIGS solar cells can also be grown in either a substrate or a superstrate configuration (see chapter 7.1). Due to favourable process conditions, where interdiffusion of CdS during high-temperature CIGS film deposition is avoided, the substrate configuration results in the highest efficiency for CIGS solar cells (Razykov et al., 2011; Chopra et al., 2004). Consequently this is the most common configuration for CIGS solar cells. An additional encapsulation layer (e.g. glass) are required to protect the cell surface when using the substrate configuration. The substrate can be either glass, metal foil (e.g. stainless steel, Mo and Ti) or polymer foil. There is several reasons for choosing a soda-lime glass as substrate: It addition to being relatively cheap, it is electrically insulating, temperature stable, and with a smooth surface.

Using a metal or polymer foil has different advantages and disadvantages (adapted from Razykov et al., 2011):

- Solar cells on metal foil are heavier than solar cells on polymer foil due to a higher density.
- Monolithic module development (see chapters 7.1 and 9.8) is more difficult on metal foils due to rough surfaces and high conductivity.
- Solar cells on metal foil often have higher conversion efficiency than those on polymer foil, because metal foils can withstand higher processing temperatures (550-600°C) than polymer foils (<450°C).
- Metal foils of stainless steel requires the deposition of a diffusion layer to protect against diffusion of impurities (e.g. Fe) into the CIGS layer.
- Electrically conductive substrates (e.g. metal foils) need an insulating barrier layer in order to contain monolithically interconnected cells (e.g.  $\text{Al}_2\text{O}_3$ ,  $\text{SiO}_x$ ) (Kessler & Rudmann, 2004; Malm, 2008).
- The insulating barrier layer can be used as diffusion barrier layer too.

Companies producing flexible CIGS modules are Global Solar Energy (stainless steel), SoloPower (stainless steel) and Ascent Solar (polymer) (Ullal & von Roedern, 2007).

### 9.3 Back electrical contact

In commercial CIGS module production, molybdenum (Mo) is the most commonly used back contact material due to its work function (see chapter 8.7), high reflectivity, resistance to alloying with Cu and In and relatively inert nature during the highly corrosive CIGS deposition conditions (Chopra et al., 2004; U.S. Department of Energy, 2012b; Singh & Patra, 2010). Mo is deposited onto the substrate by DC magnetron sputtering or e-beam evaporation. Using the sputtering method requires precise pressure to be able to control the stress in the film (U.S. Department of Energy, 2012b). During the CIGS deposition, a thin intermediate layer of  $\text{MoSe}_2$  is formed between the Mo and the CIGS layers, forming an ohmic contact and giving good adhesion. The thickness of the Mo layer is typically in the range of 0,3-1,2  $\mu\text{m}$ .

### 9.4 Absorber layer

The CIGS absorber layer is deposited onto the back electrical contact (1,0-3,0  $\mu\text{m}$  thick). Since CdS (commonly used for the buffer layer) can only be grown as n-type material, the CIGS layer must be of p-type conductivity (Markvart, 2000). The deposition of the CIGS layer can be done by a variety of methods (see Table 9.1), most of them achieving solar cell conversion efficiencies above 13%. A 0,1-0,3  $\mu\text{m}$  thick CIGS layer is sufficient for absorbing the incident light, but to ensure a compositional uniformity over a large area, the CIGS layer should be minimum 1,0  $\mu\text{m}$  thick (Marwede et al., 2013).

**Table 9.A: Methods for CIGS film deposition (Razykov et al., 2011)**

1.	Co-evaporation	6.	Hybrid evaporation/sputtering
2.	Electrodeposition/selenization	7.	Reactive sputtering
3.	Electron beam/selenization	8.	Spraying
4.	Hybrid selenization	9.	Close-spaced vapour transport
5.	Sputtering selenization		

In the next subsections, two of the most common methods for CIGS deposition will be explained: The co-evaporation process and the selenization/sulfurization of precursor materials.

#### **9.4.1 Co-evaporation processes**

Using vacuum co-evaporation for CIGS deposition has the given the best results in terms of efficiency. During this vacuum process, the different elements (Cu, In, Ga, Se) are evaporated simultaneously from multiple sources in single or sequential processes, before they deposit onto a heated substrate at 400-600°C (see Figure 9.2) (Razykov et al., 2011; Singh & Patra, 2010; U.S. Department of Energy, 2012b). Selenium is offered in excess during the whole deposition process (Romeo et a., 2004). Parameters like the rate of sources, their position, the geometry of the deposition chamber and the movement of the substrates affect the material composition in the CIGS layer (Malm, 2008). Typically, an in-line process is used with stationary sources and the substrates moving past them. The main challenges with the co-evaporation process is to coat large areas with sufficient process stability and homogeneity (Dhere, 2007).

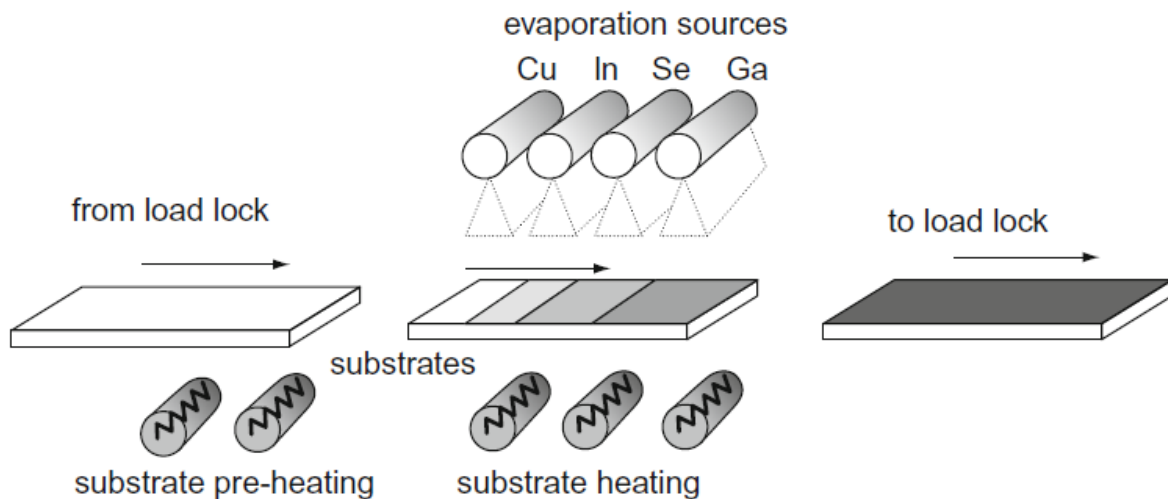


**Figure 9.2: Illustration of an in-line deposition system for co-evaporation of CIGS absorber layer from line-sources (McEvoy et al, 2012).**

The variation of the copper (Cu) content has proven to strongly affect the CIGS film growth and the different co-evaporation processes are therefore classified according to their copper evaporation profile (see Figure 9.3 for details). There are three different co-evaporation processes:

- **The single-stage/constant rate process:** All fluxes (of copper, indium, gallium and selenium) are constant throughout the deposition processes.
- **The Bilayer/Boeing process:** The process conditions are first copper-rich, and then indium- and gallium-rich.
- **The 3-stage process:** The process conditions alternates between being copper-rich and copper-poor. This process has yielded the most efficient CIGS solar cells so far.

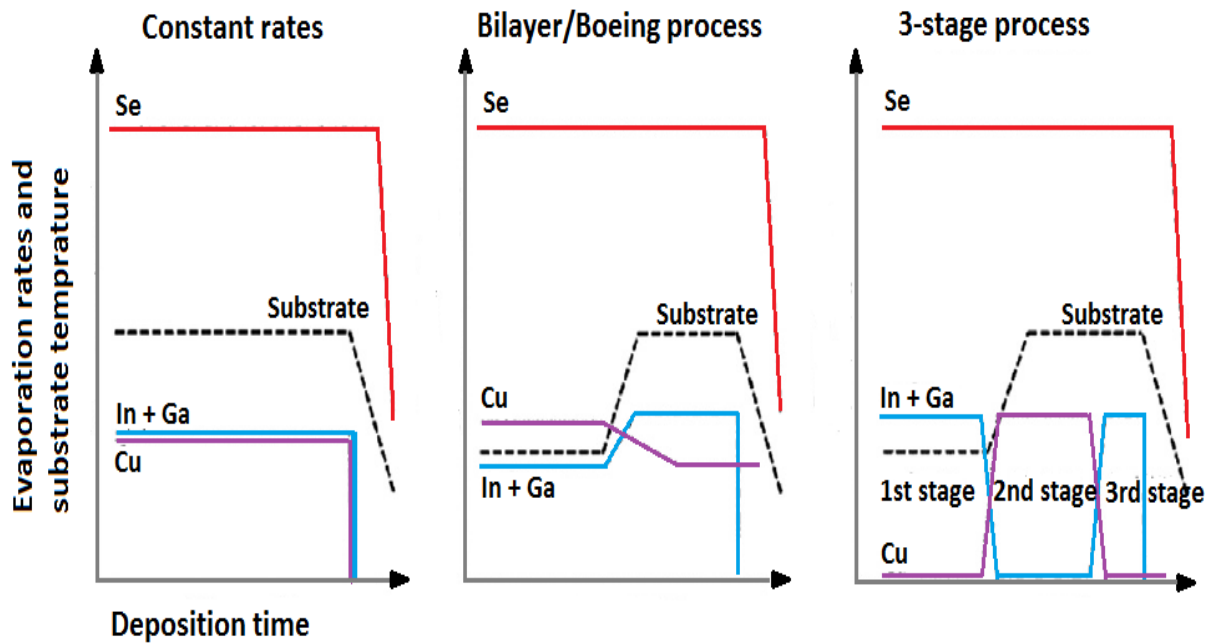
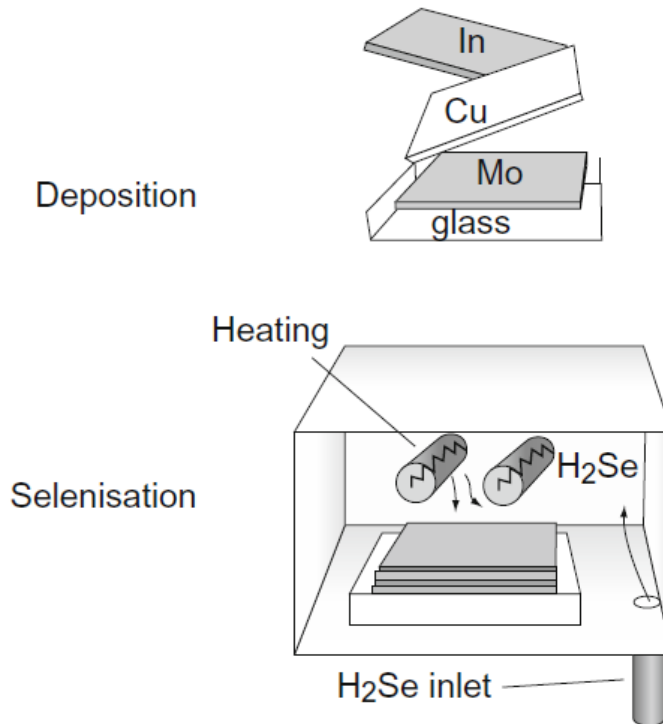


Figure 9.3: Diagrams representing the recipes in the co-evaporation methods used for deposition of the CIGS absorber layer (Razykov et al., 2011, edited for readability). The methods are defined according to the variation in the copper (Cu) content.

#### 9.4.2 Selenization/sulfurization of precursor materials

The advantages of the selenization/sulfurization process are that it can produce uniform films of high-quality material over large areas, suitable for module production, and having good control of the film composition and thickness (Markvart, 2000; Razykov et al., 2011). During this two-stage process, a precursor material is deposited onto the molybdenum back contact (e.g. by sputtering, thermal evaporation or electrodeposition), before undergoing a thermal annealing treatment in a chalcogen-containing environment, forming a layer of  $\text{Cu}(\text{In}, \text{Ga})\text{Se}_2$ . The precursor materials are a stack or alloy of the constituents copper, indium and gallium. The chalcogen source can be selenium (Se) or sulfur (S) in an elemental form as vapour or as a hydride gas ( $\text{H}_2\text{Se}$  or  $\text{H}_2\text{S}$ ) (Wolden et al., 2011). It is also possible to employ both selenium and sulfur at the same time. This is known as the sulfidization after selenization (SAS) scheme.



**Figure 9.4: Illustration of the selenization of precursors materials for deposition of the CIGS absorber layer (McEvoy et al, 2012). The process happens in two steps: A stack of metal (Cu, In, Ga) layers are deposited by e.g. sputtering, thermal evaporation or electrodeposition, before the stack is selenized in H<sub>2</sub>Se atmosphere and converted into CIGS.**

## 9.5 Buffer layer

A buffer layer should prevent shunting at the TCO/CIGS interface and reduce carrier recombination at the buffer/CIGS interface (Minemoto & Julayhi, 2013). To form a heterojunction with CIGS in the solar cells, CdS is the most common material used as buffer layer in commercial production. CdS has a high resistivity, so the buffer layer should be as thin as possible (Biccari A, 2013). The thickness of this layer is typically around 40-100 nm. CdS has continuously yielded high-efficiency cells and is usually deposited by using chemical bath deposition (see chapter 8.4.1) (Razykov et al., 2011). This deposition method is however not compatible with in-line vacuum-based production methods. The cadmium (Cd) is of concern due to the toxicity (see chapter 7.3), and the low bandgap of CdS hinders high-energy photons from reaching the CIGS absorber layer. These issues have driven the research towards investigation of other "Cd-free" wide-bandgap semiconductors and other deposition methods compatible with in-line processes.

### 9.5.1 Alternative buffer materials

Due to its relatively low bandgap of 2,42 eV, the CdS layer absorbs almost all of the incident light in the green/blue end of the spectrum (Markvart, 2000; Biccari, 2012b). This effect is to a certain extent reduced by utilizing the thinnest CdS layer as possible. However, to improve the blue response of the CIGS solar cell, thereby increasing the voltage and current, and to remove the concern of toxicity related to cadmium, investigations of other materials which can replace CdS are of interest. Several materials have been investigated as alternative candidates, but only a few have so far been commercialized.

Ideally, the buffer material should have a bandgap between 2,0 and 3,4 eV (Razykov et al., 2011). Looking at the research literature, the trend seems to be that mainly chalcogenides (oxides, sulphides and selenides) of two elements, zinc and indium, are investigated as alternative buffer layers. The following list gives an overview over what is found in literature:

- **Cadmium based buffers:**  $Cd_{1-x}Zn_xS$  (zinc addition).
- **Indium based buffers:**  $In_2S_3$ ,  $InS$ ,  $In(OH)_3$ ,  $In_2Se_3$ .
- **Zinc based buffers:**  $ZnS$ ,  $ZnO$ ,  $ZnSe$ ,  $ZuInSe_x$ ,  $ZnMgO$ ,  $ZnS:Al$  (Al-doped ZnS).
- **Double layered buffers:**  $In_x(OH, S)_y/CdS$ ,  $In_x(OH, S)_y/ZnS$ ,  $ZnS/CdS$ .

(Hariskos et al., 2005; Bhattacharya et al., 2006; Buecheler et al., 2009; Islam et al., 2009; Hariskos et al., 2009; Powalla, 2009; Yagioka and Nakada, 2009; Matsunaga et al., 2009; Shin et al., 2010; Chelvanathan et al., 2010; Rousset et al., 2011; Li et al., 2011; Razykov et al., 2011; Naghavi et al., 2011; Nagamani et al., 2012; Wang et al., 2012; Bae et al., 2013a; McPeak et al., 2013; Minemoto & Julayhi, 2013).

There are a few companies which are using alternative buffer layers with success. The largest CIGS PV manufacturer, Solar Frontier, utilizes  $Zn(S,OH)_x$  as buffer layer, while Honda Soltec utilizes  $In(S, OH)_x$  (Kushiya, 2012).

### 9.6 Sodium incorporation

An improvement in conversion efficiency can be achieved by incorporating sodium (Na) into the CIGS layer. The effect of sodium increases the p-type conductivity, the open-circuit voltage and the performance ratio. The sodium incorporation can be done either via the soda-lime glass substrate by sodium diffusion from the glass during CIGS layer deposition (most common), or by introducing sodium from a separate, external source during or after the CIGS layer deposition (Razykov et al., 2011). The second alternative gives increased controllability and reliability, and is especially used in the case of Na-free substrates (metal and polymer foils). Na-free substrates includes soda-lime glass covered with barrier layers (e.g.  $Al_2O_3$ ,  $Si_3N_4$ ,  $SiO_2$ , Cr; McEvoy et al., 2012), inhibiting sodium diffusion from the glass substrate. Sodium incorporation with an external source can be done either by co-evaporation or by deposition of a thin precursor of Na compound, e.g. NaF,  $Na_2Se$ ,  $Na_2S$ , on

the substrate (Razykov et al., 2011). For CIGS solar cells on metal or polymer foils, a layer of precursor is applied prior to or after the CIGS layer deposition.

## 9.7 Front electrical contact

The front contact is applied to the top of the solar cell to help collect the light-generated current (Solar Thin Film Inc., 2007a). The most appropriate front contacts for CIGS solar cells are TCOs with bandgaps above 3,0 eV (Razykov et al., 2011). High optical transparency (above 85%) and good electrical conductivity makes them well suited for this type of application. Commercial production usually use a bi-layer of zinc oxide (ZnO): First an intrinsic, highly resistive layer of ZnO (i-ZnO), and then a thick n-type aluminium-doped ZnO layer (ZnO:Al, AZO) deposited by RF magnetron sputtering or chemical vapour deposition (Kushiya, 2012; U.S. Department of Energy, 2012a). The layer of i-ZnO is usually 40-140 nm thick, while the layer of AZO has a thickness of 0,2-1,0  $\mu\text{m}$ . In addition to protecting the surface from damage in subsequent process steps, the intrinsic layer of ZnO evens out the potential (Malm, 2008). As an alternative to aluminium doping, boron has shown to be a feasible dopant for ZnO (ZnO:B, BZO), using metal organic chemical vapour deposition (Kushiya, 2012). Solar Frontier currently use BZO. ITO is another alternative front contact (together with a thin layer of i-ZnO), but are so far used less frequently.

To achieve a sufficiently high conversion efficiency and avoid interdiffusion across the CdS/CIGS interface, the temperature during TCO deposition should not exceed 150°C (Razykov et al., 2011). Since the front contact of a CIGS cell lets the incident light through, the front contact is also sometimes referred to as the window layer in the CIGS solar cell structure.

## 9.8 CIGS solar cell and PV module

In CIGS PV modules, the solar cells can be interconnected monolithically, meaning that the series connection is performed during the deposition of the different layers making up the module (similar procedure as for the CdTe PV modules). The series interconnection is done by patterning the thin film layers during the in-line processing (Malm, 2008). Usually, three patterning steps are required.

Figure 9.5 illustrates the sequence of the patterning steps for cell interconnection: The first patterning step, P1, happens through laser scribing of the back contact layer (Mo). The back contact layer is separated for the different cells by trenches/scribing lines in the Mo metal layer, defining the number of cells and the cell area/width. The width of the cells are usually in the order of 0,5-1 cm (McEvoy et al., 2012). After the deposition of the absorber-, buffer-, and intrinsic front contact layers (i-ZnO), a new trench is made by mechanical scribing. The trench do not penetrate the back contact layer. This second patterning step, P2, can also be performed before the deposition of the intrinsic front contact layer. During the deposition of



the n-type front contact (AZO), the front contact forms an ohmic contact to the back contact of the next cell in the P2 trench. The third and final patterning step, P3, is made by mechanical scribing through all the layers, except the back electrical contact, separating the front contact of adjacent cells from each other (Malm, 2008). The length of the solar cell is the same as the length of the scribes, and can be more than 1 m. The interconnection width is in the order of 300  $\mu\text{m}$ , meaning that 3-5% of the solar cell area is sacrificed to the interconnects (McEvoy et al., 2012). Figure 9.6 shows the monolithic cell interconnections between two CIGS solar cells, together with the trenches from the three patterning steps.

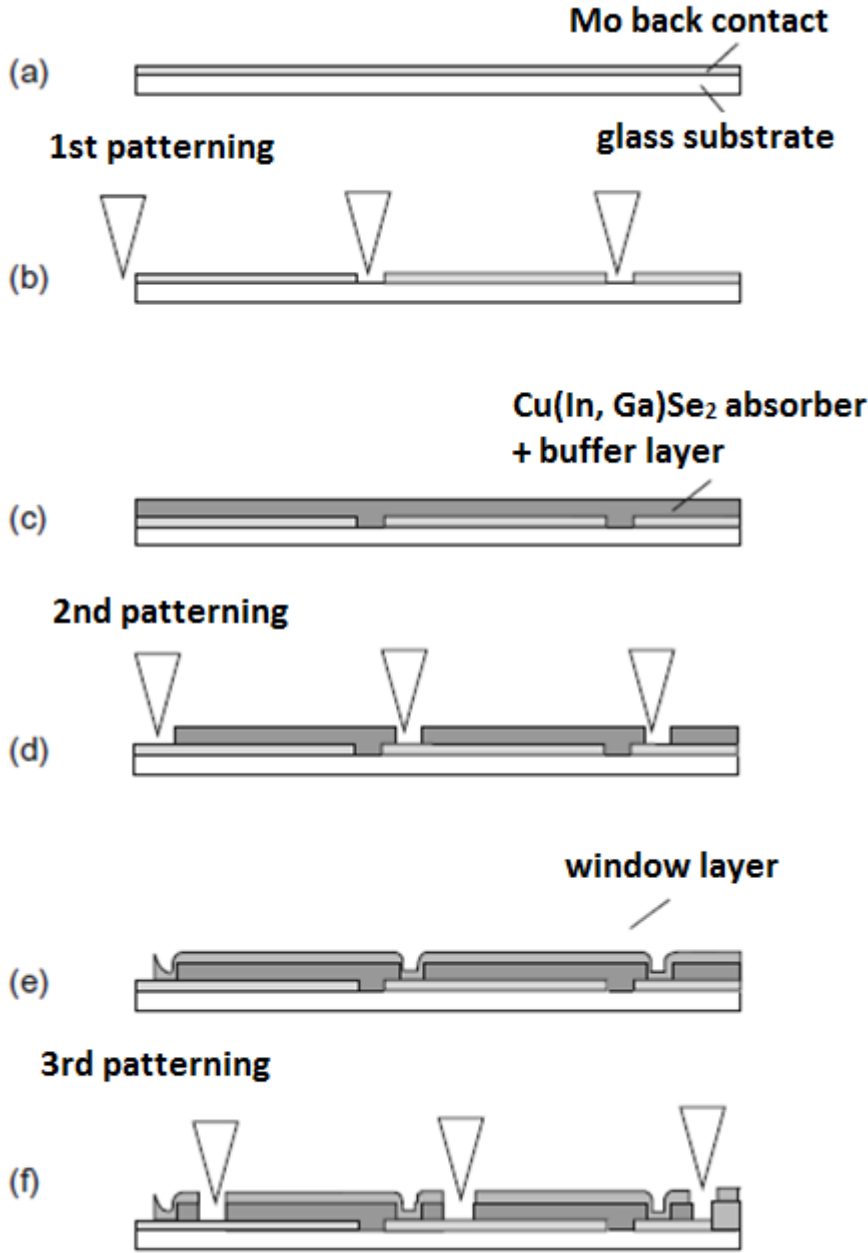
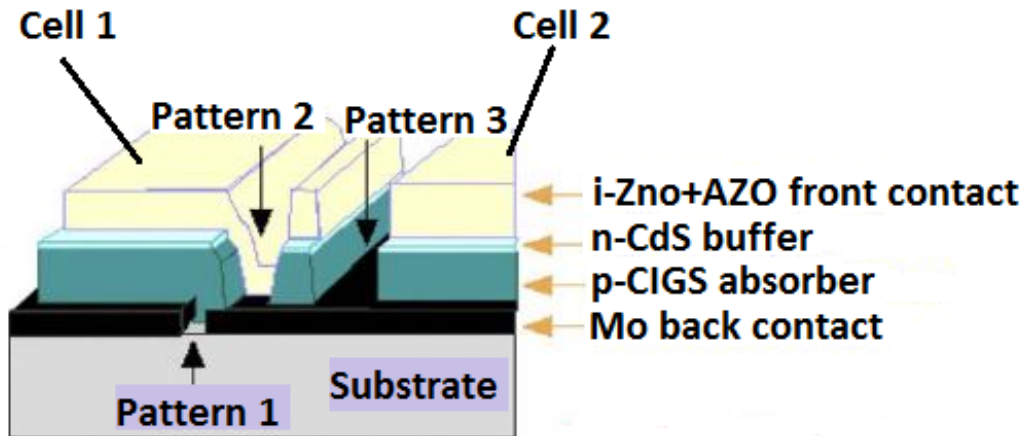


Figure 9.5: Deposition and patterning sequence to obtain a monolithically integrated CIGS PV module (McEvoy et al., 2012, edited for readability). The window layer refers to the front contact.



**Figure 9.6: Patterning scheme for monolithic cell interconnections in an integrated CIGS module (Kushiya et al., 2009, edited for readability). P1 is performed by laser scribing, while P2 and P3 usually are performed by mechanically scribing.**

To increase the collection of electrical current, metal grids may be deposited on top of the front contact layer. The grids are usually made of nickel (Ni) and aluminium (Al), and deposited by e-beam evaporation (Repins et al., 2008; Singh & Patra, 2010).

The rest of the manufacturing happens in the same way as the CdTe module manufacturing: The CIGS modules have conducting solar cells at each ends for external contacting. Metallic conductors (strips) are attached to these and then connected by contact bands traversing a point in the back cover of the module (typically glass), making up the bus bar attach. To protect against humidity, the module is encapsulated with an adhesive, EVA, before a low iron cover glass is applied (referred to as lamination). The CIGS PV module is very sensitive to moisture exposure, making it essential that the CIGS module is properly encapsulated to avoid degradation of the electrical contacts (Razykov et al., 2011). An anti-reflective coating, e.g.  $MgF_2$ , may be applied to the front surface of the cover glass, before lamination with EVA (Repins et al., 2008; Singh & Patra, 2010; Marwede et al., 2013). The contact bands of the module are attached to a junction box to enable series connection of modules. The edges of the module are hermetically sealed by laser ablation. An exterior frame is applied if necessary. The module manufacturing is completed by performing testing of the module performance using a solar simulator. The modules are classified according to conversion efficiency and packed for shipment.

The cross-sectional structure of a finished CIGS PV module in the substrate configuration can be found in Figure 9.7. Note that this is the standard structure, and that there may be other options for the different layers.

Incident light



Low iron cover glass	2,0-4,0 mm
Encapsulant: EVA	0,7 mm
Al-Ni grid	
Front contact: ZnO:Al (AZO)	0,2-1,0 $\mu\text{m}$
Front contact: i-ZnO	40-140 nm
Buffer: n-CdS	40-100 nm
Absorber: p-CIGS	1,0-3,0 $\mu\text{m}$
Back contact: Mo	0,3-1,2 $\mu\text{m}$
Substrate: Soda-lime glass	2,0-4,0 mm

Figure 9.7: Cross-section of a finished CIGS PV module in substrate configuration (standard structure). Note that a layer of antireflective coating (e.g. EVA) may be applied to the front surface of the low iron cover glass facing the incident light.

## **10 The rest of the PV production value chain**

Chapters 6, 8 and 9 presented the specific production value chains upstream of the PV module, including the module itself, for the three different PV technologies investigated in this report. However, a PV module do not represent an entire PV system by itself. The production value chain downstream of the PV module, i.e. the components of the balance of system and the manufacturing of the complete rooftop PV system, will be briefly presented in this chapter.

### **10.1 Balance of system**

The mounting structure, inverter and cabling makes out the balance of system (BOS) of the PV module. The mounting structure is necessary in order to be able to mount the PV module onto the roof or on the ground. In this study an on-roof mounting structure is used. The inverter transforms the DC-current produced from the PV module into an AC-current, which is compatible with the electric system in the building or the local electricity grid (Markvart, 2000). The electricity is transported through cables. The cables are attached to the junction box on each individual PV module. These components will not be further discussed.

### **10.2 Rooftop PV system**

Combining the PV modules with the BOS components creates the complete PV system (U.S. Department of Energy, 2012c). To produce the necessary amount of electricity, the PV modules are series connected together in arrays and mounted onto the roof of a building.

Figure 10.1 illustrates the difference between a solar cell, a PV module and a PV array (adapted from U.S. Departmentet of Energy, 2012 c): A solar cell produces only a small amount of power. To produce more power, several solar cells may be interconnected to form a PV module. The PV modules can in turn be connected into PV arrays to produce even more power. Because of this modularity, PV systems can be designed to meet any electrical requirement.

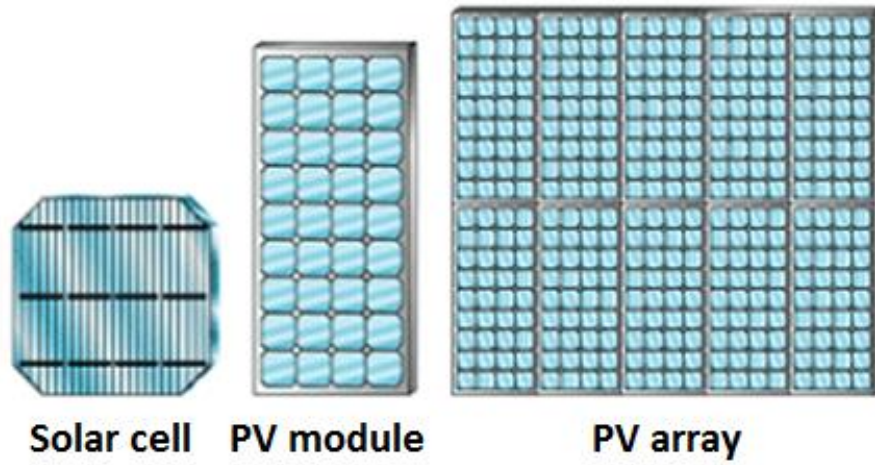


**Figure 10.1: Illustration showing the difference between a solar cell, a PV module and a PV array (U.S. Department of Energy, 2012c).**

## 11 Life cycle inventory

In this chapter, the life cycle inventory (LCI) of the four different cases investigated will be described in terms of where and when the data comes from and how they have been obtained. The complete inventories will not be presented here, since they are too extensive for this. However, a brief presentation of some important yield ratios for the mc-Si cases will be given in the last section. Please see the attached appendices for the complete inventories used in the four cases (appendices A-I). Table 11.1 and Table 11.2 will provide a summary over which data sources have been used and in which appendices to find the inventories. All cases assumes a lifetime of 30 years for the PV module, cabling and mounting structure, while the lifetime of the inverter is assumed to be 15 years.

### 11.1 Collection of inventories

In this section follows general descriptions on the data collections for each case.

#### 11.1.1 Case 1: Mc-Si Sim

The mc-Si Sim-case represents the most commonly used SoG-Si technology, i.e. the modified Siemens process. This case is based on inventory gathered for a chapter on PV technology in the upcoming UNEP (United Nations Environment Programme) report called "*Environmental assessment of low-GHG electricity supply technologies*" (Gibon et al., forthcoming). These data have been gathered from different sources, but mainly within a Chinese context. Specific data on MG-Si production and SoG-Si production were gathered from two factories in Sichuan Province and Jiangsu Province in China. For the factory in Sichuan, the annual production capacity was 3 000 ton of SoG-Si.

Data for the rest of the foreground processes were mainly obtained from a anonymous company, Company A. Company A is one of the international PV system integrators who has several important suppliers in China (Gibon et al., forthcoming). The remaining data were collected from field interviews in other factories and from Ecoinvent v2.2. Entries using Ecoinvent data exist in the inventory of MG-Si, SoG-Si, mounting structure, inverter and cabling.

The data which were collected directly from factories include material inputs, electricity and part of the emissions. All of the materials were converted to units of mass (Gibon et al., forthcoming). In the cases where the factories report contained insufficient information to do the mass conversion, densities and other dimensions were obtained from online resources and product specification sheets (Gibon et al., forthcoming).

### 11.1.2 Case 2: Mc-Si ESS

The mc-Si ESS-case represents an estimate case for the Elkem Solar Silicon metallurgical production process (ESS) for SoG-Si production. In this report, this is assumed to be the currently best SoG-Si technology in terms of energy requirements. Elkem Solar is based in Kristiansand, Norway. The mc-Si ESS-case is based on an updated version of the inventory used in Johansen (2008). The main difference between the inventory used for the ESS-case in this report and the inventory used in Johansen (2008), is the inventory for the SoG-Si production. This inventory has been almost completely updated in the ESS-case. Only a few entries in the LCI for SoG-Si production from Johansen (2008) have been reused, these are confidential material inputs given from researches at Elkem Solar (2008). They will therefore be omitted from this report. The inventory for the SoG-production has been updated with numbers on energy supply, emissions and waste from the Climate and Pollution Agency of Norway (Klif, 2012). These numbers have been reported by Elkem Solar for the year 2011 and can be found on the website [www.norskeutslipp.no](http://www.norskeutslipp.no). The production in 2011 was approximately 4 000 ton SoG-Si (Lande, 2012). The rest of the SoG-Si inventory is made by upscaling numbers on MG-Si production given in either Jungbluth et al. (2012) or Andresen (2008). The upscaling factor is set to 1,5. According to a contact at Elkem Carbon in Kristiansand, Marit Torp, the MG-Si loss from Elkem Solars SoG-Si production is roughly 50% (2012). The upscaling factor of 1,5 can therefore be seen as a reasonable estimate.

The data from Andresen (2008) is data collected from Elkem's MG-Si plant at Thamshavn, Norway. These data are taken from the years 2006 - 2007 (Andresen, 2008). The production was 40 000 ton MG-Si and 5 000 ton silica dust. The data from Jungbluth et al. (2012) is a gathering of the most recent information available on life cycle inventories of photovoltaic production technologies. For the mc-Si PV technology, a large part of these data are based on what was found by Alsema et al. (2006) and de Wild-Scholten et al. (2006) in the Crystal Clear project (will be explained in the next section).

The remaining data for the rest of the PV system value chain downstream of the SoG-Si production are collected from Alsema et al. (2006) and de Wild-Scholten et al. (2006). This dataset were gathered as a part of the Crystal Clear project, founded by the European Commission. The Crystal Clear project investigated and generated up-to-date life cycle inventory data of the crystalline silicon PV technology, covering the entire value chain from silicon production to module manufacturing (Alsema et al., 2006; Jungbluth et al., 2012). Data were provided by 11 commercial European and U.S photovoltaic companies for the reference year 2005, supplemented by numbers from the literature (Fthenakis et al., 2011a). Due to data availability and confidentiality, the ingot growing and wafer cutting were aggregated into one process. Some new additional entries have been added in the inventory for the wafer, solar cell and module, gathered from Jungbluth et al. (2012). Especially the wafer inventory has been altered by additional numbers on emissions to water and new material inputs. For the inverter, cabling, mounting structure and complete PV system, the inventory from Alsema et al. (2006) and de Wild-Scholten et al. (2006) is completely reused.

### **11.1.3 Case 3: CdTe**

The CdTe-case is built on two different data sets which have been integrated into one single CdTe inventory.

The first data set consist of inventories taken from Jungbluth et al. (2012), Alsema et al.(2006) and de Wild-Scholten et al. (2006). The inventory from Jungbluth et al. (2012) is used for the CdTe PV module, while inventories from Alsema et al.(2006) and de Wild-Scholten et al. (2006) are used for the inverter, cabling, mounting structure and complete PV system.

As previously mentioned, the data from Jungbluth et al. (2012) is a gathering of the most recent information available on life cycle inventories of photovoltaic production technologies. The CdTe data were collected from the First Solar production facilities in Germany, Malaysia and the United States for the year 2010, together with additional information from the authors of the publications "*Life cycle impact analysis of cadmium in CdTe PV production*" (Fthenakis, 2004) and "*Energy use and greenhouse gas emissions in the life cycle of the CdTe photovoltaics*" (Fthenakis & Kim, 2005). The data were then adjusted to represent the production mix of Europe, i.e. the share of the PV modules produced in Germany, Malaysia and United States and then installed in Europe. The following production mix of CdTe PV modules installed in Europe was used: 22,5% German production, 12,2% USA production and 65,4% Malaysian production.

The second data set is provided from Gibon et al. (forthcoming). The data for the CdTe PV module were obtained from the National Renewable Energy Laboratory (NREL), a national laboratory for the U.S. Department of Energy. The data were collected for the year 2010. It has not been possible to obtained further details on how these data were collected, but it is likely to assume that First Solar (the largest CdTe PV producer) has been one of the PV companies providing information (Bergesen, 2013). The remaining data on mounting structure, inverter and cabling were collected from Ecoinvent v2.2.

The two data sets have been integrated into one single inventory by using the average value of each entry. Entries only occurring in one of the two data sets have been kept unchanged in the integrated inventory. Entries from Ecoinvent v2.2 in the inventory of the mounting structure, inverter and cabling, have been disaggregated to be able to integrate them with the data from Alsema et al.(2006) and de Wild-Scholten et al. (2006).

### **11.1.4 Case 4: CIGS**

The CIGS-case is also built on two different data sets which have been integrated into one single CIGS inventory. The data sets have been taken from the same sources as the CdTe data sets. Details follow below.



The first data set consist of inventories taken from Jungbluth et al. (2012), Alsema et al.(2006) and de Wild-Scholten et al. (2006). The inventory from Jungbluth et al. (2012) is used for the CIGS PV module, while inventories from Alsema et al.(2006) and de Wild-Scholten et al. (2006) are used for the inverter, cabling, mounting structure and complete PV system.

In Jungbluth et al. (2012), the CIGS data were mainly collected directly from Würth Solar in Germany for the year 2007. Publications by Ampenberger et al. (1998), Naujoks (2000), Rauegi (2005) and Rauegi (2007a) were used for verification. The share of the different coating materials (metals) was estimated by the help of Ampenberger et al. (1998). The cadmium emissions to air were estimated by using Fthenakis & Kim (2005) as a worst-case estimate. However, it is worth noticing that these data refer to another type of process than what was used by Würth Solar.

The second data set is provided from Gibon et al. (forthcoming). The data for the CIGS PV module were obtained from NREL and collected for the year 2010. It has not been possible to obtain further details on how these data have been collected, but it is likely to assume that at Solar Frontier (the largest CIGS PV producer) has been one of the PV companies providing information (Bergesen, 2013). The remaining data on mounting structure, inverter and cabling were collected from Ecoinvent v2.2.

The two data sets have been integrated into one single inventory by using the average value of each entry. Entries only occurring in one of the two data sets have been kept unchanged in the integrated inventory. Entries from Ecoinvent v2.2 in the inventory of the mounting structure, inverter and cabling, have been disaggregated to be able to integrate them with the data from Alsema et al.(2006) and de Wild-Scholten et al. (2006).

It is **very** important to note the following assumption concerning **electricity consumption**: In Jungbluth et al. (2012), an electricity consumption of 122 kWh/m<sup>2</sup> module is given, which is almost an order of magnitude higher than what is given in Gibon et al. (forthcoming). The value was obtained as the gross electricity use of the Würth Solar factory divided by the number of PV modules produced. This means that not only the electricity for the production machines was included, but also electricity for air-conditioning, water purification etc. The time of this data collection was when the Würth Solar facility was still in a pilot production stage, and it is assumed that the provided number is an overestimate. It has therefore been decided to use the number for electricity consumption given in Gibon et al. (forthcoming), and not an average value.

### 11.1.5 Overview

Table 11.1 lists the different sources of data collection. Table 11.2 gives an overview of which sources have been used for the foreground processes in the different cases, and in which appendices the complete inventories can be found.

**Table 11.A: Data sources for the life cycle inventories used in this study.**

Label	Data source
a	Johansen (2008) - Confidential numbers from Elkem Solar (2008).
b	Alsema et al.(2006) and de Wild-Scholten et al. (2006).
c	Climate and Pollution Agency of Norway (2012).
d	Jungbluth et al. (2012).
e	Andresen (2008). Numbers from Elkem Thamshavn (2006-2007).
f	Gibon et al. (forthcoming)
g	Lande (Elkem Solar, 2012)
h	Torp (Elkem Carbon, 2012)

**Table 11.B: Overview of data sources used in this study and in which appendices the LCIs can be found.**

Foreground process	Info	Mc-Si Sim	Mc-Si ESS	CdTe and CIGS
MG-Si	Date source	f	-	
	Appendix	A.1		
SoG-Si	Date source	f	a, c, d, e, g, h	
	Appendix	B.1	B.2	
Ingot	Date source	f	-	
	Appendix	C.1		
Wafer	Date source	f	b, d	
	Appendix	D.1	D.2	
Solar cell	Date source	f	b, d	d, f
	Appendix	E.1	E.2	E.3
PV module	Date source	f	b, d	d, f
	Appendix	F.1	F.2	F.3, F.4
Mounting structure	Date source	f	b	b, f
	Appendix	G.1	G.2	G.3
Inverter and cabling	Date source	f	b	b, f
	Appendix	H.1	H.2	H.3
PV system	Date source	f	b	b, f
	Appendix	I.1	I.2	I.3

## 11.2 Yield ratios

Table 11.3 present some important yield ratios between the different foreground processes used in the life cycle inventories of the mc-Si cases.

The mc-Si Sim-case assumes a 50% lower yield ratio for the wafer and 16% lower yield ratio for the PV module compared to the mc-Si ESS-case. This might be due to the difference in

when these inventories were collected. However, the mc-Si ESS-case assumes a lower solar cell loss, with a 28% lower yield ratio for the solar cell compared to the mc-Si Sim-case. The yield ratio for the MG-Si and SoG-Si production are approximately the same for both mc-Si cases.

**Table 11.C: Yield ratios for foreground processes in the two mc-Si cases.**

<b>Process:</b>	<b>Mc-Si Sim</b>	<b>Mc-Si ESS</b>
Metallurgical grade silicon	2,68 kg silica sand/kg MG-silicon	2,70 kg silica sand/kg MG-Si (used in the upscaling, from Jungbluth et al., 2012)
Solar grade silicon	1,50 kg MG-Si/kg SoG-Si	1,50 kg MG-Si/kg SoG-Si used as upscaling factor
Ingot	1,33 kg SoG-Si/kg ingot	N/A
Wafer	0,485 kg ingot/m <sup>2</sup> wafer = 0,645 kg SoG-Si/m <sup>2</sup> wafer	1,30 kg SoG-Si/m <sup>2</sup> wafer
Solar cell	1,47 m <sup>2</sup> wafer/ m <sup>2</sup> solar cell	1,06 m <sup>2</sup> wafer/ m <sup>2</sup> solar cell
PV module	0,753 m <sup>2</sup> solar cell/ m <sup>2</sup> module	0,888 m <sup>2</sup> solar cell/ m <sup>2</sup> module

## 12 Results and analysis

In this chapter, the results from the life cycle impact assessment will be presented and explained. The results are given per functional unit, being amount of environmental impact per m<sup>2</sup> of PV system. The results from the sensitivity analysis will be presented and explained as well.

In the first section, the results from the LCA of the four cases will be briefly compared by normalizing the impact scores to the PV technology (case) resulting in the highest score within each impact category (Figure 12.1). This is an easy way to get a quick overview of how the four cases perform relative to each other. The results are obtained by using the average European electricity mix (UCTE). Note that the normalization done here is **not** the same as normalization for weighting impact categories against each other (see chapter 4.4.4).

In the second section, an advanced contribution analysis will be conducted. The calculated impacts from the LCA will be distributed over the different foreground processes (see chapters 4.6.5 and 5.3.1), and normalized to the highest impact score across the four different PV technologies (Figures 12.2-5). Note that the normalization done here is **not** the same as normalization for weighting impact categories against each other (see chapter 4.4.4).

The results from the sensitivity analysis will be presented in the last section, mainly with regards to climate change. The base case will be the impact results obtained by using the average European electricity mix (UCTE). The GWP results will be transformed to a per kWh basis to be able to compare the result with those of wind power (referred to as the windband). The sensitivity of the GWP for changes in the parameters PV module conversion efficiency, performance ratio, lifetime, direct normal irradiation, lifetime electricity generation, electricity mix, energy efficiency (electricity) and material efficiency will be presented in Figures 12.6-13. Figure 12.14 will present the area of overall GWP performance of the four PV technologies (cases) by changing several parameters at a time.

### 12.1 Relative performance

To see how the four different cases perform compared to each other, the impacts results have been normalized to the PV technology resulting in the highest impact potential within each impact category. The case having the highest value within an impact category then consequently has the normalized value equal to 100%. All results are obtained by using the average European electricity mix (UCTE). It is important to stress that the normalization done here in this chapter is **not** the same as normalization for comparing/weighting impact categories (see chapter 4.4.4). The normalized values are shown in Figure 12.1. For abbreviations used for the impact categories, please see Table 5.1.

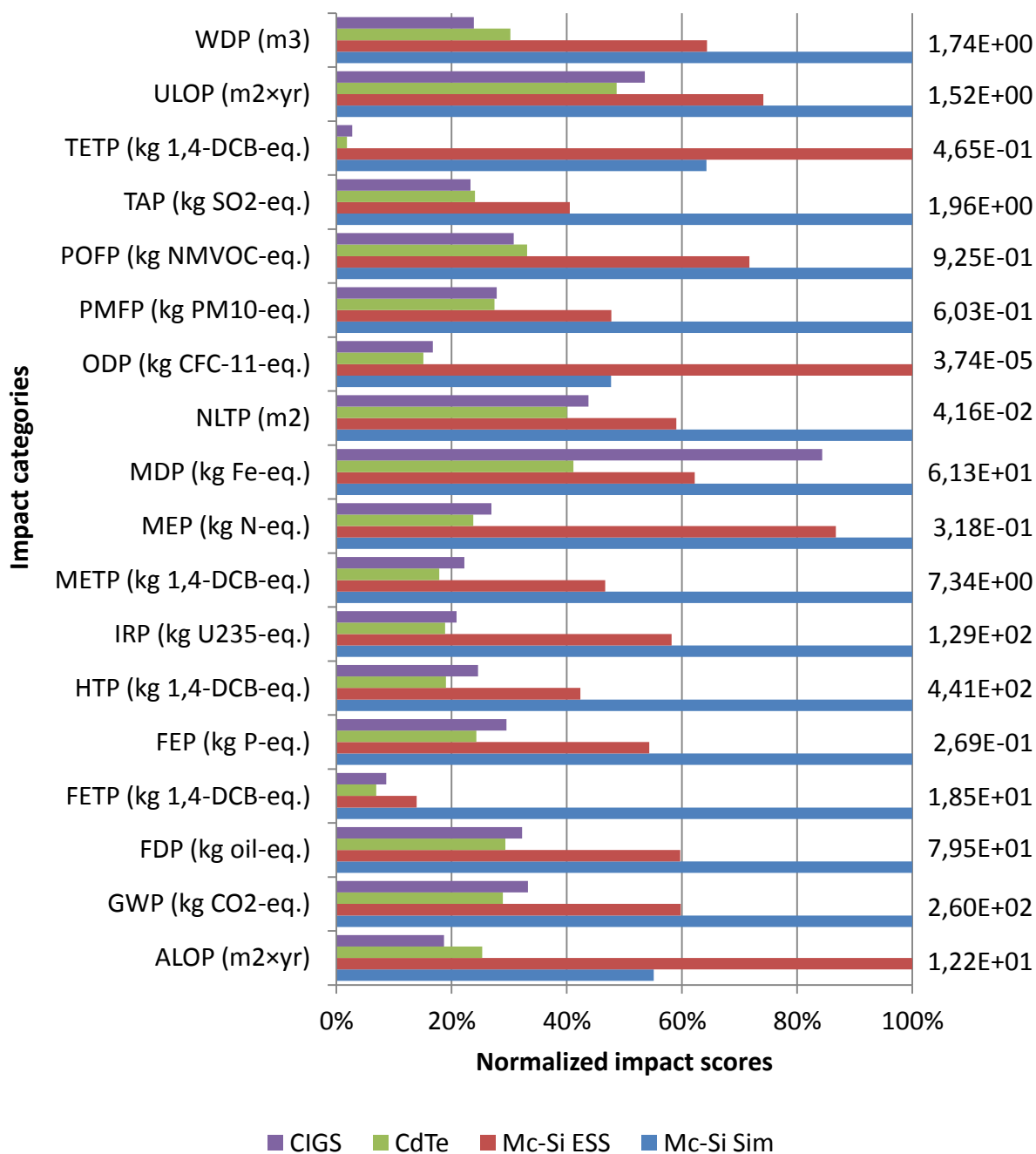


**Figure 12.1: Relative performance of PV technologies (UCTE el mix). Impact scores normalized to highest impact score across the different PV technologies. The aggregated impact value for the case with the highest score is given per m<sup>2</sup> of PV system. (For abbreviations see Table 5.1).7**

In terms of having the highest environmental impacts, the mc-Si Sim-case outperforms all the three other cases in almost all impact categories, except in the three impact categories:

Terrestrial ecotoxicity (TETP), ozone depletion (ODP) and agricultural land occupation (ALOP). The mc-Si ESS-case has the highest score in these three impact categories.

The differences between the impact potentials of the two thin film cases (CdTe and CIGS) are generally small, indicating inherent uncertainties and that one should be careful to argue that one is better than the other. An exception appears for metal depletion potential (MDP), where the CIGS-case has a score twice as high as the CdTe. Only mc-Si Sim has a higher metal depletion potential than CIGS.

Except for metal depletion, the differences between the mc-Si cases and the thin film cases are large, indicating that mc-Si PV technology gives higher environmental impacts than thin film PV technology.

## 12.2 Advanced contribution analysis

By performing an advanced contribution analysis, one seeks to identify how the different foreground processes are contributing to the total impacts resulting from the product system investigated. In this section, the contribution from the foreground processes within each impact category will be presented and explained. The impact results have been normalized to the highest impact score across the four different PV technologies. The PV technology having the highest value within an impact category then consequently has the normalized value equal to 100%. When the text refers to the "*normalized share/contribution*" from a process, the meaning is the normalized, relative share/contribution of that process. It is important to stress that the normalization done here in this chapter is **not** the same as normalization for comparing/weighting impact categories (see chapter 4.4.4). The contribution analysis makes it possible to identify where the emissions/environmental burdens are occurring and where improvement may be done in order to reduce these environmental burdens. All results are obtained by using the average European electricity mix (UCTE). For abbreviations used for the impact categories, please see Table 5.1.

### 12.2.1 Case 1: Mc-Si Sim

Figure 12.2 displays the normalized contribution from the foreground processes to the impact categories by using the mc-Si Sim-inventory together with the aggregated impact potentials.

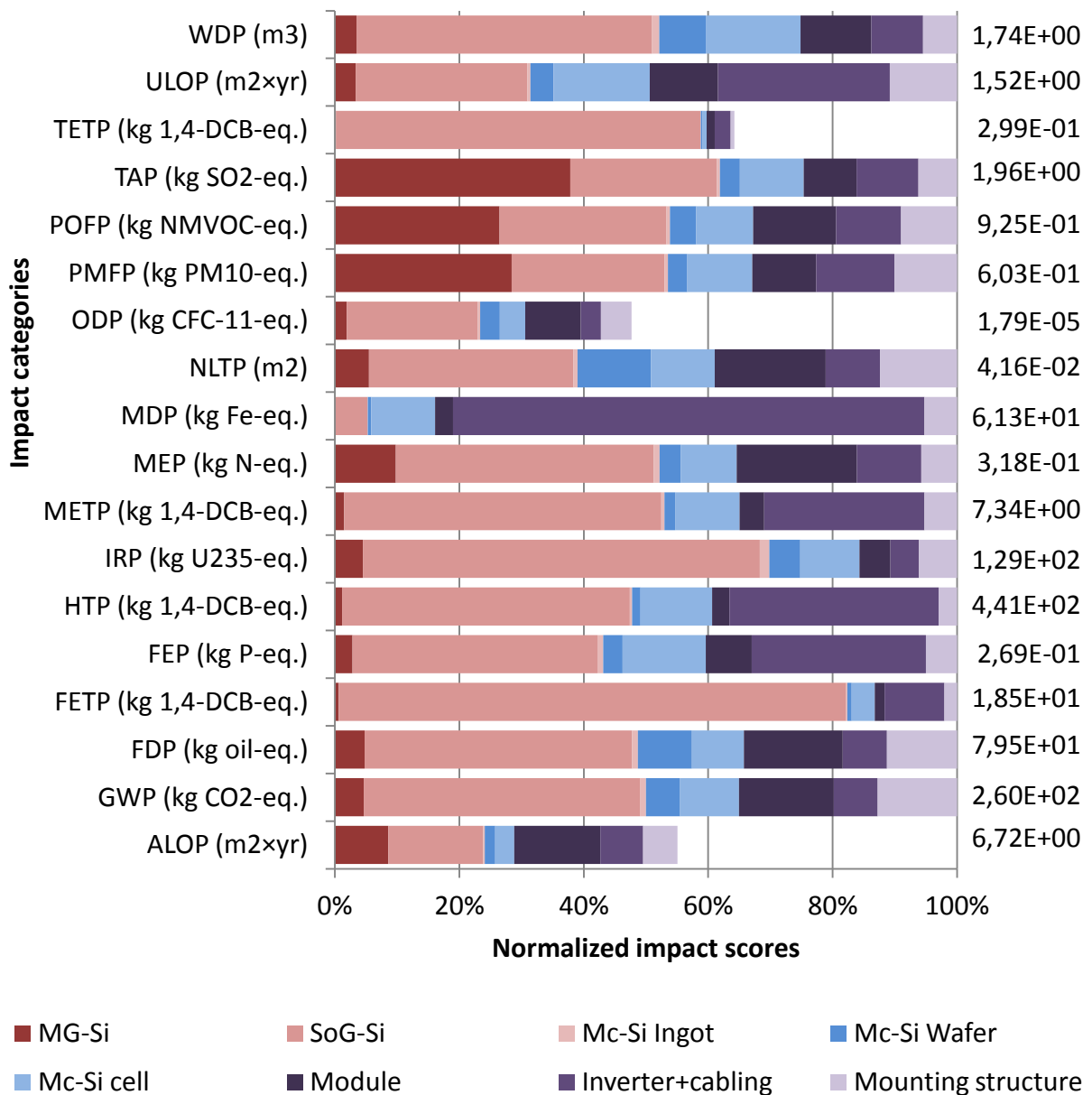


**Figure 12.2: Mc-Si Sim, UCTE el mix. Relative contribution from foreground processes to impact categories normalized to highest impact score across the different PV technologies. Aggregated impact results per m<sup>2</sup> PV system. (For abbreviations see Table 5.1).**

The production of SoG-Si has significant contributions in all of the impact categories, except for the metal depletion, where the inverter and cabling account for as much as 76% of the impacts (explained later). The SoG-Si production actually contributes with the highest normalized share in 15 out of 18 impact categories. The exceptions are the metal depletion (MDP), particulate matter formation (PMFP) and terrestrial acidification (TAP).

The normalized contribution from the production of SoG-Si range from 5% (MDP) up to 82% (freshwater ecotoxicity potential, FETP). As much as 73% of the freshwater ecotoxicity

potential is due to direct impacts from the SoG-production itself. The SoG-Si production has high normalized shares in the other toxicity categories too:

- 59% of the terrestrial ecotoxicity potential (TETP). As much as 88% of this contribution is due to direct impacts from the SoG-production itself.
- 51% of the marine ecotoxicity potential (METP). 30% of this contribution is direct impacts from the SoG-Si production.
- 46% of the human toxicity potential (HTP). 28% of this contribution is direct impacts from the SoG-Si production.

The contribution from the SoG-production to these toxicity potentials comes from the emissions of chlorine to rivers. The chlorine is used in a membrane cell during the SoG-Si production.

Other significant contributions from the SoG-Si production are 64% to the ionising radiation potential (IRP) and 47% to the water depletion potential (WDP). These contributions are related to indirect impacts resulting from the background processes. 65% of the contribution to the IRP is impacts from uranium milling, used in nuclear power plants to generate electricity, while 47% of the contribution to the WDP comes from the use of decarbonised water and tap water.

28% of the particulate matter formation potential, 26% of the photochemical oxidation potential (POFP) and 38% of the terrestrial acidification potential are related to the production of MG-Si. These are direct impacts resulting from emissions of sulphur dioxide and nitrogen oxides. The SoG-Si production contributes with approximately the same normalized shares as the MG-Si production in these three impact categories: 25% of the PMFP, 27% of the POFP and 24% of the TAP, respectively. These are indirect impacts.

The total GWP is 260 kg CO<sub>2</sub>-eq./m<sup>2</sup>. The SoG-production is also here the main contributor with a normalized share of 44% of the impacts. The high impact potential is due to the fact that the modified Siemens process is very energy intensive, generating indirect impacts from the background energy supply system.

The electric infrastructure of the PV system consists of the inverter and the cabling. These components contribute with the highest normalized share of 76% of the metal depletion potential. The use of metals like copper and tin in the making of components for the inverter and cabling stand for 65% of the metal depletion potential. The inverter and cabling processes also have high normalized shares within the impact categories human toxicity (34%), freshwater eutrophication (FEP, 28%), marine ecotoxicity (26%) and urban land occupation (ULOP, 28%). All of these contributions are due to indirect impacts resulting from disposal of sulfidic tailings (from mining of metals).

For the manufacturing of the module, the normalized contribution ranges from 1-19%. The highest normalized contributions from the module occur in the impact categories



agricultural land occupation (ALOP), fossil depletion (FDP), marine eutrophication (MEP) and natural land transformation (NLTP). Most of the impacts from the module are related to the background production of the aluminium for the frame and the sheets of cover glass, some also to the corrugated board used for packaging.

The ingot growing has more or less negligible contributions compared to the other foreground processes. The highest normalized contribution from this process is only 1,5% (IRP). Other processes with low normalized contributions compared to the foreground processes mentioned so far, are the wafer production, the solar cell production and the mounting structure. The impacts resulting from the wafer production are due to the silicon carbide used for the sawing slurry. The normalized contributions from this process are 12% or lower in all of the impact categories. The normalized contributions from the solar cell production are 15% or lower in all of the impact categories. These impacts are mainly related to the production of silver used in the metallization paste for front and back electrical contact. Other impacts are related to the use of hydrogen fluoride for etching of phosphor glass. The normalized contributions from the solar cell range from 0,7-15% (urban land occupation potential, and water depletion potential, WDP). For the mounting structure, the normalized contributions are 13% or lower. These impacts are due to the production of aluminium used in the mounting structure.

### **12.2.2 Mc-Si ESS**

Figure 12.3 displays the normalized contribution from the foreground processes to the impact categories by using the mc-Si ESS-inventory together with the aggregated impact potentials.

Note that Figure 12.3 in this section differ from Figure 12.2 in the previous section, even though both PV technologies are built on the mc-Si value chain. In Figure 12.3 the production of MG-Si and SoG-Si silicon happens in an integrated process, developed by Elkem Solar (denoted "SoG-Si"). In addition, the wafer production includes ingot growing (denoted "Mc-Si wafer") and the cabling and inverter are disaggregated into two process instead of one.

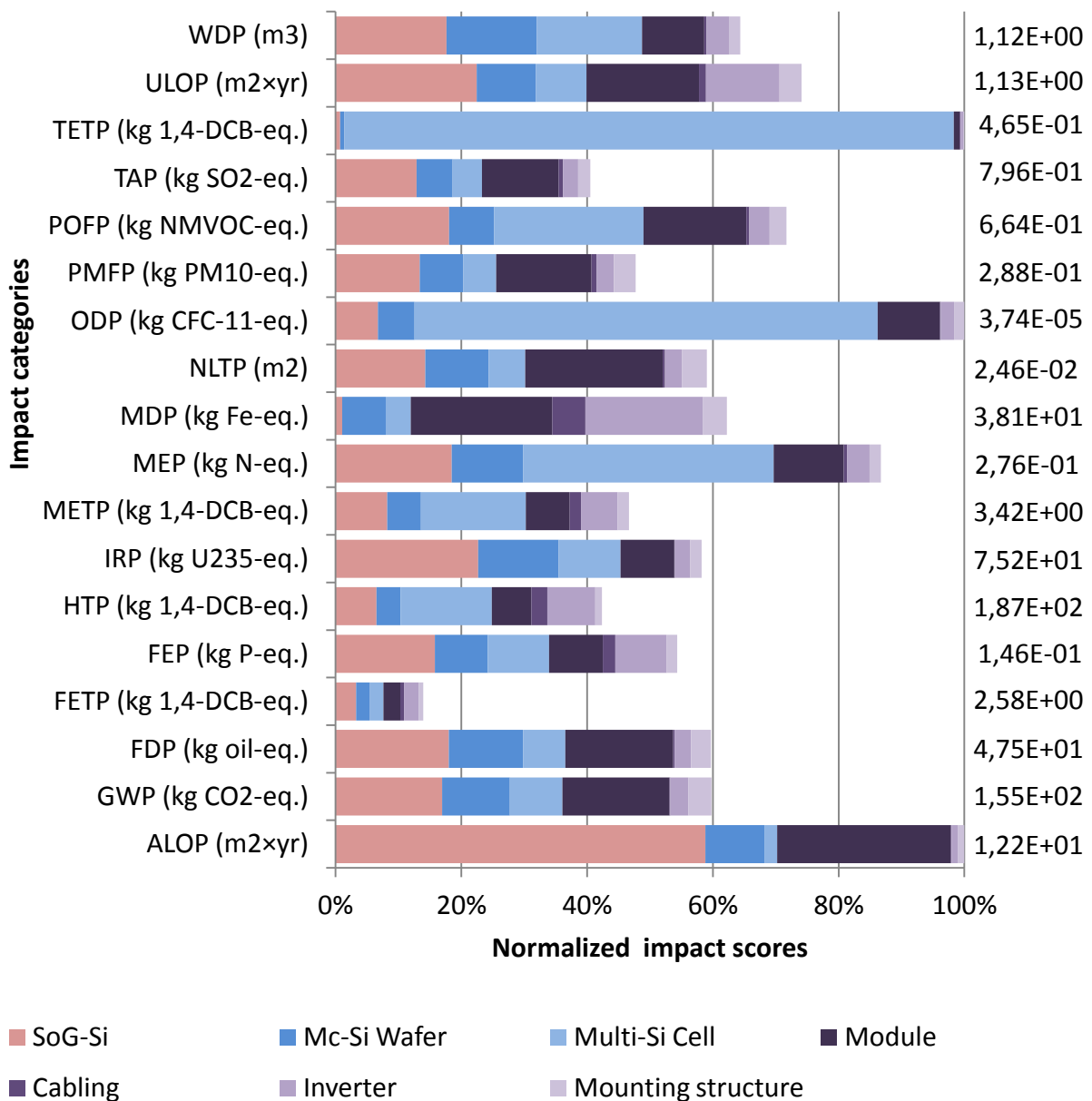


**Figure 12.3: Mc-Si ESS, UCTE el mix. Relative contribution from foreground processes to impact categories normalized to highest impact score across the different PV technologies. Aggregated impact results per m<sup>2</sup> of PV system. (For abbreviations see Table 5.1).**

The picture of broken down impacts over foreground processes are quite different for the mc-Si ESS-case compared to the mc-Si Sim-case. The solar cell production and the module manufacturing have become more important contributors. The production of SoG-Si is now the largest contributor in "only" 9 out of 18 impact categories: Agricultural land occupation (ALOP), climate change (GWP), fossil fuel depletion (FDP), freshwater ecotoxicity (FETP), freshwater eutrophication (FEP), ionising radiation (IRP), terrestrial acidification (TAP), urban

land occupation (ULOP) and water depletion (WDP). The normalized contribution from the production of SoG-Si range from 0,7% (TETP) up to 59% (ALOP).

It is natural to start commenting the three impact categories where the mc-Si ESS-case achieves higher impact scores than in the mc-Si Sim-case: The terrestrial ecotoxicity (TETP), ozone depletion (ODP) and agricultural land occupation (ALOP). 59% of the agricultural land occupation potential results from the SoG-Si production. This is due to indirect impacts from the softwood chips used as reduction agent in the ESS-process. For the terrestrial ecotoxicity potential (TETP) and the ozone depletion potential (ODP), the solar cell is by far the dominating process, with a normalized contribution of 97% and 74% respectively. The contribution to the terrestrial ecotoxicity potential comes from the direct air emissions of silver during the solar cell production itself. Silver is the main ingredient in the paste used in the front and back electrical contacts of the cell. 41% of the ozone depletion potential comes from the tetrafluoroethylene used in the solar cell production.

Except for the freshwater ecotoxicity potential, the solar cell production is the largest normalized contributor in the rest of the toxicity categories too. The solar cell is responsible for 15% of the human toxicity potential (HTP) and 17% of the marine ecotoxicity potential (METP). These impacts come from the solar cell production itself (silver emissions) and from production of metallization pastes. Also worth mentioning is the normalized contribution of 40% to the marine eutrophication potential (MEP) and 24% to the photochemical oxidant formation (POFP) from the solar cell. 38% of the marine eutrophication potential is due to the treatment of effluent cell waste, while 26% of the photochemical oxidation formation potential is due to direct emissions of non-methane volatile organic compounds (NMVOC) during the solar cell production. The total HTP-score and the total METP-score for the mc-Si ESS-case are both lower than the part of the HTP-score and the part of the METP-score resulting from producing SoG-Si in the mc-Si Sim-case.

The total GWP-score for the mc-Si ESS-case is actually approximately the same as the part of the GWP-score resulting from producing the SoG-Si and the PV module in the mc-Si Sim-case. The total GWP is 155 kg CO<sub>2</sub>-eq./m<sup>2</sup>, a decrease of 40% relative to the mc-Si Sim-case. The SoG-Si production and the module each contributes to 17% of the GWP. The reasons for the contribution from these processes are the energy feedstock/electricity mix used in the SoG-production and the production of aluminium for frame and solar glass for the module. Comparing the inventories of the mc-Si Sim-case and the mc-Si ESS-case, the modified Siemens process uses 1 098 MJ/kg SoG-Si produced (305 kWh), while the Elkem Solar process uses 200 MJ/kg SoG-Si produced (55 kWh). In other words, the energy demand for the ESS-process makes up under one fifth of the energy demand of the modified Siemens process. Considering that Elkem Solars technology is an integrated process, where the MG-Si and SoG-Si production is done in the same process step, makes this process even more energy efficient than the modified Siemens process. If the energy used in the MG-production for the Sim-case also were to be added, the total energy demand would be 1 144 MJ/kg MG-

Si AND SoG-Si produced (318 kWh). In addition, Elkem Solar uses a larger share of wood as reduction agent than what is given in the inventory of the Sim-case. While Elkem Solar uses 2,8 kg of softwood chips/kg SoG-Si produced, the modified Siemens process uses 0,19 kg of charcoal/kg MG-Si produced.

The production of SoG-Si accounts for 23% of the ionising radiation potential (IRP), caused by the share of nuclear power in the UCTE electricity mix. The 22% normalized contribution from the SoG-Si to the urban land occupation (ULOP) are due to the softwood used for the chips as reduction agent in the ESS-process.

The module and the inverter each accounts for 22% and 19% of the metal depletion potential (MDP) respectively. This is due to the tin, copper, manganese and steel used in either the components for the module or inverter. The total MDP-score for this case is lower than the part of the MDP-score caused by the inverter and cabling in the Sim-case. The normalized contributions from the inverter in the rest of the impact categories are 12% or lower. These impacts are related to the use of e.g. gold, manganese and tin and to disposal of sulfidic tailings.

The module accounts for 28% of the ALOP due to the production of corrugated board paper for packaging. It also accounts for 22% of the natural land transformation potential (NLTP) due to the production of aluminium and solar glass. The normalized contributions from the module in the rest of the impact categories are 18% or less. These impacts are mainly related to the use of primary aluminium in the frame, solar glass and copper for cell interconnections.

The environmental impacts from the mounting structure are more or less negligible compared to the other foreground processes, its normalized shares ranging from 0,2-4% (NLTP). These impacts are mostly related to the production of aluminium (some also to the steel) used in the mounting structure. The normalized shares of impacts from the cabling are low and range from 0,1-5,3% (MDP). These impacts are related to the production of copper and disposal of sulfidic tailings.

The impacts resulting from the wafer production (ingot growing included) are mainly due to the electricity supply. The normalized contributions from the wafer production are 14% or lower in all of the impact categories. It is worth noticing that even though the inventory of the mc-Si ESS-case is more detailed (has more entries), the normalized contribution from the wafer production in the mc-Si Sim-case is approximately at the same level as the wafer production in the mc-Si ESS-case, with 12% or lower normalized contribution. Adding the ingot process to the wafer process in the mc-Si Sim-case, the normalized contribution get even closer that of the mc-Si ESS-case where the wafer process actually includes the ingot growing.

### 12.2.3 Case 3: CdTe

Figure 12.4 displays the normalized contribution from the foreground processes to the impact categories by using the CdTe-inventory, together with the aggregated impact potentials.

Due to company confidentiality, it has not been possible to disaggregate the data set provided by the NREL for the CdTe technology. This means a low resolution concerning the module manufacturing and the components making up the solar cell. Due to less process steps, Figure 12.4 are simpler than Figure 12.2 and Figure 12.3 for the mc-Si PV technologies.

**Note that the x-axis stops at 50% normalized contribution.**

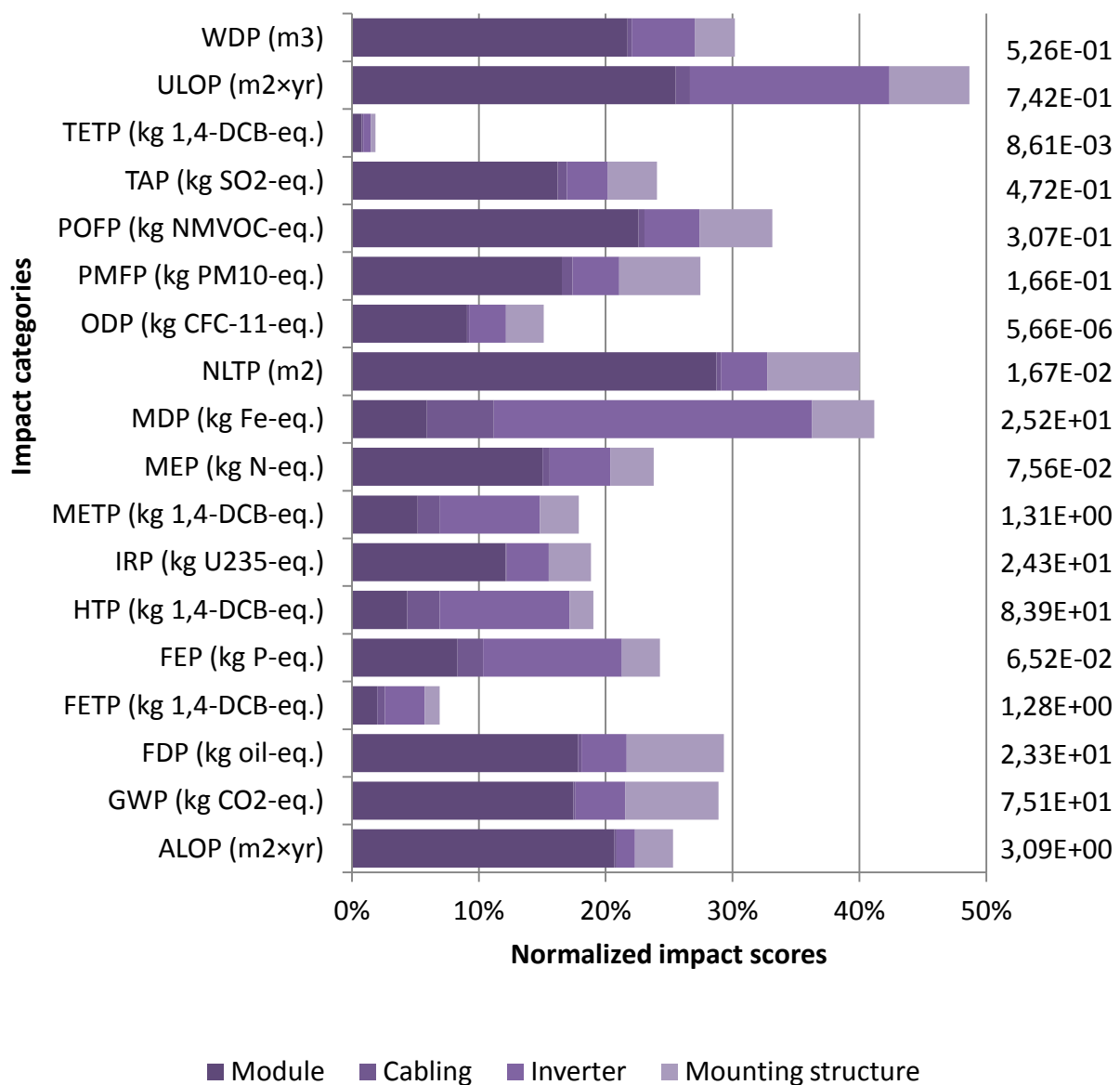


**Figure 12.4: CdTe, UCTE el mix. Relative contribution from foreground processes to impact categories normalized to highest impact score across the different PV technologies. Aggregated impact results per m<sup>2</sup> of PV system. (For abbreviations see Table 5.1).**

The module manufacturing has the highest normalized contribution in all of the impact categories except for freshwater ecotoxicity (FETP), freshwater eutrophication (FEP), human toxicity (HTP), marine ecotoxicity (METP) and metal depletion (MDP), where the normalized contribution from the inverter are higher. The normalized contribution from the production of the module range from 0,8% (terrestrial ecotoxicity potential, TETP) up to 29% (natural land transformation potential, NLTP). 16% of the contribution to the natural land occupation potential and 23% of the contribution to the urban land occupation (ULOP) come from the infrastructure for the module production, i.e. the photovoltaic panel factory. The rest of the NLTP impact (65%) mainly comes from well for exploration and production, due to the use of fossil fuel for transportation. The module accounts for 23% of the photochemical oxidation formation (POFP) and 21% of the agricultural land occupation (ALOP). For the photochemical oxidation potential, 24% comes from the transport of materials to the module factory by freight ship, while 18% comes from the glass used for the module. 39% of the agricultural land occupation potential are due to indirect impacts from the softwood used for the corrugated board paper in the packaging.

The total GWP is 75 kg CO<sub>2</sub>-eq./m<sup>2</sup>, a decrease of 71% relative to the mc-Si Sim-case. The main contributor is the module, with a normalized share of 17%. Glass used for the module account for 15% of the GWP, while primary aluminium for the back electrical contact accounts for 6,5%. The total GWP-score for this case is lower than the part of the GWP-score resulting from the SoG-Si production in the mc-Si Sim-case.

The manufacturing of the inverter accounts for 25% of the metal depletion potential, caused by the use of copper, manganese and tin in the inverter components (e.g. printed wiring board and transformer). The normalized contribution of 11% to the freshwater eutrophication potential from the inverter is due to the disposal of sulfidic tailings resulting from the production of gold and copper used for the printed wiring board.

The cabling and mounting structure have small normalized contributions compared to the module and inverter. The normalized contributions range from 0,1-5,3% (MDP) for the cabling and 0,4-7,7% for the mounting structure. The use of copper is usually the reason for the impacts from the cabling. For the mounting structure, the impacts result from the use of primary aluminium (sometimes also steel). Note that the normalized contributions from the cabling in the CdTe-case are more or less the same as the normalized contributions from the cabling in the mc-Si ESS-case, due to approximately the same cabling-inventory.

#### **12.2.4 Case 4: CIGS**

Figure 12.5 displays the normalized contribution from the foreground processes to the impact categories by using the CIGS-inventory, together with the aggregated impact

potentials. **Note that the x-axis has been cut off at 60% normalized contribution and that the MDP actually goes to 84% normalized contribution.**

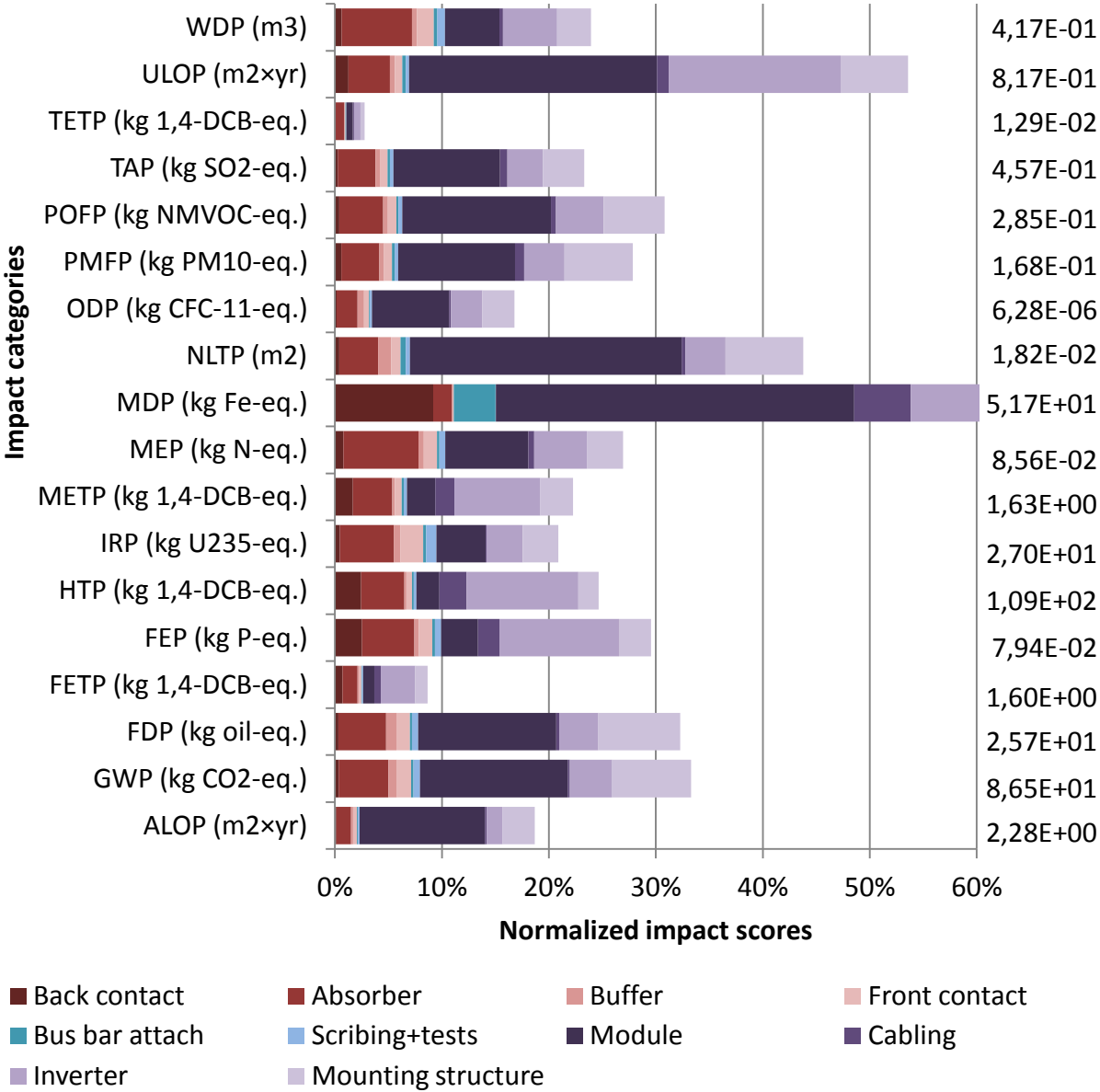


**Figure 12.5: CIGS, UCTE el mix. Relative contribution from foreground processes to impact categories normalized to highest impact score across the different PV technologies. Aggregated impact results per m<sup>2</sup> of PV system. (For abbreviations see Table 5.1). The graph has been cut off at 60% normalized contribution, and the MDP has in realty a normalized contribution of 84%.**

The module manufacturing has the highest normalized shares in all of the impact categories except for freshwater ecotoxicity (FETP), freshwater eutrophication (FEP), human toxicity (HTP) and marine ecotoxicity (METP), where the normalized shares from the inverter are

higher, and for terrestrial ecotoxicity (TETP) and water depletion (WDP), where the normalized shares from the absorber are higher. The normalized contribution from the production of the module range from 0,6% (terrestrial ecotoxicity potential, TETP) up to 34% (metal depletion potential, MDP). 46% of the contribution to the metal depletion comes from production of tin. The module accounts for 25% of the natural land transformation (NLTP), 23% of the urban land occupation (ULOP) and 14% of the photochemical oxidation formation (POFP). 61% of the contribution to the natural land transformation are indirect impacts caused by well for exploration and production, due to use of fossil fuels in the glass production, and 15% are related to the module factory. This is similar to the contributions from the module to the NLTP in the CdTe-case. 21% of the urban land occupation comes from the PV module factory. 19% of the photochemical oxidation potential comes from the glass used for the module.

The total GWP is 86 kg CO<sub>2</sub>-eq./m<sup>2</sup>, a decrease of 67% relative to the mc-Si Sim-case. The main contributor is the module with a normalized share of 14%. Glass for the module accounts for 12%, while primary aluminium for the frame accounts for 6,9%. These contributions are similar to the ones from the module in the CdTe-case. However, note that in the CdTe-case, the use of aluminium is related to the back contact, while in the CIGS-case, the use of aluminium is related to the frame. (The CdTe module is frameless). Like for the CdTe-case, the total GWP-score for the CIGS-case is also lower than the part of the GWP resulting from the SoG-Si production in the mc-Si Sim-case.

The inverter accounts for 26% of the metal depletion, 16% of the urban land occupation, 11% of the freshwater eutrophication and 10% of the human toxicity. The rest of the normalized contributions from this process are 5,1% or lower. The contribution to the metal depletion is connected to the use of metals like copper, manganese, tin and gold. 12% of the urban land occupation, 54% of the freshwater eutrophication and 66% of the human toxicity are related to the disposal of sulfidic tailings.

The normalized contributions from the mounting structure range from 0,4-7,7% and are also in this case mainly related to the use of primary aluminium (some also to steel).

Even though the resolution in this case is higher than in the CdTe-case (disaggregated into more process steps), the additional processes do not contribute with much impacts compared with the module and inverter. The back contact contributes with a normalized share of 9,2% of the metal depletion, due to the use of molybdenum. The absorber (CIGS) accounts for 7,0% of the marine eutrophication (MEP), related to the use of ethylenediaminetetraacetic acid in the gallium production, and 6,6% of the water depletion (WDP), related to the leaching residues from indium production. The rest of the normalized contribution from the back contact range from 0,02-2,5% (FEP), while for the absorber the rest of the normalized contribution range from 0,9-5,1% (IRP).



The production of the buffer, front contact, bus bar attach and scribing+tests have virtually no environmental impacts related to them, their normalized contribution range between 0,03% and 3,9%. The impacts from these three processes are related to the electricity use.

The normalized contribution from the cabling range from 0,1-5,3% (MDP). This is similar to the normalized contribution from the cabling in the CdTe-case and is due to the use of the same cabling inventory.

### 12.3 Sensitivity analysis

As explained in chapter 5.1, the impact results from the sensitivity analysis will be compared with impact results for generating 1 kWh of electricity by wind power. The range of impact values from the wind power system will be referred to as the *windband*, meaning the impact values between the minimum and the maximum of what is found in chosen literature. (When the text refer to that a certain PV technology/case has the potential to "*reach the windband*", the meaning is that the PV technology in question can reach an impact value equal to or lower than the maximum impact value caused by wind power).

The windband values for the GWP are chosen according to what is found in Arvesen & Hertwich (2012); a review of the existing LCAs of wind power. They found that most of the studies gave a GWP between 9,0-24,0 g CO<sub>2</sub>-eq./kWh. This is what is used for the GWP windband in this report (often only referred to as the windband in the text).

The windband values for other impact categories is chosen according to what is found in Hertwich et al. (2013), where the minimum values are the impact results from onshore wind power and the maximum values are the impact results from offshore wind power.

The impact scores for the PV system are initially given on a per m<sup>2</sup>-basis. In order to present the impact scores on a per kWh-basis, the following equation has been used:

$$PIE = \frac{PIA}{G} \quad (12.1)$$

where, *PIE* is the impact score per energy [kWh<sup>-1</sup>], *PIA* is the impact score per area [(m<sup>2</sup>)<sup>-1</sup>] and *G* is the lifetime electricity generation [kWh/m<sup>2</sup>].

Transforming the impact score onto a per kWh-basis makes it possible to compare the results of this analysis with other similar studies and with other energy technologies, in this case wind power.

The last section will present the possible GWP-range for the different PV technologies. This will be referred to as the *overall performance envelope*.

For future reference, the base case scenario can be found in Table 12.1.

**Table 12.A: Overview of parameters for the base case scenario.**

<b>Parameter:</b>	<b>Value:</b>	<b>Comment:</b>								
Conversion efficiency [%]	<table border="0"> <tr> <td>Mc-Si Sim</td> <td>16,0</td> </tr> <tr> <td>Mc-Si ESS</td> <td>13,2</td> </tr> <tr> <td>CdTe</td> <td>11,7</td> </tr> <tr> <td>CIGS</td> <td>11,0</td> </tr> </table>	Mc-Si Sim	16,0	Mc-Si ESS	13,2	CdTe	11,7	CIGS	11,0	The PV module conversion efficiencies are chosen according to what have been the basis for the collected inventories. For the CdTe and CIGS, the weighted average of the conversion efficiency in the two data sets has been used. (It should be noted that the efficiency of the CIGS in this LCA is slightly misleading in terms of reflecting the current technology on the market. The efficiency of CIGS PV modules is usually higher than those of CdTe PV modules (see chapter 3.2.1) (DayStar Technologies Inc, 2013a)).
Mc-Si Sim	16,0									
Mc-Si ESS	13,2									
CdTe	11,7									
CIGS	11,0									
Performance ratio [%]	75%	Default value for rooftop PV systems recommended in Fthenakis et al. (2011b).								
Lifetime [years]	30 years	Default value for mature PV module technologies recommended in Fthenakis et al. (2011b).								
Direct normal irradiation [kWh/m <sup>2</sup> /year]	1 700	Estimate for the direct normal irradiation reaching an optimally inclined surface in South Europe during a year (de Wild-Scholten, 2011). I.e. installation location assumed to be Southern Europe.								
Lifetime electricity generation [kWh/m <sup>2</sup> ]	<table border="0"> <tr> <td>Mc-Si Sim</td> <td>6 120</td> </tr> <tr> <td>Mc-Si ESS</td> <td>5 049</td> </tr> <tr> <td>CdTe</td> <td>4 425</td> </tr> <tr> <td>CIGS</td> <td>4 208</td> </tr> </table>	Mc-Si Sim	6 120	Mc-Si ESS	5 049	CdTe	4 425	CIGS	4 208	Electricity generated from a PV system during its entire lifetime. Found by plotting the previous parameter values into equation 3.3.
Mc-Si Sim	6 120									
Mc-Si ESS	5 049									
CdTe	4 425									
CIGS	4 208									
Electricity mix	UCTE el mix	PV system assumed produced in Southern Europe.								

Using equation 12.1, and the base case parameters in Table 12.1, the resulting GWP in g CO<sub>2</sub>-eq./kWh for the four cases are: 42,5 for the mc-Si Sim-case, 30,8 for the mc-Si ESS-case, 16,8 for the CdTe-case and 20,6 for the CIGS-case.

### 12.3.1 Conversion efficiency

Figure 12.6 displays the GWP results from varying the PV module conversion efficiency. **Note that the x-axis starts at 8% conversion efficiency.** The range of possible conversion efficiency values vary according to the different PV technologies. The choice for the efficiency limits has been based on the following:

- **Lowest estimate:** For the mc-Si PV technologies based on what is presented in Jäger-Waldau (2012), where the current efficiency range for commercial mc-Si PV modules is 12-17%. For the thin film technologies, based on the lowest of what is used in previous LCA studies of thin film PV systems, 8% for CdTe and 10% for CIGS (see appendices J.1-3).
- **Highest estimate:** Based on the highest of the expected/predicted future conversion efficiencies for PV technologies presented in IEA (2010) and in Dimmler (2012). For the mc-Si PV technologies the estimate of 21% for the development between the years 2020-2030 in IEA (2010) has been used. For the thin film PV technologies the estimates of 17% for CdTe and 19% for CIGS for the development towards the year 2040 in Dimmler (2012) have been used.

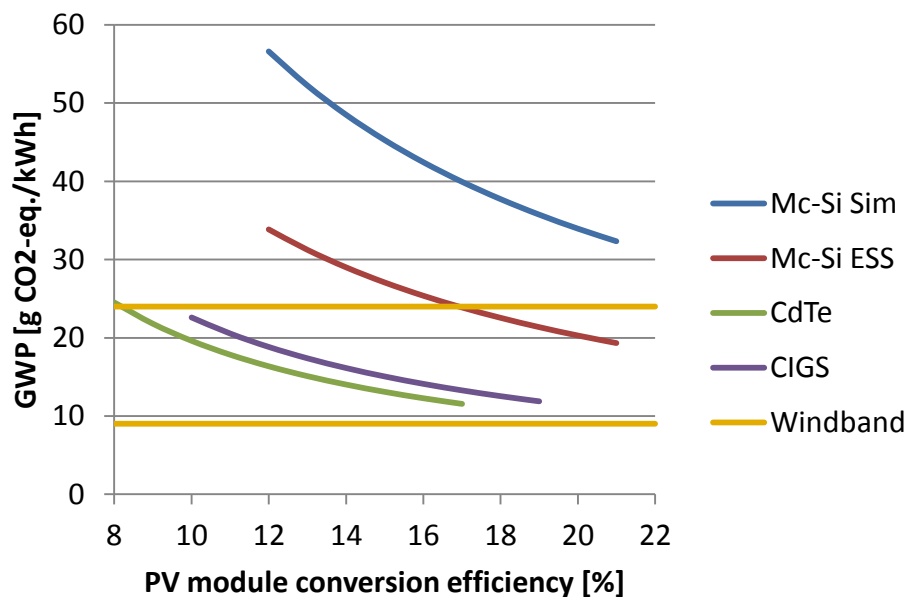


Figure 12.6: GWP [g CO2-eq./kWh] related to change in PV module conversion efficiency. GWP values for wind power included for comparison (windband).

The relative reductions in GWP when going from the lowest to the highest conversion efficiencies are:

- 43% for both mc-Si cases. This gives average reductions in GWP of 2,7 g CO<sub>2</sub>-eq. per % improvement in conversion efficiency for the mc-Si Sim-case, and 1,6 g CO<sub>2</sub>-eq. per % improvement in conversion efficiency for the mc-Si ESS-case.
- 53% for CdTe, giving an average reduction in GWP of 1,4 g CO<sub>2</sub>-eq. per % improvement in conversion efficiency.
- 47% for CIGS, giving an average reduction in GWP of 1,2 g CO<sub>2</sub>-eq. per % improvement in conversion efficiency.

Even with the lowest possible conversion efficiencies, both CdTe and CIGS are within the windband. However, none of them reach the minimum value of the windband (9 g CO<sub>2</sub>-eq./kWh) with the highest conversion efficiencies. They are not far from it though. CdTe with 17% conversion efficiency gives a GWP equal to 11,5 g CO<sub>2</sub>-eq./kWh, while CIGS with 19% conversion efficiency gives a GWP equal to 11,9 g CO<sub>2</sub>-eq./kWh.

Mc-Si ESS can reach the windband with a conversion efficiency of 17% or higher, while mc-Si Sim can not reach the windband at all with only conversion efficiency improvements. Even with high conversion efficiencies, the mc-Si PV technologies are far from reaching the minimum value of the windband: With a conversion efficiency of 21%, mc-Si ESS achieves a GWP of 19,3 g CO<sub>2</sub>-eq./kWh and mc-Si Sim a GWP of 32,4 g CO<sub>2</sub>-eq./kWh.

### 12.3.2 Performance ratio

Figure 12.7 displays the GWP results from varying the performance ratio of the PV system between 70 and 90%.

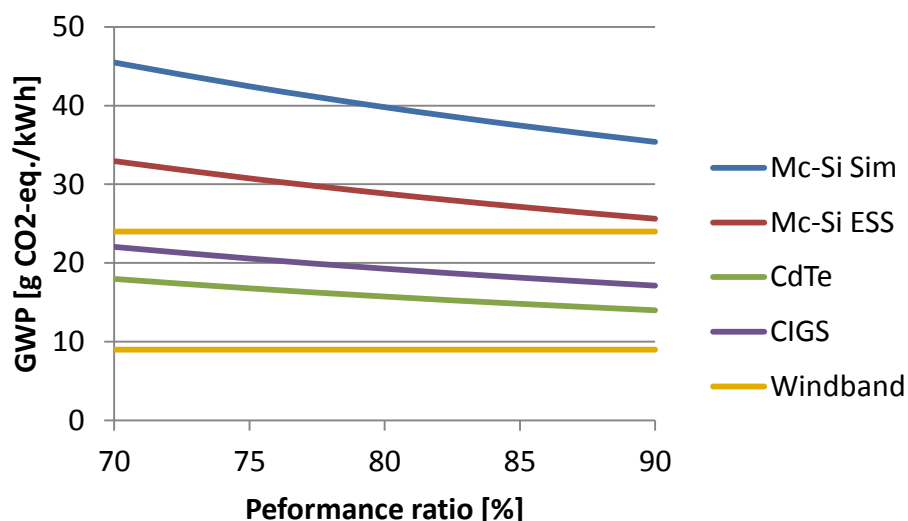


Figure 12.7: GWP [g CO<sub>2</sub>-eq./kWh] related to change in performance ratio of the PV system. GWP values for wind power included for comparison (windband).

The relative reduction in GWP when going from a performance ratio of 70 to 90% is 22%. This gives average reductions of 0,5 g CO<sub>2</sub>-eq. per % improvement in performance ratio for the mc-Si Sim case, 0,4 g CO<sub>2</sub>-eq. per % improvement in performance ratio for the mc-Si ESS-case and 0,2 g CO<sub>2</sub>-eq. per % improvement in performance ratio for both the CdTe-case and the CIGS-case.

Both thin film technologies are already within the windband with the lowest possible performance ratio of 70%. With a performance ratio of 90%, the GWP is 14,0 g CO<sub>2</sub>-eq./kWh for the CdTe and 17,1 g CO<sub>2</sub>-eq./kWh for the CIGS, meaning that they do not reach the minimum value of the windband.

Neither of the mc-Si PV technologies can reach the windband with only improvements in performance ratio. With a performance ratio of 90%, the GWP are 35,4 and 25,6 g CO<sub>2</sub>-eq./kWh for mc-Si Sim and mc-Si ESS respectively.

### 12.3.3 Lifetime

Figure 12.8 displays the GWP results from varying the lifetime of the PV system between 20 and 30 years.

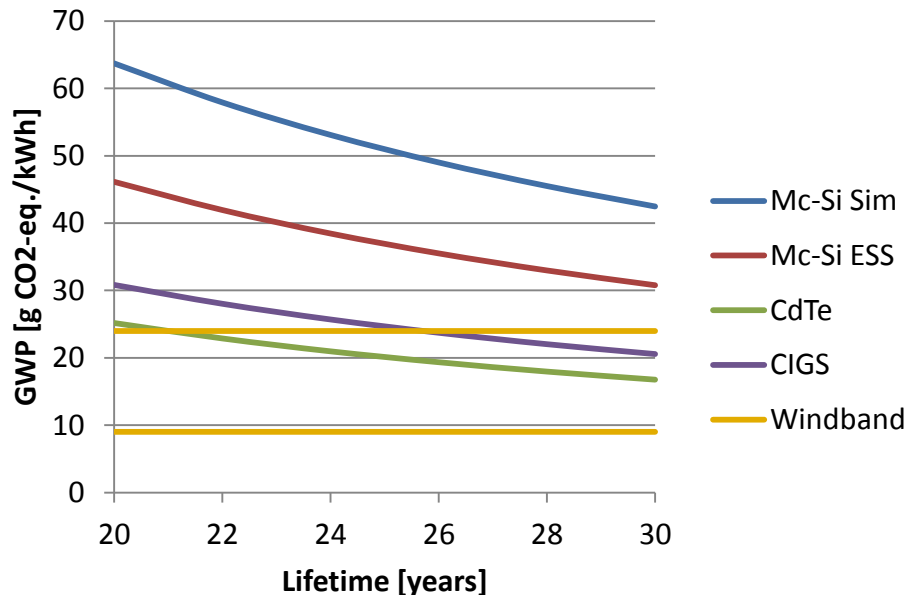


Figure 12.8: GWP [g CO<sub>2</sub>-eq./kWh] related to change in lifetime of the PV system. GWP values for wind power included for comparison (windband).

The relative reduction in GWP when going from a lifetime of 20 to 30 years is 33%.

The CdTe reach the windband after approximately 21 years lifetime, the CIGS at approximately 25,5 years. With a lifetime of 30 years (equal to base case), they can reach a GWP-score of 16,8 and 20,6 g CO<sub>2</sub>-eq./kWh respectively.

The mc-Si PV technologies do not have the possibility to reach the windband at all with only improvements in lifetime. At 30 years lifetime the mc-Si Sim achieves a GWP of 42,5 g CO<sub>2</sub>-eq./kWh and the mc-Si ESS a GWP of 30,8 g CO<sub>2</sub>-eq./kWh.

### 12.3.4 Direct normal irradiation

Figure 12.9 displays the GWP results from varying the direct normal irradiation reaching a PV system during a year. The chosen minimum value of 1 200 kWh/m<sup>2</sup>/year equals the average, yearly direct normal irradiation in Germany (Zuser & Rehnberger, 2011). The chosen maximum value of 2 400 kWh/m<sup>2</sup>/year equals the average, yearly direct normal irradiation in the USA. This value also corresponds the direct normal irradiation reaching locations in South America and Africa during a year (Zuser & Rehnberger, 2011).

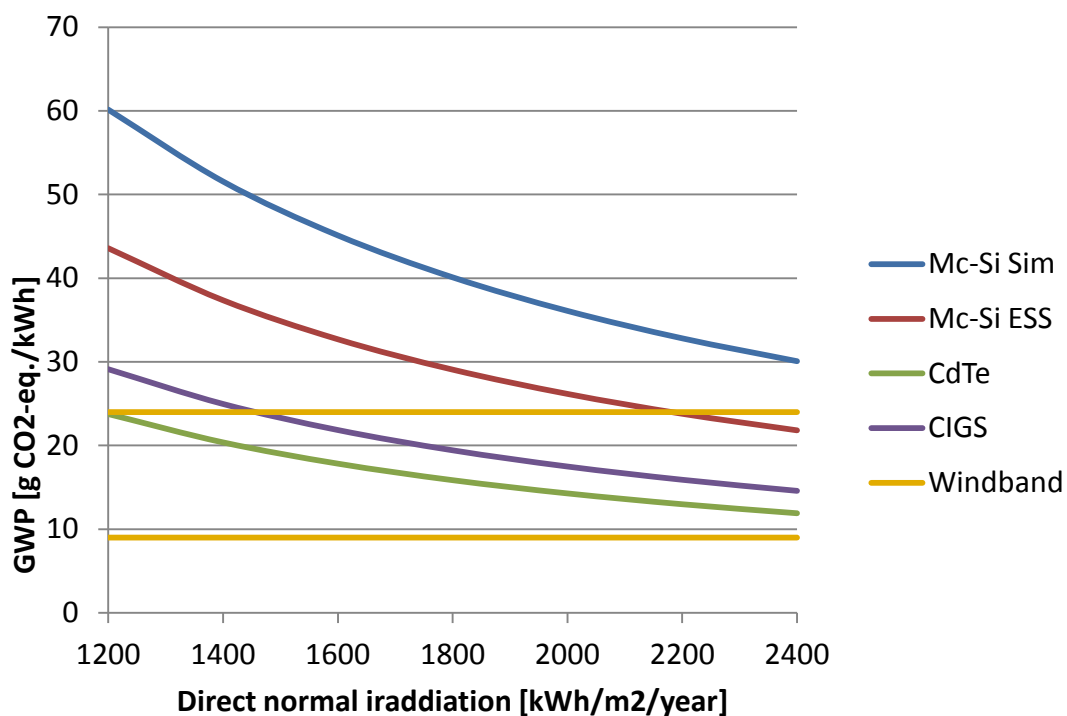


Figure 12.9: GWP [g CO<sub>2</sub>-eq./kWh] related to change in the direct normal irradiation. GWP values for wind power included for comparison (windband).

The relative reduction in GWP when going from a direct normal irradiation of 1 200 up to 2 400 kWh/m<sup>2</sup>/year is 50%.

All of the investigated PV technologies, except for mc-Si Sim, have the potential to reach the windband: CdTe is within the windband already at the minimum irradiation value of 1 200 kWh/m<sup>2</sup>/year. CIGS reach the windband at approximately 1 500 kWh/m<sup>2</sup>/year and mc-Si ESS at approximately 2 200 kWh/m<sup>2</sup>/year.

At the maximum irradiation of 2 400 kWh/m<sup>2</sup>/year, the corresponding GWP values in g CO<sub>2</sub>-eq./kWh are: 30,1 for mc-Si Sim, 21,8 for mc-Si ESS, 11,9 for CdTe and 14,6 for CIGS, meaning that none of the investigated cases can reach the minimum value of the windband with only increase in the direct normal irradiation.

### 12.3.5 Lifetime electricity generation

The lifetime electricity generation of a PV system is (as stated earlier in equation 3.3) equal to the product of the conversion efficiency, performance ratio, lifetime and direct normal irradiation. Due to the large range of possible values for the lifetime electricity generation, it has been decided to present the GWP as a function of the ratio of the varying lifetime electricity generation ( $G$ ) and the base case lifetime electricity generation ( $G_{base}$ ). Table 12.2 presents how the minimum and maximum values for the x-axis in Figure 12.10 have been decided.

**Table 12.B: Choice for x-value limits - ratio of lifetime electricity generation relative to base case.**

	Lowest estimate	Base case	Highest estimate
<b>Parameters:</b>			
Efficiency, mc-Si Sim [%]	12,0	16,0	20,0
Efficiency, mc-Si ES [%]		13,2	
Efficiency, CdTe [%]	8,0	11,7	17,0
Efficiency, CIGS [%]	10,0	11,0	19,0
Performance ratio [%]	70	75	90
Lifetime [years]	20	30	30
Direct normal irradiation [kWh/m <sup>2</sup> /year]	1 200	1 700	2 400
<b>Lifetime electricity generation, <math>G</math> [kWh/m<sup>2</sup>]:</b>			
Mc-Si Sim	2 016	6 120	13 608
Mc-Si ESS		5 049	
CdTe	1 344	4 475	11 016
CIGS	1 680	4 208	12 312

Ratio of lifetime electricity generation relative to base case, $G/G_{base}$ :			
Mc-Si Sim	0,3	1,0	2,2
Mc-Si ESS	0,4		2,7
CdTe	0,3		2,5
CIGS	0,4		2,9

Figure 12.10 shows the GWP results for varying the lifetime electricity generation relative to the base case ( $G/G_{base}$ ). When the "ratio of lifetime electricity generation relative to base case" is equal to one, this represents the lifetime electricity generation resulting from using the parameters defined in the base case (see Table 12.1). This point is also marked off at Figure 12.10.

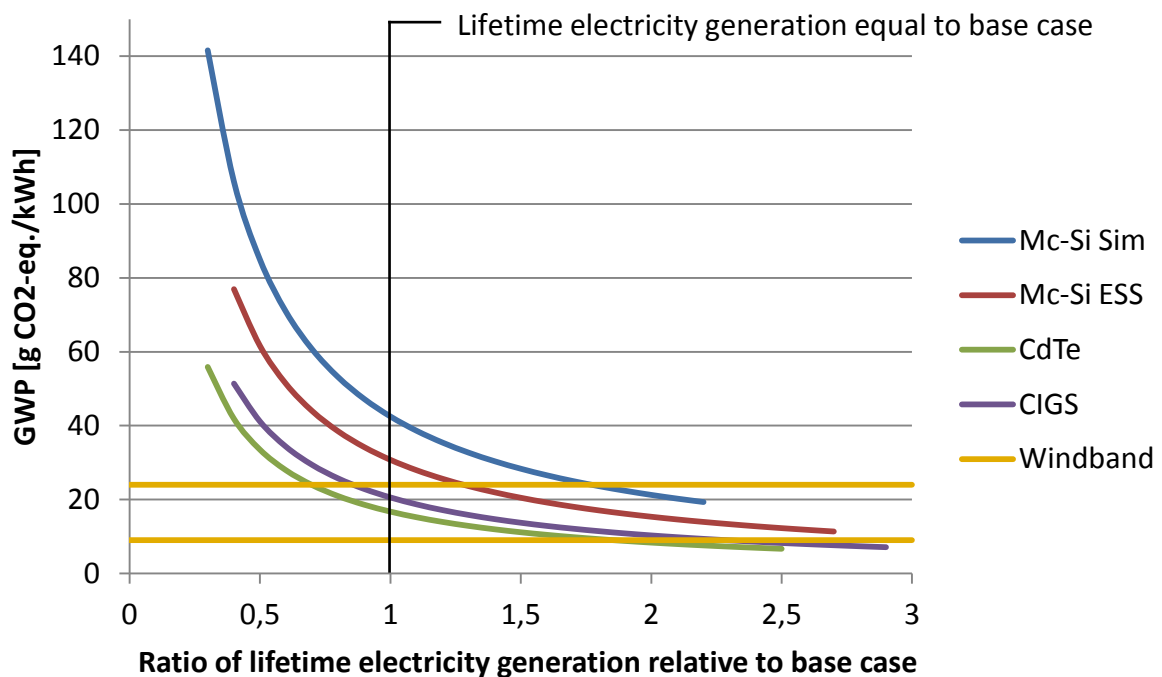


Figure 12.10: GWP [g CO<sub>2</sub>-eq./kWh] related to change in the ratio of electricity generation relative to base case. GWP values for wind power included for comparison (windband).

Looking at Figure 12.10, all of the PV technologies have the potential to reach the windband:

- Mc-Si Sim reaches the windband at  $x=1,8$ , meaning a 80% increase in the lifetime electricity generation relative to the base case.



- Mc-Si ESS reaches the windband at  $x=1,3$ , meaning a 30% increase in the lifetime electricity generation relative to the base case.
- CdTe reaches the windband at 0,7, meaning a 30% decrease in the lifetime electricity generation relative to the base case.
- CIGS reaches the windband at 0,9, meaning a 10% decrease in the lifetime electricity generation relative to the base case.

Only the thin film PV technologies have the potential to reach the minimum value of the windband. To achieve this, CdTe must have an increase in the lifetime electricity generation of 90% ( $x=1,9$  in Figure 12.10) and CIGS of 130% ( $x=2,3$  Figure 12.10), relative to the base case. With the right conditions, these two PV technologies can obtain an even lower GWP than the minimum value of the windband: CdTe achieves a GWP of 6,7 g CO<sub>2</sub>-eq./kWh at point  $x=2,5$  in Figure 12.10, meaning an increase of 150% in the lifetime electricity generation relative to the base case. CIGS achieves a GWP of 7,1 g CO<sub>2</sub>-eq./kWh at point  $x=2,9$  in Figure 12.10, meaning an increase of 190% in the lifetime electricity generation relative to the base case. The lowest obtainable GWP for the mc-Si PV technologies are 19,3 g CO<sub>2</sub>-eq./kWh for mc-Si Sim at  $x=2,2$  and 11,4 g CO<sub>2</sub>-eq./kWh for mc-Si ESS at  $x=2,7$ .

### 12.3.6 Electricity mix

Figure 12.11 shows how the GWP varies with the use of different electricity supplies for the PV value chain. The electricity mixes used are: Hard coal (DE), natural gas (DE), UCTE el mix, wind power (RER) and hydropower (NO). The GWP values resulting from using these electricity supplies for the PV value chain have been marked off in Figure 12.11.

Note that the denotation "CC" on the x-axis refers to climate change, i.e. the GWP value for generating 1kWh electricity from the specific energy source/technology.

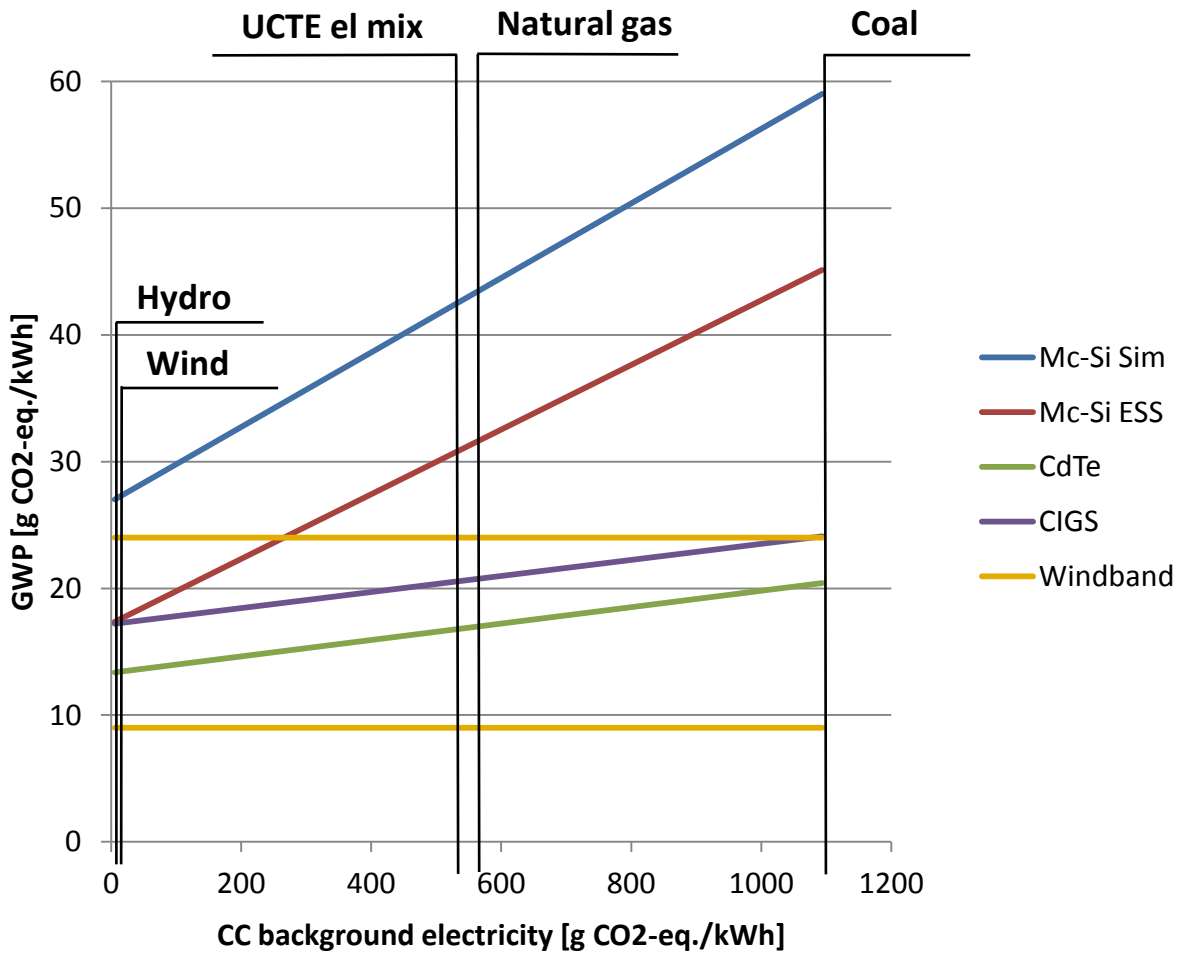


Figure 12.11: GWP [g CO2-eq./kWh] related to change in electricity supply mix (marked off on figure). GWP values for wind power included for comparison (windband).

The relative reductions in GWP when going from coal power to hydropower as electricity supply mix are:

- 54% for mc-Si Sim.
- 62% for mc-Si ESS.
- 35% for CdTe.
- 29% for CIGS.

The GWP of mc-Si Sim never reaches the windband, no matter what type of electricity mix is used. Mc-Si ESS has the potential to reach the the windband if the electricity supply comes from renewable energy like wind power or hydropower. The thin film PV technologies are within the windband even with coal power as electricity supply. Note that the GWP of mc-ESS and CIGS are approximately equal when using hydropower as electricity supply. None of the PV technologies get below the minimum value of the windband. When using

hydropower for electricity supply, the resulting GWP values in g CO<sub>2</sub>-eq./kWh are: 27,0 for mc-Si Sim, 17,4 for mc-Si ESS, 13,4 for CdTe and 17,2 for CIGS.

As one can see from Figure 12.11, using either wind power or hydropower as energy feedstock gives approximately equal GWP-scores. Coal as energy feedstock gives significantly higher GWP. Especially the two technologies for producing mc-Si PV systems, are sensitive to the electricity mix/energy feedstock. The electricity mix is often dependent on location. For examples, the typical Norwegian power mix consist of almost 99% hydropower, while the typical German power mix consist of a large share of thermal power from coal and gas. By switching from the coal power mix to the hydropower mix, one can assume that the whole value chain of the PV system takes place in Norway.

### 12.3.7 Energy efficiency (electricity)

Figure 12.12 displays how the GWP vary with improvements in energy efficiency, with the main focus on reduced electricity consumption during manufacturing.

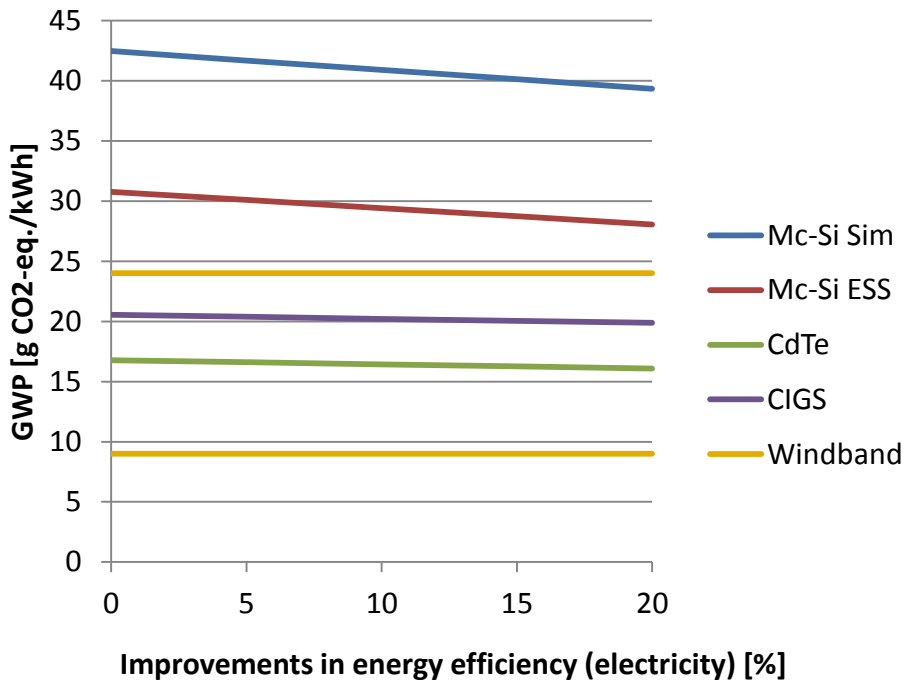


Figure 12.12: GWP [g CO<sub>2</sub>-eq./kWh] related to improvements in energy efficiency (electricity). GWP values for wind power included for comparison (windband).

The relative reductions in GWP when going from the current technology (no improvements in energy efficiency) to 20% improvements in energy efficiency are:

- 7% for mc-Si Sim, giving an average reduction in GWP of 0,2 g CO<sub>2</sub>-eq. per % improvement in energy efficiency .
- 9% for mc-Si ESS, giving an average reduction in GWP of 0,1 g CO<sub>2</sub>-eq. per % improvement in energy efficiency.
- 4% for CdTe, giving an average reduction in GWP of 0,03 g CO<sub>2</sub>-eq. per % improvement in energy efficiency.
- 3% for CIGS, giving an average reduction in GWP of 0,03 g CO<sub>2</sub>-eq. per % improvement in energy efficiency.

Improvements in energy efficiency have most impact on the GWP for the mc-Si PV technologies, due to their energy intensive production. With an improvement of 20% in energy efficiency, the GWPs are 39,3 g CO<sub>2</sub>-eq./kWh for mc-Si Sim and 28,1 g CO<sub>2</sub>-eq./kWh for mc-Si ESS, indicating that an energy efficiency improvement far above 20% is needed for these technologies in order to be able to reach the windband.

The thin film PV technologies are already within the windband without energy efficiency improvements. However, they do not reach the minimum value of the windband. 20% improvement in energy efficiency results in a GWP of 16,1 g CO<sub>2</sub>-eq./kWh for CdTe and 19,9 g CO<sub>2</sub>-eq./kWh for CIGS.

### **12.3.8 Material efficiency**

Figure 12.13 displays how the GWP, HTP, MDP, PMFP and POFP vary with improvements in material efficiency (for abbreviations, see Table 5.1). For comparison reasons, the HTP-score resulting from generating 1 kWh of electricity by the use of natural gas, has also been included.

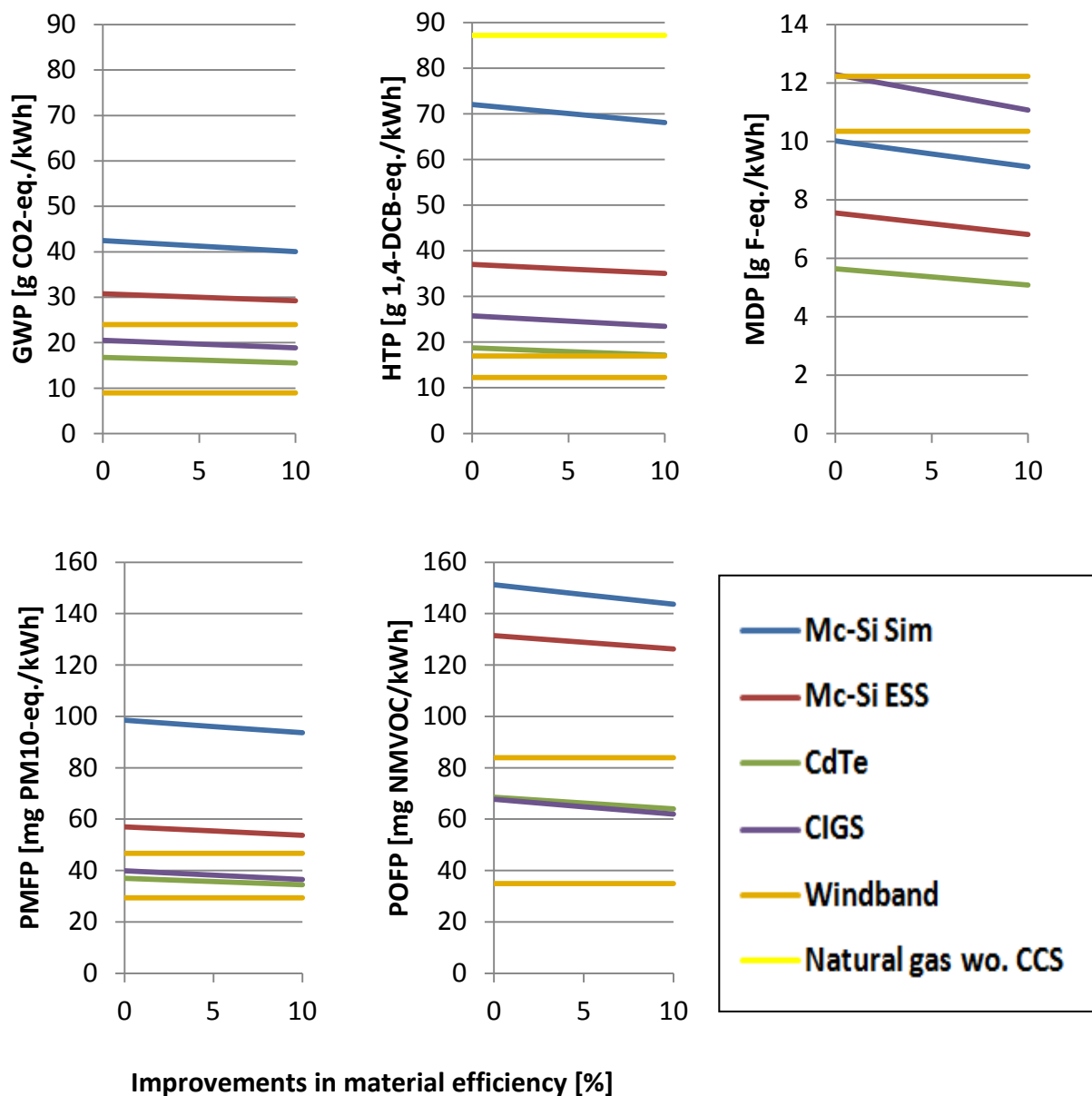


Figure 12.13: GWP, HTP, MDP, PMFP and POFP related to improvements in material efficiency, measured in per kWh electricity produced by the PV system. Impact values for natural gas without CSS and for wind power included for comparison (windband).

The relative reductions in GWP when going from the current technology (no improvements in material efficiency) to 10% improvements in material efficiency are:

- 5,7% for mc-Si Sim, giving an average reduction in GWP of 0,2 g CO<sub>2</sub>-eq. per % improvement in material efficiency.
- 5,0% for mc-Si ESS, giving an average reduction in GWP of 0,2 g CO<sub>2</sub>-eq. per % improvement in material efficiency.

- 7,2% for CdTe, giving an average reduction in GWP of 0,1 g CO<sub>2</sub>-eq. per % improvement in material efficiency.
- 8,0% for CIGS, giving an average reduction in GWP of 0,2 g CO<sub>2</sub>-eq. per % improvement in material efficiency.

The GWPs in g CO<sub>2</sub>-eq./kWh, resulting from 10% improvement in material efficiency, are 40,0 for mc-Si Sim, 29,2 for mc-Si ESS, 15,6 for CdTe and 18,9 for CIGS.

The graphs for GWP, PMFP and POFP, reflects the same trend: The thin film PV technologies are within the windband with current technology (i.e. no improvements in material efficiency), while the mc-Si PV technologies do not reach the windband. The thin film PV technologies do however not reach the minimum value of the windband with only material efficiency improvements.

Already at no material efficiency improvements, all PV technologies, except CIGS, lies below the minimum MDP value of the windband. CIGS do not reach the minimum value of the windband with only material efficiency improvements.

For the HTP, CdTe can reach the maximum value of the windband at 10% material efficiency improvements. The rest of the PV technologies have HTP-scores above the windband, but below the HTP of natural gas without carbon capture and storage (CSS).

### 12.3.9 Overall performance envelopes

In order to see which GWP range can be achieved when varying all the parameters at once, overall performance envelopes have been constructed based on a worst case scenario and a best case scenario. The worst case scenario is based on the current PV technology, i.e. no improvements in energy efficiency or material efficiency, with coal power for electricity supply. The best case scenario is based on the "future" PV technology with maximum improvements in both energy efficiency (20%) and material efficiency (10%), and with hydropower for electricity supply.

Figure 12.14 shows the overall performance envelopes for the four different PV cases. It has been decided to present the GWP as a function of the ratio of the varying lifetime electricity generation and the base case lifetime electricity generation. The conversion efficiency, performance ratio, lifetime and direct normal irradiation are (indirectly) varied by varying the lifetime electricity generation of the PV system. When the "ratio of lifetime electricity generation relative to base case" is equal to one, this represents the lifetime electricity generation resulting from using the parameters defined in the base case (see Table 12.1). In Figure 12.14, the dark, solid lines represents the GWP values for the base case (i.e. the current PV technology with UCTE el. mix), while the light colored areas around the line represent the range of possible GWP values between the worst case and the best case scenario. The values of the x-axis have been decided according to Table 12.2.

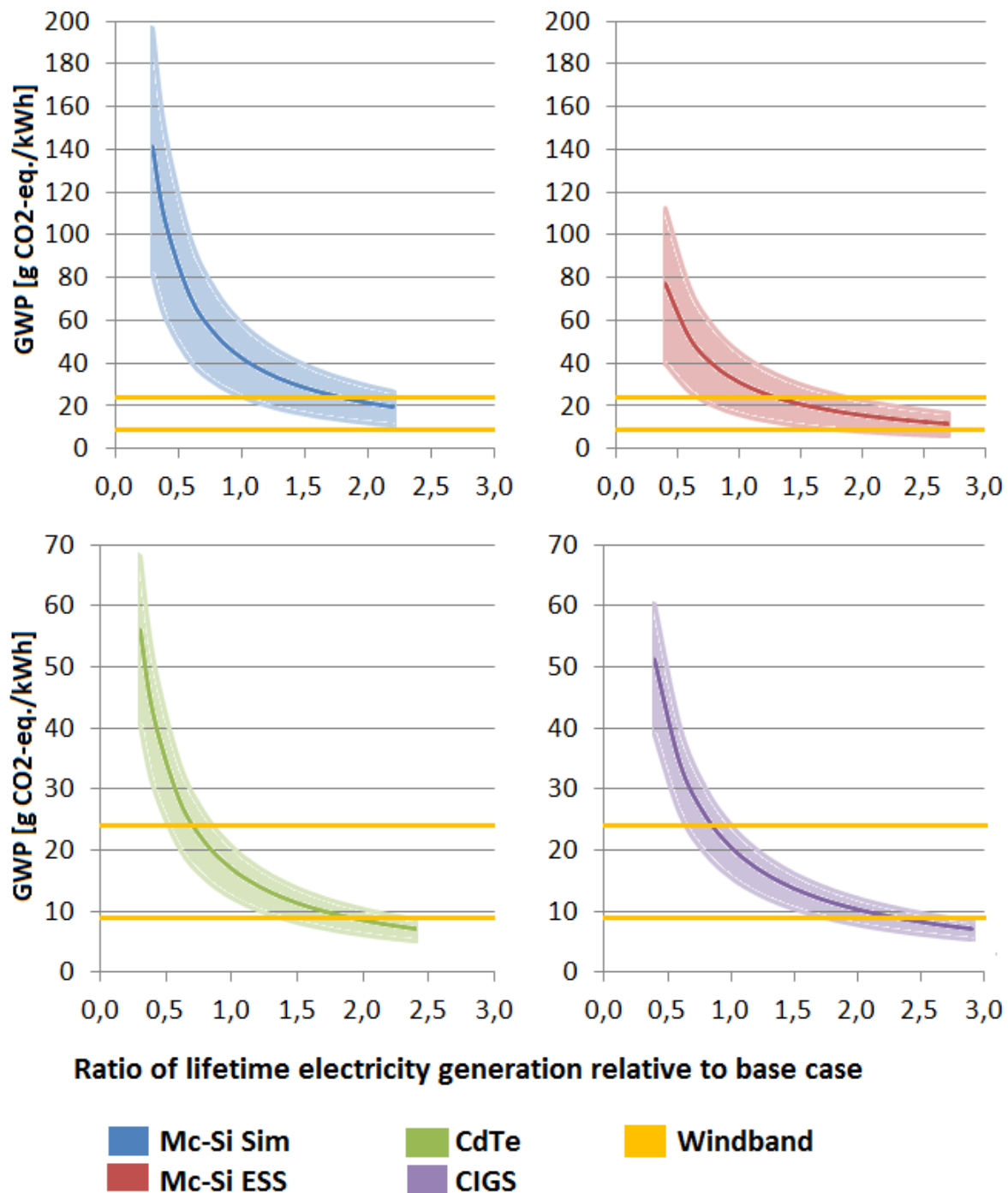


Figure 12.14: Overall performance envelopes for GWP values. Worst case scenario: Coal power, no improvements. Best case scenario: Hydropower, 20% improved energy efficiency, 10% improved material efficiency. Dark line: Base case scenario, UCTE electricity mix, no improvements.

The performance envelopes show that it is possible for the PV technologies to reach the windband by performing different measures. The necessary change in lifetime electricity generation to reach the windband is dependent on what scenario is used, i.e. what type of

electricity supply and the amount of improvements in energy efficiency and/or material efficiency. Note that the best case scenario for mc-Si Sim gives approximately the same GWP values as the worst case scenario for CIGS, and that the best case scenario for mc-Si ESS gives approximately the same GWP values as the best case scenario for CIGS.

All of the PV technologies have the potential to reach the maximum value of the windband. However, if the electricity supply is coal power with no improvements (worst case scenario), the mc-Si Sim-case can not reach the maximum windband value. In order to reach the maximum value of the windband, mc-Si Sim requires an improvement of 10-80% in lifetime electricity generation relative to the base case (depending on electricity mix). For the best case scenario, the mc-Si ESS can reach the windband at a 30% lower lifetime electricity generation than the base case. Using the current mc-Si ESS PV technology with the UCTE electricity mix or coal power requires an improvement of 30-90% in lifetime electricity generation relative to the base case.

It is interesting to see that the current PV technology for both CdTe and CIGS, with coal power as electricity supply and an electricity generation equal or lower to that of the base case, already fulfills the maximum value of the windband. The thin film technologies do consequently not require any improvements in either energy efficiency, material efficiency or lifetime electricity generation (or the parameters related to this quantity) to reach the windband. CdTe can reach the windband at a lifetime electricity generation 10-50% lower than the base case, while CIGS can reach the windband at a lifetime electricity generation 0-30% lower than the base case (depending on electricity mix).

The mc-Si Sim-case does not have the possibility to reach the minimum value of the windband. At 120% improvement in lifetime electricity generation relative to base case (maximum improvement), the GWP range from 11,1 to 26,8 CO<sub>2</sub>-eq./kWh for the best and worst case respectively.

The mc-Si ESS-case can only reach the minimum value of the windband and below it with hydro as energy supply and maximum improvements in energy efficiency (20%) and material efficiency (10%). This requires an improvement in lifetime electricity generation of 80% or more relative to the base case. At maximum improvement, meaning 170% increased lifetime electricity generation relative to the base case, the mc-Si ESS-case has a GWP equal to 5,8 g CO<sub>2</sub>-eq./kWh (best case scenario).

CdTe and CIGS can achieve a GWP equal to the minimum value of the windband, even with coal power as electricity supply (worst case scenario). This requires an overall improvement in lifetime electricity generation of 40-130% for the CdTe-case and 80-170% for the CIGS-case, relative to the base case, depending on the type of electricity supply mix and the amount of improvements in energy efficiency and material efficiency. At maximum improvement, meaning 140% increased lifetime electricity generation for CdTe relative to base case and 190% increase lifetime electricity generation for CIGS relative to base case,



the GWPs range between 5,1-8,5 g CO<sub>2</sub>-eq./kWh for CdTe and 5,4-8,3 g CO<sub>2</sub>-eq./kWh for CIGS, depending on type of scenario. The achievable level of GWP with maximum improvement in both electricity mix, energy efficiency, material efficiency and lifetime electricity generation is in other words quite similar for the mc-Si ESS-, CdTe- and CIGS-cases (5,1-5,8 g CO<sub>2</sub>-eq./kWh). However, the thin film technologies are less sensitive to the electricity mix, and this gives a larger flexibility in terms of energy feedstock than for the mc-Si ESS-case.

## 13 Discussion and conclusion

The first section in this chapter will give a recap of the main results from the LCA and the sensitivity analysis. The quality of data, model choices, limitations and implications from the modelling will be discussed in the second section. The results from this report will then be compared with already existing LCA studies. Finally, possible options for improving the PV production value chain will be presented, before a conclusion is reached.

### 13.1 Objective completeness

In this report, a comparative life cycle assessment of a rooftop, grid-connected PV system, has been conducted with the primary objective of assessing the environmental life cycle impacts of the system. Even though several environmental impacts were analyzed, the main consideration has been put on the global warming potential (GWP), as this is an important environmental issue. In total, four different PV cases have been investigated: Two cases on multicrystalline silicon (mc-Si), one on cadmium telluride (CdTe) and one on copper indium gallium selenide (CIGS). For the two mc-Si cases the main difference was the production method used for SoG-Si. The mc-Si Sim-case built upon the most common production method; the modified Siemens process, while the mc-Si ESS-case built upon the metallurgical SoG-Si production method by Elkem Solar (ESS).

There were large difference between the impact potentials from the mc-Si technologies and the thin film technologies (CdTe and CIGS), favouring the thin film technologies over the mc-Si technologies in terms of lower environmental impacts. With few exceptions, the mc-Si Sim-case gave the highest environmental impact in all of the impact categories. One exception worth noticing is that CIGS had the second highest metal depletion potential among all four cases (explained later). Comparing CdTe and CIGS, the differences in impact potentials were small, indicating that one should be careful to argue that one of these technologies is better than the other.

The relative, normalized contributions from the foreground processes to the impact scores were different for each investigated case: For the mc-Si Sim-case, most of the environmental burdens were connected to the production of either MG-Si or SoG-Si. For the mc-Si ESS-case, the SoG-Si production and the solar cell were the main contributors, the later especially in the toxicity categories and the ozone depletion category. The PV module was the third most important contributor in the mc-Si ESS-case, while it dominated most of the impact potential in both the CdTe-case and the CIGS-case. The contributions from the PV module were mainly related to the use of glass and primary aluminium for the frame and back contact (CdTe). Other contributions from the module were connected to copper and tin for cell- and module interconnections and corrugated board for packaging. The use of fossil fuels for transport of

materials and the module infrastructure (factory halls) itself were more important in some impact categories in the thin film cases, than in the mc-Si cases.

For all four cases, the following seemed to be the trend: The contributions from the other foreground processes in the PV value chain were generally less significant, with the exception of the inverter (up to 76% normalized, relative contribution). The use of metals like copper, manganese, tin and gold in these components has a large influence on the metal depletion potential, in terms of production of these metals and in terms of generating sulfidic tailings which have to be disposed off. In the CIGS-case, the metal depletion potential was also affected by the use of tin in the module and molybdenum for the back contact.

Considering the global warming potential, the following GWP values in kg CO<sub>2</sub>-eq./m<sup>2</sup> of PV system were obtained: 260 for the mc-Si Sim-case, 155 for the mc-Si ESS-case, 75 for the CdTe-case and 86 for the CIGS-case (using the UCTE electricity mix). For the CdTe- and the CIGS-cases, the main contribution came from the primary aluminium for frame and the glass used in the production of the PV module. This was also the case for the mc-Si PV technologies, together with a high share of indirect impacts resulting from the energy feed stock/electricity supply mix used in the SoG-Si production.

The secondary objective was to perform a sensitivity analysis in order to see how the change in different parameters affected the environmental performance (mainly the GWP) of PV system. The sensitivity analysis were conducted with varying eight parameters: PV module conversion efficiency, performance ratio, lifetime, direct normal irradiation, lifetime electricity generation, electricity mix, energy efficiency (main focus electricity) and material efficiency. Using a base case with a performance ratio of 75%, a lifetime of 30 years and a direct normal irradiation of 1 7000 kWh/m<sup>2</sup>/year, gave the following GWP values in g CO<sub>2</sub>-eq./kWh: 42,5 for the mc-Si Sim-case (16,0% conversion efficiency), 30,8 for the mc-Si ESS-case (13,2% conversion efficiency), 16,8 for the CdTe-case (11,7% conversion efficiency) and 20,6 for the CIGS-case (11,0% conversion efficiency).

The results showed that the GWP was very sensitive to changes in the electricity supply mix. Carbon intensive energy supply, i.e. fossil energy sources like coal and gas power, contributed significantly to higher GWP. Due to a much lower energy requirements during production, the thin film technologies were less sensitive to the electricity mix, giving a larger flexibility in terms of energy feedstock than for the mc-Si cases.

Across the four cases, the GWPs had an average reduction in the ranges of 1,2-2,7 g CO<sub>2</sub>-eq. per % improvement in conversion efficiency, 0,03-0,2 g CO<sub>2</sub>-eq. per % improvement in energy efficiency (electricity) and 0,1-0,2 g CO<sub>2</sub>-eq. per % improvement in material efficiency. In other words, improvements in conversion efficiencies affecte the GWP more than improvements in energy efficiency or material efficiency, and this may be low-hanging

fruits to enhance the environmental performance in terms of lower GWP from the PV systems.

Comparing the results from the sensitivity analysis with the GWP-scores of wind power (9,0-24,0 g CO<sub>2</sub>-eq./kWh) showed that the thin film PV technologies, and sometime also mc-Si ESS, have the potential to reach this windband (maximum value) with improvement in only one of the eight parameters. However, to get below the minimum value of the windband, a combination of improvements were required at the same time. This could be done by different measures. The thin film technologies could achieve GWPs below the windband regardless of energy supply, while this was only possible for mc-Si ESS with hydropower as electricity supply, and maximum improvements in both energy efficiency (20%) and material efficiency (10%). This was assuming that these three cases increased their lifetime electricity generation relative to the base case. With maximum improvements in both electricity mix, energy supply, material efficiency and lifetime electricity generation, mc-Si ESS, CdTe and CIGS could achieve a GWP in the range of 5,1-5,8 g CO<sub>2</sub>-eq./kWh. Mc-Si Sim was unable to get below the minimum value of windband and can only get below the maximum value of the windband by undergoing a combination of improvements.

## **13.2 Result robustness**

### **13.2.1 Quality of analysis**

The data used in this report are considered to be of good quality, as they have been collected first hand from reliable sources. Most of the data are quite recent numbers. The exceptions are the data for the value chain downstream of SoG-Si production in the mc-Si ESS-case, and the data on the inverter, cabling and mounting structure for mc-Si EES, CdTe and CIGS from Alsema et al. (2006) and de Wild-Scholten et al. (2006). It is hard to say how much the technology, production methods and material composition for these three components have changed during the last years, and how much this might influence the results, but it is a fact that the development in PV technology in general has been very rapid.

Concerning the inventories on SoG-Si production, the mc-Si Sim-case mainly used collected data from production facilities in China. For the mc-Si ESS-case, the majority of data on energy requirements, airborne and waterborne emissions are numbers reported from Elkem to the Climate and Pollution Agency of Norway in the year 2011. The estimates in the rest of the SoG-Si inventory for the ESS-case, found by upscaling numbers from MG-Si production, were shown to be reasonable estimates for the metallurgical SoG-Si production method by Elkem Solar in the previous work of Bekkelund (2013).

The rest of the inventory used in mc-Si ESS is data from the Crystal Clear project, collected from 11 different PV manufacturers. Sine some of these data are obtained by aggregation in order to keep sensitive information confidential, it is possible that this has introduced some

uncertainties in the data. The data are collected for the reference year of 2005, i.e. eight years ago. Since the PV industry is in continuously rapid development, these data used for the processes downstream of the SoG-production may not be representative numbers anymore. This can be seen by comparing the yield ratios of the two different mc-Si cases, where mc-Si Sim has a lower yield ratio for both the wafer- and PV-module production per m<sup>2</sup> (see Table 11.3). In fact, the yield ratio for the wafer process is only half of the yield ratio used in mc-Si ESS.

It is important to note that the mc-Si ESS-inventory in general is more extensive and detailed than what is the case with the mc-Si Sim-inventory. This is especially notable for the inventory of SoG-Si, wafer and solar cell production, where the ESS-case has a much more extensive list of airborne and waterborne emissions. Some important processes have been left out from the modelling of the mc-Si Sim-case, making it appear less complete compared to the mc-Si ESS-case: Waste management have not been included at all, neither has raw material transportation for MG-Si production and infrastructure for the processes happening before the wafer production step. Leaving these processes out, may give a misleading result, i.e. lower environmental impacts than what actually is the case. The use of Ecoinvent-data in the mc-Si Sim-inventory for the inverter, cabling and mounting structure, may introduce more uncertainties than if process specific data were collected.

A weakness in the modelling of the mc-Si Sim-case is that recycling of slurry used in the wafer production is not included. The slurry consists of silicon carbide and triethylene glycol (polyethylene in the Sim-case). This sawing slurry can be partly recycled and reused in the PV industry (Jungbluth et al., 2012). According to Alsema & de Wild-Scholten (2007), slurry recycling can reduce the wafer energy requirement with about 15%. However, compared to other foreground processes, the environmental burdens resulting from the wafer process is small, at least in this study, so the implications of leaving this process out may not be that significant.

Both the CdTe-case and CIGS-case have been modelled by integrating two different inventories into one inventory, using the weighted average of the entries. This integration may have introduced uncertainties. There is not much detail on how the PV modules have been manufactured and what each material input has been used for. Due to the large range of possible deposition methods and no standardized production processes, it may be that the PV module have been produced differently in the two inventories used for integration in each of the cases. If two different materials have been used for serving the same function in a production process, this will introduce a kind of "double counting" of material and the related emissions and waste. The integrated inventory will end up with too many material inputs and waste-/emissions outputs, than what is actually required.

In both the CdTe-case and the CIGS-case, the inventory for the inverter, cabling and mounting structure from Gibbon et al. (forthcominig) is built up of Ecoinvent-processes. These have been disaggregated to be able to integrate them with the data from Alsema et

al. (2006) and de Wild-Scholten et al. (2006). One should be aware that not all of the sub-processes coming from an Ecoinvent process have been included in the integrated inventory. This would require further disaggregation of Ecoinvent processes and making assumptions without a proper basis. (See appendices G.3 and H.3 for details).

One of the datasets used in each of the CdTe-case and the CIGS-case, has been collected by the NREL from PV different producers. These data are presented in Gibon et al. (forthcoming) in an aggregated form, in order to keep sensitive information confidential. It is possible that this have introduced some uncertainties in the data. On the other hand, since more than one PV producer has been involved in the data collection, one may say that the current state of art of the PV technologies are reflected.

Resolution of the dataset on the CdTe PV module could have been better. There was not supplied enough information in either Jungbluth et al. (2012) or Gibon et al. (forthcoming) to disaggregate the module manufacturing into more process-specific step upstream of the module, like with the CIGS-case. This limits the transparency and may "hide" important aspects. It would have been interesting to see how the different solar cell components/layers contribute to the total impact potential resulting from the module. The contribution from the buffer- and absorber layer in the toxicity categories would have been valuable information, due to the skepticism of some for using cadmium in these components.

It is worth noticing that the primary aluminium input to the manufacturing of the CdTe PV module is used for the back electrical contact, and not for a frame. The CdTe module can therefore be considered frameless in this study. This is important to remember since the other cases are modelled with an aluminium frame. If the CdTe module inventory had included an aluminium frame, the impact potentials resulting from the CdTe-case would have been higher.

The CIGS technology is so far less mature than the CdTe technology. The gap of three years between the two inventories used in the CIGS-case may be problematic due to technological advances during these years.

The dataset on the CIGS PV module from Gibbon et al. (forthcoming) included internal recycling of the metals copper, indium, gallium, selenium and molybdenum during manufacturing. In the provided inventory from Gibbon et al. (forthcoming), the reclaimed metals had been allocated according to price (economic allocation by using the partitioning approach, see chapter 4.6.6). The allocation may have introduced uncertainties. The reclaimed metal entries were represented by credits, i.e. negative contributions. When integrating the inventory from Gibbon et al. (forthcoming) with the inventory from Jungbluth et al. (2012), these credits were included under the production of the absorber layer (CIGS) and the production of the back contact (Mo). This may be inconsistent, but since the metal recycling happens as an integrated part of each process step, and not as recycling at the end-

of- life of the module, it was decided to include it with the absorber layer and the back contact processes, instead of modelling a separate recycling process. It is interesting to note that even though the dataset from Jungbluth et al. (2012) do not include metal recycling during manufacturing, the values for these metal inputs (indium, gallium, selenium and molybdenum) are actually lower (14-80%) than the ones from Gibbon et al. (forthcoming). Considering the credits given in Gibbon et al. (forthcoming) for the recycling of these metals, one might have expected the opposite result. The exception is the input of copper, which is actually 602% higher in Jungbluth et al. (2012) than in Gibbon et al (forthcoming). These differences underlines the fact that the CIGS technology is still a relatively immature technology, which has not yet been standardized in terms of production processes. Note that except for the slurry recycling mentioned earlier, none of the other three cases investigated includes recycling of manufacturing losses/-waste during PV production.

It can be discussed whether transportation should have been included in the modelling of the two mc-Si cases. As it is now, only the transportation of raw materials going to the SoG-Si production is included (not included for the mc-Si Sim-case). This builds on the assumption that the production of the PV system is happening as an "integrated" process, where the foreground processes (production steps) are all happening at the same geographical location, but within separate production facilities (factory halls/infrastructure). Since many PV companies specialize on one or more production steps, it may seem more realistic to include transportation between these steps in the modelling of the mc-Si PV system. Even though certain PV companies cover the whole PV chain, their facilities have often different geographical locations. However, including transportation would have implications on the electricity mix used, as different countries have different electricity mix. As mentioned earlier, the choice of electricity mix have a significant influence on the impact results. In addition, including the transportation would mean that assumptions on type of transportation, as well as distance travelled, would have to be made. All of this would introduce uncertainties to the modelling, indicating that leaving the transportation out of the modelling may be better in terms of generating more reliable results (less uncertainty). However, it can be argued that since transportation of materials are included in the modelling of the two thin film cases, transportation should also have be included in the mc-Si Sim-case and mc-Si ESS-case to ensure a best comparative basis. Alternatively, modelling of the transportation should have be excluded all together in all the cases. The manufacturing of CdTe- and CIGS PV modules are less complex than the mc-Si PV module manufacturing in terms of fewer process steps. This means that the whole value chain usually is covered at one location, avoiding transportation between different facilities. The only required transportation is transportation of raw materials and chemicals to the PV plant, and the transportation of the PV module to the installation site. Note that this last step is not included in any of the four cases in this report.

The foreground system modelled in this report is missing the end-of-life treatment of PV modules. One foreground process which will probably become more important in the future

is the recycling of PV modules. It has not been possible to obtain reliable life cycle inventory on this process. The recycling of PV modules is still a young industry; the current volumes of PV module waste are low, due to the long technical lifetime of up to 30 years and most PV systems being installed quite recently (in the 1990s)(PV Cycle, 2013d). Recycling of PV modules have the potential for reducing the environmental impacts from the value chain of a PV system (Held, 2009). A non-for-profit association called PV Cycle are managing operational collections and recycling solutions for PV modules in Europe (PV Cycle, 2013b). They strive to organize the recycling of all available PV technologies. It is already possible to recover the glass, ferrous (e.g. aluminium) and non-ferrous metals from the modules, as well as junction boxes, plastics and cables (PV Cycle, 2013a; PV Cycle, 2013c). According to PV Cycle (2013d), 1% of all collected PV modules had reached the end of their lifetime. Most of the PV module waste collected by PV Cycle comes from transport or installation damages. However, it is expected that a significant amount of PV module waste will be generated the next 10-15 years (PV Cycle, 2013d). According to Müller et al. (2005), the volume of end-of-life PV modules is estimated to rise to 33 500 tons in 2040. As more PV module waste is generated, the PV module recycling industry will probably become more mature and reliable data may be recorded for use in LCA studies.

Only a few published LCAs assess how the end-of-life treatment affect the environmental performance of a PV system. Müller et al. (2005) performed a LCA of a recycling process for crystalline silicon PV modules. The recycling process of Deutsche Solar, run at a pilot plant scale, was investigated and compared with two other end-of-life options; municipal incineration and shredding. First, the solar cells were removed from the PV module by burning off the laminate. The metals from the frame and glass were delivered to recycling partners. Then the front- and back contacts, anti-reflection coating and p-n junction of the solar cell were removed by chemical etching, while the wafer were reprocessed in a standard solar cell production line and integrated into a PV module. The burden (positive contribution) of the recycling process was compared with the disburden (negative contribution) caused by the reuse of recovered wafers and the material of other components (Müller et al., 2005). In all impact categories investigated, the impact potentials were reduced. The highest contribution to the disburden was related to the reused of recovered wafers. The GWP was found to be reduced by 52,6 kg CO<sub>2</sub>-eq./m<sup>2</sup> of PV module. The municipal incineration had significantly lower energy requirements than the recycling process, but the negative contribution (disburden) to the GWP was higher for the recycling process. The shredding process had an energy requirement of two orders magnitude lower than the recycling process. However, the recycling process produced recycled materials with higher value, justifying the higher energy consumption.

Regarding the thin film PV technologies, recycling of disposed PV modules is especially interesting due to the possible recovery of rare metals like tellurium, indium and gallium. Held (2009) performed a LCA of CdTe PV module recycling using current available industry data from First Solar's facility in Germany. In general, the recycling process consisted of



mechanical and hydrometallurgical treatments, divided into five steps: Shredding and milling, extraction/film removal, solid/liquid separation, glass-laminate separation and glass rinsing, precipitation and dewatering. In the study, environmental benefits from the recycling were accounted for with credits. In all impact categories investigated, the benefits due to the material recycling and energy recovery outweighed the impacts from the recycling process itself and therefore lead to a reduction of the investigated impact potentials (Held, 2009). The highest contribution to the recycling benefits came from the recycling of the glass cullet and the copper recycling from the junction boxes and wires. The burdens came from the energy demand and the use of hydrogen peroxide (an auxiliary). In total, the GWP was reduced with 8,5 kg CO<sub>2</sub>-eq./m<sup>2</sup> of PV module. An additional recycling benefit contributed to reducing the GWP, namely the melting process of the recycled glass cullet, avoiding CO<sub>2</sub>-emissions from the carbon reduction of limestone, dolomite or soda ash (raw materials in glass production). It is important to note that this LCA did not account for the recycling of semiconductor materials (filter cake) sent to a third party for recycling, due to unavailable data.

### **13.2.2 Benchmarking**

As mentioned in chapter 1.2, the differences in e.g. system boundaries, data sources, level of detail, production methods for manufacturing the PV system, type of PV system and other assumptions make it difficult to compare the results from this LCA study with other, published LCA studies. The PV system can be either rooftop, ground mounted or building integrated, and grid-connected or stand-alone. Stand-alone PV systems require batteries for power storage. The geographical place where the production takes place is of significance due to the electricity supply mix.

To be able to compare the environmental performance of a PV system with other energy technologies, most of the existing studies present the results on a per kWh-basis, and not per m<sup>2</sup> of PV system as used in this report. As mentioned in chapter 5.1, this means that assumptions regarding direct normal irradiation (i.e. location for the installation of the PV system), PV module conversion efficiency, performance ratio and lifetime of the PV system have to be made. This introduces uncertainties which are important to document in the LCA study. IEA has published a report on how to make model choices when conducting a LCA on PV systems (Fthenakis et al., 2011b). Production methods and conversion efficiencies may vary across manufacturers. Due to the continuous research on solar cells and the rapid development of PV technology the last decade, one has to keep in mind that previous LCA studies of PV systems may not reflect the current technologies on the market.

For benchmarking with existing studies, a base case with a PV-system placed in South-Europe (direct normal irradiation of 1700 kWh/m<sup>2</sup>/year), a performance ratio of 75% and a lifetime of 30 years will be used. PV module conversion efficiencies will be 16,0% for the mc-Si Sim-case, 13,2% for the mc-Si ESS-case, 11,7% for the CdTe-case and 11,0% for the CIGS

case. (For future reference, please see Table 12.1). The UCTE electricity mix is used for the whole PV value chain.

The existing LCA studies (see references in chapter 1.2 and appendices J.1-3) on PV systems mainly assess the GWP and the energy-payback time of the PV system. The results from this report are within the expected GWP ranges stated in chapter 1.2: The GWP values of **30,8-42,5 g CO<sub>2</sub>-eq./kWh** for the mc-Si-cases are well within the range of **18,0-72,4 g CO<sub>2</sub>-eq./kWh**. The GWP of **16,8 g CO<sub>2</sub>-eq./kWh** for the CdTe-case lie in the lower end of the range **15,5-66,0 g CO<sub>2</sub>-eq./kWh**. The same goes for the CIGS-case; with a GWP of **20,6 g CO<sub>2</sub>-eq./kWh**, the results lie in the lower end of the range **20,5-95,0 g CO<sub>2</sub>-eq./kWh**. It is a high variability in how well the existing LCA studies documents their assumptions, data collections and results, i.e. how transparent they are.

It is easier to find LCAs on mc-Si PV systems than on thin film PV systems, because mc-Si PV technology is a more mature technology. The thin film PV technology have only been commercially produced the recent years. Consequently, fewer LCAs on these technologies have been conducted, especially on CIGS. Many of the LCAs on thin film PV systems are LCAs on ground mounted PV systems, and not on roof mounted systems.

The LCA studies chosen for comparison are recent studies with the most similar assumptions to those used in this report, ensuring a best possible comparative basis. Note that only LCA studies on rooftop PV system have been considered. If not otherwise stated, the studies have assumed the same direct normal irradiation, performance ratio, lifetime and PV module conversion efficiency as for the base case in this report. If these assumptions differ from the base case in this report, the parameters in the base case will be adjusted to those of the specific study to provide a more correct basis for comparing the GWP values.

### ***Mc-Si PV systems***

In Alsema et al. (2006), a GWP of 32,0 g CO<sub>2</sub>-eq./kWh for mc-Si PV was found. The collection efficiency was 13,2%, the same collection efficiency as assumed for the mc-Si ESS-case. The study used data collected as a part of the Crystal Clear project, i.e. the study used many of the same data as what was used in the ESS-case, except for the SoG-Si production (see chapter 11.1.2). Alsema et al. (2006) used a modified Siemens process, while the ESS-case used the Elkem Solar Silicon metallurgical production process (ESS), giving a GWP of 30,8 g CO<sub>2</sub>-eq./kWh. This is approximately the same as the result from Alsema et al. (2006). Since the ESS is less energy intensive than the modified Siemens process and use a larger part of biogenic reduction agent (i.e. softwood chips), one might expect that the difference in GWP would be larger. However, there are some important aspects distinguishing the mc-Si ESS-case from Alsema et al. (2006): In Alsema et al. (2006), the silicon feedstock production (i.e. MG-Si and SoG-Si production) is assumed located at a site with low electricity cost, and the electricity supply is a mix of hydropower and high-efficiency combined cycle gas turbines.

The rest of the PV value chain uses the UCTE electricity mix. The sensitivity analysis in this report have already demonstrated the significant influence of electricity supply mix on the GWP results. Using another, more carbon intensive electricity mix for the silicon feedstock production, e.g. the UCTE electricity mix, the GWP result from Alsema et al. (2006) would probably be significantly higher.

The two mc-Si cases in this report uses on-roof mounting, leaving the existing roofing material in place, while Alsema et al. (2006) uses in-roof mounting, where the modules take over the function of the roof-tiles (de Wild-Scholten et al., 2006). Alsema et al. (2006) have taken into account the savings of roof tile material in the LCA analysis (credits), which probably has resulted in lower impacts from this type of mounting structure compared to a on-roof mounting structure. This is further supported by the work of de Wild-Scholten et al. (2006), where different mounting structures were analyzed. The in-roof mounting structures gave net negative GWP, while the on-roof mounting structures gave net positive GWP.

Comparing with the mc-Si Sim-case (42,5 g CO<sub>2</sub>-eq./kWh), this GWP is relatively higher than in Alsema et al. (2006). Adjusting the conversion efficiency of the mc-Si Sim base case down to that of the study (13,2%), gives a GWP of 51,5 g CO<sub>2</sub>-eq./kWh. Even though both studies use the modified Siemens process, and the data in the mc-Si Sim-case are more recent, there are a few possible reasons for the difference in the results (in addition to those already mentioned): The data for the mc-Si Sim-case is collected from China, while the data in Alsema et al. (2006) are from Western-Europe and the USA. The environmental regulation is generally considered to be stricter in these countries than in China, and the technology used is often "cleaner". Process-specific data on MG-Si have been collected for the mc-Si Sim-case, while data on this in Alsema et al. (2006) are taken from Ecoinvent. The inventory for SoG-Si used in the mc-Si Sim-case is more detailed, especially in terms of airborne and waterborne emissions. It is worth mentioning that in the modelling of the SoG-Si production in Alsema et al. (2006), the only airborne emissions given were waste heat (Johansen, 2008). The inadequate data on other airborne emissions may give lower results than what actually is the case.

A GWP of 34,0 g CO<sub>2</sub>-eq./kWh for a mc-Si PV system is presented in de Wild-Scholten (2011). De Wild-Scholten (2011) also used the modified Siemens process for SoG-Si production, with PV modules with a conversion efficiency of 14,1%. The data are taken from 2009. The main differences between de Wild-Scholten (2011) and the mc-Si cases investigated in this report is that de Wild-Scholten (2011) used hydropower in the production of SoG-Si, and takeback and recycling of the PV modules were included. The relative contribution from the recycling process to the total GWP was not large compared to the other foreground processes. It has already been shown in this report how sensitive GWP results are to different electricity mixes. The use of biogenic reduction agents and higher energy efficiency of the ESS-process compared to the modified Siemens process, can explain the slightly lower GWP value for the mc-Si ESS-case (30,8 g CO<sub>2</sub>-eq./kWh). Adjusting the conversion efficiency of the mc-Si ESS

base case up to that of the study (14,1%), gives a GWP of 28,7 g CO<sub>2</sub>-eq./kWh. For the mc-Si Sim-case, the GWP is 48,2 g CO<sub>2</sub>-eq./kWh when adjusted down to the conversion efficiency of the study. The data collection from a Chinese context may explain the higher GWP value for the mc-Si Sim-case, in addition to the use of UCTE electricity mix and not hydropower for the SoG-Si production. The UCTE electricity mix is more carbon intensive than hydropower.

Very interesting indeed is the fact that de Wild-Scholten & Gløckner (2012) performed an LCA of the Elkem Solar Silicon production process in 2011. The study assumed a conversion efficiency of 14,3%. The LCA also included the take back and recycling of PV modules by the scheme of PV Cycle. The SoG-Si process used electricity and heat from a mix of hydropower and combined heat and power. For the rest of the PV value chain downstream of the SoG-Si production, electricity mixes were based on production locations in the world. A GWP of 29,0 g CO<sub>2</sub>-eq./kWh was presented in de Wild-Scholten & Gløckner (2012). Adjusting the conversion efficiency of the mc-Si ESS base case up to that of the study, gives a GWP of 28,3 g CO<sub>2</sub>-eq./kWh. This is indeed very close to the result from de Wild-Scholten & Gløckner (2012), and the result obtained for the mc-Si ESS-case therefore seems reliable. The small difference may be explained by the difference in electricity mix. The take back and recycling of the PV modules are not included in the mc-Si ESS-case, which means that it do not take recycling credits into account, but at the same time transportation and energy are "saved". Distributed onto the foreground processes, the take back- and recycling process accounted for 1,3 g CO<sub>2</sub>-eq./kWh of the total GWP in de Wild-Scholten & Gløckner (2012), i.e. accounting for 4,6% of the GWP.

There has also been done some LCA-studies on PV-systems using the Fluidized Bed Reactor (FBR) process for SoG-Si production, a technology not investigated in this report (see chapter 6.2.4). However, it is still interesting to see how the results from these analyses perform compared to the mc-Si ESS-case and mc-Si Sim-case. Stoppato (2008) presented a GWP value of 123 kg CO<sub>2</sub>-eq./m<sup>2</sup> using the FBR technology. The study assumed a conversion efficiency of 16% and a lifetime of 28 years. This GWP value is 21% lower than for the mc-Si ESS-case (155 kg CO<sub>2</sub>-eq./m<sup>2</sup>) and as much as 53% lower than for the mc-Si Sim-case (260 kg CO<sub>2</sub>-eq./m<sup>2</sup>). Even though the FBR-technology is considered to be less energy intensive than the modified Siemens process, the results from Stoppato (2008) may not give an unambiguous answer as to how much, because the manufacturing of the BOS-components are left out from the LCA. If the BOS-components had been included, the aluminium used in the mounting structure would probably have resulted in a higher GWP.

Westgaard et al. (2012) performed a LCA of a PV system in 2011, manufactured by the Renewable Energy Corporatio (REC). REC is one of the global integrated PV solar producers, covering the entire value chain of a PV system. The data were actual production data from REC facilities in the first quarter of 2011. Recycling of PV modules was included using generic data from the Energy Research Centre of the Netherlands (ECN). The PV system was located in Southern Europe, using the same direct normal irradiation as the base case in this report.

The performance ratio was 84%, thus 9% higher than in the base case. For a PV system made of SoG-Si from the USA and wafer, cells and modules produced in Singapore, a GWP of 21,0 g CO<sub>2</sub>-eq./kWh was found, while for modules with wafers and cells produced in Norway, the corresponding GWP was 18,0 g CO<sub>2</sub>-eq./kWh. These GWP values lies in the lower range of the GWP values found in the existing literature. The author of this report has not been able to find the conversion efficiency used in the study, but PV modules from REC generally have a conversion efficiency of 14,2-15,5% (REC, 2013b; REC, 2013c). With an exact value for the conversion efficiency, it would be possible to adjust the base case for mc-Si ESS and mc-Si Sim, giving a GWP result per kWh with similar assumptions to those of the study.

Compared to the mc-Si ESS-case and the mc-Si Sim-case, the GWP result from Westgaard et al. (2012) outperforms both of these cases in terms of lower GWP. This may indicate that the FBR-method is even more energy efficient than the ESS-method. Other processes in the value chain may also differ from what is used in this report. However, in dept information about the inventory used in Westgaard et al. (2012) were not found (only an abstract of the analysis were found). The fact that the LCA has it outset from two/three different production sites plays an influential part in terms of electricity mix and transportation. For the SoG-Si production in the USA and the rest of the processes situated in Norway, the energy was supplied from hydropower, while the processes situated in Singapore used natural gas power (REC, 2011a). If the whole PV value chain in the mc-Si ESS- and mc-Si Sim-cases were to be placed in Norway, with hydropower as electricity supply, this would lead to a GWP of 17,4 g CO<sub>2</sub>/kWh and 27,0 g CO<sub>2</sub>/kWh respectively. In this case, the result shows that the ESS-method may be equally energy efficient as the FBR-method used in Westgaard et al. (2012).

### ***CdTe PV systems***

Raugei et al. (2007a) reported a GWP of 48,0 g CO<sub>2</sub>-eq./kWh for CdTe PV system, using the UCTE electricity mix. The conversion efficiency was 9% and the lifetime 20 years. The study was performed within the framework of PVACCEPT. PVACCEPT was a European research project on the public acceptability of advanced PV technologies. It ran from 2001 to 2004 and was funded by the European Commission (PVACCEPT, 2013). The data were based on actual production data from the PV producer Antec Solar. Since Antec Solar was the only producer of CdTe PV modules on the market at that time, the GWP result from the study represents the state of art of the CdTe PV modules in Europe in early 2005 (Raugei et al.,2007a). Adjusting the conversion efficiency and lifetime of the CdTe base case down to that of the study, increases the GWP with 95% up to 32,7 g CO<sub>2</sub>-eq./kWh. Still, this value is 32% lower than the GWP from Raugei et al. (2007a). Technical advances in CdTe PV technology and production since then may explain the difference.

The data of some main inputs to the CdTe PV module and BOS manufacturing processes are given, enabling a deeper investigation of the differences between the results in Raugei et al.

(2007a) and the CdTe-case, even after the adjustments. Raugei et al. (2007a) has a higher consumption of glass, steel, electricity and fuel oil. The CdTe-case uses 15 kg glass, 14 kg steel and 29,1 kWh electricity per m<sup>2</sup> of PV module, while Raugei et al. (2007a) uses as much as 25 kg glass, 25 kg steel and 236 kWh electricity per m<sup>2</sup> PV module, in addition to 10,8 MJ fuel oil per m<sup>2</sup> of PV module for installation. The electricity consumption in Raugei et al. (2007a) seem unreasonable high. There might be a misprint in the article, and that the actual electricity consumption is 23,6 kWh electricity. This is supported by an earlier LCA study conducted by the same authors (Raugei et al., 2005) which builds on many of the same data from PVACCEPT and Antec Solar. Here they state an electricity consumption of 24 kWh per m<sup>2</sup> of PV module. There are also other differences between the inventory of the CdTe-case and Raugei et al. (2007a). The CdTe-cases uses 0,97 kg EVA and 178 kg water per m<sup>2</sup> of PV module, while Raugei et al. (2007a) uses 0,63 kg EVA and only 1,25 kg water per m<sup>2</sup> of PV module. The water consumption in the CdTe-case is especially high compared to Raugei et al. (2007a).

It should also be noted that Raugei et al. (2007a) uses CML 2 baseline 2000 as the characterization model, not ReCiPe. This is very likely to affect the results, and one may assume that the outcome would have been different if ReCiPe had been used instead.

Raugei et al. (2005) presented a GWP of 53,0 g CO<sub>2</sub>-eq./kWh, but the assumptions for conversion efficiency, performance ratio and lifetime were different from the CdTe base case in this report. Adjusting the parameters of the CdTe base case to those of Raugei et al. (2005), i.e. the conversion efficiency down to 8,0%, the performance ratio up to 80% and the lifetime down to 20 years, increases the GWP with 105% up to 34,5 g CO<sub>2</sub>-eq./kWh. Still, this value is 35% lower than the GWP from Raugei et al. (2005).

A GWP of 19,0 g CO<sub>2</sub>-eq./kWh for CdTe PV is presented in de Wild-Scholten (2011). The PV modules had a conversion efficiency of 11,3%. The data were taken from the production facilities of First Solar in Germany, the USA and Malaysia for the year 2010. One of the inventories used in the CdTe-case in this report is also based on production data from First Solar. The GWP value is very close to what is found for the CdTe-case. Adjusting the conversion efficiency and lifetime of the CdTe base case down to that of the study, increases the GWP with 4% up to 17,4 g CO<sub>2</sub>-eq./kWh, even closer to the GWP from de Wild-Scholten (2011). Both de Wild-Scholten (2011) and the CdTe-case uses frameless modules. Due to lack of transparency in de Wild-Scholten (2011), it is impossible to give further reasons for the differences.

Kato et al. (2001) was among the earliest LCAs conducted on a rooftop, residential CdTe PV system. The study analyzed three PV systems with different nominal power output: 10 MWp/yr with 10,3% conversion efficiency, 30 MWp/yr with 11,2% conversion efficiency and 1000 MWp/yr with 12,4% conversion efficiency. The resulting GWP were 51,0, 42,0 and 33,0 g CO<sub>2</sub>-eq./kWh respectively. In addition to the difference in conversion efficiency, Kato et al. (2001) assumed a performance ratio of 81%, lifetime of 20 years and direct normal

irradiation of 1430 kWh/m<sup>2</sup>/year. Using these parameter values for the CdTe-case in this report gives a GWP of 26,1-31,4 g CO<sub>2</sub>-eq./kWh, depending on what type of conversion efficiency is used. The differences may be explained by technological advances the last 12 years. According to a review by Kim et al. (2012), Kato et al. (2001) built on hypothetical cases, which may have influenced the results.

Fthenakis and Kim (2007) found a GWP of 16,0 g CO<sub>2</sub>-eq./kWh for a CdTe PV system produced and installed in Europe (direct normal irradiation equaled 1700 kWh/m<sup>2</sup>/year). The conversion efficiency was 9%. Adjusting the conversion efficiency of the CdTe base case down to that of the study, increases the GWP with 30% up to 21,8 g CO<sub>2</sub>-eq./kWh. Lack of transparency makes it difficult to explain possible reasons for the difference between the adjusted CdTe base case and Fthenakis & Kim (2007).

In the presentation of de Wild-Scholten & Schottler (2009), a GWP of 15,5 g CO<sub>2</sub>-eq./kWh is presented for a CdTe PV system. The presentation gives very few details, but the PV system were assumed installed in Southern Europe, the data were from 2008 and the conversion efficiency was 10,7%. The performance ratio is not given, making it impossible to adjust the CdTe base case without making assumptions. Regardless of this, the GWP of the CdTe-case is very close to that of de Wild-Scholten & Schottler (2009), only 8% higher.

Fillippidou et al. (2010) gives a more conservative GWP estimate of 137 kg CO<sub>2</sub>-eq./m<sup>2</sup>. This is 83% higher than what is found for the CdTe-case. The conversion efficiency was 9% and the direct normal irradiation 1420 kWh/m<sup>2</sup>/year, but this does not affect the GWP results since they are given on a per m<sup>2</sup>-basis. The electricity supply mix is not stated. This study also lack in depth details to give further explanation for the differences.

### ***CIGS PV systems***

Raugei et al. (2007a) reported a GWP of 95,0 g CO<sub>2</sub>-eq./kWh for CIGS PV module, using the UCTE electricity mix. The lifetime was 20 years. The study was performed within the framework of PVACCEPT (see chapter 13.2.2; ***CdTe PV systems*** for details). The data was collected from a prototype batch line at Würth Solar in Germany. This is the same PV producer as one of the inventories used in the CIGS-case was based on. Würth Solar was the only producer of CIGS PV modules on the market at that time. The GWP result from the study can therefore be seen as representative for the state of art of the CIGS PV modules in Europe in early 2005 (Raugei et al.,2007a). However, according to Raugei et al. (2007a), it should be noted that the CIGS production would probably undergo large improvements in the near future before standard production would begin. Adjusting the lifetime of the CIGS base case down to that of the study, increases the GWP with 49% up to 30,7 g CO<sub>2</sub>-eq./kWh- Still, this is very low (68% lower) compared to the GWP from Raugei et al. (2007a). The fact that the data in Raugei et al. (2007a) do not represent current standard production, may probably explain some of this difference.

The data of some main inputs to the CIGS PV module and BOS manufacturing processes are given. Rauegi et al. (2007a) has a higher consumption of glass, steel and fuel oil. The CIGS-case uses 14,4 kg glass and 14 kg steel per m<sup>2</sup> of PV module, while Rauegi et al. (2007a) uses as much as 25 kg glass and 25 kg steel per m<sup>2</sup> of PV module, in addition to 10,8 MJ fuel oil per m<sup>2</sup> of PV module for installation. The high glass consumption may reflect a very high percentage of breakage in the prototype line (Kim et al., 2012). Production of glass is an energy intensive process, and the difference in amount used in the module may explain some of the difference in GWP between the CdTe-case and Rauegi et al. (2007a).

There are other, although smaller differences too: The CIGS-cases uses 1,17 kg EVA, 2,67 kg water and 26,6 kWh electricity per m<sup>2</sup> of PV module, while Rauegi et al. (2007a) has a lower consumption of these entries, using 0,88 kg EVA, 1,25 kg water and 24,3 kWh electricity per m<sup>2</sup> of PV module.

It should be noted that Rauegi et al. (2007a) uses CML 2 baseline 2000 as the characterization model, not ReCiPe. This is very likely to affect the results, and the outcome would probably have been different if ReCiPe had been used instead.

De WildScholten (2011) presented a GWP of 31,0 g CO<sub>2</sub>-eq./kWh for a CIGS rooftop PV system installed in Southern Europe. The data came from Germany for the year 2010 (source not given). This GWP value is 51% higher than the GWP found for the CIGS base case in this report. Due to lack of transparency in de Wild-Scholten (2011), it is impossible to give further reasons for the differences.

Clarius (2011) presented a GWP of 140,3 kg/m<sup>2</sup> for a PV module manufactured by Avancis, including BOS-components. This result is 63% higher than the GWP found for the CIGS-case. The transportation were only modeled for the front- and substrate glass, while the transportation of the rest of the components was not considered due to their low mass. The end-of-life treatment was included as waste landfilled at the Torgau plant, which may have affected the results. One of the inventories used in the CIGS-case includes internal recycling of the metals copper, indium, gallium, selenium and molybdenum during manufacturing. This do not seem to be included in Clarius (2011). Lack of transparency makes it impossible to give further reasons for the differences.

In the presentation of de Wild-Scholten & Schottler (2009), a GWP of 15,5 g CO<sub>2</sub>-eq./kWh was stated. The presentation gives very few details, but the PV system was assumed installed in Southern Europe, the data was from 2008 and the conversion efficiency was 10,7%. The performance ratio was not given, making it impossible to adjust the CIGS base case without making assumptions. Regardless of this, the GWP of the CIGS-case is not too far away from that of de Wild-Scholten & Schottler (2009), but is in relative terms 33% higher. The study lack in depth details to give further explanation for the differences.



### 13.3 Insights and implications

The comparative LCA and sensitivity analysis give valuable insights on how the environmental performance of a PV system may be improved, in terms of reduced lifecycle impacts.

The sensitivity analysis showed how influential the choice of electricity supply is for the GWP. A considerable reduction of the GWP could be achieved if the electricity supply was switched towards renewable energy sources like wind- and hydropower. This is especially relevant for the mc-Si technologies, which have significantly higher energy requirements than the thin film technologies. The energy intensive process steps for purification of silicon (MG-Si and SoG-Si) should ideally be performed in countries with a high share of renewable energy in the electricity mix. One may expect that other environmental impact potentials would be reduced too by performing such a switch, particular in impact categories where energy use plays an important part.

The electricity supply mix is related to the production site. This is very important to have in mind considering the current globalization trend, where the production of solar cells, PV modules and BOS components is shifted towards Asia. In particular China and Taiwan have been large producers the recent years (see chapter 2.1). The share of solar cell and PV module production happening in these countries are expected to increase further in the next years. Chinese electricity supply is highly dependent on carbon intensive coal power (Hsu et al., 2012). This will have a large influence on the environmental performance of PV systems. On the other hand, Hsu et al. (2012) suggest that companies may install PV systems to supply a part of the electricity required for manufacturing, thereby decreasing the facility's GHG emissions. Looking at the existing LCA literature, many studies are based on the PV manufacturing taking place in Europe or the USA. These sites are generally considered to have a stricter environmental legislation/regulation than e.g. China.

There should still be a continuously research on conversion efficiency improvement. This study has showed that by improving the PV module conversion efficiency by 1%, an average GWP reduction of 1,2-2,7 g CO<sub>2</sub>-eq./kWh can be achieved, depending on what type of PV technology is used. The mc-Si technologies have already achieved a certain level of conversion efficiency, while the thin film technologies still have a way to go before reaching the same levels. To improve the spectral response and thereby the conversion efficiency of the thin film PV modules, the search for another buffer layer material, replacing CdS, should be continued. Among the thin film PV technologies, CIGS is among the technologies which is considered to have the highest potential for conversion efficiency improvements (Dhere, 2007). On a research level, CIGS has in some cases achieved conversion efficiencies as high as those of the crystalline silicon technology (not yet confirmed under standard conditions, see chapter 7.3), but implementation into commercial production has so far proven to be more difficult. This may be due to difficulties between laboratory- and large-scale production

technologies (Razykov et al., 2011). An increased R&D effort of research institutions in cooperation with commercial PV producers is probably required to solve this challenge.

The lifetime electricity generation of a PV system is affected by the conversion efficiency, performance ratio, lifetime and direct normal irradiation. Improvements in conversion efficiency seems to have a higher potential for GWP reductions than improvements of the other parameters affecting the lifetime electricity generation. It is possible to achieve performance ratios up to 90%. Improving the performance ratio by 1% gives an average GWP reduction of 0,2-0,5 g CO<sub>2</sub>-eq./kWh, depending on type of PV technology. The choice of performance ratio in this study was 75%, recommended in Fthenakis et al. (2011b), but it is possible that a higher performance ratio would have reflected the current technology on the market in a better way. It is important to remember that processes will always involve energy losses, and therefore the potential for improvements in performance ratio is limited. The technical lifetime of a PV system is already considered to be sufficiently high (30 years), so the potential for improvements is also in this case limited. The direct normal irradiation had a certain effect on the GWP. However, this parameter is more difficult to "control", due to the fact that the direct normal irradiation is related to the geographical site of installation. To achieve the lowest possible GWP, the PV systems should be installed at sites with a high direct normal irradiation.

Improvements in energy efficiency and/or material efficiency are feasible measures that should be investigated to reduce the GWP of the PV system. The improvements in material efficiency can e.g. come from reducing material losses during manufacturing or from using less material in the final product (e.g. thinner mc-Si wafers, thinner layers in the thin film solar cell). Today, the thickness of crystalline silicon wafers range between 180 and 285 µm, giving an average wafer thickness of 200 µm on the market (Zuser & Rehnberger, 2011). Since silicon has an indirect bandgap, a certain thickness is required to ensure sufficient light absorption. At the same time, reducing the wafer thickness will increase the chance of breakage during manufacturing and transport. It is therefore difficult to put a measurement on how much the wafer thickness may be reduced, but Dhere (2007) states that it is an increased probability of wafer breakage when the wafer thickness is reduced to 100 µm. Alsema et al. (2006) predicts a wafer thickness of 150 µm in the future.

Striving to improve the material efficiency is important for the thin film PV technologies in terms of reducing the consumption of scarce elements like tellurium, indium and gallium. The production of thin film PV systems is expected to increase further and a market share of approximately 20% is forecasted for thin film PV modules for the year 2020 (Held, 2009). There is a concern that the availability of scarce metals may limit the growth of thin film PV technology (see chapter 7.3). However, it is worth mentioning that the LCA results in this report indicate that the part of the metal depletion potential (MDP) caused by the inverter components are usually dominating the part of the MDP caused by the thin film layers in the PV module. Currently, the average thickness of the absorber layer in CdTe is in the range of

1,0-3,3  $\mu\text{m}$ , while it is in the range of 1,3-2,5  $\mu\text{m}$  for CIGS (Zuser & Rehnberger, 2011). Reducing the thickness of the absorber layer and other layers like e.g. the back contact layer of molybdenum in CIGS would reduce the GWP, and at the same time reduce the requirements of primary metals.

In parallel with the material efficiency measures already mentioned, the commercial producers should increase their efforts on implementing "internal", closed-loop recycling of manufacturing waste during the different process steps in the value chain. This will make it possible to reuse recycled materials in production, reducing the demand of primary material. Recycled material with insufficient quality to be reused in the PV value chain can be exported to other industries. If it is impossible to recycle or/and reuse the manufacturing waste in production, the waste should be properly handled. This is particularly important during the manufacturing of mc-Si solar cell, where the LCA of the mc-Si technologies showed a large contribution from the solar cell in e.g. the toxicity categories. The commercial producers of mc-Si PV systems should investigate the possibility of recycling ingot cut-offs, wafer- and cell waste during the manufacturing steps. Slurry recycling during wafer production should be implemented. According to Zuser & Rehnberger (2011), the material losses in the mc-Si value chain are mainly caused during ingot growing and kerf loss during the wafer sawing. These losses can be in the range of 45-51% (Zuser & Rehnberger, 2011). The commercial producers of thin film technologies should consider the possibility of recycling rare metals during manufacturing. Material losses occurring during manufacturing in the thin film value chain can be related to e.g. overspray which coats equipment and deposition chambers and has to be removed regularly, waste from scribing for monolithic cell interconnections and from laser edge cleaning of the module (Marwede & Reller, 2012).

Improvements in energy efficiency are most relevant for the mc-Si PV technologies with an average GWP reduction of 0,1-0,2 g CO<sub>2</sub>-eq. per % improvement, while it only has a minor effect on the GWPs for the thin film technologies (much lower energy demand). The improvements in energy efficiency can e.g. come from reducing energy losses during manufacturing, or from using other, less energy intensive process steps for manufacturing of the PV system.

The results from the LCA conducted in this report implicates that for the SoG-Si production the ESS-process has an environmental advantage in terms of using biogenic carbon sources, e.g. chips, as part of the reduction agents and being less energy intensive than the modified Siemens process. As both the mc-Si ESS-case and mc-Si Sim-case show, the SoG-Si production accounts for a large part of the environmental impacts caused by the PV system, especially to the GWP. A switch towards using more energy efficient methods for SoG-Si production, as the ESS-process and/or FBR-process, instead of the modified Siemens process should be considered. It should also be consider whether it is a possibility of implementing energy recovery during the SoG-Si production, in order to reduce the external energy requirement.

For the mc-Si Sim-case, the production of MG-Si is an important contributor. This is an energy intensive process, and energy recovery should be considered when possible. The possibility of using more biogenic carbon sources as reduction agents would reduce the CO<sub>2</sub>-emissions from the MG-Si production. Using renewable energy sources, e.g. hydropower, for the energy supply would (as already mentioned) contribute to further emission reductions.

Another important process in the PV value chain, for all cases, is the manufacturing of the PV module. Aluminium and (solar) glass are the main reasons for the environmental burdens caused by the PV module, contributing to e.g. the GWP. Possible improvements may be to use less aluminium in the frame, shift towards using more steel or use recycled (secondary) aluminium for the frame and for the mounting structure, as this is less energy intensive. The energy requirement of secondary aluminium may be as low as 8 MJ/kg, while primary aluminium requires 200 MJ/kg (Alsema & de Wild-Scholten, 2007). Using frameless modules may remove the requirement of aluminium to the frame completely. For this to become a possibility, frameless modules must be able to offer the same long lifetime as framed modules do. This is particularly relevant for the thin film PV technologies, where the PV modules can be frameless as long as the solar cells are encapsulated between two sheets of glass. Solibro Solar, MiaSolé and HelioVolt are among those companies which produce PV modules with a frameless design. Using flexible solar cells integrated in building facades would also remove the requirement of a frame. In-roof mounting structure should be used instead of on-roof mounting structure, as they uses less material than on-roof mounting structure and replaces roof tiles. Instead of aluminium, other metals should be considered to be used as back electrical contact in the CdTe PV module.

Recycling of the PV module after end-of-life should of course be considered, in order to recover the aluminium, glass sheet, rare metals and other materials. However, the recycling of mc-Si solar cells from the modules may become more difficult to perform as wafer- and therefore also solar cell thicknesses continues to decrease, which is the current trend, making them easier to break. The same will be the case for recycling of end-of-life thin film modules, with very thin compound layers in the solar cell structure. The recycling of rare metals could replace the requirement of primary material in the production of thin film PV modules. With thinner solar cells, it should be investigated how to design for recycling of PV modules, so that the disassembly/treatment of end-of-life modules can be made as easy as possible. (It is important to have in mind that end-of-life recycling will introduce new energy- and material requirements).

Governments should implement economical incentives and support schemes for PV technology to promote production and installation of PV systems. This is necessary in order for PV technology to be competitive with other energy sources/-technologies and to be able to reach grid parity. Take-back schemes and collection systems for end-of-life PV modules should be set up to ensure a proper waste management. This will be important in the future years when the amount of PV scrap is expected to increase. Both government and

commercial PV producers should take their part of the responsibility and cooperate to find out how the end-of-life management can be solved in a best possible way.

### 13.4 Conclusion

The comparative LCA which has been conducted in this report indicates that the mc-Si PV technologies results in higher environmental impacts than the thin film PV technologies (CdTe and CIGS). The modified Simens process (Sim) for SoG-Si production resulted in significantly higher environmental impacts than using the metallurgical process by Elkem Solar (ESS). The differences between impact potentials of CdTe and CIGS PV systems were small, indicating that one should be careful to argue that one of these technologies is better than the other.

The mc-Si ESS-case gave a GWP of 155 kg CO<sub>2</sub>-eq./m<sup>2</sup> of PV system, while the mc-Si Sim-case gave a score of 260 kg CO<sub>2</sub>-eq./m<sup>2</sup> of PV system. This is related to the high energy requirement and the energy feedstock used in the SoG-Si production. The GWP-scores for the CdTe and CIGS PV systems were 75 and 86 kg CO<sub>2</sub>-eq./m<sup>2</sup> of PV system, mainly related to the glass and the primary aluminium used in the frame of the module or for the back contact in the CdTe solar cells .

For comparison with existing LCA studies, a base case was used. The corresponding GWP values in g CO<sub>2</sub>-eq./kWh electricity produced by the PV system were 42,5 for mc-Si Sim, 30,8 for mc-Si ESS, 16,8 for CdTe and 20,6 for CIGS. These values are well within the range of values published in other similar studies. However, CdTe and CIGS generated values in the lower end of the scale. The lack of transparency and few published LCAs on thin film PV technology limited the benchmarking. It is important to be aware of the assumptions made when comparing with other studies.

The relative contribution from foreground process to the impact scores were different within each case investigated, but some main trends could be observed: The energy intensive production of MG-Si and SoG-Si, in addition to the use of primary aluminium and (solar) glass in the PV manufacturing, were often large contributors in many categories in the mc-Si cases, while the manufacturing of the PV module dominated the contribution in the thin film cases. The main contributions came from the glass and aluminium to the frame and back contact (CdTe). In all cases, the metal depletion potential got most of its impacts from the copper and tin in the inverter and cabling components. The metallization pastes used in the mc-Si solar cell production contributed to the toxicity potentials.

A sensitivity analysis showed that PV technology has the potential of competing with wind power by performing different combinations of measures. In the best case scenario, with hydropower for electricity supply and maximum improvements in energy efficiency (main focus electricity), material efficiency and lifetime electricity generation, mc-Si ESS, CdTe and

CIGS achieved GWPs in the range of 5,1-5,8 g CO<sub>2</sub>-eq./kWh, i.e. lower than the GWP of 9,0 g CO<sub>2</sub>-eq./kWh from wind power.

The sensitivity analysis revealed that choice of the energy supply and conversion efficiency has a significant effect on the GWP. The electricity supply should be switched towards a larger share of renewable energy sources, like wind or hydropower, especially in the energy intensive silicon purification steps in the mc-Si value chain. There should be continuously research on how to improve the conversion efficiency further, e.g. by replacing the current buffer layer of CdS in thin film solar cells with other materials.

The SoG-Si production needs to be made even more energy-efficient. Promising methods like the Elkem Solar production process and Fluidized Bed Reactor process are steps in the right direction. The implementation of energy recovery and larger use of biogenic reduction agents may reduce the environmental impacts further. Recycled aluminium or steel should be used in the PV module and mounting structure in order to reduce the environmental impacts from these manufacturing processes. Frameless PV modules would remove the need for a frame. The possibility of using metallization pastes with less silver should be investigated for the mc-Si PV value chain, reducing the toxicity potentials.

Recycling of manufacturing scrap and end-of-life module should be implemented/improved, reducing the demand for primary material. Reducing the thickness of the mc-Si wafers or the compound layers in the thin film solar cell will increase the material efficiency and contribute to further GWP-reductions.

Most of the modelling did not include the recycling of internal manufacturing waste and end-of-life treatment of PV modules. It is unsure how much the inclusion of these processes would have affected the results. Currently, the waste of PV modules is quite low.

## References

- ABB (2012). *Project report: Lightning in a bottle? Solar power in a chip. Silicon purification process "under control" by ABB.* 3BSE069611. Available: <http://www.abb.com/> (Downloaded 04.01.13)
- Aberle, A.G. (2009). Thin-film solar cells. *Thin Solid Films*, 517 (17) , pp. 4706-4710. Available: <http://dx.doi.org/10.1016/j.tsf.2009.03.056> (Downloaded 13.02.13)
- Aliyu, M.M., Islam, M.A., Hamzah, N.R., Karim, M.R., Matin, M.A., Sopian, K., Amin, N. (2012). Recent developments of flexible CdTe solar cells on metallic substrates: Issues and prospects. *International Journal of Photoenergy*, vol. 2012, Article ID 351381, 10 pages. Available: <http://dx.doi.org/10.1155/2012/351381> (Downloaded 10.06.13)
- Alsema, E.A., de Wild-Scholten, M.J. (2007). Reduction of the environmental impacts in crystalline silicon module manufacturing. *22nd European Photovoltaic Solar Energy Conference, Milan, Italy, September 3-7, 2007.* ECN report ECN-M--07-027. Available: <http://www.ecn.nl/publicaties/ECN-M--07-027> (Downloaded 01.02.13)
- Alsema, E.A., de Wild-Scholten, M.J., Fthenakis, V.M. (2006). Environmental impacts of PV electricity generation - A critical comparison of energy supply options. *21st European Photovoltaic Solar Energy Conference, Dresden, Germany, September 4-8, 2006.* ECN report ECN-RX--06-016. Available: <http://www.ecn.nl/publicaties/ECN-RX--06-016> (Downloaded: 01.02.13)
- Amendola, S. (2011). *Overview of manufacturing processes for solar-grade silicon.* Available: <http://www.yumpu.com/en/document/view/4616920/overview-of-manufacturing-processes-for-solar-grade-rsi-silicon> (Downloaded 01.06.13)
- Ampenberger, A., Hellriegel, E., Köhler, D. (1998). *Massen- und Energiebilanzen für die Herstellung von CIS-Dünnschichtsolarmodulen.* Forschungsstelle für Energiewirtschaft (FfE), München, Germany.
- Andersson, B.A., Azar, C., Holmberg, J., Karlsson, S. (1998). *Material constraints for thin-film solar cells.* *Energy*, 23 (5), pp. 407-411. Available: [http://dx.doi.org/10.1016/S0360-5442\(97\)00102-3](http://dx.doi.org/10.1016/S0360-5442(97)00102-3) (Downloaded 19.06.13)
- Andresen, S.R. (2008). *Life cycle assessment of silicon production: Environmental analysis of present production and relevant alternatives.* Project thesis. Norwegian University of Science and Technology, Trondheim, Norway.
- Arvesen, A., Hertwich, E. G. (2012). Assessing the life cycle environmental impacts of wind power: A review of present knowledge and research needs. *Renewable and Sustainable*

*Energy Reviews*, 16 (8), pp. 5994-6006. Available:

<http://dx.doi.org/10.1016/j.rser.2012.06.023> (Downloaded 14.06.13)

AVANCIS GmbH. (2013). *CIS solar modules - Excellent performance even in low light and shade*. Available: <http://www.avancis.de/en/cis-technology/advantages-of-a-cis-solar-system/performance-in-low-light-conditions/> (Downloaded 29.07.13)

Bae, D., Gho, J., Shin, M., Kwon, S. (2013a). Effect of zinc addition on properties of cadmium sulfide layer and performance of Cu(In,Ga)Se<sub>2</sub> solar cell. *Thin Solid Films*, 535, pp. 162-165. Available: <http://dx.doi.org/10.1016/j.tsf.2012.11.077> (Downloaded 26.02.13)

Bae, D., Kwon, S., Oh, J., Kim, W.K., Park, H. (2013b). Investigation of Al<sub>2</sub>O<sub>3</sub> diffusion barrier layer fabricated by atomic layer deposition for flexible Cu(In,Ga)Se<sub>2</sub> solar cells. *Renewable Energy*, 55, pp. 62-68. Available: <http://dx.doi.org/10.1016/j.renene.2012.12.024> (Downloaded 26.02.13)

Bekkelund, K. (2013). *Life cycle assessment of PV solar systems*. Project thesis. Norwegian University of Science and Technology, Trondheim, Norway.

Berger, W., Simon, F-G., Weimann, K., Alsema, E.A. (2010). A novel approach for the recycling of thin film photovoltaic modules. *Resources, Conservation and Recycling*, 54 (10), pp. 711-718. Available: <http://dx.doi.org/10.1016/j.resconrec.2009.12.001> (Downloaded 05.03.13)

Bergesen, J. (2013). PhD Student, MESM, Bren School of Environmental Science & Management, University of California, Santa Barbara, the USA. E-mail correspondence.

Bhattacharya, R.N., Contreras, M.A., Egaas, B., Noufi, R.N., Kanevce, A., Sites, J.R. (2006). High efficiency thin-film CuIn<sub>1-x</sub>Ga<sub>x</sub>Se<sub>2</sub> photovoltaic cells using a Cd<sub>1-x</sub>Zn<sub>x</sub>S buffer layer. *Applied Physics Letters*, 89 (25), Article ID 253503, 2 pages. Available: <http://dx.doi.org/10.1063/1.2410230> (Downloaded 12.02.13)

Biccari, F. (2012a). *CdTe solar cells*. Power point presentation. University of Rome, Italy. Available: <http://biccari.altervista.org/c/fisica/fotovoltaico/> (Downloaded 03.06.13)

Biccari, F. (2012b). *CuIn<sub>1-x</sub>Ga<sub>x</sub>Se<sub>2</sub> solar cells*. Power point presentation. University of Rome, Italy. Available: <http://biccari.altervista.org/c/fisica/fotovoltaico/> (Downloaded 03.06.13)

Biccari, F. (2012c). *Why thin film solar cells?* Power point presentation. University of Rome, Italy. Available: <http://biccari.altervista.org/c/fisica/fotovoltaico/> (Downloaded 03.06.13)

Birkmire, R.W., McCandless, B.E. (2010). CdTe thin film technology: Leading thin film PV into the future. *Current Opinion in Solid State and Materials Science*, 14 (6), pp. 139-142. Available: <http://dx.doi.org/10.1016/j.cossms.2010.08.002> (Downloaded 18.03.13)



- Birkmire, R.W., Meyers, P.E. (2001). *Processing issues for thin-film CdTe cells and modules*. Institute of Energy Conversion, University of Delaware, Newark, the USA. Available: <http://www.udel.edu/iec/Resumes/Birkmire/Pubs/> (RWB55)(Downloaded 10.06.13)
- Blösch, P., Nishiwaki, S., Chirila, A., Kranz, L., Fella, C., Pianezzi, F., Adelhelm, C., Franzke, E., Buecheler, S., Tiwari, A.N. (2013). Sodium-doped molybdenum back contacts for flexible Cu(In,Ga)Se<sub>2</sub> solar cells. *Thin Solid Films*, 535, pp. 214-219. Available: <http://dx.doi.org/10.1016/j.tsf.2012.10.080> (Downloaded 06.03.13)
- Bonnet, D. (2000). Manufacturing of CSS CdTe solar cells. *Thin Solid Films*, 361–362, pp. 547-552. Available: [http://dx.doi.org/10.1016/S0040-6090\(99\)00831-7](http://dx.doi.org/10.1016/S0040-6090(99)00831-7) (Downloaded 30.04.13)
- Bosio, A., Menossi, D., Mazzamuto, S., Romeo, N. (2011). Manufacturing of CdTe thin film photovoltaic modules. *Thin Solid Films*, 519 (21), pp. 7522-7525. Available: <http://dx.doi.org/10.1016/j.tsf.2010.12.137> (Downloaded 18.03.13)
- Braga, A.F.B., Moreira, S.P., Zampieri, P.R., Bacchin, J.M.G, Mei, P.R. (2008). New processes for the production of solar-grade polycrystalline silicon: A review. *Solar Energy Materials & Solar Cells*, 92 (4), pp. 418-424. Available: <http://dx.doi.org/10.1016/j.solmat.2007.10.003> (Downloaded 01.02.13)
- Breierova, L., Choudhari, M. (1996). *An introduction to sensitivity analysis*. Prepared for the MIT System Dynamics in Education Project. Massachusetts Institute of Technology, Cambridge, the USA.
- Buecheler, S., Corica, D., Guettler, D., Chirila, A., Verma, R., Müller, U., Nielsen, T.P., Palm, J., Tiwari, A.N. (2009). Ultrasonically sprayed indium sulfide buffer layers for Cu(In,Ga)Se<sub>2</sub> thin-film solar cells. *Thin Solid Films*, 517 (7), pp. 2312-2315. Available: <http://dx.doi.org/10.1016/j.tsf.2008.10.135> (Downloaded 06.03.13)
- Candelise, C., Speirs, J.F., Gross, R.J.K. (2011). Materials availability for thin film (TF) PV technologies development: A real concern? *Renewable and Sustainable Energy Reviews*, 15 (9), PP. 4972-4981. Available: <http://dx.doi.org/10.1016/j.rser.2011.06.012> (Downloaded 12.02.13)
- Carcia, P.F., McLean, R.S., Hegedus, S. (2010). Encapsulation of Cu(InGa)Se<sub>2</sub> solar cell with Al<sub>2</sub>O<sub>3</sub> thin-film moisture barrier grown by atomic layer deposition. *Solar Energy Materials & Solar Cells*, 94 (12), pp. 2375-2378. Available: [dx.doi.org/10.1016/j.solmat.2010.08.021](http://dx.doi.org/10.1016/j.solmat.2010.08.021) (Downloaded 05.03.13)
- Centre for Alternative Technology (CAT) (2013). *How long do solar electricity PV panels last?* Available: <http://info.cat.org.uk/questions/pv/life-expectancy-solar-PV-panels> (Downloaded 01.02.13)

Chelvanathan, P., Hossain, M.I., Amin, N. (2010). Performance analysis of copper-indium-gallium-diselenide (CIGS) solar cells with various buffer layers by SCAPS. *Current Applied Physics*, 10 (3), pp. S387-S391. Available: <http://dx.doi.org/10.1016/j.cap.2010.02.018> (Downloaded 26.02.13)

Chopra, K.L., Paulson, P.D., Dutta, V. (2004). Thin-film solar cells: An overview. *Progress in Photovoltaics: Research and Applications*, 12 (2-3), pp. 69-92. Available: <http://dx.doi.org/10.1002/pip.541> (Downloaded 05.03.13)

Chu, Y. (2011). Review and comparison of different solar energy technologies. (Edited by Meisen, P.). Global Energy Network Institute (GENI). Available: <http://www.geni.org/globalenergy/research/index.shtml> (Downloaded 08.05.13)

Ciftja, A., Engh, T.A., Tangstad, M. (2008). *Refining and recycling of silicon: A review*. Norwegian University of Science and Technology, Trondheim, Norway. Available: <http://urn.kb.se/resolve?urn=urn:nbn:no:ntnu:diva-1942> (Downloaded 01.02.13)

Clarius, T. (2011). *Life cycle analysis (LCA): Modeling of photovoltaics*. Available: [http://www.slideshare.net/ICV\\_eV/lca-avancis-for-icv](http://www.slideshare.net/ICV_eV/lca-avancis-for-icv) (Downloaded 02.05.13)

Climate and Pollution Agency of Norway (Klif) (2012). *Norske utslipp - Elkem Solar (utslipp, avfall, energiforbruk)*. Available: <http://www.norskeutslipp.no> (Downloaded 30.09.2012)

Compaan, A.D. (2007). Materials challenges for terrestrial thin-film photovoltaics. *JOM*, 59 (12), pp. 31-36. Available: <http://dx.doi.org/10.1007/s11837-007-0149-6> (Downloaded 12.02.13)

Cunningham, D., Rubcich, M., Skinner, D. (2002). Cadmium telluride PV module manufacturing at BP Solar. *Progress in Photovoltaics: Research and Applications*, 10 (2), pp. 159-168. Available: <http://dx.doi.org/10.1002/pip.417> (Downloaded 18.03.113)

DayStar Technologies Inc. (2013a). *CIGS on glass*. Available: <http://www.daystartechinc.com/cigsonglass.html> (Downloaded 29.07.13)

DayStar Technologies Inc. (2013b). *Solar Photovoltaics and CIGS*. Available: <http://www.daystartechinc.com/solar.html> (Downloaded 29.07.13)

De Wild-Scholten, M. (2011). Environmental profile of PV mass production: Globalization. *26th European Photovoltaic Solar Energy Conference, Hamburg, Germany, September 5-9, 2011*. Available: <http://www.smartgreenscans.nl/publications.html> (both paper and power point presentation) (Downloaded 01.02.13)

De Wild-Scholten, M., Alsema, A. (2004). Towards cleaner solar PV. *Refocus*, 5 (5), p.46-49. Available: [http://dx.doi.org/10.1016/S1471-0846\(04\)00225-2](http://dx.doi.org/10.1016/S1471-0846(04)00225-2) (Download 01.02.13)

De Wild-Scholten, M.J., Alsema, E.A. (2006). "Environmental Life Cycle Inventory of Crystalline Silicon Photovoltaic System Production." Excel file, ECN report ECN-E--06-019. Available: <http://www.ecn.nl/publications/ECN-E--06-019> (Downloaded: 13.09.12)

De Wild-Scholten, M.J., Alsema, E.A. ter Horst, E.W., Bächler, M., Fthenakis, V.M. (2006). A cost and environmental impact comparison of grid-connected rooftop and ground-based PV systems. *21th European Photovoltaic solar Energy Conference, Dresden, Germany, September 4-8, 2006*. ECN report ECN-RX--06-024. Available: <http://www.ecn.nl/publicaties/ECN-RX--06-024> (Downloaded 01.03.13)

De Wild-Scholten, M., Gløckner, R. (2012). Environmental footprint of Elkem Solar Silicon. *Silicon for the Chemical and Solar Industry XI, Bergen-Ulvik, Norway, June 25-29, 2012*. Available: <http://www.smartgreenscans.nl/publications.html> (Downloaded 01.02.13)

De Wild-Scholten, M., Schottler, M. (2009). Solar as an environmental product: Thin-film modules - production processes and their environmental assessment. *Thin Film Industry Forum, Berlin, Germany, April 23-24, 2009*. ECN report ECN-M--09-072. Available: <http://www.ecn.nl/publicaties/ECN-M--09-072> (Downloaded 19.06.13)

Dhere, N.G. (2007). Toward GW/year of CIGS production within the next decade. *Solar Energy Materials and Solar Cells, 91 (15-16), pp. 1376-1382*. Available: <http://dx.doi.org/10.1016/j.solmat.2007.04.003> (Downloaded 12.02.13)

Dimmler, B. (2012). CIGS and CdTe based thin film PV modules, an industrial r/evolution. *Photovoltaic Specialists Conference (PVSC), 38th IEEE, Austin, Texas, the USA, June 3-8, 2012, pp.002494-002499*. Available: <http://dx.doi.org/10.1109/PVSC.2012.6318101> (Downloaded 24.04.13)

Dominguez-Ramos, A., Held, M., Aldaco, R., Fischer, M., Irabien, A. (2010). Prospective CO<sub>2</sub> emissions from energy supplying systems: Photovoltaic systems and conventional grid within Spanish frame conditions. *The International Journal of Life Cycle Assessment, 15 (6), pp 557-566*. Available: <http://dx.doi.org/10.1007/s11367-010-0192-3> (Downloaded 22.04.13)

Ecoinvent Centre (2012). *The ecoinvent database*. Dübendorf, Zürich, Switzerland: Swiss Centre for Life Cycle Inventories. Available: <http://www.ecoinvent.org/database> (Downloaded 21.12.2012)

Edoff, M. (2013). Professor, Department of Engineering Sciences, Solid State Electronics, Uppsala University, Uppsala, Sweden. E-mail correspondance.

Elkem Solar (2012a). *Elkem Solar Silicon (ESS<sup>TM</sup>) for multicrystalline application*. Available: <http://www.elkem.com/en/Solar/Products/> (Downloaded 03.01.2013)

Elkem Solar (2012b). *Products*. Available: <http://www.elkem.com/en/Solar/Products/> (Downloaded 13.12.2012)

Elowe, P.R., Stempki, M.A., Rozeveld, S.J., DeGroot, M.W. (2011). Development of direct cell inorganic barrier film technology providing exceptional device stability for CIGS solar cells. *Chemistry of Materials*, 23 (17), pp. 3915-3920. Available: <http://dx.doi.org/10.1021/cm201281v> (Downloaded 05.03.13)

European Photovoltaic Industry Association (EPIA) (2011). *Solar generation 6: Solar photovoltaic electricity empowering the world*. Brussels, Belgium: EPIA. Available: <http://www.epia.org/news/publications/> (Downloaded 09.01.2013)

European Photovoltaic Industry Association (EPIA) (2013). *Global market outlook for photovoltaics 2013-2017*. Brussels, Belgium: EPIA. Available: <http://www.epia.org/news/publications/> (Downloaded 08.05.13).

European Commission (2012a). *Life cycle Impact Assessment (LCIA)*. Joint Research Centre, Institute for Environment and Sustainability. Available: <http://lca.jrc.ec.europa.eu/lcainfohub/lciaPage.vm> (Downloaded 21.12.12)

European Commission (2012b). *Photovoltaics*. Research & Innovation. Available: [http://ec.europa.eu/research/energy/eu/index\\_en.cfm?pg=research-photovoltaics](http://ec.europa.eu/research/energy/eu/index_en.cfm?pg=research-photovoltaics) (Downloaded 09.01.13)

European Commission (2012c). *Photovoltaics: Technical background- future prospects*. Research & Innovation. Available: [http://ec.europa.eu/research/energy/eu/index\\_en.cfm?pg=research-photovoltaics-background](http://ec.europa.eu/research/energy/eu/index_en.cfm?pg=research-photovoltaics-background) (Downloaded 21.12.12)

European Commission (2012d). *Photovoltaics: Technical background - Technology*. Research & Innovation. [http://ec.europa.eu/research/energy/eu/index\\_en.cfm?pg=research-photovoltaics-background](http://ec.europa.eu/research/energy/eu/index_en.cfm?pg=research-photovoltaics-background) (Downloaded 22.11.12)

EV Group (2013). *Photovoltaics - Anti-reflective coating*. Available: [http://www.evgroup.com/de/solutions/photovoltaics/anti\\_reflective\\_coatings/](http://www.evgroup.com/de/solutions/photovoltaics/anti_reflective_coatings/) (Downloaded 03.08.13)

Fang, Z., Wang, X.C., Wu, H.C., Zhao, C.Z. (2011). Achievements and challenges of CdS/CdTe solar cells. *International Journal of Photoenergy*, vol. 2011, Article ID 297350, 8 pages. Available: <http://dx.doi.org/10.1155/2011/297350> (Downloaded 10.06.13)

Filippidou, F., Botsaris, P.N., Angelakoglou, K., Gaidajis, G. (2010). A comparative analysis of a CdTe and a poly-si photovoltaic module installed in North Eastern Greece. *Applied Solar Energy*, 46 (3), pp. 182-191. Available: <http://dx.doi.org/10.3103/S0003701X10030060> (Downloaded 23.01.13)

Fraunhofer Institut für Solare Energiesysteme (ISE) (2012). *Photovoltaic report*. Available: <http://www.ise.fraunhofer.de/en/news/news-2012/fraunhofer-ise-publishes-photovoltaics-report> (Downloaded 08.05.13)

Fthenakis, V.M. (2004). Life cycle impact analysis of cadmium in CdTe PV production. *Renewable and Sustainable Energy Reviews*, 8(4), pp. 303-334. Available: <http://dx.doi.org/10.1016/j.rser.2003.12.001> (Downloaded 05.03.13)

Fthenakis, V. (2009). Sustainability of photovoltaics: The case for thin-film solar cells. *Renewable and Sustainable Energy Reviews*, 13 (9), pp. 2746-2750. Available: <http://dx.doi.org/10.1016/j.rser.2009.05.001> (Downloaded 13.02.13)

Fthenakis, V., Alsema, E. (2006). Photovoltaics energy payback times, greenhouse gas emissions and external costs: 2004-early 2005 status. *Progress in Photovoltaics: Research and Applications*, 14 (3), pp. 275-280. Available: <http://dx.doi.org/10.1002/pip.706> (Downloaded 01.02.13)

Fthenakis, V., Frischknecht, R., Raugei, M., Kim, H.C., Alsema, E., Held, M., de Wild-Scholten, M. (2011b). *Methodology guidelines on life cycle assessment of photovoltaic electricity*. 2nd edition. IEA PVPS Task 12, International Energy Agency, Photovoltaic Power systems Programme. Available: <http://www.iea-pvps-task12.org/45.0.html> (01.02.13)

Fthenakis, V., Kim, H. C. (2005). Energy use and greenhouse gas emissions in the life cycle of CdTe photovoltaics. *Material Research Society (MRS) proceedings*, 895. Available: <http://dx.doi.org/10.1557/PROC-0895-G03-06> (Downloaded 01.02.13)

Fthenakis, V.M., Kim, H.C. (2006). CdTe photovoltaics: Life cycle environmental profile and comparisons. *European Material Research Society Meeting, Symposium O, Nice, France, May 29-June 2, 2006*. Available: <http://www.bnl.gov/pv/biblio.asp> (Downloaded 23.01.13)

Fthenakis, V.M., Kim, H.C. (2007). Greenhouse-gas emissions from solar electric- and nuclear power: A life-cycle study. *Energy Policy*, 35 (4), pp. 2549-2557. Available: <http://dx.doi.org/10.1016/j.enpol.2006.06.022> (Downloaded 23.04.13)

Fthenakis, V.M., Kim, H.C., Alsema, E. (2008). Emissions from photovoltaic life cycles. *Environmental Science and Technology*, 42 (6), pp. 2168-2174. Available: <http://dx.doi.org/10.1021/es071763q> (Downloaded 01.02.13)

Fthenakis, V.M., Kim, H.C., Colli A., Kirchsteiger C. (2006). Evaluation of risks in the life cycle of photovoltaics in a comparative context. *21st European Photovoltaic Solar Energy Conference, Dresden, Germany, September 4-8, 2006*. Available: <http://www.bnl.gov/pv/biblio.asp> (Downloaded 19.06.13)

- Fthenakis, V., Kim, H.C., Frischknecht, R., Raugei, M., Sinha, P., Stucki, M. (2011a). *Life cycle inventories and life cycle assessment of photovoltaic systems*. International Energy Agency (IEA). PVPS Task 12, Report T12-02:2011. Available: <http://www.clca.columbia.edu/publications.html> (Downloaded 23.01.13)
- Fthenakis, V. M., Wang, W. (2006). Extraction and separation of Cd and Te from cadmium telluride photovoltaic manufacturing scrap. *Progress in Photovoltaics: Research and Applications*, 14 (4), pp. 363–371. Available: <http://dx.doi.org/10.1002/pip.676> (Downloaded 19.06.13)
- Gessert, T.A. (2008). Review of photovoltaic energy production using CdTe thin-film modules. Extended abstract, preprint. *U.S. Workshop on the Physics and Chemistry of II-VI Materials, Las Vegas, Nevada, the USA, November 11–13, 2008*, 7 pages. NREL Report No. AB-520-44128.
- Gibon, T. et al. (forthcoming). Methodology. In: *Environmental assessment of low-GHG electricity supply technologies*. (Edited by E.G. Hertwich et al.). Paris, France: UNEP.
- Gledhill, S.E., Zykov, A., Rissom, T., Caballero, R., Kaufmann, C.A., Fischer, C.-H., Lux-Steiner, M., Efimova, V., Hoffman, V., Oswald, S. (2011). The role of spray pyrolysed Al<sub>2</sub>O<sub>3</sub> barrier layer in achieving high efficiency solar cells on flexible steel substrates. *Applied Physics A*, 104 (1), pp. 407-413. Available: <http://dx.doi.org/10.1007/s00339-010-6176-0> (Downloaded 05.03.13)
- Gløckner, R., Odden, J.-O., Halvorsen, G., Tronstad, R., de Wild-Scholten, M.J. (2008). Environmental life cycle assessment of the Elkem Solar metallurgical process route to solar grade silicon with focus on energy consumption and greenhouse gas emissions. *Silicon for the Chemical and Solar Industry IX, Oslo, Norway, June 23-26, 2008*. ECN Report ECN-M--08-069. Available: <http://www.ecn.nl/publicaties/ECN-M--08-069> (Downloaded 01.02.13)
- Goedkoop, M., Heijungs, R., Huijbregts, M., Schryver, A.D., Struijs, J., van Zelm, R. (2012). *ReCiPe 2008: A life cycle impact assessment method which comprises harmonised category indicators at the midpoint and endpoint level. Report I: Characterization*. 1st edition. Available: <http://www.pre-sustainability.com/reports> (Downloaded: 01.02.13)
- Green, M.A., Emery, K., Hishikawa, Y., Warta, W., Dunlop, E.D. (2013). Solar cell efficiency tables (version 42). *Progress in Photovoltaics: Research and Applications*, 21 (5), pp. 827–837. Available: <http://dx.doi.org/10.1002/pip.2404> (Downloaded 29.07.13)
- Gupta, A., Compaan, A.D. (2004). All-sputtered 14% CdS/CdTe thin-film solar cell with ZnO:Al transparent conducting oxide. *Applied Physics Letters*, 85 (4), pp. 684-686. Available: <http://dx.doi.org/10.1063/1.1775289> (Downloaded 16.05.13)
- Hariskos, D., Fuchs, B., Menner, R., Naghavi, N., Hubert, C., Lincot, D., Powalla, M. (2009). The Zn(S, O, OH)/ZnMgO buffer in thin-film Cu(In, Ga)(Se,S)<sub>2</sub>-based solar cells part II:

Magnetron sputtering of the ZnMgO buffer layer for in-line co-evaporated Cu(In, Ga)Se<sub>2</sub> solar cells. *Progress in Photovoltaics: Research and Applications*, 17 (7), pp.479-488. Available: <http://dx.doi.org/10.1002/pip.897> (Downloaded 07.03.13)

Hariskos, D., Spiering, S., Powalla, M. (2005). Buffer layers in Cu(In,Ga)Se<sub>2</sub> solar cells and modules. *Thin Solid Films*, 480-481, pp. 99-109. Available: <http://dx.doi.org/10.1016/j.tsf.2004.11.118> (Downloaded 05.03.13)

Held, M. (2009). Life cycle assessment of CdTe module recycling. *24th European Photovoltaic Solar Energy Conference, Hamburg, Germany, September 21-25, 2009*. Available: <http://dx.doi.org/10.4229/24thEUPVSEC2009-3CO.7.4> (Downloaded 13.02.13)

Held, M., Ilg, M. (2011). Update of environmental indicators and energy payback time of CdTe PV systems in Europe. *Progress in Photovoltaics: Research and Applications*, 19 (5), pp. 614-626. Available: <http://dx.doi.org/10.1002/pip.1068> (Downloaded 13.02.13)

Hertwich, E.G., Gibon, T., Bouman, E.A., Arvesen, A., Suh, S., Ramirez, A., Coloma, M.V., Bergesen, J.D., Saurat, M., Lei, S., Heath, G. (2013). Resource and environmental implications of low-carbon electricity supply. *Proceedings of the National Academy of Science*, forthcoming.

Herz, K., Eicke, A., Kessler, F., Wächter, R., Powalla, M. (2003). Diffusion barriers for CIGS solar cells on metallic substrates. *Thin Solid Films*, 431-432, pp. 392-397. Available: [http://dx.doi.org/10.1016/S0040-6090\(03\)00259-1](http://dx.doi.org/10.1016/S0040-6090(03)00259-1) (Downloaded 26.02.13)

Hsu, D.D., O'Donoghue, P., Fthenakis, V., Heath, G.A., Kim, H.C., Sawyer, P., Jun-Ki Choi, J., Turney, D.E. (2012). Life cycle greenhouse gas emissions of crystalline silicon photovoltaic electricity generation - Systematic review and harmonization. *Journal of Industrial Ecology*, 16 (s1), pp. S122-S135. Available: <http://dx.doi.org/10.1111/j.1530-9290.2011.00439.x> (Downloaded 24.06.13)

Intergovernmental Panel on Climate Change (IPCC) (2007). Climate Change 2007: Synthesis Report - Summary for policy makers. In: *IPCC Fourth Assessment Report: Climate Change 2007 (AR4)*. Available: [http://www.ipcc.ch/publications\\_and\\_data/publications\\_ipcc\\_fourth\\_assessment\\_report\\_synthesis\\_report.htm](http://www.ipcc.ch/publications_and_data/publications_ipcc_fourth_assessment_report_synthesis_report.htm) (Downloaded 12.02.2013)

International Energy Agency (IEA) (2008). *Energy Technology Perspectives 2008 - Scenarios and strategies to 2050*. Paris, France: OECD/IEA. Available: [http://www.iea.org/etp/publications\\_factsheets/previouseditions/](http://www.iea.org/etp/publications_factsheets/previouseditions/) (Downloaded 09.07.13)

International Energy Agency (IEA) (2010). *Technology roadmap: Solar photovoltaic energy*. Paris, France: OECD/IEA. Available: <http://www.iea.org/publications/freepublications/publication/name,3902,en.html> (Downloaded 02.05.13)

International Energy Agency (IEA) (2012a). *Energy Technology Perspectives 2012 - Pathways to a clean energy system. Executive summary*. Paris, France: OECD/IEA. Available: <http://www.iea.org/w/bookshop/add.aspx?id=425> (Downloaded 09.07.13)

International Energy Agency (IEA) (2012b). *World energy model documentation*. Paris, France: OECD/IEA. Available: <http://www.worldenergyoutlook.org/weomodel/> (Downloaded 08.07.13).

International Energy Agency (IEA) (2012c). *World Energy Outlook 2012. Chapter 7 - Renewable energy outlook*. Paris, France: OECD/IEA. Available: <http://www.worldenergyoutlook.org/publications/weo-2012/> (Downloaded 04.06.13)

International Energy Agency (IEA). (2013a). *About energy technology perspectives*. Available: <http://iea.org/etp/aboutetp/> (Downloaded 08.07.1)

International Energy Agency (IEA) (2013b). *ETP 2012 data visualisation*. Available: <http://www.iea.org/etp/explore/> (Downloaded 09.07.13)

International Energy Agency (IEA) (2013c). *EPT methodology*. <http://iea.org/etp/aboutetp/methodology/> (Downloaded 08.07.13)

International Energy Agency (IEA) (2013d). *Medium-Term Renewable Energy Market Report 2013 - Market Trends and Projections to 2018. Executive summary*. Paris, France: OECD/IEA. Available: <http://www.iea.org/W/bookshop/add.aspx?id=453> (Downloaded 10.07.13)

International Organization for Standardization (2006a). *ISO 14040: Environmental management - Life cycle assessment - Principle and framework*.

International Organization for Standardization (2006b). *ISO 14044: Environmental management - Life cycle assessment - Requirements and guidelines*.

Irfan, I., Lin, H., Xia, W., Wu, H.N., Tang, C.W., Gao, Y. (2012). The effect of MoO<sub>x</sub> inter-layer on thin film CdTe/CdS solar cell. *Solar Energy Materials and Solar Cells*, 105, pp. 86-89. Available: <http://dx.doi.org/10.1016/j.solmat.2012.04.006> (Downloaded 05.03.13)

Islam, M.M., Ishizuka, S., Yamada, A., Sakurai, K., Niki, S., Sakurai, T., Akimoto, K. (2009). CIGS solar cells with MBE-grown ZnS buffer layer. *Solar Energy Materials & Solar Cells*, 93 (6-7), pp. 970-972. Available: <http://dx.doi.org/10.1016/j.solmat.2008.11.047> (Downloaded 06.03.13)

Ito, M., Kato, K., Komoto, K., Kichimi, T., Kurokawa, K. (2008). A comparative study on cost and life-cycle analysis for 100 MW very large-scale PV (VLS-PV) systems in deserts using m-Si, a-Si, CdTe, and CIS modules. *Progress in Photovoltaics: Research and Applications*, 16 (1), pp. 17-30. Available: <http://dx.doi.org/10.1002/pip.770> (Downloaded 22.04.13)



Ito, M.; Komoto, K.; Kurokawa, K. (2009). A comparative LCA study on potential of very-large scale PV systems in Gobi desert. *Photovoltaic Specialists Conference (PVSC), 34th IEEE, Philadelphia, the USA, June 7-12, 2009*, pp.000729-000732. Available: <http://dx.doi.org/10.1109/PVSC.2009.5411180> (Downloaded 22.04.13)

Ito, M., Komoto, K., Kurokawa, K. (2010). Life-cycle analyses of very-large scale PV systems using six types of PV modules. *Current Applied Physics, 10 (2)*, pp. S271-S27. Available: <http://dx.doi.org/10.1016/j.cap.2009.11.028> (Downloaded 22.04.13)

Ito, M., Kudo, M., Nagura, M., Kurokawa, K. (2011). A comparative study on life cycle analysis of 20 different PV modules installed at the Hokuto mega-solar plant. *Progress in Photovoltaics: Research and Applications, 19 (7)*, pp. 878-886. Available: <http://dx.doi.org/10.1002/pip.1070> (Downloaded 19.06.13)

Johansen, B.A. (2008). *Life cycle assessment of a roof-mounted photovoltaic system with focus on the environmental benefits of the Elkem Solar silicon feedstock route relative to the modified Siemens process*. Project thesis. Norwegian University of Science and Technology, Trondheim, Norway.

Jungbluth, N., Stucki, M., Flury, K., Frischnecht, R., Büsser, S. (2012). *Life cycle inventories of photovoltaics*. Swiss Federal Office of Energy (SFOE). Zürich, Switzerland: ESU-services Ltd. Available: <http://www.esu-services.ch/projects/pv/> (Downloaded 01.02.13)

Jäger-Waldau, A. (2012). *PV status report 2012: Research, solar cell production and market implementation of photovoltaics*. European Commission, Joint Research Centre, Institute for Energy and Transport. Available: <http://dx.doi.org/10.2788/44478> (Downloaded 08.05.13)

Kato, K., Hibino, T., Komoto, K., Ihara, S., Yamamoto, S., Fujihara, H. (2001). A life-cycle analysis on thin-film CdS/CdTe PV modules. *Solar Energy Materials and Solar Cells, 67 (1-4)*, pp. 279-287. Available: [http://dx.doi.org/10.1016/S0927-0248\(00\)00293-2](http://dx.doi.org/10.1016/S0927-0248(00)00293-2) (Downloaded 18.03.13)

Keithley Instruments Inc. (2010). Electrical characterization of photovoltaic materials and solar cells with the model 4200-SCS Semiconductor Characterization System: I-V, C-V, C-f, DLCP, pulsed I-V, resistivity, and hall voltage measurements. *Keithley Application Note Series, no. 3026*. Available: <http://www.scribd.com/doc/107498220/1-DLCP-PV-SolarCellAppNote> (Downloaded 16.06.13)

Kessler, F., Rudmann, D. (2004). Technological aspects of flexible CIGS solar cells and modules. *Solar Energy, 77 (6)*, pp. 685-695. Available: <http://dx.doi.org/10.1016/j.solener.2004.04.010> (Downloaded 12.02.13)

Khallaf, H., Oladeji, I.O., Chai, G., Chow, L. (2008). Characterization of CdS thin films grown by chemical bath deposition using four different cadmium sources. *Thin Solid Films, 516 (21)*,

pp. 7306-7312. Available: <http://dx.doi.org/10.1016/j.tsf.2008.01.004> (Downloaded 09.05.13)

Khan, A. (2009). *Screen printed silicon solar cells*. University of South Alabama, Mobile, Alabama, the USA. Available: <http://www.southalabama.edu/engineering/ece/faculty/akhan/Courses/EE590-Renewable/supporting%20material/PVDevices/pvcdrom/Ch05/scrnprt.htm> (Downloaded 04.01.2013)

Kim, H.C., Fthenakis, V., Choi, J.-K. and Turney, D.E. (2012). Life cycle greenhouse gas emissions of thin-film photovoltaic electricity generation. *Journal of Industrial Ecology*, 16 (s1), pp. S110–S121. Available: <http://dx.doi.org/10.1111/j.1530-9290.2011.00423.x> (Downloaded 19.03.13)

Krishnakumar, V., Han, J., Klein, A., Jaegermann, W. (2001). CdTe thin film solar cells with reduced CdS film thickness. *Thin Solid Films*, 519 (21), pp. 7138-7141. Available: <http://dx.doi.org/10.1016/j.tsf.2010.12.118> (Downloaded 18.03.13)

Kushiya, K. (2012). CuInSe<sub>2</sub>-based thin-film photovoltaic technology in the gigawatt production era. *Japanese Journal of Applied Physics*, 51 (10), pp. 10NC01-10NC01-5. Available: <http://dx.doi.org/10.1143/jjap.51.10nc01> (Downloaded 23.04.13)

Kushiya, K., Tanaka, Y., Hakuma, H., Goushi, Y., Kijima, S., Aramoto, T., Fujiwara, Y. (2009). Interface control to enhance the fill factor over 0,70 in a large-area CIS-based thin film PV technology. *Thin Solid Films*, 517 (7), pp. 2108-2110. Available: <http://dx.doi.org/10.1016/j.tsf.2008.10.125> (Downloaded 13.02.13)

Lande, J.H. (2012). Employee, Elkem Solar, Kristiansand, Norway. Phone call 08.10.2012.

LDK Solar (2011a). *Products - Cell - Multicrystalline*. Available: [http://www.ldksolar.com/pro\\_cell\\_mul.php](http://www.ldksolar.com/pro_cell_mul.php) (Downloaded 03.01.2013)

LDK Solar (2011b). *Products - Silicon - Production*. Available: [http://www.ldksolar.com/pro\\_silicon\\_production.php](http://www.ldksolar.com/pro_silicon_production.php) (Downloaded 03.01.2013)

Li, Z.Q., Shi, J.H., Zhang, D.W., Liu, Q.Q., Sun, Z., Chen, Y.W., Yang, Z., Huang, S.M. (2011). Cu(In,Ga)Se<sub>2</sub> solar cells with double layered buffers grown by chemical bath deposition. *Thin Solid Films*, 520 (1), pp. 333-337. Available: <http://dx.doi.org/10.1016/j.tsf.2011.06.100> (Downloaded 26.02.13)

Lian, R. (2013). *Top 10 PV module suppliers in 2012*. PV TECH. Available: [http://www.pv-tech.org/guest\\_blog/top\\_10\\_pv\\_module\\_suppliers\\_in\\_2012](http://www.pv-tech.org/guest_blog/top_10_pv_module_suppliers_in_2012) (Downloaded 01.06.13)

Liu, W, Mitzi, D.B., Yan, M., Kellock, A.J., Chey, S.J. Gunawan, O. (2010). 12% efficiency CuIn(S<sub>e</sub>,S)<sub>2</sub> photovoltaic device prepared using a hydrazine solution process. *Chemistry of*

*Materials*, 22 (3), pp. 1010-1014. Available: <http://dx.doi.org/10.1021/cm901950q>  
(Downloaded 13.02.13)

Luque, A., Hegedus, S. (2011). *Handbook of Photovoltaic Science and Engineering*. 2nd edition. Chichester, United Kingdom: John Wiley & Sons, Ltd.

Malm, U. (2008). Modelling and degradation characteristics of thin-film CIGS solar cells . *Digital Comprehensive Summaries of Uppsala Dissertations from the Faculty of Science and Technology*, 554, 81 pp. Acta Universitatis Upsaliensis, Uppsala, Sweden. Available: <http://urn.kb.se/resolve?urn=urn:nbn:se:uu:diva-9291> (Downloaded 10.06.13)

Markvart, T. (2000). *Solar electricity*. 2nd edition. UNESCO. Chichester, United Kingdom: John Wiley & Sons, Ltd.

Martello, E.D. (2012). *Impurity distribution and reduction behavior of quartz in the production of high purity silicon*. PhD thesis. Norwegian University of Science and Technology, Trondheim, Norway. Available: <http://urn.kb.se/resolve?urn=urn:nbn:no:ntnu:diva-17363> (Downloaded 01.02.13)

Marwede, M., Berger, W., Schlummer, M., Mäurer, A., Reller, A. (2013). Recycling paths for thin-film chalcogenide photovoltaic waste - Current feasible processes. *Renewable Energy*, 55, pp. 220-229. Available: <http://dx.doi.org/10.1016/j.renene.2012.12.038> (Downloaded 12.02.13)

Marwede, M., Reller, A. (2012). Future recycling flows of tellurium from cadmium telluride photovoltaic waste. *Resources, Conservation and Recycling*, 69, pp. 35-49. Available: <http://dx.doi.org/10.1016/j.resconrec.2012.09.00> (Downloaded 06.03.13)

Matin, M.A, Aliyu, M.M., Quadery, A.H., Amin, N. (2010). Prospects of novel front and back contacts for high efficiency cadmium telluride thin film solar cells from numerical analysis. *Solar Energy Materials and Solar Cells*, 94 (9), pp. 1496-1500. Available: <http://dx.doi.org/10.1016/j.solmat.2010.02.042> (Downloaded 27.07.13)

Matsunaga, K., Komaru, T., Nakayama, Y., Kume, T., Suzuki, Y. (2009). Mass-production technology for CIGS modules. *Solar Energy Materials and Solar Cells*, 93 (6–7), pp. 1134-1138. Available: <http://dx.doi.org/10.1016/j.solmat.2009.02.015> (Downloaded 13.02.13)

McEvoy, A., Tom Markvart, T., Castaner, L. (2012). *Practical Handbook of Photovoltaics: Fundamentals and Applications*. 2nd edition. Kidlington, Oxford, United Kingdom: Elsevier Ltd.

McIntyre, R. (2010). State of the art of photovoltaic technologies. *Science Progress*, 93 (4), pp. 361-392. Available: [dx.doi.org/ 10.3184/003685010X12871589883476](http://dx.doi.org/10.3184/003685010X12871589883476) (Downloaded 05.03.13)

McPeak, K.M., Opananont, B., Shibata, T., Ko, D-K., Becker, M.A., Chattopadhyay, S., Bui, H.P., Beebe, T.P, Bunker, B.A., Murray, C.B., Baxter, J.B. (2013). Microreactor chemical bath deposition of laterally graded Cd<sub>1-x</sub>Zn<sub>x</sub>S thin films: A route to high-throughput optimization for photovoltaic buffer layers. *Chemistry of Material*, 25 (3), pp. 297-306. Available: [dx.doi.org/10.1021/cm3023506](http://dx.doi.org/10.1021/cm3023506) (Downloaded 05.03.13)

MiaSolé. (2011). *Thin film*. Available: <http://miasole.com/thin-film> (Downloaded 29.07.13)

Miles, R.W., Hynes, K.M., Forbes, I. (2005). Photovoltaic solar cells: An overview of state-of-the-art cell development and environmental issues. *Progress in Crystal Growth and Characterization of Materials*, 51 (1–3), pp. 1-42. Available: <http://dx.doi.org/10.1016/j.pcrysgrow.2005.10.002>. (Downloaded 22.04.13)

Minemoto, T., Julayhi, J. (2013). Buffer-less Cu(In,Ga)Se<sub>2</sub> solar cells by band offset control using novel transparent electrode. *Current Applied Physics*, 13 (1), pp. 103-106. Available: <http://dx.doi.org/10.1016/j.cap.2012.06.019> (Downloaded 26.02.13)

Morales-Acevedo, A. (2006). Thin film CdS/CdTe solar cells: Research perspectives. *Solar Energy*, 80 (6), pp. 675-681. Available: <http://dx.doi.org/10.1016/j.solener.2005.10.008> (Downloaded 18.03.13)

Muñoz-García, M.A., Marin, O., Alonso-García, M.C., Chenlo, F. (2012). Characterization of thin film PV modules under standard test conditions: Results of indoor and outdoor measurements and the effects of sunlight exposure. *Solar Energy*, 86 (10), pp. 3049-3056. Available: <http://dx.doi.org/10.1016/j.solener.2012.07.015> (Downloaded 13.02.13)

Müller, A., Wamback, K., Alsema, E. (2005). Life cycle analysis of solar module recycling process. *Material Research Society (MRS) Proceedings*, 895. Available: <http://dx.doi.org/10.1557/PROC-0895-G03-07> (Downloaded 24.06.13).

Nagamani, K., Prathap, P., Lingappa, Y., Miles, R.W., Reddy, K.T.R. (2012). Properties of Al-doped ZnS films grown by chemical bath deposition. *Physics Procedia*, 25, pp. 137-142. Available: <http://dx.doi.org/10.1016/j.phpro.2012.03.062> (Downloaded 05.03.13)

Naghavi, N., Renou, G., Bockelee, V., Donsanti, F., Genevee, P., Jubault, M., Guillemoles, J.F., Lincot, D. (2011). Chemical deposition methods for Cd-free buffer layers in Cl(G)S solar cells: Role of window layers. *Thin Solid Films*, 519 (21), pp. 7600-7605. Available: <http://dx.doi.org/10.1016/j.tsf.2011.01.091> (Downloaded 13.02.13)

Nair, P.K., Nair, M.T.S., García, V.M., Arenas, O.L., Peña, Y., Castillo, A., Ayala, I.T., Gomezdaza, O., Sánchez, A., Campos, J., Hu, H., Suárez, R., Rincón, M.E. (1998). Semiconductor thin films by chemical bath deposition for solar energy related applications. *Solar Energy Materials and Solar Cells*, 52 (3–4), pp. 313-344. Available: [http://dx.doi.org/10.1016/S0927-0248\(97\)00237-7](http://dx.doi.org/10.1016/S0927-0248(97)00237-7) (Downloaded 09.05.13)

National Renewable Energy Laboratory (NREL) (2007a). *National solar technology roadmap: CdTe PV. Management report*. NREL Report No. MP-520-41736.

National Renewable Energy Laboratory (NREL) (2007b). *National solar technology roadmap: CIGS PV. Management report*. NREL Report No. MP-520-41737.

Naujoks, I. (2000). *Ökologischer und ökonomischer Vergleich von CuInS<sub>2</sub>- und CuInSe<sub>2</sub>-Dünnschichtsolarmodulen Über den Lebenszyklus*. Diploma Thesis. Technische Universität, Berlin, Germany.

Niki, S., Matsubara, K., Sakurai, K.-I., Ishizuka, S., Tampo, H., Yamada, A., Nakanishi, H., Terada, N. (2006). Research and progress of CIGS solar cells at AIST. *The 2nd Joint International Conference on "Sustainable Energy and Environment (SEE 2006)", Bangkok, Thailand, November 21-23, 2006*.

Noufi, R. (2013). *CIGS PV technology: Challenges, opportunities, and potential*. Power point presentation. National Center for Photovoltaics, NREL, Golden, Colorado.

Noufi, R., Zweibel, K. (2006). High-efficiency CdTe and CIGS thin-film solar cells: Highlights and challenges. *2006 IEEE 4th World Conference on Photovoltaic Energy Conversion, Waikoloa, Hawaii, the USA, May 7-12, 2006*. Piscataway, New Jersey, the USA: Institute of Electrical and Electronics Engineers Inc. (IEEE), 1, pp. 317-320. NREL Report No. CP-520-41276. Available: <http://dx.doi.org/10.1109/WCPEC.2006.279455> (Downloaded 23.04.3)

Odden, J.O., Halvorsen, G., Rong, H., Gløckner, R. (2008). Comparison of the energy consumption in different production processes for solar grade silicon. *Silicon for the Chemical and Solar Industry IX, Oslo, Norway, June 23-26, 2008*. Available: <https://elkem.com/en/Solar/Innovation/Research-papers/> (Downloaded 01.02.13)

Pacca, S., Sivaraman, D., Keoleian, G.A. (2007). Parameters affecting the life cycle performance of PV technologies and systems. *Energy Policy*, 35 (6), pp. 3316-3326. Available: <http://dx.doi.org/10.1016/j.enpol.2006.10.003> (Downloaded 01.02.13)

Parida, B., Iniyar, S., Goic, R. (2011). A review of solar photovoltaic technologies. *Renewable and Sustainable Energy Reviews*, 15 (3), pp. 1625-1636. Available: <http://dx.doi.org/10.1016/j.rser.2010.11.032> (Downloaded 13.02.13)

Photovoltaic-software (2013). *How to calculate the annual solar energy output of a photovoltaic system*. Available: <http://photovoltaic-software.com/PV-solar-energy-calculation.php> (Downloaded 01.06.13)

Pisarkiewicz, T., Jankowski, H., Schabowska-Osiowska, E., Maksymowicz, L.J. (2003). Fabrication of thin film polycrystalline CIS photovoltaic heterostructure. *Opto-Electronics Review*, 11 (4), pp. 297-304.

- Platzer, M.D. (2012). *U.S Solar photovoltaic manufacturing: Industry trends, global competition, federal support*. Congressional Research Service. Available: <http://www.fas.org/sgp/crs/misc/> (Downloaded 13.09.2012)
- Powalla, M., Voorwinden, G., Hariskos, D., Jackson, P., Kniese, R. (2009). Highly efficient CIS solar cells and modules made by the co-evaporation process. *Thin Solid Films*, 517 (7), pp. 2111-2114. Available: <http://dx.doi.org/10.1016/j.tsf.2008.10.126> (Downloaded 12.02.13)
- PVACCEPT (2013). *Introduction*. Available: <http://pvaccept.de/eng/index.htm> (Downloaded 15.06.13)
- PV Cycle (2013a). *FAQs*. Available: <http://www.pvcycle.org/frequently-asked-questions-faq/> (Downloaded 11.01.2013)
- PV Cycle (2013b). *Homesite*. Available: <http://www.pvcycle.org/> (Downloaded 11.01.2013)
- PV Cycle (2013c). *Recycling*. Available: <http://www.pvcycle.org/about/recycling> (Downloaded 11.01.2013)
- PV Cycle (2013d). *Waste prognosis*. Available: <http://www.pvcycle.org/about/waste-prognosis/> (Downloaded 11.01.2013).
- Pålsson, A-C., Mattsson, J. (2011). *Performing the environmental impact assessment in the LCA*. Tosca. Available: <http://www.tosca-life.info/getting-started-guides/life-cycle-assessment/how-to-perform-an-lca/phases-in-an-lca-study/impact-assessment/> (Downloaded 01.02.12)
- Rajendra, B. V., Kekuda, D. (2012). Flexible cadmium telluride/cadmium sulphide thin film solar cells on mica substrate. *Journal of Materials Science: Materials in Electronics*, 23 (10), pp. 1805-1808. Available: <http://dx.doi.org/10.1007/s10854-012-0666-0> (Downloaded 05.03.13)
- Raugei, M. (2005). *Advances in Life cycle assessment: Method integration and geographic allocation of environmental impact*. PhD thesis. Università degli Studie di Siena, Siena, Italy.
- Raugei, M., Bargigli, S., Ulgiati, S. (2005). Energy and life cycle assessment of thin film CdTe photovoltaic modules. *20th European PVSC Conference, Barcelona, Spain, 2005*.
- Raugei, M., Bargigli, S., Ulgiati, S. (2007a). Life cycle assessment and energy pay-back time of advanced photovoltaic modules: CdTe and CIS compared to poly-Si. *Energy*, 32(8), pp. 1310-1318. Available: <http://dx.doi.org/10.1016/j.energy.2006.10.003>. (Downloaded 26.02.13)
- Raugei, M., Frankl, P., Alsema, E., de Wild-Scholten, M., Fthenakis, V., Kim H.C. (2007b). Life cycle assessment of present and future photovoltaic systems. *Renewable Energy 2007 Symposium on "Expectations and Advanced Technologies in Renewable Energy"*, Chiba,

Japan, October 11, 2007. Available: <http://clca.columbia.edu/presentations.html>  
(Downloaded 01.02.13)

Raugei, M., Fthenakis, V. (2010). Cadmium flows and emissions from CdTe PV: Future expectations. *Energy Policy*, 38 (9), pp. 5223-5228. Available: <http://dx.doi.org/10.1016/j.enpol.2010.05.007> (Downloaded 06.03.13)

Raugei, M., Isasa, M., Palmer, P.F. (2012). Potential Cd emissions from end-of-life CdTe PV. *The International Journal of Life Cycle Assessment*, 17 (2), pp. 192-198. Available: : <http://dx.doi.org/10.1007/s11367-011-0348-9> (Downloaded 23.01.13)

Razykov, T.M., Ferekides, C.S., Morel, D., Stefanakos, E., Ullal, H.S., Upadhyaya, H.M. (2011). Solar photovoltaic electricity: Current status and future prospects. *Solar Energy*, 85 (8), pp. 1580-1608. Available: <http://dx.doi.org/10.1016/j.solener.2010.12.002> (Downloaded 12.03.13)

ReCiPe (2012). *Characterisation*. Available: <http://www.lcia-recipe.net/> (Downloaded 01.13.3)

Reenaas, T.W. (2013). Associate Professor, Department of Physics, Norwegian University of Science and Technology (NTNU), Trondheim, Norway. Personal communication and e-mail correspondance.

Renewable Energy Corporation (REC) (2011a). *Annual report 2011*. Available: <http://www.recgroup.com/view?feed=R/136555/PR/201203/1598640.xml> (Downloaded 18.09.2012)

Renewable Energy Corporation (REC) (2011b). *Granual polysilicon productivity: Benefit of FBR granular polysilicon to increase efficiency of PV ingot manufacturing by increasing crucible polysilicon charge weight*. REC Silicon Inc. Available: <http://www.recgroup.com/en/Downloads/Silicon-product-downloads/?feed=Whitepapers> (Downloaded 03.01.2013)

Renewable Energy Corporation (REC) (2013a). *REC's fluidized bed reactor (FBR) process*. Available: <http://www.recgroup.com/en/tech/FBR/> (Downloaded 04.01.2013)

Renewable Energy Corporation (REC) (2013b). *REC peack energy pluss series*. Available: <http://www.recgroup.com/en/products/SolarPanels/REC-Peak-Energy-Plus/> (Downloaded 11.01.2013)

Renewable Energy Corporation (REC) (2013c). *REC peak energy series*. Available: <http://www.recgroup.com/en/products/SolarPanels/recpeakenergyseries/> (Downloaded 11.01.2013)

Renewable Energy Policy Network for the 21st century (REN21). (2013a). *Renewables 2013: Global status report*. Available:

<http://www.ren21.net/REN21Activities/GlobalStatusReport.aspx> (Downloaded 22.07.13)

Renewable Energy Policy Network for the 21st century (REN21). (2013b). *Renewables - Global futures report 2013*. Available:

<http://www.ren21.net/REN21Activities/GlobalFuturesReport.aspx> (Downloaded 08.05.13)

Repins, I., Contreras, M. A., Egaas, B., DeHart, C., Scharf, J., Perkins, C. L., To, B., Noufi, R. (2008). 19,9%-efficient ZnO/CdS/CuInGaSe<sub>2</sub> solar cell with 81,2% fill factor. *Progress in Photovoltaics: Research and Applications*, 16 (3), pp. 235–239. Available:

<http://dx.doi.org/10.1002/pip.822> (Download 07.03.13)

Romeo, A., Terheggen, M., Abou-Ras, D., Bätzner, D.L., Haug, F.-J., Kälin, M., Rudmann, D., Tiwari, A. N. (2004). Development of thin-film Cu(In,Ga)Se<sub>2</sub> and CdTe solar cells. *Progress in Photovoltaics: Research and Applications*, 12 (2-3), pp. 93-111. Available:

<http://dx.doi.org/10.1002/pip.527> (Downloaded 07.03.13)

Romeo, N., Bosio, A., Mazzamuto, S., Romeo, A., Vaillant-Roca, L. (2007). High efficiency CdTe/CdS thin film solar cells with a novel back-contact. *22nd European Photovoltaic Solar Energy Conference, Milan, Italy, September 3-7, 2007*. WIP-Renewable Energies, pp. 1919-1921. Available: <http://profs.sci.univr.it/~romeo/Publications/> (Downloaded 16.05.13)

Romeo, N., Bosio, A., Tedeschi, R., Canevari, V. (2000). Growth of polycrystalline CdS and CdTe thin layer for high efficiency thin film solar cells. *Materials Chemistry and Physics*, 66 (2–3), pp. 201-206. Available: [http://dx.doi.org/10.1016/S0254-0584\(00\)00316-3](http://dx.doi.org/10.1016/S0254-0584(00)00316-3) (Downloaded 27.07.13)

Rosenkilde, C. (2012). Employee Norsk Hydro. *Solar cell technology*. Lectures in the course: TMT4285 Hydrogen technology, fuel cells and solar cells, 16.-17.02.2012, Norwegian University of Technology and Science, Trondheim, Norway.

Rousset, J., Donsanti, F., Genevée, P., Renou, G., Lincot, D. (2011). High efficiency cadmium free Cu(In,Ga)Se<sub>2</sub> thin film solar cells terminated by an electrodeposited front contact. *Solar Energy Materials & Solar Cells*, 95 (6), pp. 1544-1549. Available:

<http://dx.doi.org/10.1016/j.solmat.2010.12.009> (Downloaded 06.03.13)

Saga, T. (2010). Advances in crystalline silicon solar cell technology for industrial mass production. *NPG Asia Materials*, 2, pp. 96-102. Available:

<http://dx.doi.org/10.1038/asiamat.2010.82> (Downloaded 10.01.2013)

Shi, C.Y., Sun, Y., He, Q., Li, F.Y., Zhao, J.C. (2009). Cu(In,Ga)Se<sub>2</sub> solar cells on stainless-steel substrates covered with ZnO diffusion barriers. *Solar Energy Materials & Solar Cells*, 93 (5), pp. 654-656. Available: <http://dx.doi.org/10.1016/j.solmat.2008.12.004> (Downloaded 06.03.13)



Shin, D.H., Larina, L., Yoon, K.H., Ahn, B.T. (2010). Fabrication of Cu(In,Ga)Se<sub>2</sub> solar cell with ZnS/CdS double layer as an alternative buffer. *Current Applied Physics*, 10 (2), pp. S142-S145. Available: <http://dx.doi.org/10.1016/j.cap.2009.11.019> (Downloaded 26.02.13)

Simon, F.-G., Holm, O., Berger, W. (2013). Resource recovery from urban stock, the example of cadmium and tellurium from thin film module recycling. *Waste Management*, 33 (4), pp. 942-947. Available: <http://dx.doi.org/10.1016/j.wasman.2012.12.025> (Downloaded 05.03.13)

Singh, U.P., Patra, P. (2010). Progress in polycrystalline thin-film Cu(In, Ga)Se<sub>2</sub> solar cells. *International Journal of Photoenergy*, vol. 2010, Article ID 468147, 19 pages. Available: <http://dx.doi.org/10.1155/2010/468147> (Downloaded 12.02.13)

Sinha, P., Kriegner, C.J., Schew, W.A., Kaczmar, S.W., Traister, M., Wilson, D.J. (2008). Regulatory policy governing cadmium-telluride photovoltaics: A case study contrasting life cycle management with the precautionary principle. *Energy Policy*, 36 (1), pp. 381-387. Available: <http://dx.doi.org/10.1016/j.enpol.2007.09.017> (Downloaded 17.06.13)

SMA Solar Technology AG (2010). *Performance ratio: Quality factor of the PV plant*. Available: <http://files.sma.de/dl/7680/Perfratio-UEN100810.pdf> (Downloaded 01.02.13)

Solar Construction Sustainability Technology (SOLTECTURE). (2013). *CIS = CIGS & CIGSe*. Available: <http://www.solteature.com/technology/cis-cigs-cigse.html> (Downloaded 01.06.03)

Solar Thin Film Inc. (2007a). *CIGS technology*. Available: [http://www.solarthinfilms.com/active/en/home/photovoltaics/cigs\\_technology.html](http://www.solarthinfilms.com/active/en/home/photovoltaics/cigs_technology.html) (Downloaded 01.06.13)

Solar Thin Film Inc. (2007b). *Thin-film photovoltaics*. Available: [http://www.solarthinfilms.com/active/en/home/photovoltaics/photovoltaics\\_and\\_thinfilms/thinilm\\_photovoltaics.html](http://www.solarthinfilms.com/active/en/home/photovoltaics/photovoltaics_and_thinfilms/thinilm_photovoltaics.html) (Downloaded 01.06.13)

Solar World (2012). *Solar panel assembly*. Available: <http://www.solarworld-usa.com/solar-for-home/solar-101/making-solar-panels/solar-panel-assembly.aspx> (Downloaded 05.01.2012)

Statistics Norway (SSB) (2005). *Energiinhold, tetthet og virkningsgrad*. Available: <http://www.ssb.no/magasinet/miljo/tabell.html> (Downloaded 20.11.2012)

Stoppato, A. (2008). Life cycle assessment of photovoltaic electricity generation. *Energy*, 33 (2), pp. 224-232. Available: <http://dx.doi.org/10.1016/j.energy.2007.11.012> (Downloaded: 01.02.13 )

Strømman, A.H. (2010). *Methodological Essentials of Life Cycle Assessment*. Trondheim, Norway: Norwegian University of Science and Technology.

- Sumper, A., Robledo-García, M., Villafáfila-Robles, R., Bergas-Jané, J., Andrés-Peiró, J. (2011). Life-cycle assessment of a photovoltaic system in Catalonia (Spain). *Renewable and Sustainable Energy Reviews*, 15 (8), pp. 3888-3896. Available: <http://dx.doi.org/10.1016/j.rser.2011.07.023> (Downloaded 19.06.13)
- Sustainability Evaluation of Solar Energy Systems (SENSE) (2008). *LCA analysis*. Available: <http://www.sense-eu.net/30.html> (Downloaded 23.01.13).
- Torp, M. (2012). Employee Elkem Carbon, Kristiansand, Norway. Phone call 10.12.2012.
- Ullal, H.S. (2008). Overview and challenges of thin film solar electric technologies. *World Renewable Energy Congress X and Exhibition, Glasgow, Scotland, July 19–25, 2008*, 7 pages. NREL Report No. CP-520-43355.
- Ullal, H. S., von Roedern, B. (2007). Thin film CIGS and CdTe photovoltaic technologies: commercialization, critical issues, and applications. Preprint. *22nd European Photovoltaic Solar Energy Conference (PVSEC) and Exhibition, Milan, Italy, September 3-7, 2007*, 7 pages. NREL Report No. CP-520-42058.
- U.S. Department of Energy. (2012a). *Cadmium Telluride*. Available: [http://www1.eere.energy.gov/solar/sunshot/pv\\_cdte.html](http://www1.eere.energy.gov/solar/sunshot/pv_cdte.html) (Downloaded 01.06.13).
- U.S. Department of Energy. (2012b). *Copper Indium Gallium Diselenide*. Available: [http://www1.eere.energy.gov/solar/sunshot/pv\\_cigs.html](http://www1.eere.energy.gov/solar/sunshot/pv_cigs.html) (Downloaded 01.06.13).
- U.S. Department of Energy. (2012c). *Photovoltaic systems*. Available: [http://www.eere.energy.gov/basics/renewable\\_energy/pv\\_systems.html](http://www.eere.energy.gov/basics/renewable_energy/pv_systems.html) (Downloaded 01.06.13).
- Wadia, C., Alivisatos, A.P, Kammen, D.M. (2009). Materials availability expands the opportunity for large-scale photovoltaics deployment. *Environmental Science & Technology*, 43 (6), pp. 2072-207. Available: <http://dx.doi.org/10.1021/es8019534> (Downloaded 17.06.13)
- Wang, L.-P., Chiang, C.-C., Wang, Y.-Y., Yeh, T.-K., Chen, W.-C., Tsai, S.-Y. (2012). Flexible Cd-free Cu(In,Ga)Se<sub>2</sub> solar cells with non-vacuum process. *Surface & Coatings Technology*. Available: <http://dx.doi.org/10.1016/j.surfcoat.2012.02.018> (Downloaded 26.02.13)
- Wang, S. (2011). Tellurium, its resourcefulness and recovery. *JOM*, 63 (8), pp. 90-93. Available: <http://dx.doi.org/10.1007/s11837-011-0146-7> (Downloaded 12.02.13)
- Werner, F., Althaus, H.-J., Künniger, T., Richter, K., Jungbluth, N. (2007). *Life cycle inventories of wood as fuel and construction material. Ecoinvent report No.9*. Dübendorf, Zürich, Switzerland: Ecoinvent centre - Swiss Centre for Life Cycle Inventories.

- Westgaard, T., Olson, C.L., Veltkamp, A.C. (2012). Life cycle analysis of photovoltaic modules: A multicrystalline silicon case study. Abstract. *Photovoltaics International*, 15, p. 122-128. ECN Report ECN-V--12-001. Available: <http://www.ecn.nl/publications/ECN-V--12-001> (Downloaded 10.01.13)
- Wolden, C.A., Kurtin, J., Baxter, J.B., Repins, I., Shaheen, S.E., Torvik, J.T., Rockett, A.A., Fthenakis, V.M., Aydil, E.S. (2011). Photovoltaic manufacturing: Present status, future prospects, and research needs. *Journal of Vacuum Science & Technology A*, 29 (3), Article ID 030801, 16 pages. Available: <http://dx.doi.org/10.1116/1.3569757> (Downloaded 15.05.13)
- Wu, X. (2004). High-efficiency polycrystalline CdTe thin-film solar cells. *Solar Energy*, 77 (6), pp. 803-814. Available: <http://dx.doi.org/10.1016/j.solener.2004.06.006> (Downloaded 13.02.13)
- Wu, X., Dhere, R.G., Albin, D.S., Gessert, T.A., DeHart, C., Keane, J.C., Duda, A., Coutts, T.J., Asher, S., Levi, D.H., Moutinho, H.R., Yan, Y., Moriarty, T., Johnston, S., Emery, K., Sheldon, P. (2001). High-efficiency CTO/ZTO/CdS/CdTe polycrystalline thin-film solar cells. Preprint. *NCPV Program Review Meeting, Lakewood, Colorado, the USA, October 14-17, 2001*, 4 pages. NREL Report No. CP-520-31025.
- Wu, X., Zhou, J., Keane, J.C., Dhere, R.G., Albin, D. S., Gessert, T.A., DeHart, C., Duda, A., Ward, J.J., Yan, Y., Teeter, G., Levi, D.H., Asher, S., Perkins, C., Moutinho, H.R., To, B. (2005). Advances in CdTe R&D at NREL. *DOE Solar Energy Technologies Program Review Meeting, Denver, Colorado, the USA, November 7-10, 2005*, 5 pages. NREL Report No. CP-520-38954.
- Wuerz, R., Eicke, A., Frankenfeld, M., Kessler, F., Powalla, M., Rogin, P., Yazadani-Assl, O. (2009). CIGS thin-film solar cells on steel substrates. *Thin Solid Films*, 517 (7), pp. 2415-2418. Available: <http://dx.doi.org/10.1016/j.tsf.2008.11.016> (Downloaded 06.03.13)
- Yagioka, T., Nakada, T. (2009). Cd-free flexible Cu(In,Ga)Se<sub>2</sub> thin film solar cells with ZnS(O,OH) buffer layers on Ti foils. *Applied Physics Express*, 2, Article ID 042201, 3 pages. Available: <http://dx.doi.org/10.1143/apex.2.072201> (Downloaded 06.03.13)
- Yun, J.H., Kim, K.H., Kim, M.S., Ahn, B.T., Ahn, S.J., Lee, J.C., Yoon, K.H. (2007). Fabrication of CIGS solar cells with a Na-doped Mo layer on a Na-free substrate. *Thin Solid Films*, 515 (15), pp. 5876-5879. <http://dx.doi.org/10.1016/j.tsf.2006.12.156> (Downloaded 06.03.13)
- Zuser, A., Rehnberger, H. (2011). Considerations of resource availability in technology development strategies: The case study of photovoltaics. *Resources, Conservation and Recycling*, 56 (1), pp. 56-65. Available: <http://dx.doi.org/10.1016/j.resconrec.2011.09.004> (Downloaded 06.03.12)



## Appendices

### A Inventory MG-Si

#### A.1 Mc-Si Sim

**Table A: Inventory for MG-Si production, mc-Si Sim-case.**

	Location	Unit	Amount	Comment
<b>PRODUCT:</b>				
MG-Si		kg	1,00	Produced in electrical furnace. Reducing agent: Charcoal free.
<b>MATERIALS:</b>				
silica sand, at plant	DE	kg	2,68	Represents the quartz input.
graphite, at plant	RER	kg	1,20E-01	Graphite electrodes.
<b>ENERGY:</b>				
electricity, medium voltage, production UCTE, at grid	UCTE	kWh	12,7	
charcoal, at plant	GLO	kg	1,90E-01	Reduction agent.
hard coal, at regional storage	WEU	kg	9,60E-01	
petroleum coke, at refinery	RER	kg	6,00E-01	Reduction agent.
<b>RESOURCES:</b>				
water, unspecified natural origin		m <sup>3</sup>	1,20E-01	
<b>EMISSIONS TO AIR:</b>				
carbon dioxide, fossil, unspecified		kg	3,58	
nitrogen oxides, unspecified		kg	1,62E-01	
sulfur dioxide, unspecified		kg	5,71E-01	
silicon, unspecified		kg	5,40E-01	Assumption for silicon dioxide.

## B Inventory SoG-Si

### B.1 Mc-Si Sim

Table B: Inventory for SoG-Si production by using the modified Siemens method, mc-Si Sim-case.

	Location	Unit	Amount	Comment
<b>PRODUCT:</b>				
SoG-Si		kg	1,00	Produced with modified Siemens technology.
<b>INPUT FROM FOREGROUND:</b>				
MG-Si		kg	1,50	
<b>MATERIALS:</b>				
chlorine, gaseous, membrane cell, at plant	RER	kg	1,00	
hydrogen, liquid, at plant	RER	kg	1,31E-01	
sodium hydroxide, 50% in H2O, production mix, at plant	RER	kg	44,0	
<b>ENERGY:</b>				
electricity, medium voltage, production UCTE, at grid	UCTE	kWh	190	
heat, at cogen 1MWe lean burn, allocation exergy	RER	MJ	414	
<b>RESOURCES:</b>				
water, unspecified natural origin		m3	1,70E-02	
water, cooling, unspecified natural origin		m3	4,54E-01	
<b>EMISSIONS TO AIR:</b>				
silicon, unspecified		kg	8,00E-01	
hydrogen chloride, unspecified		kg	9,00E-02	
fluorine, unspecified		kg	1,00E-04	
silicon tetrafluoride, low population		kg	8,00E-03	
<b>EMISSIONS TO WATER:</b>				
chlorine, river		kg	1,00	
solids, inorganic, river		kg	5,18	

## B.2 Mc-Si ESS

**Table C: Inventory for SoG-Si production by using the metallurgical production method by Elkem Solar, mc-Si ESS-case.**

	Location	Unit	Amount	Comment	Source
<b>PRODUCT:</b>					
SoG-Si		kg	1,00	Produced with Elkem Solar technology.	
<b>MATERIALS:</b>					
silica sand, at plant	DE	kg	4,05	Represents quartz input, raw material for MG-Si production	Upscaled numbers from MG-Si production, Jungbluth et al. (2012), p.24.
limestone, crushed, for mill	CH	kg	1,50E-02		Upscaled number from Mg-Si production, Andresen (2008).
anode, aluminium electrolysis	RER	kg	1,20E-01		
sodium hydroxide, 50% in H <sub>2</sub> O, production mix, at plant	RER	kg	3,48E-01		Ecoinvent; "silicon, solar grade, modified Siemens process, at plant".
N/A				Rest of inputs. Omitted because of confidentiality.	Johansen (2008).
<b>ENERGY:</b>					
electricity, medium voltage, production UCTE, at grid	UCTE	kWh	55,2		Climate and Pollution Agency of Norway (2012).
light fuel oil, burned in industrial furnace 1MW, non-modulating	RER	MJ	9,37E-01	Energy content: 43,1 MJ/kg (SSB, 2005).	
liquefied petroleum gas, at service station	CH	kg	2,78E-02		
chips, Scandinavian softwood (plant-debarked), u=70%, at plant	NORDEL	m <sup>3</sup>	1,67E-02	Reduction agent. Density: 169kg/m <sup>3</sup> (Werner et al.,	

				2007, p. 41).	
hard coal coke, at plant	RER	MJ	10,6	Reduction agent. Energy content: 28,5 MJ/kg (SSB, 2005).	
hard coal, at mine	RNA	kg	3,14	Reduction agent.	
diesel, at refinery	RER	kg	9,75E-03		Upscaled number from Mg-Si production, Andresen (2008).
<b>TRANSPORT:</b>					
transport, transoceanic tanker	OCE	tkm	35,7		Upscaled number from Mg-Si production, Andresen (2008).
transport, lorry 16-32t, EURO5	RER	tkm	3,57	Assumed 10% of transport by transoceanic tanker.	
<b>INFRASTRUCTURE:</b>					
silicone plant	RER	P	1,00E-11		Ecoinvent; "silicon, solar grade, modified Siemens process, at plant".
<b>WASTE:</b>					
disposal, slag from MG silicon production, 0% water, to inert material landfill	RER	kg	1,98		
iron scrap, at plant	RER	kg	5,33E-02	Assumed that "mixed metall scrap" equals iron scrap. Iron scrap is generated in MG-Si production (Andersen, 2008).	Climate and Pollution Agency of Norway (2012).



disposal, hazardous waste, 25% water, to hazardous waste incineration	CH	kg	2,84E-01	Assumption for hazardous waste.	
disposal, refinery sludge, 89.5% water, to sanitary landfill	CH	kg	1,41E-01		
<b>RESOURCES:</b>					
water, unspecified natural origin		m3	1,83E-01		Climate and Pollution Agency of Norway (2012).
<b>EMISSIONS TO AIR:</b>					
carbon dioxide, fossil, unspecified		kg	3,25		Climate and Pollution Agency of Norway (2012).
sulfur dioxide, unspecified		kg	3,18E-02		
nitrogen oxides, unspecified		kg	5,85E-02		
carbon dioxide, biogenic, unspecified		kg	10,3		
carbon monoxide, fossil, unspecified		kg	9,50E-03		
particulates, > 2.5 um, and < 10um, unspecified		kg	1,65E-03		
dinitrogen monoxide, unspecified		kg	1,00E-04		
methane, fossil, unspecified		kg	3,75E-04		
NM VOC, non-methane volatile organic compounds, unspecified origin		kg	2,75E-04		
PAH, polycyclic aromatic hydrocarbons, unspecified		kg	4,00E-06		
dioxins, measured as 2,3,7,8-tetrachlorodibenzo-p-dioxin, unspecified		kg	5,00E-12		
mercury, unspecified		kg	1,23E-07		
arsenic, unspecified		kg	9,00E-07		
cadmium, unspecified		kg	7,50E-09		
zinc, unspecified		kg	1,07E-06		
lead, unspecified		kg	4,13E-07		

copper, unspecified		kg	5,95E-07			
chromium, unspecified		kg	1,25E-08			
molybdenum, unspecified		kg	1,88E-07			
nickel, unspecified		kg	3,25E-07			
aluminium, unspecified		kg	2,33E-06		Upscaled numbers from Mg-Si production, Jungbluth et al. (2012), p.24.	
antimony, unspecified		kg	1,18E-08			
boron, unspecified		kg	4,19E-07			
tin, unspecified		kg	1,18E-08			
calcium, low population density		kg	1,16E-06			
cyanide, unspecified		kg	1,03E-05			
fluorine, unspecified		kg	5,82E-08			
hydrogen fluoride, unspecified		kg	7,50E-04			
hydrogen sulfide, unspecified		kg	7,50E-04			
iron, unspecified		kg	5,82E-06			
potassium, low population density		kg	9,30E-05			
silicon, unspecified		kg	1,13E-02			
sodium, unspecified		kg	1,16E-06			
<b>EMISSIONS TO WATER:</b>						
aluminium, unspecified		kg	6,03E-06			Climate and Pollution Agency of Norway (2012).
arsenic, ion, unspecified		kg	1,38E-06			
iron, ion, unspecified		kg	1,52E-05			
copper, ion, unspecified		kg	2,03E-06			
chromium, ion, unspecified		kg	1,90E-06			
nickel, ion, unspecified		kg	4,40E-06			
zinc, ion, unspecified		kg	6,75E-07			
sulfur, unspecified		kg	2,10E-05		Upscaled number from Mg-Si production, Andresen (2008).	

## C Inventory ingot

### C.1 Mc-Si Sim

Table D: Inventory for mc-Si ingot growing, mc-Si Sim-case.

	Location	Unit	Amount	Comment
<b>PRODUCT:</b>				
Ingot		kg	1,00	Traditional method.
<b>INPUT FROM FOREGROUND:</b>				
SoG-Si		kg	1,33	
<b>MATERIALS:</b>				
argon, liquid, at plant	RER	kg	3,02E-05	For crystal growing.
hydrogen, liquid, at plant	RER	kg	4,89E-08	
<b>ENERGY:</b>				
electricity, medium voltage, production UCTE, at grid	UCTE	kWh	8,89	
<b>RESOURCES:</b>				
water, unspecified natural origin		m3	8,89E-03	

## D Inventory mc-Si wafer

### D.1 Mc-Si Sim

Table E: Inventory for mc-Si wafer production, mc-Si Sim-case.

	Location	Unit	Amount	Comment
<b>PRODUCT:</b>				
Mc-Si Wafer		m <sup>2</sup>	1,00	Area: 243 cm <sup>2</sup> (156x156 mm <sup>2</sup> ). Thickness: 180 μm. Average weight per area: 0,431 kg/m <sup>2</sup> .
<b>INPUT FROM FOREGROUND:</b>				
Ingot		kg	4,85E-01	
<b>MATERIALS:</b>				
polyethylene, HDPE, granulate, at plant	RER	kg	1,31	For sawing slurry.
sodium hydroxide, 50% in H <sub>2</sub> O, production mix, at plant	RER	kg	5,75E-02	For wafer cleaning.
silicon carbide, at plant	RER	kg	1,18	For sawing slurry.
water, deionised, at plant	CH	kg	45,5	For wafer cleaning.
corrugated board base paper, testliner, at plant	RER	kg	1,60	
<b>ENERGY:</b>				
electricity, medium voltage, production UCTE, at grid	UCTE	kWh	3,15	
<b>INFRASTRUCTURE:</b>				
wafer factory	DE	P	3,04E-06	

### D.2 Mc-Si ESS

Table F: Inventory for mc-Si wafer production (including wafer growing), mc-Si ESS-case.

	Location	Unit	Amount	Comment	Source
<b>PRODUCT:</b>					
Mc-Si wafer (incl. ingot growing)		m <sup>2</sup>	1,00	Area: 243 cm <sup>2</sup> (156x156 mm <sup>2</sup> ). Average thickness: 240μm.	Alsema et al. (2006); de Wild-Scholten et al. (2006).
<b>INPUT FROM FOREGROUND:</b>					

SoG-Si		kg	1,30	Assumed produced with Elkem Solar technology. Value equals the total silicon needed minus internally recycled silicon from ingot cut-offs and broken wafers.	Alsema et al. (2006); de Wild-Scholten et al. (2006).
<b>MATERIALS:</b>					
glass wool mat, at plant	CH	kg	1,00E-02	Glass for temporarily attachment of bricks to wire sawing equipment.	Alsema et al. (2006); de Wild-Scholten et al. (2006).
wire drawing, steel	RER	kg	1,49	Steel wire for wafer cutting.	
silicon carbide, at plant	RER	kg	4,90E-01	For sawing slurry.	
silicon carbide, recycling, at plant	RER	kg	2,14	For sawing slurry.	
nitrogen, liquid, at plant	RER	kg	5,33E-02	For ingot growing.	
argon, liquid, at plant	RER	kg	3,04E-01	For ingot growing.	
helium, at plant	GLO	kg	1,36E-04	For ingot growing.	
triethylene glycol, at plant	RER	kg	1,10E-01	Assumption for polyethylene glycol for sawing slurry.	
triethylene glycol, recycling, at plant	RER	kg	2,60	Assumption for polyethylene glycol for sawing slurry.	
dipropylene glycol monomethyl ether, at plant	RER	kg	3,03E-01	For wafer cleaning.	
acrylic binder, 34% in H <sub>2</sub> O, at plant	DE	kg	2,00E-03	Assumption for adhesive for temporarily attachment of bricks to wire sawing-equipment.	
alkylbenzene sulfonate, linear, petrochemical, at plant	RER	kg	2,37E-01	Assumption for tenside for wafer cleaning.	
sodium hydroxide, 50% in H <sub>2</sub> O, production mix, at plant	RER	kg	1,49E-02	For wafer cleaning.	
hydrochloric acid, 30% in H <sub>2</sub> O, at plant	RER	kg	2,72E-03	For wafer cleaning.	
acetic acid, 98% in H <sub>2</sub> O, at	RER	kg	3,90E-02	For wafer cleaning.	

plant					
tap water, at user	RER	kg	6,41E-03	For ingot sawing.	
water, deionised, at plant	CH	kg	64,9	For wafer cleaning.	
paper, woodfree, coated, at integrated mill	RER	kg	1,90E-01		Jungbluth et al. (2012), p.54.
polystyrene, high impact, HIPS, at plant	RER	kg	2,00E-01	For packaging.	
packaging film, LDPE, at plant	RER	kg	1,00E-01	For packaging.	
brass, at plant	CH	kg	7,45E-03	Wire saws, high resistance brass-coated steel with carbon content in the range 0,7-0,9%, 5 g/kg brass.	
steel, low-alloyed, at plant	RER	kg	1,48	Wire saws, high resistance brass-coated steel with carbon content in the range 0,7-0,9%, 5 g/kg brass.	
<b>ENERGY:</b>					
electricity, medium voltage, production UCTE, at grid	UCTE	kWh	30,0	Total energy consumption incl. direct and indirect process energy and overhead energy.	Alsema et al. (2006); de Wild-Scholten et al. (2006).
natural gas, burned in industrial furnace low-NO <sub>x</sub> >100kW	RER	MJ	3,96	For removing adhesive after sawing.	
<b>INFRASTRUCTURE:</b>					
wafer factory	DE	p	1,79E-07	Area: 2 400 m <sup>2</sup> . Lifetime: 25 years. Production: 30 MWp/yr (9 millions wafers).	Alsema et al. (2006); de Wild-Scholten et al. (2006).
<b>WASTE:</b>					
disposal, waste, silicon wafer production, 0% water, to underground deposit	DE	kg	1,70E-01	Silicon waste, not recycled part of ingot (top).	Alsema et al. (2006); de Wild-Scholten et al. (2006).
<b>EMISSIONS TO AIR:</b>					
heat, waste, unspecified		MJ	28,8		Jungbluth et al. (2012), p.54.

<b>EMISSIONS TO WATER:</b>				
AOX, Adsorbable Organic Halogen as Cl, river		kg	5,01E-04	
cadmium, ion, river		kg	6,05E-06	
chromium, ion, river		kg	3,03E-05	
COD, Chemical Oxygen Demand, river		kg	2,96E-02	
copper, ion, river		kg	6,05E-05	
lead, river		kg	3,03E-05	
mercury, river		kg	6,05E-06	
nickel, ion, river		kg	6,05E-05	
nitrogen, river		kg	9,94E-03	
phosphate, river		kg	5,01E-04	
BOD5, Biological Oxygen Demand, river		kg	2,96E-02	
DOC, Dissolved Organic Carbon, river		kg	1,11E-02	
TOC, Total Organic Carbon, river		kg	1,11E-02	

Jungbluth et al. (2012), p.54.

## E Inventory solar cell

### E.1 Mc-Si Sim

Table G: Inventory for mc-Si solar cell production, mc-Si Sim-case.

	Location	Unit	Amount	Comment
<b>PRODUCT:</b>				
Mc-Si solar cell		m2	1,00	Area: 243 cm <sup>2</sup> (156x156 mm <sup>2</sup> ).
<b>INPUT FROM FOREGROUND:</b>				
Wafer		m2	1,47	
<b>MATERIALS:</b>				
silver, at regional storage	RER	kg	2,88E-02	For metallization paste front side and back side.
aluminium, production mix, wrought alloy, at plant	RER	kg	8,83E-01	For metallization paste back side.
ammonia, liquid, at regional storehouse	RER	kg	4,11E-03	For silicon nitride deposition.
hydrochloric acid, from the reaction of hydrogen with chlorine, at plant	RER	kg	7,81E-02	For surface etching.
hydrogen fluoride, at plant	GLO	kg	1,20	For etching phosphor glass.
nitric acid, 50% in H2O, at plant	RER	kg	5,05E-01	For etching phosphor glass.
sodium hydroxide, 50% in H2O, membrane cell, at plant	RER	kg	9,86E-02	For etching and cleaning.
polylactide, granulate, at plant	GLO	kg	8,22E-03	
water, deionised, at plant	CH	kg	120	
<b>ENERGY:</b>				
electricity, medium voltage, production UCTE, at grid	UCTE	kWh	27,1	
<b>INFRASTRUCTURE:</b>				
photovoltaic cell factory	DE	P	4,47E-07	
<b>RESOURCES:</b>				
water, unspecified natural origin		m3	3,61E-01	



## E.2 Mc-Si ESS

Table H: Inventory for mc-Si solar cell production, mc-Si ESS-case.

	Location	Unit	Amount	Comment	Source
<b>PRODUCT:</b>					
Mc-Si solar cell		m <sup>2</sup>	1,00	Area: 243 cm <sup>2</sup> (156x156 mm <sup>2</sup> ). Thickness may vary.	Alsema et al. (2006); de Wild-Scholten et al. (2006).
<b>INPUT FROM FOREGROUND:</b>					
Multi-Si wafer		m <sup>2</sup>	1,06	+6% cell loss.	Alsema et al. (2006); de Wild-Scholten et al. (2006).
<b>MATERIALS:</b>					
phosphoric acid, fertiliser grade, 70% in H <sub>2</sub> O, at plant	GLO	kg	1,45E-03	Phosphorus paste for emitter formation.	Alsema et al. (2006); de Wild-Scholten et al. (2006).
metallization paste, front side, at plant	RER	kg	7,40E-03	For electric contact.	
metallization paste, back side, at plant	RER	kg	4,93E-03	For electric contact.	
metallization paste, back side, aluminium, at plant	RER	kg	7,19E-02	For electric contact.	
polystyrene, expandable, at plant	RER	kg	4,07E-04	For packaging.	
nitrogen, liquid, at plant	RER	kg	1,85		
oxygen, liquid, at plant	RER	kg	1,02E-01	Diffusion.	
argon, liquid, at plant	RER	kg	2,57E-02	Diffusion and damage etching.	
tetrafluoroethylene, at plant	RER	kg	3,16E-03	Assumption for fluorinated compound mix (CF <sub>4</sub> , C <sub>2</sub> F <sub>6</sub> ), aggregated value for different fluorinated source gases.	
ammonia, liquid, at regional storehouse	RER	kg	6,73E-03	For silicon nitride deposition.	

silicon tetrahydride, at plant	RER	kg	1,21E-03	Assumption for silane (SiH <sub>4</sub> ) for silicon nitride deposition.	
sodium hydroxide, 50% in H <sub>2</sub> O, production mix, at plant	RER	kg	1,57E-01	For etching and cleaning.	
acetic acid, 98% in H <sub>2</sub> O, at plant	RER	kg	2,83E-03	For cleaning.	
hydrochloric acid, 30% in H <sub>2</sub> O, at plant	RER	kg	4,55E-02	For surface etching.	
hydrogen fluoride, at plant	GLO	kg	3,77E-02	For etching phosphor glass.	
nitric acid, 50% in H <sub>2</sub> O, at plant	RER	kg	2,67E-02	For etching phosphor glass.	
phosphoryl chloride, at plant	RER	kg	2,17E-04	For emitter formation.	
phosphoric acid, industrial grade, 85% in H <sub>2</sub> O, at plant	RER	kg	7,61E-03	For emitter formation.	
sodium silicate, spray powder 80%, at plant	RER	kg	7,47E-02		
calcium chloride, CaCl <sub>2</sub> , at plant	RER	kg	2,16E-02		
titanium dioxide, production mix, at plant	RER	kg	1,42E-06	Assumption for tetraisopropyltitanate (TPT, a titanium precursor) for titanium dioxide antireflection coating deposition.	
isopropanol, at plant	RER	kg	7,87E-02	For cleaning.	
ethanol from ethylene, at plant	RER	kg	6,39E-04	Assumption for ethanol to cleaning.	
solvents, organic, unspecified, at plant	GLO	kg	1,43E-03	For cleaning.	
water, deionised, at plant	CH	kg	137		
<b>ENERGY:</b>					
electricity, medium voltage, production UCTE, at grid	UCTE	kWh	30,2		Alsema et al. (2006); de Wild-Scholten et al. (2006).
natural gas, burned in industrial furnace low-NO <sub>x</sub> >100kW	RER	MJ	4,75		

light fuel oil, burned in industrial furnace 1MW, non-modulating	RER	MJ	1,17	Density: 36,2 MJ/L (SSB, 2005).	
<b>INFRASTRUCTURE:</b>					
photovoltaic cell factory	DE	P	1,90E-07	Area: 1 600 m <sup>2</sup> . Lifetime: 25 years. Production: 30 MWp/yr (9 millions cells).	Alsema et al. (2006); de Wild-Scholten et al. (2006).
<b>WASTE:</b>					
disposal, waste, Si waferprod., inorg, 9.4% water, to residual material landfill	CH	kg	2,76E-01	Photovoltaic cell waste.	Alsema et al. (2006); de Wild-Scholten et al. (2006).
treatment, PV cell production effluent, to wastewater treatment, class 3	CH	m3	2,17E-01	Waste to treatment, mix of: Neutral solution, alkaline solution, acid solution, organic waste.	
<b>RESOURCES:</b>					
water, unspecified natural origin, cooling		m3	1,00	Cooling water.	Alsema et al. (2006); de Wild-Scholten et al. (2006).
<b>EMISSIONS TO AIR:</b>					
aluminium, unspecified		kg	7,74E-04		Alsema et al. (2006); de Wild-Scholten et al. (2006).
hydrogen chloride, unspecified		kg	2,66E-04		
hydrogen fluoride, unspecified		kg	4,84E-06		
lead, unspecified		kg	7,74E-04		
particulates, < 2.5 um, unspecified		kg	2,66E-03		
silicon, unspecified		kg	7,26E-05	Assumption for silicon dioxide.	
silver, high population		kg	7,74E-04		
sodium hydroxide, high population		kg	4,84E-05		
tin, unspecified		kg	7,74E-04		
NMVOC, non-methane volatile organic compounds, unspecified		kg	1,94E-01		

carbon dioxide, fossil, unspecified		kg	2,82	Emission from FC-gases (CF <sub>4</sub> , C <sub>2</sub> F <sub>6</sub> ) in CO <sub>2</sub> -eq.	
nitrogen oxides, unspecified		kg	5,00E-05	Due to nitric acid use.	Jungbluth et al. (2012), p.64.
heat, waste, unspecified		MJ	109		

### E.3 CIGS

Table I: Inventory for deposition of back contact in solar cell, CIGS-case. "UNEP" refers to number from Gibon et al. (forthcoming), while "ESU" refers to numbers from Jungbluth et al. (2012), p. 86.

	Location	Unit	Amount (average value)	UNEP	ESU	Comment
<b>PRODUCT:</b>						
Back contact		m <sup>2</sup>	1,00			Deposited by sputtering.  <i>UNEP:</i> Thickness: 0,5-1,0 µm. <i>ESU:</i> Thickness: 0,5 µm.
<b>MATERIALS:</b>						
molybdenum, at regional storage	RER	kg	1,22E-02	1,34E-02	1,10E-02	<i>UNEP:</i> Including credits for recycling, economic allocation, materials sold back at 30% of price.
silicon, electronic grade, at plant/DE/kg	DE	kg	9,26E-04	9,26E-04		
<b>ENERGY:</b>						
electricity, medium voltage, production UCTE, at grid	UCTE	kWh	1,30	1,30		
<b>TRANSPORT:</b>						
transport, lorry >16t, fleet average	RER	tkm	1,51E-01	5,28E-03	2,96E-01	<i>UNEP:</i> Including transport to

						recycling facility.
--	--	--	--	--	--	---------------------

**Table J: Inventory for deposition of absorber layer in solar cell, CIGS-case. "UNEP" refers to number from Gibon et al. (forthcoming), while "ESU" refers to numbers from Jungbluth et al. (2012), p.86.**

	Location	Unit	Amount (average value)	UNEP	ESU	Comment
<b>PRODUCT:</b>						
Absorber		m <sup>2</sup>	1,00			Deposited by co-evaporation.  <i>UNEP:</i> Thickness: 1,5 µm. <i>ESU:</i> Thickness: 2,0 µm.
<b>MATERIALS:</b>						
copper, at regional storage	RER	kg	2,57E-02	6,41E-03	4,50E-02	<i>UNEP:</i> Including credits for recycling, economic allocation, materials sold back at 30% of price.
indium, at regional storage	RER	kg	1,64E-02	2,72E-02	5,49E-03	
gallium, semiconductor-grade, at regional storage	RER	kg	1,19E-02	1,28E-02	1,10E-02	
selenium, at plant	RER	kg	1,87E-02	2,64E-02	1,10E-02	
<b>ENERGY:</b>						
electricity, medium voltage, production UCTE, at grid	UCTE	kWh	13,0	13,0		
<b>TRANSPORT:</b>						
transport, lorry >16t, fleet average	RER	tkm	6,98E-01	2,44E-02	1,37	<i>UNEP:</i> Transport of CIGS to PV module factory (200 km) and transport to recycling facility.

Table K: Inventory for deposition of buffer layer in solar cell, CIGS-case. "UNEP" refers to number from Gibon et al. (forthcoming), while "ESU" refers to numbers from Jungbluth et al. (2012), p.86.

	Location	Unit	Amount (average value)	UNEP	ESU	Comment
<b>PRODUCT:</b>						
Buffer		m <sup>2</sup>	1,00			Deposited by chemical bath deposition.  <i>UNEP:</i> Thickness: 70 nm. <i>ESU:</i> Thickness: 50 nm.
<b>MATERIALS:</b>						
cadmium sulphide, semiconductor- grade, at plant	US	kg	3,40E-02		3,40E-02	
ammonia, liquid, at regional storehouse	RER	kg	2,93E-01		2,93E-01	Dip coating for CdS.
urea, as N, at regional storehouse	RER	kg	1,25E-01		1,25E-01	Dip coating for CdS.
<b>ENERGY:</b>						
electricity, medium voltage, production UCTE, at grid	UCTE	kWh	1,67	1,67		
<b>TRANSPORT:</b>						
transport, lorry >16t, fleet average	RER	tkm	1,22E-01	4,28E-03	2,40E-01	

**Table L: Inventory for deposition of front contact in solar cell, CIGS-case. "UNEP" refers to number from Gibon et al. (forthcoming), while "ESU" refers to numbers from Jungbluth et al. (2012), p.86.**

	Location	Unit	Amount (average value)	UNEP	ESU	Comment
<b>PRODUCT:</b>						
Front contact		m2	1,00			<b>ESU:</b> Deposited by sputtering. Thickness: 0,05 µm i-ZnO + 1,0 µm ZnO:Al.
<b>MATERIALS:</b>						
zinc oxide, at plant	RER	kg	5,56E-04	5,56E-04		Transparent conductive oxide.
<b>ENERGY:</b>						
electricity, medium voltage, production UCTE, at grid	UCTE	kWh	6,48	6,48		
<b>TRANSPORT:</b>						
transport, lorry >16t, fleet average	RER	tkm	3,17E-03	1,11E-04	6,23E-03	

**Table M: Inventory for bus bar attach to solar cell, CIGS-case. "UNEP" refers to number from Gibon et al. (forthcoming), while "ESU" refers to numbers from Jungbluth et al. (2012), p.86.**

	Location	Unit	Amount (average value)	UNEP	ESU	Comment
<b>PRODUCT:</b>						
Bus bar attach		m2	1,00			
<b>MATERIALS:</b>						
solder, paste, Sn95.5Ag3.9Cu0.6, for electronics industry, at plant	GLO	kg	1,69E-03	1,69E-03		Tin solder.
indium, at regional storage	RER	kg	7,05E-04	7,05E-04		Indium solder.
<b>ENERGY:</b>						
electricity, medium voltage, production UCTE,	UCTE	kWh	7,87E-01	7,87E-01		

at grid						
<b>TRANSPORT:</b>						
transport, lorry >16t, fleet average	RER	tkm	1,37E-02	4,79E-04	2,69E-02	Transport of solder and electronics.

**Table N: Inventory for scribing of solar cells for cell interconnection, CIGS-case. "UNEP" refers to number from Gibon et al. (forthcoming), while "ESU" refers to numbers from Jungbluth et al. (2012), p.86.**

	Location	Unit	Amount (average value)	UNEP	ESU	Comment
<b>PRODUCT:</b>						
Scribing		m2	1,00			Laser scribe P1, mechanical scribe P2 and laser scribe P3 for cell interconnections, laser edge isolation.
<b>ENERGY:</b>						
electricity, medium voltage, production UCTE, at grid	UCTE		2,08	2,08		



**Table O: Inventory for test of solar cell performance, CIGS-case. "UNEP" refers to number from Gibon et al. (forthcoming), while "ESU" refers to numbers from Jungbluth et al. (2012), p.86.**

	Location	Unit	Amount (average value)	UNEP	ESU	Comment
<b>PRODUCT:</b>						
Tests		m2	1,00			Intermediate IV test, high potential test and final IV test.
<b>ENERGY:</b>						
electricity, medium voltage, production UCTE, at grid	UCTE	kWh	8,61E-01	8,61E-01		

## F Inventory PV module

### F.1 Mc-Si Sim

Table P: Inventory for mc-Si PV module manufacturing, mc-Si Sim-case.

	Location	Unit	Amount	Comment
<b>PRODUCT:</b>				
Mc-Si module		m2	1,00	This inventory is based on total module area with frame: 1,94 m <sup>2</sup> (1,956x0,992 m <sup>2</sup> ). Without frame, only considering glass area of the module, the area is 1,61 m <sup>2</sup> (1,634x0,986 m <sup>2</sup> ). TPT thickness: 125µm. PET thickness: 0,2mm. Nominal output: 230 W. Conversion efficiency: 16% (glass area, excluding frame). Lifetime: 30 yr.
<b>INPUT FROM FOREGROUND:</b>				
Multi-Si cell		m2	7,53E-01	
<b>MATERIALS:</b>				
aluminium, production mix, wrought alloy, at plant	RER	kg	1,09	Aluminium profile for frame.
flat glass, uncoated, at plant	RER	kg	6,75	Area: 1,61 m <sup>2</sup> (1,634x0,986 m <sup>2</sup> ). Thickness: 3,2 mm
triple superphosphate, as P2O5, at regional storehouse	RER	kg	4,95E-01	
corrugated board base paper, testliner, at plant	RER	kg	20,6	Packaging.
ethylene vinyl acetate copolymer, at plant	RER	kg	7,99E-01	EVA thickness: 2x0,5mm.
plaster mixing	CH	kg	1,03E-01	Assumption for silicon-resin plaster.
welding, arc, steel	RER	m	8,47E-02	
<b>ENERGY:</b>				
electricity, medium voltage, production UCTE, at grid	UCTE	kWh	2,32	
<b>RESOURCES:</b>				
water, unspecified natural origin		m3	7,73E-04	

## F.2 Mc-Si ESS

Table Q: Inventory for mc-Si PV module manufacturing, mc-Si ESS-case.

	Location	Unit	Amount	Comment	Source
<b>PRODUCT:</b>					
Mc-Si PV module		m <sup>2</sup>	1,00	Type: Solar World SW 220 sun module. This inventory is based on total module area with frame: 1,68 m <sup>2</sup> (1,675x1,001 m <sup>2</sup> ). Without frame, only considering glass area of the module, the area is 1,60 m <sup>2</sup> (1,618x0,986 m <sup>2</sup> ). Weight: 21,2 kg. Nominal output: 220 W. Conversion efficiency: 13,2% (glass area, excluding frame). Lifetime: 30 yr.	Alsema et al. (2006); de Wild-Scholten et al. (2006).
<b>INPUT FROM FOREGROUND:</b>					
Multi-Si cell		m <sup>2</sup>	8,88E-01	+2% cell loss	Alsema et al. (2006); de Wild-Scholten et al. (2006).
<b>MATERIALS:</b>					
aluminium, production mix, at plant	RER	kg	2,48	Aluminium profile for frame.	Alsema et al. (2006); de Wild-Scholten et al. (2006).
polyphenylene sulfide, at plant	GLO	kg	1,52E-01	Assumption for polyphenylenoxid to junction box.	
solar glass, low-iron, at regional storage	RER	kg	9,61	+1% loss. Thickness: 4 mm. Density: 2,5 g/cm <sup>3</sup> .	
ethylvinylacetate, foil, at plant	RER	kg	9,68E-01	EVA consumption: 0,96 kg/m <sup>2</sup> , +6% more than glass area.	

polyvinylfluoride film, at plant	US	kg	1,05E-01	Assumption for back foil; 2x37 µm polyvinylfluoride in 350 µm thick back foil (with area density equal to 0,488g/m <sup>2</sup> ). +7% cutting loss.
polyethylene terephthalate, granulate, amorphous, at plant	RER	kg	3,55E-01	Assumption for back foil; 250 µm polyethylene terephthalate in 350 µm thick back foil (with area density equal to 0,488g/m <sup>2</sup> ). +7% cutting loss.
copper, at regional storage	RER	kg	1,05E-01	Copper ribbons for cell interconnection.
tin, at regional storage	RER	kg	5,30E-03	Sn60Pb40 plating on tabbing material. Sn interconnect/terminal ribbons.
lead, at regional storage	RER	kg	2,93E-03	Sn60Pb40 plating on tabbing material. Some manufacturers use lead free.
nickel, 99.5%, at plant	GLO	kg	1,56E-04	Ni plating on interconnect/terminal ribbons.
1-propanol, at plant	RER	kg	7,74E-03	Soldering flux.
acetone, liquid, at plant	RER	kg	1,24E-02	Cleaning fluid.
silicone product, at plant	RER	kg	1,16E-01	2,2 g for diaphragm of laminator, 114 g for silicon kit to attach frame and junction box.
packaging, corrugated board, mixed fibre, single wall, at plant	RER	kg	1,05	For packaging.
tap water, at user	RER	kg	20,6	For glass rinsing and general use.

<b>ENERGY:</b>					
electricity, medium voltage, production UCTE, at grid	UCTE	kWh	6,36	Total process energy.	Alsema et al. (2006); de Wild-Scholten et al. (2006).
<b>INFRASTRUCTURE:</b>					
photovoltaic panel factory	GLO	P	1,31E-07	Area: 4 200 m <sup>2</sup> . Lifetime: 25 years. Production: 30 MWp/yr (180 000 modules).	Alsema et al. (2006); de Wild-Scholten et al. (2006).
<b>WASTE:</b>					
disposal, plastics, mixture, 15.3% water, to municipal incineration	CH	kg	3,87E-02	Assumption for ethylvinylacetate foil to waste incineration.	Alsema et al. (2006); de Wild-Scholten et al. (2006).
disposal, polyvinylfluoride, 0.2% water, to municipal incineration	CH	kg	3,48E-02	Assumption for back foil to waste incineration.	
<b>EMISSIONS TO AIR:</b>					
heat, waste, unspecified		MJ	17,0	From electricity use.	Jungbluth et al. (2012), p.72.

### F.3 CdTe

Table R: Inventory for CdTe PV module manufacturing, CdTe-case. "UNEP" refers to number from Gibon et al. (forthcoming), while "ESU" refers to numbers from Jungbluth et al. (2012), p. 79-80.

	Location	Unit	Amount (average value)	UNEP	ESU	Comment
<b>PRODUCT:</b>						
CdTe PV module		m <sup>2</sup>	1,00			<p><b>UNEP:</b> Total module area with frame: 0,72 m<sup>2</sup>. Nominal output: 84 W. Conversion efficiency: 11,6%. Lifetime: 30 yr.</p> <p><b>ESU:</b> Module from First Solar. Production mix of CdTe PV modules installed in Europe: 22,5% German production, 12,2% USA production and 65,4% Malaysian production. Total module area with frame: 0,72 m<sup>2</sup> (1,2x0,6 m<sup>2</sup>). Weight: 12,0 kg. Nominal output: 84 W. Conversion efficiency: 11,7%. Lifetime: 30 yr.</p> <p>Average conversion efficiency assumed in study: 11,7%.</p>
<b>MATERIALS:</b>						
solar glass, low-iron, at regional storage	RER	kg	7,52		8,39	<p>Back/cover glass (annealed).</p> <p><b>UNEP:</b> Thickness: 3,2 mm.</p>

						<p>Total glass <b>UNEP:</b> 13,52 kg. Total glass <b>ESU:</b> 16,55 kg.</p> <p>Assumed in study: 50% going to solar glass and 50% going to flat glass.</p>
flat glass, uncoated, at plant	RER	kg	7,52	13,52	8,16	<p>Front/substrate glass. Soda lime glass.</p> <p><b>UNEP:</b> Thickness: 3,2 mm.</p> <p>Total glass <b>UNEP:</b> 13,52 kg. Total glass <b>ESU:</b> 16,55 kg.</p> <p>Assumed in study: 50% going to solar glass and 50% going to flat glass.</p>
tempering, flat glass	RER	kg	7,52	6,76	8,39	<p>Tempering of solar glass.</p> <p>Total glass <b>UNEP:</b> 13,52 kg. Total glass <b>ESU:</b> 16,55 kg.</p> <p>Assumed in study: 50% going to solar glass and 50% going to flat glass.</p>
ethylvinylacetate, foil, at plant	RER	kg	9,72E-01	1,46	4,84E-01	<p>Encapsulant.</p> <p><b>UNEP:</b> Density: 0,96 g/cm<sup>3</sup>. Area: 2,16 m<sup>2</sup> (both sides of module). Thickness: 0,76 mm.</p>
cadmium telluride,	US	kg	2,21E-02	2,05E-02	2,37E-02	Absorber.

semiconductor-grade, at plant						<b>UNEP:</b> Thickness: 2,5 µm. <b>ESU:</b> Deposited by vapour transport deposition.
cadmium sulphide, semiconductor-grade, at plant	US	kg	2,00E-03	4,80E-04	3,52E-03	Buffer.  <b>UNEP:</b> Thickness: 100 nm. <b>ESU:</b> Deposited by vapour transport deposition.
cadmium chloride, semiconductor-grade, at plant	US	kg	1,22E-04	1,22E-04		Cadmium chloride vapour treatment/junction activation.
copper, at regional storage	RER	kg	1,13E-02		1,13E-02	Copper wire.
solder, bar, Sn95.5Ag3.9Cu0.6, for electronics industry, at plant	GLO	kg	3,75E-04	3,75E-04		Tin free solder for bus bar attach.
indium, at regional storage	RER	kg	3,91E-04	3,91E-04		Indium solder for bus bar attach.
chromium, at regional storage	RER	kg	3,60E-04	3,60E-04		Back contact. Density: 7,19 g/cm <sup>3</sup> . Thickness: 50 nm.
aluminium, production mix, at plant	RER	kg	2,70E-03	2,70E-03		Back contact. Density: 2,70 g/m <sup>3</sup> . Thickness: 1,0 µm.
silicone product, at plant	RER	kg	3,07E-03		3,07E-03	
nitric acid, 50% in H <sub>2</sub> O, at plant	RER	kg	5,73E-02		5,73E-02	Used during the manufacturing process for cleaning, etching, and waste treatment during operation and maintenance.
sulphuric acid	RER	kg	3,93E-02		3,93E-02	
sodium hydroxide, 50% in H <sub>2</sub> O, production mix, at plant	RER	kg	4,93E-02		4,93E-02	
isopropanol, at plant	RER	kg	2,08E-03		2,08E-03	
silica sand, at plant	DE	kg	4,68E-02		4,68E-02	
sodium chloride,	RER	kg	4,53E-02		4,53E-02	



powder, a plant						
hydrogen peroxide, 50% in H <sub>2</sub> O, at plant	RER	kg	1,67E-02		1,67E-02	
chemicals inorganic, at plant	GLO	kg	3,76E-02		3,76E-02	
chemicals organic, at plant	GLO	kg	9,75E-03		9,75E-03	Sum up of several chemicals.
nitrogen, liquid, at plant	RER	kg	7,33E-02		7,33E-02	
helium, at plant	GLO	kg	3,64E-02		3,64E-02	
corrugated board, mixed fibre, single wall, at plant	RER	kg	5,23E-01		5,23E-01	Packaging.
glass fibre, reinforced plastic, polyamide, injection moulding at plant	RER	kg	1,08E-01		1,08E-01	
tap water, at user	RER	kg	180		180	Associated with substrate and glass cleaning, module cleaning, chemical solutions and laboratory uses.
<b>ENERGY:</b>						
electricity, medium voltage, production UCTE, at grid	UCTE	kWh	29,1	28,5	29,6	<b>ESU:</b> Includes film deposition, etching, cleaning, module assembly, environmental control, lightening, health and safety controls.
natural gas, burned in modulating >100k W	RER	MJ	2,65		2,65	
<b>TRANSPORT:</b>						
transport, lorry >16t, fleet average	RER	tkm	3,29	3,00	3,58	<b>ESU:</b> Standard distance 50 km.
transport,	RER	tkm	7,64		7,64	Standard distance

freight, rail						200 km.
transport, transoceanic freight ship	OCE	tkm	367		367	Import of modules from the USA: 6 300 km. Import of modules from Malaysia: 15 100 km.
<b>INFRA-STRUCTURE:</b>						
photovoltaic panel factory/	GLO	p	4,00E-06		4,00E-06	Assumption for production facility.
<b>WASTE:</b>						
disposal, waste, Si waferprod., inorg, 9.4% water, to residual material landfill	CH	kg	5,01E-03	5,01E-03		
disposal, municipal solid waste, 22,9% water, to municipal incineration	CH	kg	3,00E-02		3,00E-02	Production waste.
disposal, plastics, mixture, 15,3% water, to municipal incineration	CH	kg	7,09E-01		7,09E-01	
treatment, sewage, unpolluted, to wastewater treatment, class 3	CH	m3	1,52E-02		1,52E-02	Treated in an internal wastewater plant. Effluent released to sewer grid in Germany and the USA, and to surface water in Malaysia.
<b>EMISSIONS TO AIR:</b>						
heat, waste, unspecified	MJ		209	209	209	
cadmium, unspecified	kg		1,32E-08	2,10E-08	5,35E-09	
<b>EMISSIONS TO WATER:</b>						
cadmium, ion	kg		4,43E-07		4,43E-07	Dissolved cadmium emissions from

						municipal waste water plants.
--	--	--	--	--	--	-------------------------------

#### F.4 CIGS

Table S: Inventory for CIGS PV module manufacturing, CIGS-case. "UNEP" refers to number from Gibon et al. (forthcoming), while "ESU" refers to numbers from Jungbluth et al. (2012), p.86.

	Location	Unit	Amount (average value)	UNEP	ESU	Comment
<b>PRODUCT:</b>						
CIGS PV module		m2	1,00			<p><b>UNEP:</b> Total module area with frame: 1,08 m<sup>2</sup>. Nominal output: 154 W. Conversion efficiency: 12%. Lifetime: 30 yr.</p> <p><b>ESU:</b> Module from Würth Solar. Total module area with frame: 0,72 m<sup>2</sup> (1,2x0,6 m<sup>2</sup>). Weight: 12,6 kg. Nominal output: 75-80 W. Conversion efficiency: 10%. Lifetime: 30 yr.</p> <p>Average conversion efficiency assumed in study: 11%.</p>
<b>INPUT FROM FOREGROUND:</b>						
Back contact		m2	1,00			<p>Mo-layer deposited by sputtering.</p> <p><b>UNEP:</b> 0,5-1,0 µm. <b>ESU:</b> 0,5 µm.</p>

Absorber		m2	1,00			CIGS-layer deposited by co-evaporation.  <b>UNEP:</b> 1,5 µm. <b>ESU:</b> 2,0 µm.
Buffer		m2	1,00			CdS-layer deposited by chemical bath deposition.  <b>UNEP:</b> 70 nm. <b>ESU:</b> 50 nm.
Front contact		m2	1,00			<b>ESU:</b> 0,05 µm i-ZnO + 1,0 µm ZnO:Al deposited by sputtering.
Bus bar attach		m2	1,00			
Scribing		m2	1,00			
Tests		m2	1,00			
<b>MATERIALS:</b>						
solar glass, low-iron, at regional storage	RER	kg	7,22	6,94	15,0	Front/cover glass. Tempered extra clear glass.  <b>UNEP:</b> Thickness: 3,2 mm. <b>ESU:</b> Thickness: 2-4 mm.  Total glass <b>UNEP:</b> 13,89 kg. Total glass <b>ESU:</b> 15,000 kg.  Assumed in study: 50% going to solar glass and 50% to flat glass.
flat glass, uncoated, at plant	RER	kg	7,22	6,94		Back/substrate glass. Annealed soda lime glass.  <b>UNEP:</b> Thickness: 3,2 mm. <b>ESU:</b> Thickness: 2-4 mm.

						<p>Total glass <b>UNEP:</b> 13,89 kg. Total glass <b>ESU:</b> 15,00 kg.</p> <p>Assumed in study: 50% going to solar glass and 50% to flat glass.</p>
tempering, flat glass	RER	kg	7,22		15,0	<p>Tempering of solar glass.</p> <p>Total glass <b>UNEP:</b> 13,89 kg. Total glass <b>ESU:</b> 15,00 kg.</p> <p>Assumed in study: 50% going to solar glass and 50% to flat glass.</p>
ethylvinylacetate, foil, at plant	RER	kg	1,17	1,46	8,68E-01	<p>Encapsulant.</p> <p><b>UNEP:</b> Density: 0,96 g/cm<sup>3</sup>. Area: 2,16 m<sup>2</sup> (both sides of module). Thickness: 0,76 mm.</p>
aluminium alloy, AlMg3, at plant	RER	kg	1,57		1,57	
glass fibre reinforced plastic, polyamide, injection moulding, at plant	RER	kg	4,00E-02		4,00E-02	
acetone, liquid, at plant	RER	kg	1,18E-02		1,18E-02	Cleaning agent.
argon, liquid, at plant	RER	kg	7,20E-03		7,20E-03	Protection gas.
nitrogen, liquid, at plant	RER	kg	2,78		2,78	Protection gas.
zinc, primary, at regional storage	RER	kg	1,21E-02		1,21E-02	

tin, at regional storage	RER	kg	1,10E-02		1,10E-02	
tap water, at user	RER	kg	2,67		2,67	
<b>ENERGY:</b>						
electricity, medium voltage, production UCTE, at grid	UCTE	kWh	4,63E-01	4,63E-01		
light fuel oil, burned in industrial furnace 1MW, non-modulating	RER	MJ	10,8		10,8	
<b>TRANSPORT:</b>						
transport, lorry >16t, fleet average	RER	tkm	1,62	3,07	1,62E-01	<b>UNEP:</b> Transport of substrate- and cover glass and chemicals. <b>ESU:</b> Standard distance 100 km.
transport, freight, rail	RER		12,5		12,5	Standard distance 600 km.
<b>INFRA-STRUCTURE:</b>						
photovoltaic panel factory	GLO	p	4,00E-06		4,00E-06	Assumption for production facility.
<b>WASTE:</b>						
treatment, glass production effluent, to wastewater treatment, class 2	CH	m3	2,53E-03	2,44E-03	2,63E-03	
disposal, waste, Si waferprod., inorg, 9.4% water, to residual material landfill	CH	kg	3,31E-02	3,19E-02	3,44E-02	Deposited waste.
disposal, plastics, mixture, 15,3% water, to municipal incineration	CH	kg	9,08E-01		9,08E-01	Plastic parts burned after recycling.
<b>EMISSIONS TO AIR:</b>						
heat, waste,	MJ		441	441	441	

unspecified						
cadmium, unspecified	kg		2,10E-08	2,10E-08	2,10E-08	

## G Inventory mounting structure

### G.1 Mc-Si Sim

Table T: Inventory for on-roof mounting structure, mc-Si Sim-case.

	Location	Unit	Amount	Comment
<b>PRODUCT:</b>				
Mounting structure		m2	1,00	Per m2 module basis.
<b>MATERIALS:</b>				
slanted-roof construction, mounted, on roof	RER	m2	4,00E-01	
flat roof construction, on roof	RER	m2	4,00E-01	

### G.2 Mc-Si ESS

Table U: Inventory for on-roof mounting structure, mc-Si ESS-case.

	Location	Unit	Amount	Comment	Source
<b>PRODUCT:</b>					
Mounting structure		m2	1,00	Per m <sup>2</sup> module area. Type: Schletter Eco05 with EcoG roof hooks.	Alsema et al. (2006); de Wild-Scholten et al. (2006).
<b>MATERIALS:</b>					
steel, low-alloyed, at plant	RER	kg	7,20E-01		Alsema et al. (2006); de Wild-Scholten et al. (2006).
aluminium, production mix, at plant	RER	kg	9,70E-01	Aluminium profile.	



### G.3 CdTe and CIGS

**Table V: Inventory for on-roof mounting structure, CdTe-case and CIGS-case. "UNEP" refers to number from Gibon et al. (forthcoming), while "ESU" refers to numbers from Alsema et al. (2006) and de Wild-Scholten et al. (2006).**

	Location	Unit	Amount (average value)	UNEP	ESU	Comment
<b>PRODUCT:</b>						
Mounting structure		m2	1,00			Per m2 module area.
<b>MATERIALS:</b>						
slanted-roof construction, mounted, on roof	RER	m2		5,00E-01		
flat roof construction, on roof	RER	m2		5,00E-01		
steel, low-alloyed, at plant	RER	kg	8,41E-01	9,61E-01	7,20E-01	<b>UNEP:</b> Decomposed from ecoinvent processes: "slanted-roof construction, mounted, on roof", "flat roof construction, on roof", "section bar extrusion, aluminium" and "sheet rolling, steel".
aluminium, production mix, at plant	RER	kg	1,84	2,71	9,70E-01	
corrugated board, mixed fibre, single wall, at plant	RER	kg	7,58E-02	7,58E-02		<b>UNEP:</b> Decomposed from ecoinvent processes: "slanted-roof construction, mounted, on roof" and "flat roof construction, on roof".
polyethylene, HDPE, granulate, at plant	RER	kg	9,62E-01	9,62E-01		
polystyrene, high impact, HIPS, at plant	RER	kg	7,66E-03	7,66E-03		

## H Inventory inverter and cabling

### H.1 Mc-Si Sim

Table W: Inventory for inverter and cabling, mc-Si Sim-case.

	Location	Unit	Amount	Comment
<b>PRODUCT:</b>				
Inverter + cabling		p	1,00	
<b>MATERIALS:</b>				
inverter, 2500W, at plant	RER	p	1,56	Nominal output: 2500 W. Includes original inverter and replacement.
electric installation, photovoltaic plant, at plant	CH	p	1,00	

### H.2 Mc-Si ESS

Table X: Inventory for inverter, mc-Si ESS-case.

	Location	Unit	Amount	Comment	Source
<b>PRODUCT:</b>					
Inverter		p	1,00	Type: Mastervolt Sunmaster 2500. Nominal output: 2500 W. Lifetime: 15 years.	Alsema et al. (2006); de Wild-Scholten et al. (2006).
<b>MATERIALS:</b>					
steel, electric, un- and low-alloyed, at plant	RER	kg	9,80	Steel casing.	Alsema et al. (2006); de Wild-Scholten et al. (2006).
aluminium, production mix, at plant	RER	kg	1,40	Aluminium casing.	
transformer, high voltage use, at plant	GLO	kg	5,50	Transformer, wire-wound.	
printed wiring board, mixed mounted, unspec., solder mix, at plant	GLO	kg	1,80	Printed Circuit Board, with electronic components.	

Table Y: Inventory for cabling, mc-Si ESS-case.

	Location	Unit	Amount	Comment	Source
<b>PRODUCT:</b>					
Cabling		m2	1,00	Per m <sup>2</sup> module area.	Alsema et al. (2006); de Wild-Scholten et al. (2006).
<b>MATERIALS:</b>					
copper, at regional storage	RER	kg	1,00E-01	2,2 m DC cable and 0,1 m AC cable.	Alsema et al. (2006); de Wild-Scholten et al. (2006).
tube insulation, elastomere, at plant	DE	kg	6,00E-02	Assumption for thermoplastic elastomere (TPE).	Alsema et al. (2006); de Wild-Scholten et al. (2006).

### H.3 CdTe and CIGS

Table Z: Inventory for inverter, CdTe-case and CIGS-case. "UNEP" refers to number from Gibon et al. (forthcoming), while "ESU" refers to numbers from Alsema et al. (2006) and de Wild-Scholten et al. (2006).

	Location	Unit	Amount (average value)	UNEP	ESU	Comment
<b>PRODUCT:</b>						
Inverter		p	1,00			Nominal output: 2500 W.  <i>ESU:</i> Type: Mastervolt Sunmaster 2500. Lifetime: 15 years.
<b>MATERIALS:</b>						
inverter, 2500W, at plant	RER	p		1,56		
electric installation, photovoltaic plant, at plant	CH	p		1,00		

steel, electric, un- and low-alloyed, at plant	RER	kg	13,0	16,1	9,80	Steel casing.  <b>UNEP:</b> Decomposed from ecoinvent process: "inverter, 2500W, at plant" and "electric installation, photovoltaic plant, at plant".
aluminium, production mix, at plant	RER	kg	1,79	2,18	1,40	Aluminium casing.  <b>UNEP:</b> Decomposed from ecoinvent process: "inverter, 2500W, at plant".
transformer, high voltage use, at plant	GLO	kg	5,50		5,50	Transformer, wire-wound.
printed wiring board, mixed mounted, unspec, solder mix, at plant	GLO	kg	1,80		1,80	Printed Circuit Board, with electronic components.

**Table AA: Inventory for cabling, CdTe-case and CIGS-case. "UNEP" refers to number from Gibon et al. (forthcoming), while "ESU" refers to numbers from Alsema et al. (2006) and de Wild-Scholten et al. (2006).**

	Location	Unit	Amount (average value)	UNEP	ESU	Comment
<b>PRODUCT:</b>						
Cabling		m <sup>2</sup>	1,00			Per m <sup>2</sup> module area.
<b>MATERIALS:</b>						
copper, at regional storage	RER	kg	1,00E-01		1,00E-01	2,2 m DC cable and 0,1 m AC cable.
tube insulation, elastomere, at plant	RER	kg	6,00E-02		6,00E-02	Assumption for thermoplastic elastomere (TPE).

## I Inventory rooftop PV-system

### I.1 Mc-Si Sim

Table BB: Inventory for complete rooftop mc-Si PV system, mc-Si Sim-case.

	Unit	Amount	Comment
<b>PRODUCT:</b>			
Rooftop PV-system	m2	1,00	
<b>INPUT FROM FOREGROUND:</b>			
Module	p	5,15E-01	Total area with frame: 1,94 m <sup>2</sup> (1,956x0,992 m <sup>2</sup> ). Conversion efficiency: 16%. Lifetime: 30 yr.
Mounting structure	p	5,15E-01	
Inverter + cabling	p	4,48E-02	Includes original inverter and inverter replacement. Nominal output: 2 500 W.

### I.2 Mc-Si ESS

Table CC: Inventory for complete rooftop mc-Si PV system, mc-Si ESS-case.

	Unit	Amount	Comment
<b>PRODUCT:</b>			
Rooftop PV-system	m2	1,00	Area: 87 m <sup>2</sup> . 4 rows of 13 SolarWorld SW220 sunmodule, with 6 x 10 multicrystalline cells of 156 mm x 156 mm. Conversion efficiency: 13,2% (glass area, excluding frame).
<b>INPUT FROM FOREGROUND:</b>			
Module	p	5,98E-01	Type: Solar World SW 220 sunmodule. Area: 1,68 m <sup>2</sup> (1,675x1,001 m <sup>2</sup> ). Weight: 21,2 kg. Conversion efficiency: 13,2% (glass area, excluding frame).
Mounting structure	p	1,15E-02	Type: Schletter Eco05 with EcoG roof hooks.
Cabling	p	1,15E-02	
Inverter	p	2,30E-02	Type: Mastervolt Sunmaster 2500. Nominal output: 2500 W. Lifetime: 15 years

### I.3 CdTe

Table DD: Inventory for complete rooftop CdTe PV system, CdTe-case. "UNEP" refers to number from Gibon et al. (forthcoming), while "ESU" refers to numbers from Alsema et al. (2006) and de Wild-Scholten et al. (2006).

	Unit	Average value (used in report)	UNEP	ESU	
<b>PRODUCT:</b>					
CdTe PV system	p	1,00			
<b>INPUTS FROM FOREGROUND:</b>					
Module	p	1,39	1,39	1,39	<p><b>UNEP:</b> Total module area with frame: 0,72 m<sup>2</sup>. Nominal output: 84 W. Conversion efficiency: 11,6%. Lifetime: 30 yr.</p> <p><b>ESU:</b> Module from First Solar. Total module area with frame: 0,72 m<sup>2</sup> (1,2x0,6 m<sup>2</sup>). Weight: 12,0 kg. Nominal output: 84 W. Conversion efficiency: 11,7%. Lifetime: 30 yr.</p> <p>Average conversion efficiency assumed in study: 11,7%.</p>
Mounting structure	p	1,39	1,39	1,39	
Cabling	p	1,39		1,39	
Inverter	p	3,08E-02	3,87E-02	2,30E-02	<p>Nominal output: 2500 W.</p> <p><b>ESU:</b> Mastervolt Sunmaster 2500. Lifetime: 15 years.</p>

## I.4 CIGS

Table EE: Inventory for complete rooftop CIGS PV system, CIGS-case. "UNEP" refers to number from Gibon et al. (forthcoming), while "ESU" refers to numbers from Alsema et al. (2006) and de Wild-Scholten et al. (2006).

	Unit	Amount (average value)	UNEP	ESU	Comment
<b>PRODUCT:</b>					
CIGS PV system	m2	1,00			
<b>INPUT FROM FOREGROUND:</b>					
Module	p	1,16	9,26E-01	1,39	<p><b>UNEP:</b> Total module area with frame: 1,08 m2. Lifetime: 30 yr. Conversion efficiency: 12%.</p> <p><b>ESU:</b> Module from Würth Solar. Total module area with frame: 0,72 m2 (1,2x0,6 m2). Weight: 12,6 kg. Nominal output: 75-80 W. Conversion efficiency: 10%. Lifetime: 30 yr.</p> <p>Average conversion efficiency assumed in base case: 11%.</p>
Mounting structure	p	1,16	9,26E-01	1,39	
Cabling	p	1,39		1,39	
Inverter	p	3,15E-02	4,00E-02	2,30E-02	<p>Nominal output: 2500 W.</p> <p><b>ESU:</b> Mastervolt Sunmaster 2500. Lifetime: 15 years</p>

## J Overview of existing LCA studies

### J.1 Mc-Si PV systems

Table FF: Overview of recent LCAs assessing the GWP of rooftop and ground mounted mc-Si PV systems.

Year	Authors	Direct normal irradiation [kWh/m <sup>2</sup> /yr]	PR [%]	Life-time [yr]	Conversion efficiency [%]	GWP [g CO <sub>2</sub> -eq./kWh]	GWP [kg CO <sub>2</sub> -eq./m <sup>2</sup> ]
<b>ROOFTOP PV SYSTEM</b>							
2012	De Wild-Scholten & Gløckner	1700	75,0	30	14,3	29,0	
2012	Westgaard et al.	1700	84,0	30	N/A	21,0 18,0	
2011	De Wild-Scholten	1700	75,0	30	14,1	34,0	
2010	Filippidou et al.	1420	N/A	N/A	14,0		317,0
2008	Stoppato	1700	80,0	28	16,0		123,0
2007	Fthenakis & Kim	1700 1800 2280	75,0	30	13,2	38,0 38,5 30,0	
2007	Pacca et al.	1359	95,0	20	12,9	54,6 72,4	
2006	Alsema et al.	1700	75,0	30	13,2	32,0	
2006	Fthenakis & Alsema	1700	75,0	30	13,2	37,0	
2006	De Wild-Scholten et al.	1700	75,0	30	13,2	35,0-38,0	
<b>LOWEST ESTIMATE</b>						18,0	
<b>HIGHEST ESTIMATE</b>						72,4	
<b>GROUND MOUNTED PV SYSTEM</b>							
2011	Ito et al.	1725	N/A	30	13,9		135,2
2010	Dominguez-Ramos et al.	1825	78,0	30	13,0	36,0	
2010	Ito et al.	1702	78,0	N/A	N/A	43,0	
2009	Ito et al.	2017	77,0	N/A	13,9	51,5	
2008	Ito et al.	2017	77,2	30	12,8 15,8	44,4 34,5	



2008	Fthenakis et al.	1700	80,0	30	13,2	42,0	
2007	Fthenakis & Kim	2060	80,0	30	13,2	33,0	
<b>LOWEST ESTIMATE</b>						33,0	
<b>HIGHEST ESTIMATE</b>						51,5	

## J.2 CdTe PV systems

Table GG: Overview of recent LCAs assessing the GWP of rooftop and ground mounted CdTe PV systems.

Year	Authors	Direct normal irradiation [kWh/m <sup>2</sup> /yr]	PR [%]	Life-time [yr]	Conversion efficiency [%]	GWP [g CO <sub>2</sub> -eq./kWh]	GWP [kg CO <sub>2</sub> -eq./m <sup>2</sup> ]
<b>ROOFTOP PV SYSTEM</b>							
2011	De Wild-Scholten	1700	75,0	30	11,3	19,0	
2010	Filippidou et al.	1420	N/A	N/A	9,0		137,0
2009	De Wild-Scholten & Schottler	1700	N/A	30	10,7	15,5	
2007	Raugei et al.	1700	75,0	20	9,0	48,0	
2007	Fthenakis & Kim	1700 1800 2280	75,0	30	9,0	16,0 22,0 17,0	
2006	Fthenakis & Alsema	1700	75,0	30	8,0	21,0	
2005	Raugei et al.	1700	80,0	20	8,0	53,0	
2001	Kato et al.	1430	81,0	20	10,3 11,2 12,4	51,0 42,0 33,0	
<b>LOWEST ESTIMATE</b>						15,5	
<b>HIGHEST ESTIMATE</b>						53,0	
<b>GROUND MOUNTED PV SYSTEM</b>							
2011	Held & Ilg	1200 1700 1900	80,0	30	10,9	29,5 20,9 18,7	86,1

2010	Ito et al.	1702	78,0	N/A	N/A	51,0	
2010	Dominguez-Ramos et al.	1825	78,0	30	9,0	17,0	
2009	Ito et al.	2017	77,0	N/A	9,0	66,5	
2009	Fthenakis et al.	1700	80,0	30	10,9	19,0 17,7 19,5	
2008	Ito et al.	2017	77,2	30	9,0	47,0	
2008	Fthenakis et al.	1700	80,0	30	9,0	21,0 26,0	
2008	SENSE	1200 1700 2200	91,2	20	10,0	66,0 46,0 36,0	
2007	Fthenakis & Kim	2060	80,0	30	9,0	21,0	
2006	Fthenakis & Alsema	1700	80,0	30	9,0	25,0	
2005	Fthenakis & Kim	1800	N/A	N/A	N/A	25,0	
<b>LOWEST ESTIMATE</b>						17,0	
<b>HIGHEST ESTIMATE</b>						66,5	

### J.3 CIGS PV systems

Table HH: Overview of recent LCAs assessing the GWP of rooftop and ground mounted CIGS PV systems.

Year	Authors	Direct normal irradiation [kWh/m <sup>2</sup> /yr]	PR [%]	Life-time [yr]	Conversion efficiency [%]	GWP [g CO <sub>2</sub> -eq./kWh]	GWP [kg CO <sub>2</sub> -eq./m <sup>2</sup> ]
<b>ROOFTOP PV SYSTEM</b>							
2011	De Wild-Scholten	1700	75,0	30	11,0	31,0	
2011	Clarius	N/A	N/A	N/A	12,0		140,3
2009	De Wild-Scholten & Schottler	1700	N/A	30	11,0	20,5	
2007	Raugei et al.	1700	75,0	20	11,0	95,0	
2005	Raugei et al.	1700	80,0	20	10,0	85,0	
<b>LOWEST ESTIMATE</b>						20,5	

<b>HIGHEST ESTIMATE</b>						95,0	
<b>GROUND MOUNTED PV SYSTEM</b>							
2011	Ito et al.	1725	N/A	30,0	10,1		67,5
2010	Ito et al.	1702	78,0	N/A	N/A	45,0	
2010	Dominguez-Ramos et al.	1825	78,0	30	10,0	33,0	
2009	Ito et al.	2017	77,0	N/A	10,1	58,8	
2008	SENSE	1200	91,2	20	11,5	61,0	
		1700				43,0	
		2200				33,0	
2008	Ito et al.	2017	77,6	30	11,0	38,5	
<b>LOWEST ESTIMATE</b>						33,0	
<b>HIGHEST ESTIMATE</b>						61,0	